Improved downscaling of meteorological data for hydrological modeling in the tropics under climate change

Von der
Fakultät Architektur, Bauingenieurwesen und Umweltwissenschaften
der Technischen Universität Carolo-Wilhelmina
zu Braunschweig

zur Erlangung des Grades eines
Doktoringenieurs (Dr.-Ing.)
genehmigte

Dissertation

von
Tien Thanh, NGUYEN
geboren am 25.10.1983
aus Hanoi, Vietnam

Eingereicht am 30.03.2016
Disputation am 31.05.2016

Berichterstatter Prof. Dr.-Ing. Günter Meon
Prof. Dr. Phan Van Tan

2016

Acknowledgements

This work was conducted at the University of Braunschweig with the financial support from the Ministry of Education and Training (MOET) of Vietnam, the German Academic Exchange Service (DAAD) and the University of Braunschweig.

First and foremost, I would like to express my deepest gratitude to my supervisor, Prof. Dr.-Ing. Günter Meon, who gave me a great opportunity to be a part of his research group as well as the EWATEC-COAST project and pursue my academic goals.

I am especially grateful to Prof. Dr.-Ing. Günter Meon with financial support of the hosting department at the Leichtweiss Institute to run the model on the cluster of the University of Braunschweig as well as his kindly support me on working equipment (powerful desktop computer). I thank him very much for his patience, invaluable guidance, constant encouragement and time which are not only about the academic parts but also are about social livings during the research period.

I would like to thank Prof. Dr. Michael P. Wistuba (University of Braunschweig) for the chairmanship of the examination board. I thank to Prof. Dr. Phan Van Tan (Department of Meteorology, VNU-Hanoi University of Science) for his participation in the examination board as well as co-reviewing my thesis. I would also like to thank to Prof. Dr. Matthias Schöniger for his participation in the examination board.

On this occasion, I would like to show my tremendous gratefulness to Dr.-Ing. Huyen Le and Assoc. Prof. Dr. Ngo Thi Thanh Van for introducing me to Prof. Dr.-Ing. Günter Meon. I would also like to acknowledge Assoc. Prof. Dr. Nguyen Van Lai, who gave me the first opportunities to take part in his projects dealing with hydrology and water resources.

I thank here also to my colleagues at the Thuy Loi University (Prof. Dr. Nguyen Quang Kim, Assoc. Prof. Dr. Pham Thi Huong Lan, Dr. Hoang Thanh Tung, Dr. Nguyen Hoang Son and Assoc. Prof. Dr. Ngo Le Long) for their reliance, encouragements as well as facilitation for my abroad study.

I would like to thank to my colleagues in the group of Hydrology, Water Management and Water Protection (HYWAG) (Dr. Gerhard Riedel, Dr. Kristian Förster, Dr. Malte, Dr. Phillip, Malte Eley, Stephanie Zeunert, Worapong, Hernita, Marlene, Tim, Karoline, Saskia, Viktoria, Karen) for sharing with me a lot of fun, for creating a very pleasant atmosphere, for supporting as well as memorable moments, both present and past at office especially for their knowledge of hydrological modeling.

I would like to thank to Mrs. Vanessa Wörner in particular, but also Dr.-Ing. Matthias and Dr. Nguyen Hoang Anh for editing my English writings. Of course, the errors in this thesis remain mine. I thank to Mrs. Susanne Festerling for her supports and time in the first days I came to Braunschweig as well as during the research period. I will always remember a short space of time when she picked me up at the Braunschweig Hbf and transferred me to the Weststadt Dormitory.

To gain the fruit of all work, I would like to acknowledge in particular the assistance of Prof. Dr. Andreas H. Fink at the University of Karlsruhe for his useful ideas and suggestions. I also thank to the members of the climate modeling groups RegCM, WRF and COSMO as well as Linux community for

admitting me as an affiliated member in their group, which allowed me to learn a lot more about weather, climate, computer science and statistics.

Last but not least, this is the time for me to express my thankfulness to my grandmother - Nghiem Thi Tan, my parents - Nguyen Van Trung and Le Thi Truong, my parents-in law for their love, my brother - Nguyen Tien Dung and my beloved wife - Le Phuong Dung, who continuously encouraged me by their understanding, unconditional helps, patience and endless loves.

Thank you very much! Danke schön! Xin chân thành cảm ơn!

Abstract

Climate change is of special interest in recent research projects dealing with the Earth's climate system due to its potentially strong influences on the society in many ways. One of the great challenges in climate modelling for the analysis of climate variability and climate change at a considerable scale of time and space is the non-linear interaction between the various components of the climate system. Parallel to the development of computing science, the understanding of the climate system behaviours and the climate model accuracy and resolution have been considerable improved. It, however, has still not been sufficient for the request of hydrologic modeling at a local scale, especially when focusing on the impacts of climate change.

Therefore, it is necessary to carry out a study for a small basin like the Thi Vai basin (approximately 500 km^2) in southern Vietnam to provide further information on local changes in climate and to quantify its impacts on hydrological characteristics for present and future periods. Within this study, the technology of statistical downscaling is improved and directly coupled with the outputs of a regional climate model, which contains dynamical downscaling techniques. The regional climate model is implemented with the three self-nesting steps to transfer the information of global climate models into local climate information. The techniques of Model Output Statistics and Two-Step Model are applied and developed to correct the daily temperature and precipitation at the finest resolution of 10 x 10 km, respectively. To quantify the possible impacts of climate change on hydrological characteristics, the water balance model PANTA RHEI is driven by the model output of the dynamic-statistical downscaling. A strategy for future analyses of the reverse effects of changes in the water balance on the outputs of downscaling models is also provided.

The main results indicate that: (i) the dynamical climate model overestimates both total precipitation and wet day frequency, although both precipitation and temperature is simulated quite well on the highest horizontal grid resolution that can be reached using a hydrostatic climate model, (ii) the combination of statistical and dynamical downscaling is an effective approach for daily precipitation and temperature series analysis, (iii) a clear climate change signal for temperature and precipitation is found for the Thi Vai basin, (iv) the simulations of the PANTA RHEI model fit well to the observational data, although PANTA RHEI has never been applied in Vietnam before and (v) the changes in meteorological components significantly contribute to potential changes in stream flow in the Thi Vai basin, even if these changes are negligible.

Zusammenfassung

Eine der großen Herausforderungen in der Klimamodellierung für die Analyse von Klimavariabilität und Klimawandel auf einer breiten Skala von Zeit und Raum ist die nicht-lineare Interaktion zwischen den verschiedenen Komponenten des Klimasystems. Zeitgleich zur Entwicklung der Computerwissenschaften verbesserten sich das Verständnis des Verhaltens des Klimasystems und die Genauigkeit und Auflösung der Klimamodelle deutlich.

Deshalb ist es notwendig, eine Studie für ein kleines Einzugsgebiet wie das Thi Vai Einzugsgebiet (ca. 500 km^2) im südlichen Vietnam durchzuführen, um weitergehende Informationen zu lokalen Klimaveränderungen zu liefern und deren Auswirkungen auf hydrologische Charakteristiken für heutige und zukünftige Zeiträume zu quantifizieren. In dieser Studie wird das statistische Downscaling verbessert und direkt mit dem Output eines regionalen Klimamodells gekoppelt, welches mit einem dynamischen Downscaling produziert wurde. Hier für wird das regionale dynamische Klimamodell zunächst mit 3 Nesting-Schritten angewandt, um die Information von globalen Klimamodellen in lokale Klimainformationen zu übertragen. Die Ergebnisse aus dem letzlen Nesting-Schritt, bei dem ein Gittesnetz von 10 x 10 km angesetzt wurde, werden statistisch wie folgt verbessert: Die MOS (Model Output Statistics)-Technik wurde angewendet, um die tägliche Temperatur zu korrigieren. Die tägliche Niederschlagsmenge wurde durch die TSM (Two-Step Model)-Technik korrigiert. Um die möglichen Auswirkungen des Klimawandels auf hydrologische Charakteristika zu quantifizieren, wird das Wasserhaushaltsmodell PANTA RGHEI mit dem Output des dynamisch-statistischen Downscaling angetrieben. Zusätzlich wird eine strategie für zukünftige Analysen der Rückkopplungseffekte eines veränderten Wasserhaushalts auf den Output von Downscaling-Modellen erarbeitet.

Die wichtigsten Ergebnisse zeigen, dass: (i) das dynamische Klimamodell sowohl die Niederschlagsmenge als auch die Anzahl an Regentagen überschätzt, obwohl Niederschlag und Temperatur in der höchstmöglichen horizontalen Auflösung eines hydrostatischen Modells gut simuliert werden, (ii) die Komination von statistischem und dynamischem Downscaling ein effektiver Ansatz für die Analyse von Tagesmittelwerten für Niederschlags- und Temperaturzeitreihen ist, (iii) ein deutliches Klimawandelsignal für Niederschlag und Temperatur identifiziert wurde, (iv) die Simulationen des PANTA RHEI-Modells die Beobachtungsdaten gut widerspiegeln, obwohl PANTA RHEI zuvor nicht für Vietnam angewandt wurde, (v) die Veränderungen der meteorologischen Komponenten deutlich zu den potentiellen Veränderungen des Abflusses in Thi Vai Einzugsgebiet beitragen, auch wenn diese Veränderungen nur geringfügig sind.

TABLE OF CONTENTS

1 INTRODUCTION 1

1.1 SCOPE OF THE RESEARCH 1
1.2 OBJECTIVES OF THE RESEARCH 2
1.3 APPROACH METHODS 2
1.3.1 Homogeneous tests for the detection of trends 2
1.3.2 Interpolation methods 3
1.3.3 Downscaling climate models from global to regional and to catchment scale 4
1.3.4 Hydrological models 6
1.4 THESIS OUTLINE AND WORKING STEPS 6

2 LITERATURE REVIEW AND BACKGROUND 9

2.1 REVIEW ON DOWNSCALING TECHNOLOGY 9
2.1.1 Dynamical downscaling 10
2.1.2 Statistical downscaling 19
2.1.3 State of the art bias correction 24
2.2 EVALUATION OF DOWNSCALING TECHNOLOGIES 27
2.3 HYDROLOGICAL MODELS 29
2.3.1 Hydrological model classification 29
2.3.2 Choice of hydrological model 30

3 SELECTION-DATA COLLECTION OF THE STUDY AREA: THI VAI RIVER CATCHMENT 33

3.1 NATURAL CONDITIONS OF THE STUDY AREA 33
3.1.1 Topography 33
3.1.2 Climate 33
3.1.3 Land use and land cover 44
3.1.4 Geology and soil texture 44
3.1.5 Hydrological characteristics 45
3.2 SOCIOECONOMIC CONDITIONS OF THE STUDY AREA 46
3.2.1 Population 46
3.2.2 Socioeconomic conditions 46
3.3 DATA COLLECTION 47
3.3.1 Station data 47
3.3.2 Raster datasets for meteorological data fields 49

4 GLOBAL AND LOCAL CLIMATE CHANGE 54

4.1 OVERVIEW OF CLIMATE CHANGE 54
4.1.1 Understanding climate, climate variability and climate change 54
4.1.2 Observed changes in climate on a global scale 55
4.2 CLIMATE CHANGE IN VIETNAM 58
4.2.1 Major climate factors in Vietnam 58
4.2.2 Climate change projects 62
4.2.3 Impacts of climate change in Vietnam 63

4.3 SELECTION OF A CLIMATE CHANGE SCENARIO FOR THE THI VAI RIVER CATCHMENT 66

5 ANALYSIS OF OBSERVATIONAL DATA 69

5.1 ESTIMATION OF MISSING PRECIPITATION RECORDS 70
5.1.1 Introduction to research methods 70
5.1.2 Analysis results 71
5.2 DOUBLE MASS CURVE 73
5.2.1 Introduction 73
5.2.2 Analysis results 74
5.3 HOMOGENEOUS TESTS FOR THE DETECTION OF TRENDS 75
5.3.1 Introduction to research methods 75
5.3.2 Analysis results 79
5.4 SPATIAL INTERPOLATION 85
5.4.1 Introduction to research methods 85
5.4.2 Analysis results 88

6 IMPROVEMENT OF DYNAMIC-STATISTICAL DOWNSCALING TECHNOLOGY IN CLIMATE CHANGE STUDIES 90

6.1 THE DYNAMICAL DOWNSCALING MODEL: AN INTRODUCTION OF THE REGCM MODEL 90
6.2 THE DYNAMICAL DOWNSCALING MODEL REGCM4: DESCRIPTION AND MODEL SETUP 92
6.2.1 Model description 92
6.2.2 Model setup 93
6.3 ANALYSIS AND EVALUATION OF MODEL RESULTS 96
6.3.1 Temperature 97
6.3.2 Precipitation 103
6.4 STATISTICAL DOWNSCALING TECHNOLOGY FOR AN IMPROVEMENT OF CLIMATE SIMULATIONS 110
6.4.1 Model Output Statistic for the “correction” of daily temperature 110
6.4.2 Development of a Two Step Model for the “correction” of daily precipitation 113
6.5 CLIMATE CHANGE SIGNALS USING THE COMBINED TECHNOLOGY OF DYNAMIC-STATISTICAL DOWNSCALING 118
6.5.1 Climate Change signals in precipitation 118
6.5.2 Climate change signals in temperature 120

7 POTENTIAL CLIMATE CHANGE IMPACTS ON STREAM FLOW 123

7.1 THE HYDROLOGICAL MODEL PANTA RHEI 123
7.2 STRUCTURE OF THE HYDROLOGICAL MODEL PANTA RHEI 124
7.2.1 Evapotranspiration 124
7.2.2 Interception 125
7.2.3 Runoff formation 125
7.2.4 Runoff concentration 127
7.3 MODEL SETUP 127
7.4 EVALUATION OF THE MODEL PERFORMANCE 128
7.5 POTENTIAL CLIMATE CHANGE IMPACTS ON STREAM FLOW 133
7.5.1 Impacts on monthly stream flow 134
7.5.2 Impacts on seasonal and annual stream flow 136
7.5.3 Impacts on the day of year of stream flow 140

8 STRATEGY FOR FUTURE ANALYSES OF THE REVERSE EFFECTS OF CHANGES IN THE WATER BALANCE ON THE OUTPUTS OF DOWNSCALING MODELS 143

8.1 BASIC THOUGHTS 143
8.2 INTERACTION OF METEOROLOGICAL AND WATER BALANCE EFFECTS 145
8.3 WORKING STRATEGY 146

9 CONCLUSIONS AND RECOMMENDATIONS 148

9.1 CONCLUSIONS 148
9.2 RECOMMENDATIONS 151

REFERENCES 153

APPENDIXES 170

LIST OF FIGURES 184

LIST OF TABLES 188

ABBREVIATIONS 189

1 INTRODUCTION

1.1 Scope of the research

Evidence of global warming is found in a wide range of climate observations as documented in the reports of the Intergovernmental Panel on Climate Change (IPCC[1]). The observed changes in climate vary geographically, depending on local conditions. Consequently, identification of whether or not climate change is occurring over a specific area is considered to be the first step in climate change projects. The detection of trends in temperature and precipitation is one of the most interesting research fields in global warming climatology due to nonhomogeneous changes in space and time. These variables are one of the most important climate variables (GCOS, 2010a). In Vietnam, a dominant focus on the investigation of climate variability is for the temperature variable. To be more precise, for the period 1961-2000, Nguyen (2007) shows an increase in temperature of about 0.4 to 0.6 degree Celsius at typical meteorological stations of Northern Vietnam's territory. An increase in mean temperature of roughly 0.5 to 0.7 degree Celsius is identified for the period 1958 to 2008 (Nguyen, 2008; Nguyen, 2009). Up to the present time, an investigation of the variability in precipitation characteristics at the scale of a small catchment in Vietnam has still not been carried out. Therefore it is essential to analyse the variability of precipitation features on a local scale to obtain evidence of climate change. The identification of climatic trends and their impact on hydrological characteristics of a small Vietnamese catchment with the help of improved meteorological downscaling techniques is the objective of this research.

Climate change has been drawing the attention of governments, scientists and people all over the world, with an increasing interest shown in scientific publications as well as in the media. It is broadly argued that climate change affect both nature and society, as pointed out in the IPCC Fourth Assessment Report (IPCC, 2007). Yet, the impacts of climate change are not clarified in considerable detail due to the complexity of the climate system as well as the strong variability of climate variables in space and time. On the temporal scale, some effects can be only detected over a span of decades or centuries. On the spatial scale, the impacts of climate change for various parts of the world vary in form and intensity. So far, a main focus on global assessments is dominating in climate change projects. Dynamical and statistical downscaling model applications are being developed for the study of climate change impacts at regional and local scales. Although they are valuable climate simulation and projection tools, the quantification of the fine-scale heterogeneity of climate change impacts is still a great challenge within tropical regions. The reason for this is that the effects of local and mesoscale processes such as turbulence or thermals on terrestrial characteristics are more dominant than synoptic influences. Within these regions, the foundation and development of convective processes play a central role in weather patterns, but they are nearly unpredictable (Wang, 2006).

[1] The Intergovernmental Panel on Climate Change (IPCC) was established in 1988 by the United Nations Environment Programme and the World Meteorological Organization to provide the world with a clear scientific view on the current state of knowledge in climate change and its potential environmental and socio-economic impacts.

Furthermore, the required set of equations describing a physical system of subgrid scale processes (e.g., convection or thunderstorm) is so complex that it cannot directly be solved in the weather and climate models (Stensrud, 2007; Warner, 2010). Consequently, these processes cannot be fully interpreted. Located within the intertropical zone under the influence of monsoon regimes, the Vietnamese climate has both tropical and monsoon characteristics. These factors play an important role in producing the different climate regions. On the catchment scale in Vietnam like the Vu Gia-Thu Bon (~10000 km^2), there are several projects dealing with climate change such as LUCCi[2] and HCPV[3]. On a small scale, however, there is still a lack of studied documents in relation to climate and flood issues. Thus, it is essential to interpret the changing climate at a small basin, where the potential changes can directly affect nature and society. Additionally, high-resolution climate model outputs are required for the prediction of climate change impacts, for example as an input for hydrological models. Also, a high-quality simulation of precipitation on a local scale is important to assess and fully interpret possible future changes of water balance.

Last but not least, water is a key resource for all forms of life. The water cycle is very sensitive to changes in climate parameters. As a result, the impacts of changing climate conditions on water resources are possible threats to nature, humans and society. Knowledge of potential future changes in the hydrological cycle is very important for agricultural planning in any locality as well as for decision makers to develop possible mitigation and adaptation strategies. Therefore, it is necessary to investigate possible climate change impacts on the water balance of small rivers.

1.2 Objectives of the research

This PhD study concentrates on a small region in southern Vietnam used as a study area. The overall goals are:

- To determine and analyse trends and changes of climate data series with a focus on precipitation and temperature variables.
- To develop and apply the technology of dynamic-statistical downscaling at high spatial and temporal resolution for a climate change impact study. Based on this technology, the climate scenario is developed for the Thi Vai River catchment located in Southern Vietnam.
- To assess climate change impacts on the water balance of the Thi Vai River catchment using a water balance model.
- To develop a strategy for future analyses of the reverse effects of changes in the water balance on the meteorological outputs of downscaling models.

1.3 Approach methods

1.3.1 Homogeneous tests for the detection of trends

Several approaches can be used for the detection and estimation of trends, such as linear regression and the graphical method. Each one, however, has its strengths and weaknesses. For instance, one of

[2] Land Use and Climate Change Interactions in Central Vietnam

[3] High-resolution Climate Projections for Vietnam

the strengths of the graphical method is the visualisation of trends, but there are no quantifiable results. Alternatively, a linear regression can provide an estimation of slope, a confidence interval and quantification of fit, but it can be affected by outliers. Furthermore, it allows the quantification of multiple influences, but there is no test for handling the missing values. Because of their advantages, the Mann-Kendall (MK) statistic test (Mann, 1945; Kendall, 1948) and Sen's method (Sen, 1968), are broadly being applied in different fields of hydrological and climatological researches and are used within this study as well. The first advantage of the MK test is that it is a non-parametric test, or rank correlation, without any need for a particular distribution of data. In other words, the data require fewer assumptions to be made. The second advantage of the test is that it is not affected by data errors and outliers. Using the MK test, an upward, downward, or absent trend is assessed at α level of significance after discarding the effect of serial correlation.

1.3.2 Interpolation methods

Precipitation is an important input parameter for water resource management and hydrologic models. With a spatially continuous distribution of precipitation, the accuracy of computing results can be further strengthened. It is, seemingly, quite difficult to find enough evenly spread weather variables to cover the entire nation in general and the area of interest in particular. In Vietnam, it is challenging to gather data for such areas due to the very coarse density of observation stations. Over Southern Vietnam, for instance, there is an overall density of approximately one station per 2500 km^2 (Giang, 2014). On the other hand, the meteorological stations and rain gauges are unevenly distributed between regions of mountains, plains, and coastal zones. So, an estimation of unknown values is unavoidable. Correspondingly, Journel and Deutsch (1992) and Burrough *et al*. (1998) introduce the techniques of extrapolation and interpolation. The present study will focus on interpolation methods.

In recent research projects, several interpolation methods were applied to estimate unknown data values, such as the two-dimensional overlapping-parabolic interpolation method (Grell *et al*., 1994), the kriging method (Ly *et al*., 2011), or the thiessen polygon method (Thiessen, 1911; Dirks *et al*., 1998). Over 40 different interpolation methods are shortly described in Li (2008). The study illustrates that every method has its advantages and disadvantages, and none of them performs best in all cases but is only the optimal choice under certain circumstances. To classify spatial interpolation methods, there are several different ways. They are generally divided into the two groups of deterministic and geostatistical methods. The main idea of these methods is to estimate the unknown data values within a region covered by known data values. So far, the interpolation methods are mainly applied on the temporal scale of monthly or annual data and on a spatial scale of thousands of square kilometers (Hevesi *et al*., 1992; Holdaway, 1996; Goovaerts, 2000). Therefore, the five different interpolation methods consisting of cressman, ordinary kriging, regression kriging, dual kriging, and inverse distance weighting are applied to identify the best method for the area of study on the spatio-temporal scale (daily, 10 km x 10 km). The interpolation procedures are necessary in order to provide climate data information for a small catchment.

1.3.3 Downscaling climate models from global to regional and to catchment scale

1.3.3.1 Dynamical downscaling

Dynamical downscaling technology refers to how to fit the output from the Global Climate Models (GCMs) into Regional Climate Models (RCMs). In other words, an RCM is driven by a GCM to simulate the regional climate. For the climate problems at a global or regional scale, a set of different mathematical equations dealing with the physical, chemical and biological laws needs to be solved. Due to the coarse resolution of the global models, some of these processes are approximated. For the outputs of RCMs, the climate information is given at higher resolution than that of GCMs. This enables RCMs to better represent the atmospheric physical processes on subgrid scale such as convective thermal exchange processes. Thus, RCMs are valuable tools for the climate impact assessments.

In most hydrological models, precipitation and temperature are the most important weather input variables. Undoubtedly, it is difficult to accurately quantify the amount of precipitation because of its spatial and temporal pattern. For Asia, tropical regions in general and for a small river catchment in southern Vietnam in particular, precipitation dramatically depends on the Asian monsoon system and tropical cyclones. A variety of regional climate models such as *PRECIS* (Providing REgional Climates for Impacts Studies) (Jones *et al*., 2004), *REMO* (Regional Model) (Lorenz and Jacob, 2005) or *COSMO* (COnsortium for SMall-scale Modeling system) (Steppeler *et al*., 2003) is applied for different studies over different regions (Van der Linden and Mitchell, 2009). In international climate programs such as the WRCP[4] CORDEX[5] initiative (Giorgi *et al*., 2009), regional climate scenarios over the world have been developed. They have become useful tools for climate change studies in the 14 CORDEX regions. Even though the grid resolution is set to 0.44 degrees (approximately 50 km) for each region except for the CORDEX Southeast Asia region (36 km), it is still not fine enough to allow hydrological models to be applied to to a small river basin in general. Hence, statistical downscaling techniques are reported by Wilby *et al*., (2004) to downscale global climate model outputs to a specific station.

Within this project, the technology of dynamical downscaling is implemented to downscale from global scale to regional scale and to catchment scale using the RegCM model version 4. This system is configured with three self-nesting steps of 60, 25 and 10 km grid cell resolution. For the purpose of diminishing the influence of global climate circulation biases on the regional climate model outputs, the model is driven by the ERA-interim reanalysis data for the period of 1981-2010 and forced by the third version of the Canadian Centre for Climate Modelling and Analysis (CCCma) Coupled Global Climate Model (CGCM3) for periods of 1961-1990 and 2071-2100.

[4] World Climate Research Programme

[5] Coordinated Regional Climate Downscaling Experiment

1.3.3.2 Statistical downscaling

The idea of stochastic approaches is to establish empirical relationships between large (predictors) and local (predictands) scale variables to discard the systematic errors and correct the bias of downscaling results (Prudhomme *et al*., 2002; Wilby *et al*., 2004). With the statistical downscaling, a set of equations that expresses the statistical relationships between predictors and predictands is applied to the climate information from GCMs or RCMs output to local climate parameters. These relationships are hold for the expected environmental changes under climate change. Reviews on statistical downscaling methods can be found in Wilby and Wigley (1997), Xu (1999), Giorgi *et al*. (2001), Wilby *et al*. (2004), Benestad *et al*. (2007), Fowler *et al*. (2007) and Maraun *et al*. (2010). Thus far, a wide range of statistical downscaling methods is available, such as a project focusing on STARDEX[6] alone (Goodess, 2005), canonical correlation analysis (CCA) (Busuioc *et al*., 2008), or LARS-WG (Semenov *et al*., 2002) and others. With a variety of statistical downscaling methods, they are categorized into three categories: (i) weather classification, (ii) regression models and (iii) weather generators as given in the IPCC Second Assessment Report (IPCC, 1996) and Wilby *et al*. (2004). Alternatively, they can be classified into three categories as suggested by Rummukainen (1997) and later on adapted by Maraun *et al*. (2010): (i) Perfect prognosis (or "perfect prog" - PP), (ii) Model output statistics (MOS) and (iii) weather generators (WGs).

Within this project, to capture the high-quality climate information for the request of hydrological model at daily scale, the MOS approach was applied to the "correction" of the daily temperature data. The output of regional climate model at a high-resolution scale instead of the output of global climate models at coarse-resolution scale (Wilby, 1997) is considered to be predictors.

1.3.3.3 Bias correction of model output

Although the spatial resolution of dynamical downscaling models has been increasingly improved, regional climate models inevitably show systematic biases in their outputs, especially for precipitation because of its local features. The biases in precipitation subsequently affect other hydrologic processes in hydrological models like surface runoff or evapotranspiration. It is stressed that neither GCM nor RCM output are valuable as input parameters for hydrologic models without a bias-correction step (Hansen *et al*., 2006; Wood *et al*., 2004; Piani *et al*., 2010a). Thus, the post-process of bias correction needs to be implemented in order to produce reliable simulation results at high-resolution scale of time and space. A variety of bias correction method is investigated in projects such as the project ENSEMBLES[7] (Hewitt and Griggs, 2004) and the Inter-Sectoral Impact Model Intercomparison Project (ISI-MIP) (Hempel *et al*., 2013). The simplest formulations of bias correction are to adjust the statistical characteristics of simulated data so that they fit to those of observed data. This can be carried out with an additive or multiplicative constant as described in Schmidli *et al*. (2006) and Lenderink *et al*. (2007). More sophisticated methods, such as the variation coefficient (Leander and Buishand, 2007), the quantile mapping (Ines and Hansen, 2006) and even the transfer function (Piani *et al*., 2010a; Piani *et al*., 2010b) are used to remove biases.

[6] Statistical and Regional dynamical Downscaling of Extremes for European regions

[7] http://ensemblesrt3.dmi.dk/

Several limitations of bias correction are pointed out, such as the limitations of linear and quantile-quantile corrections (White and Toumi, 2013). The bias correction approach is also a controversial subject as given in Ehret *et al*. (2012) but, no method is obviously implemented best in all cases. The method of bias correction becomes a criterion operation in most studies in climate change impacts and used to correct climate variables in the IPCC Fifth Assessment Report (IPCC AR5) (IPCC, 2013). This refers to their advantages rather than disadvantages. As of the limitation of time within this thesis framework, a bias correction (so-called Two Step Model-TSM) is developed to diminish the bias from dynamical downscaling model outputs (e.g., daily precipitation). As compared to other bias correction methods (e.g., Leander and Buishand, 2007), this method allows to reduce biases of the frequency and intensity of daily precipitation directly aggregated from regional climate model RegCM4 output.

1.3.4 Hydrological models

To analyse the climate change impacts on the water balance, hydrological models are major tools. Parallel to the development and improvement of the computer resource and technology, a range of hydrological models of varying complexity and scale has become available. Examples for hydrological models are MIKE SHE (Abbott *et al.*, 1986) or the Soil and Water Assessment Tool (SWAT) (Moriasi *et al.*, 2007). To date, the hydrological models at high-resolution can be performed within much shorter time compared to the past. This is an advantage for the hydrological studies to some extent detail of spatio-temporal variability. Nonetheless, hydrology is a scientific area that is closely linked to other scientific areas such as meteorology and climatology. This refers that in the context of complex interplay of climate components, it is not easy to quantify the spatiotemporal variability of water balance. It is especially in coupling hydrology and science of changes in climate that is occurring on the spatial-temporal scales. Thus, the demand for hydrological simulations in order to make projections for climate change impacts on the water cycle in near-future and far-future is increasing. In general, most studies focus on climate change effects on freshwaters (Rouse *et al.*, 1997), on runoff (Arnell, 1999) and on groundwater (Taylor *et al.*, 2013). Hydrological projects mainly focus on the sparse resolution of spatial (large scale) and of temporal (monthly, seasonal or annual changes) for Europe and North America (Fowler *et al.*, 2007). In contrary to this, there is a lack of attention to potential climate change impacts on water balance in tropical regions at small basin scale. In order to address this, the effects of climate change on flood events in coastal regions in Southern Vietnam are subject of investigation in this study.

1.4 Thesis outline and working steps

The structure of this doctoral thesis comprises 9 chapters. The main works are described in chapter 2 to chapter 8, whilst chapter 1 and chapter 9 are the introduction and conclusions, respectively. A schematic overview of the main structure of this thesis is displayed in Figure 1.1. A general introduction to the statement of the problem and the objectives of the research as well as approach methods are given in chapter 1. Chapter 2 contains a literature review as well as a description of the background of the state of the art of dynamic-statistical downscaling technologies, hydrological modeling and model evaluation. Description and analysis of natural and socioeconomic conditions of

the study area, Thi Vai catchment and the data collection for the model simulation are given in chapter 3. A background on climate change science and the analysis of observed climate change and its impacts in Vietnam are given in chapter 4. Chapter 5 presents theories and results of observational data analysis. An improvement of dynamic-statistical downscaling technology for climate change studies is presented in chapter 6. The results for the climate change signals are given using a dynamical downscaling model and two statistical models. Chapter 7 gives an overview of the water balance model PANTA RHEI. The impacts of climate change on the water balance are analysed. The reverse effects of changed stream flow on meteorological components are presented in chapter 8. Chapter 9 gives conclusions and recommendations.

The working steps are illustrated in Figure 1.1 and shortly described in the following:

(1) Literature review on climate change issues worldwide and in Vietnam.

(2) Part A contains an analysis and evaluation of obtained data. The advantage and disadvantage of obtained data is fully interpreted. Statistical analysis of meteorological variables is implemented for a long-term. Plus, the homogeneous tests for the detection of trends are implemented for meteorological variables.

(3) Part B concentrates on linking meteorological and hydrological investigations at a small catchment scale using the combined hydrometeorological models. At first, local meteorological variables are reproduced by dynamic-statistical downscaling models using the output of global climate model as the initial and lateral boundary conditions. Afterwards they are used as an input for the water balance model PANTA RHEI. An evaluation of results is included within this part.

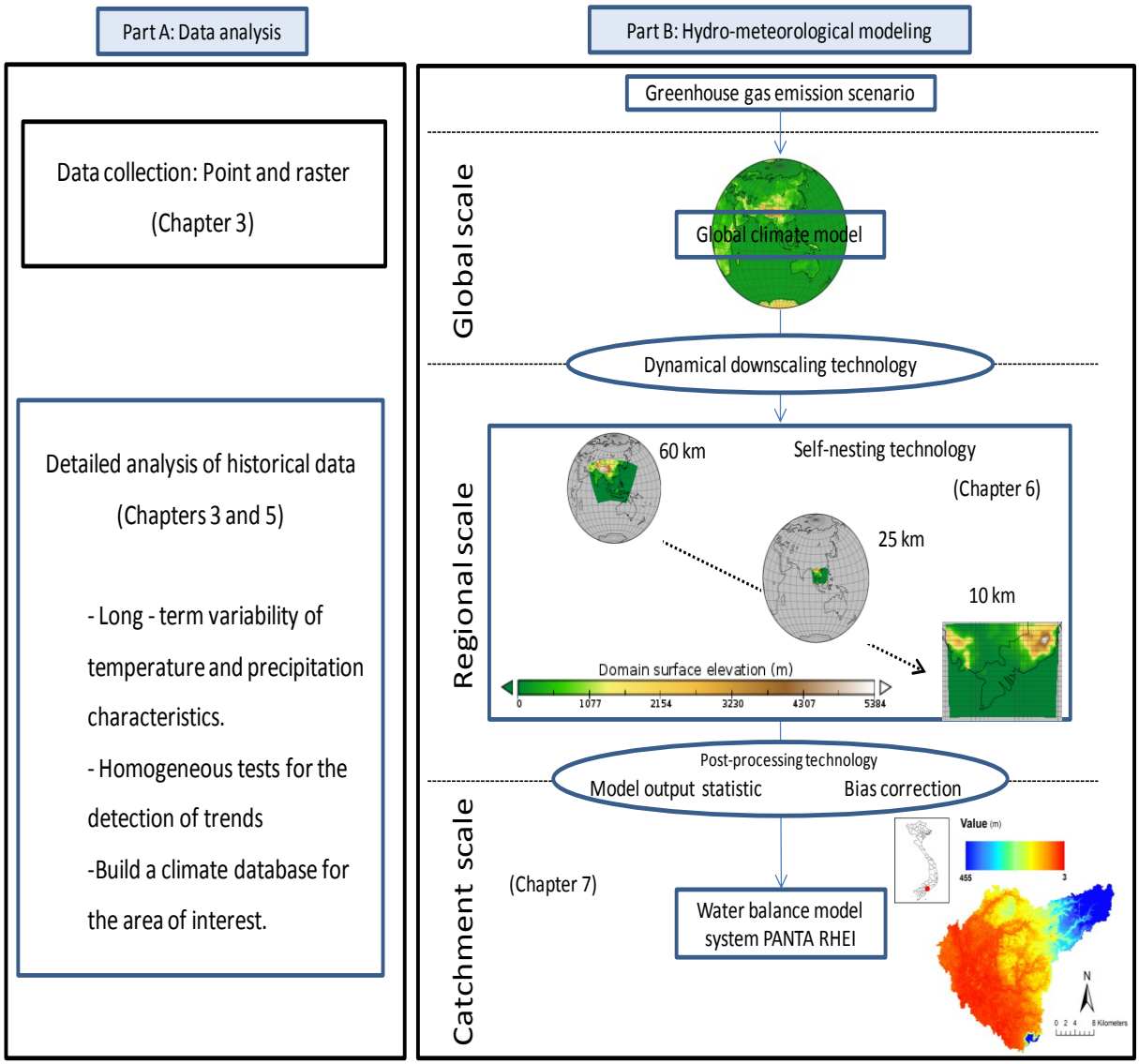

Figure 1.1: Scheme of the main structure of this thesis.

2 LITERATURE REVIEW AND BACKGROUND

2.1 Review on downscaling technology

"…Even if global climate models in the future are run at high resolution there will remain the need to "downscale" the results from such models to individual sites or localities for impact studies."

DOE (1996)

"*. . .'downscaling' techniques [are] commonly used to address the scale mismatch between coarse resolution global climate model (GCM) output and the regional or local catchment scales required for climate change impact assessment and hydrological modeling*."

Fowler *et al*. (2007)

Even if GCMs are extremely useful tools to study and understand the weather, climate and climate change behaviours, it is impossible to capture natural processes at the fine scale, such as coastal breeze wind and convective clouds due to their coarse resolution (typically 100-500 kilometres). However, these small-scale processes are important factors for the occurrence of hydrological extreme events (Maraun *et al*., 2010). Furthermore, for future projections, information about potential climate change impacts on hydrology, ecosystems, etc.,-on a spatial scale of 10 to 50 kilometres are very useful (Trzaska and Schnarr, 2014). In order to address this, a variety of "downscaling" methods has been developed to bridge the gap between the GCMs and the high-resolution simulation needed by end users. "Downscaling" methods can be applied for both, the spatial and the temporal dimension in order to get information on climate parameters at the spatio-temporal scale that is needed for further analysis. Generally, there are three main approaches to transfer large scale climate simulation from a GCM to a much smaller scale: (1) dynamical downscaling, (2) statistical downscaling and (3) a technique that combines dynamical and statistical downscaling. According to Feser *et al*. (2011), there are three different types of models for performing dynamical downscaling: (i) Limited area models, (ii) stretched grid models (or variable-resolution grids (Rummukainen, 2010)) and (iii) uniformly high resolution atmospheric GCMs. Three primary approaches for statistical downscaling are (1) regression methods, (2) weather classifications and (3) weather generators (see section 2.1.2). A general concept of downscaling is shown in Figure 2.1.

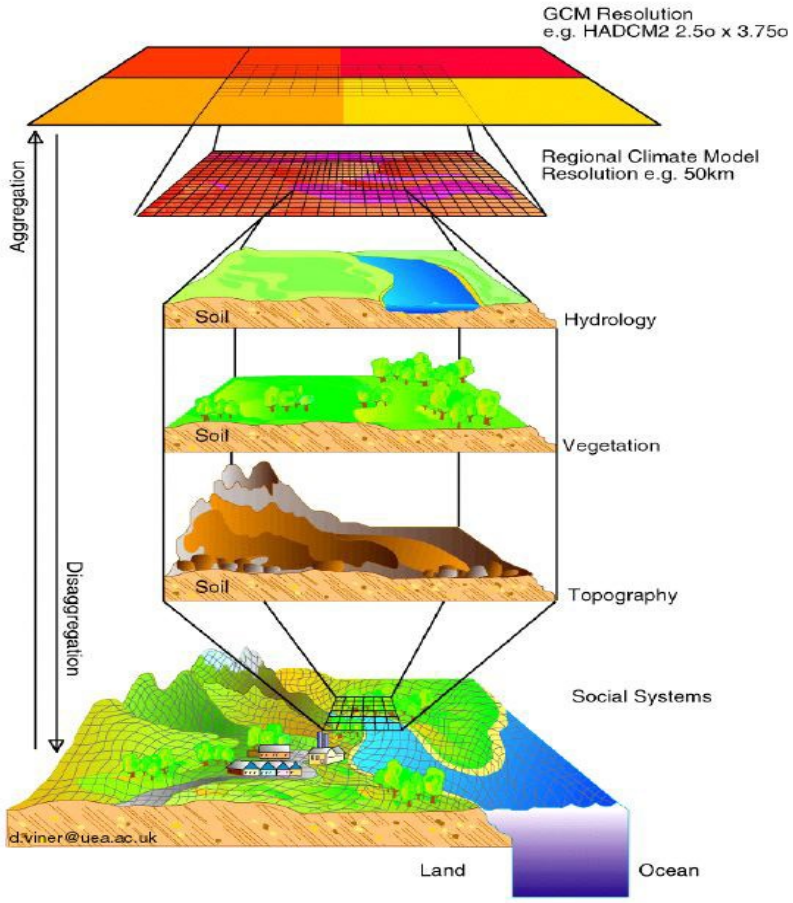

Figure 2.1: "Downscaling" scheme from coarse to fine resolution (Viner, 2012).

2.1.1 Dynamical downscaling

2.1.1.1 Global climate models (GCMs)

"*Based upon the observations that have been made, the initial state of the atmosphere is represented by a number of charts which give the distribution of seven variables from level to level in the atmosphere. With these charts as the starting point, new charts of a similar kind are to be drawn which represent the new state of the atmosphere from hour to hour*."

Bjerknes (1904)

In 1904, Vilhelm Friman Koren Bjerknes, a Norwegian physicist and meteorologist, first argued that the weather conditions could be predicted from calculations based on the physical laws of the atmosphere. A set of seven "primitive equations" describing the behaviour of heat, air motion and moisture was developed. Bjerknes (1904) suggested the graphical methods based on weather maps for solving the equations to anticipate large-scale atmospheric circulations. It was, however, not accurate enough.

Margules (1904) and Exner (1908) from the Vienna school made the first attempts to forecast the weather using numerical integration of simplified fluid equations but they were not successful. Until the 1920s, Lewis Fry Richardson, who pioneered modern mathematical techniques of weather forecasting, used the finite difference solutions of differential equations to solve the "primitive equations" with the "forecast-factory" after dividing a territory into a grid of cells (Richardson, 1922). Results from these calculations, however, were completely faulty. In the 1950s, after being able to solve the baratropic vorticity equation, weather forecasting was successfully performed for a grid of 736 km horizontal resolution with a time step of three hours over North America. The total number of grid points was limited with 270 points. Although these results strongly differed from observational data, they were good enough to explain the forecast errors. Reasons for these errors are the boundary conditions and the horizontal resolution, which is too large (Charney *et al*., 1950). The 1950s were considered as "epoch making" in the history of meteorology in general and the atmospheric numerical modeling in particular. With the development of digital computers in the 1950s it became possible to perform short-range weather predictions for the regional scale. Later, many experiments were made, for example by Philips (1956) or Lorenz (1955). These experiments are considered as the first working GCMs (Randall, 2000). The development of GCMs from the Mid-1970s, which is reflected in the implementation of more components into the models, is shown in Figure 2.2. The GCMs are based on physical laws of the interaction between the climate system components such as atmosphere and hydrosphere at each grid cell over time. Simulation results from GCMs play an important role in climate and weather researches. They are used to simulate the present climate and identify the factors that influence the climate on the regional scale. Another field of application is the projection of possible future climatic conditions. In general, GCMs are useful tools to identify the influence of natural or anthropogenic factors on a particular climatic region in the future.

It is a great challenge to develop a climate model that simulates the Earth's climate well due to a very complex climate system. The complexity derives from non-linear interactions between the various components of the climate system at different spatio-temporal scales. These components include atmosphere, hydrosphere, biosphere, geosphere and cryosphere. According to the IPCC's report (IPCC, 2001), all components are linked by mass fluxes, heat and momentum although their compositions, features and behaviours are very different. The Earth's climate as a whole is strongly dominated by the atmospheric circulation, ocean currents and incoming solar radiation at the land surface. Obviously, within each component of the climate system, many factors affect the climate of the Earth, such as for example, the atmospheric composition directly affect the amount of incoming solar radiation at different atmospheric layer as well as at land surface. Thus, to interpret the change in the Earth's climate, these factors must be introduced into the climate models. The more factors a climate model takes into account, the more complex it becomes and the more computing resources it requires. The processes, which occur on a time scale of seconds (waves) to billions of years (the formation of the Earth) or on the scale of centimetres (atmospheric turbulences) to thousands of kilometres (tropical cyclones), can be included in a simplified way or neglected depending on the particular goal. This is unavoidable when developing a climate model. In climate projects, at least the physical behaviour of the atmosphere, the ocean and the sea ice must be represented, which means

that the Atmospheric and Oceanic General Circulation Models (AGCMs and OGCMs) are the most important components of GCMs. The core of a GCM, an AGCM, simulates the atmospheric processes like the energy exchange process. The remaining parts of a climate system (ocean, sea ice, land surface processes, etc.) are coupled into AGCMs based on consistent assumptions (Sen and Hansen, 2003). The complements of the AGCMs and OGCMs are named as AOGCMs or CGCMs (e.g., the Hadley Centre Coupled Model version 3 (HadCM3) or CGCM3). In chapter 8 of IPCC AR4 (IPCC, 2007) a list of the twenty-three CGCMs that have been developed around the world is presented.

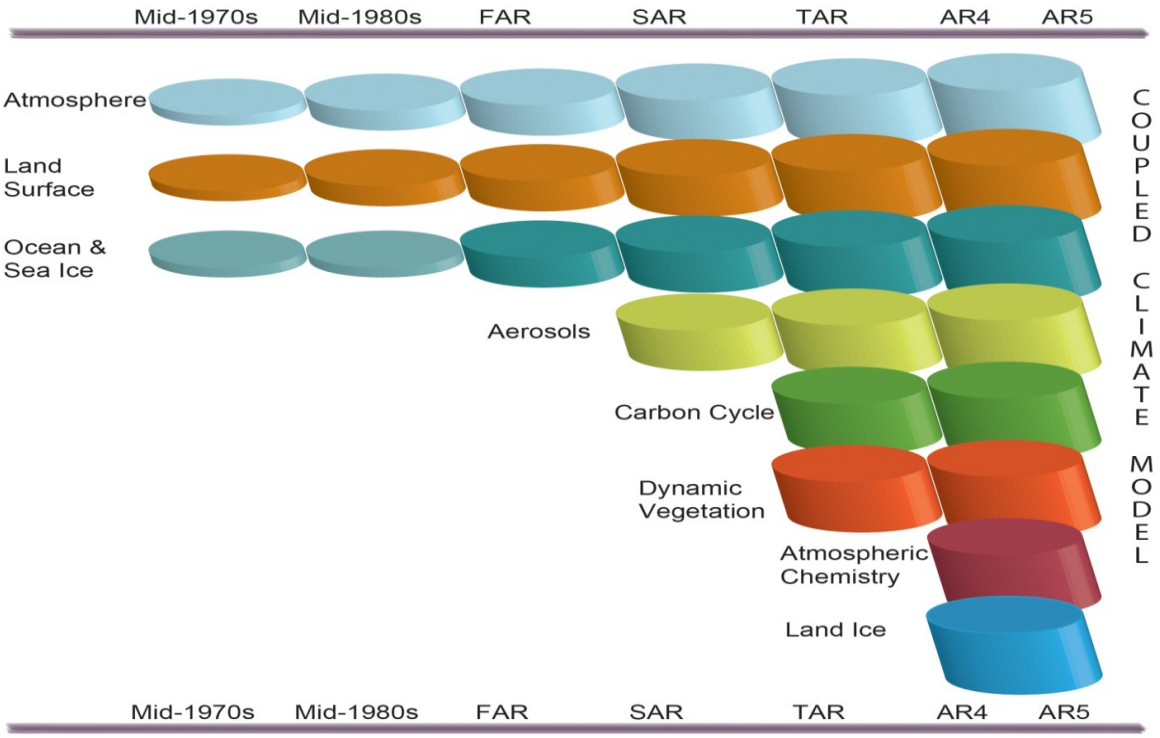

Figure 2.2: The development of climate models from the 1970s to the present. The horizontal axis stands for the time history of the climate models. The vertical axis stands for an addition of different climate components into comprehensive climate models (IPCC, 2013).

As presented in Figure 2.2, various types of GCMs include a variety of processes for modelling single aspects of the climate. To boost the accuracy of the simulations, modules for different components of the climate system are implemented to the climate models. This work is expected that the interactions and feedbacks between the climate components within the climate system will be fully interpreted. The development of GCMs started as atmospheric models and separate ocean models in the mid-1970s. Afterwards, more and more processes have been coupled together into a model. According to Goosse *et al*. (2010), Earth system models include a variety of components, such as dynamic vegetation, ice sheets and terrestrial and marine carbon cycles with the obligatory major components of atmosphere, ocean and sea ice. In other words, three-dimensional processes for all components of atmosphere, ocean, sea ice and land surface are encompassed into the Earth-system models, which has a coarse spatial resolution of hundreds of kilometres (IPCC, 2013). GCMs are forms of the highest model of the Earth system models that try to take all the important properties of the climate system at the highest affordable resolution into account as showed in the end of the

spectrum (see Figure 2.3). Currently, the grid resolutions of GCMs are typically of about 100 km to 200 km. At a simpler level, the Earth Models of Intermediate Complexity (EMICs), with a typical spatial resolution between several hundred to thousands of kilometres, are two- and three-dimensional models (IPCC, 2001). These models can allow to simulate the climate for long-term of tens of thousands of years because of more simplified physical parameter processes in comparison with GCMs (e.g., a zonally averaged atmosphere) (IPCC, 2001; Goosse *et al*., 2010). At the simplest level, the Energy Balance Models (EBMs) are considered as simple climate models in which the climate variables (e.g., temperature) over large regions and even the over whole Earth are averaged. In addition, many parameterization processes are not included, such as the land surface parameterization processes. Within these models, just two most governing physical processes are simulated as indicated by their name (i.e., global radiation balance and latitudinal energy transfer) (Stocker, 2011). So, the development of climate modelling can be improved by the further development of simple models (EMICs or EBMs) or the improvement of more complex models, GCMs, which include three-dimensional dynamics and all processes as detailed as possible.

Although some models can produce information about the behaviour of the climate system better than others do, no model can provide the best results for all cases. Results of a specific GCM may be suitable for a given region, but not for other regions. An ensemble of various model types is often the best approach to reproduce the behaviour of the climate system. This approach, however, depends on many factors. One of the most important factors is the available computing power. The sophisticated models require a large amount of computing resources. The spatio-temporal resolution, the degree of detail for natural processes and the length of the study period are the main factors that directly influence the demand for computing power. For instance, the simulation of one year can take several months depending on the spatio-temporal resolution. It is thus necessary to run climate models on the most powerful supercomputers.

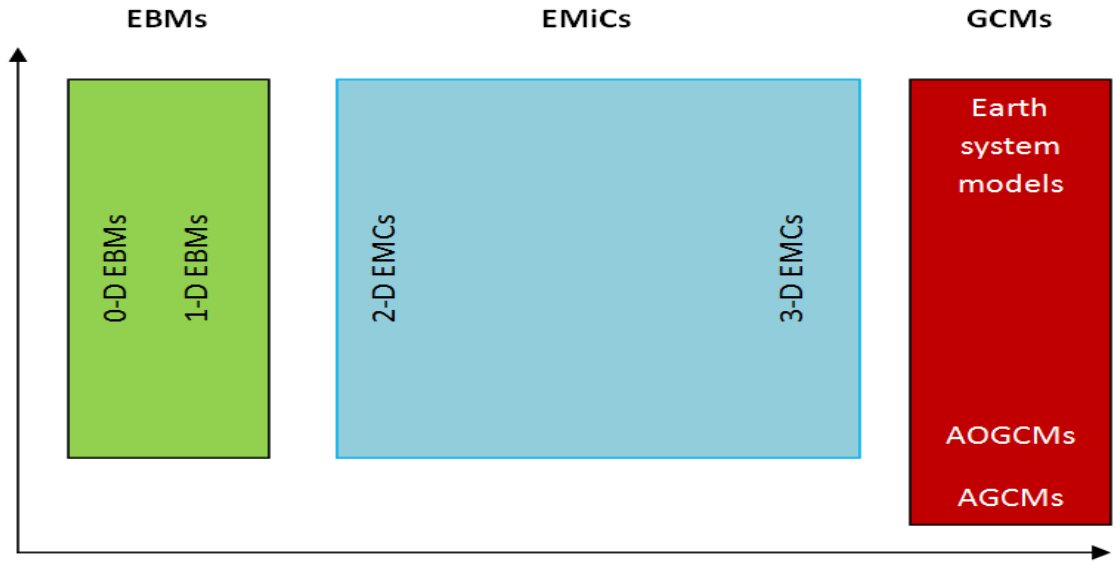

Figure 2.3: Development of climate models from zero- to three-dimensional models. The vertical axis refers to the number of interactive components of the climate system. The horizontal axis stands for details of the description and number of processes included (Goosse *et al*., 2010).

Although GCMs can simulate climate behaviour at global scales adequately, the numerical grid is still much too coarse to depict important small-scale processes (subgrid scale) such as turbulence processes in the atmospheric boundary layer or microphysical processes in clouds. To date, GCMs have been run at a coarse spatial resolution of typically ~500 km (IPCC, 1990), ~180 km (IPCC, 1996), ~250 km (IPCC, 2001), ~110 km (IPCC, 2007) or the most recent, ~100 km (IPCC, 2013). Using climate models, large-scale patterns of climate change can be assessed, but these models cannot be used for projections of the weather and climate patterns at regional or local scales (~10 km). This is especially important in climate regions that are dominated by complex topography, land use or different weather patterns such as Southeast Asia in general and Vietnam in particular. GCMs are not only limited by computing resources but also by the lack of understanding physical processes, such as oceanic deep convection. This is considered to be the main reason for insufficient representation of natural processes. Besides that, the uncertainty in models comes from parameterization schemes within GCMs that have to be built to institute subgrid-scale processes or overly complex processes such as cumulus convection and turbulence parameterizations. These parameterization schemes play a vital and necessary role in identifying model behaviours. They are the keys for understanding the behaviours of the climate system in the past, present and future. Additionally, the information on the strengths and weaknesses of global climate models can be found in the IPCC's reports and Murphy *et al*. (2009).

To date, the complexity and resolution of climate models are continuously improving. The models of chemical transport, ecosystems, ice sheets (Greenland and Antarctic) and carbon cycles are being coupled into the GCMs. These models are expected to run at a resolution finer than 20 km with the most precise parameterization schemes. This may allow a GCM to simulate the climate system in a much more realistic way.

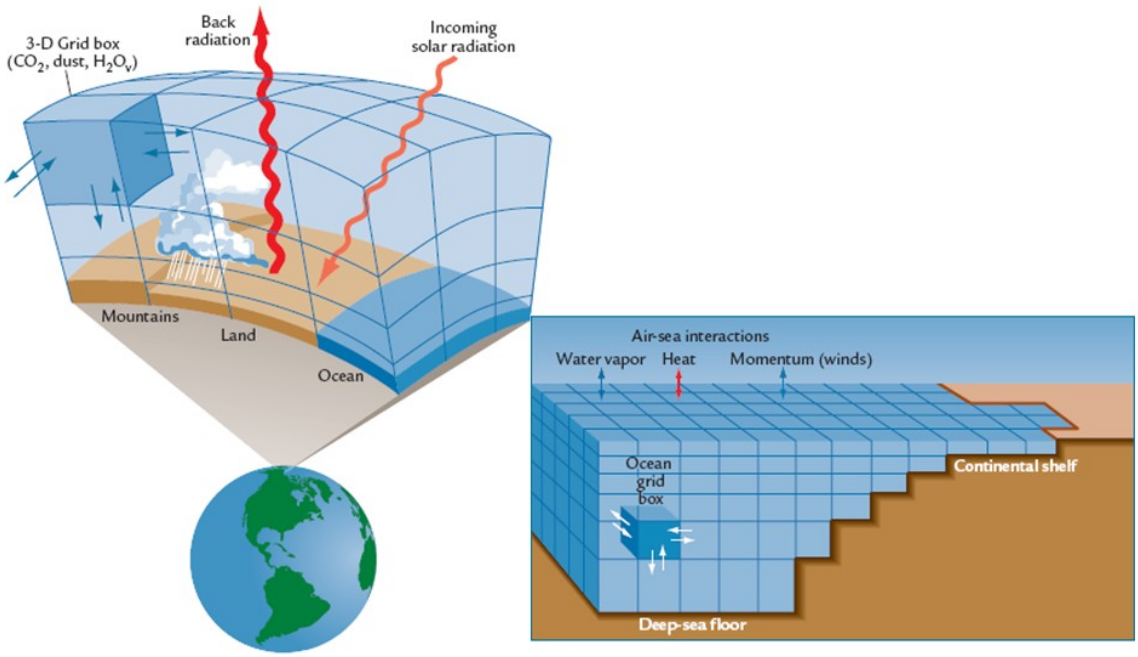

Figure 2.4: Representation of physical processes in the three-dimensional grid of AGCMs and OGCMs, represented by individual grid boxes (Ruddiman, 2007).

2.1.1.2 Regional climate models

As mentioned above, GCMs can provide useful information about climatic processes at large scales, but they cannot take into account local features like mountains or simulate small-scale atmospheric processes like cloud convection. These features significantly affect the local climate change. For that reasons, Regional Climate Models (RCMs), which have a higher resolution than GCMs, have been developed to nest in GCMs. A "nesting" technology is the connection between the regional model and a global model at different scales, while the regional model uses the output of the global model as boundary conditions. The aim is to provide more detailed information about climatic processes and possible changes in the climate system. A grid of higher resolution requires much more computing power and time, however; so it is usually configured to run for a limited area. The idea of the "nesting" strategy is originally derived from the numerical weather prediction (NWP) (Rummukainen, 2010; Warner, 2010). Phillips and Shukla (1973) showed the necessity of reducing a grid-point mesh to get a finer grid-point resolution in numerical weather prediction models. The reason of this is due to (1) the most important weather-producing phenomena occur on a scale small enough (e.g., hurricanes) and (2) these phenomena are not isolated from the large scale atmospheric variables (Phillips and Shukla, 1973). At present, two approaches for the "nesting" technology have been deploying (1) one-way nesting and (2) two-way nesting (TWN). It is noteworthy that in RCMs, solving the partial differential equations (e.g., conservation of energy or conservation of mass) requires lateral boundary conditions, which can be obtained from a global model or analyses of observations. Based on the one-way nesting technique, the application of RCMs to regional climate studies was first proposed by Dickinson *et al*. (1989). The initial and lateral boundary conditions (LBCs) for RCM simulation are provided from the output of GCMs. In the one-way nest, there is no feedback to the GCMs from the RCM's output; all information that is exchanged between the parent (GCM) and the son (RCM) domains is strictly downscaled.

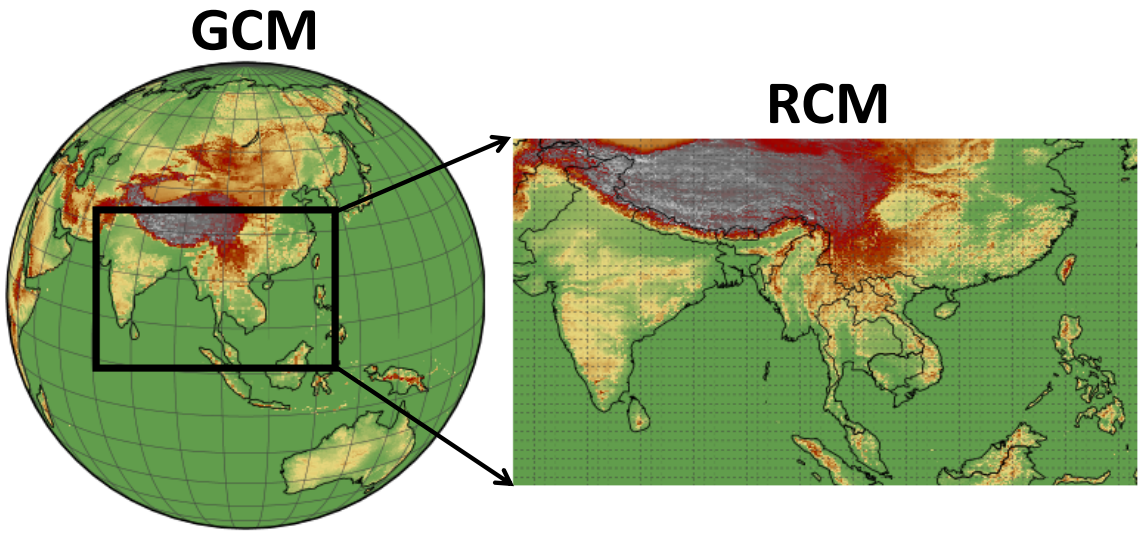

Figure 2.5: The nesting of a regional climate model within a global climate model. The right hand figure shows the regional domain over Asia with the horizontal grid (dot lines) (adapted from Giorgi, 2006).

"*The main advantage of RCM nesting is that it is a physical based downscaling approach, which implies on the one hand that all climate variables are calculated in a physical consistent way and on the other hand that RCMs are general tools applicable for a wide variety of studies.*"

Giorgi (2006)

Based on the "nesting" technique, regional climate studies in the United States and Europe were conducted (Giorgi, 1990; Giorgi *et al*., 1990; Jones *et al*., 1995). Giorgi (1990) applied a limited-area model (LAM), which was nested in a GCM to simulate the climate in January over the western United States, which has a complex topography as shown in Figure 2.6b (Giorgi, 1990). The initial and LBCs of LAM at 60 x 60 km were provided from a GCM at a 7.5° × 4.5° (R15) and 2.89° × 2.89° (T42) resolution. The horizontal grid resolution of R15 and T42 is about 800 and 300 km, respectively. The simulation results for climate parameters (e.g., zonal wind, temperature or cloudiness) in January performed at R15 and T42 resolutions were more realistic than the large scale observations. Giorgi *et al*. (1990) used a LAM nested in a GCM to simulate climate parameters in January for a 10-year period over Europe as shown in Figure 2.6a. The large-scale meteorological fields from a GCM at a 7.5° × 4.5° (R15) grid resolution were used to force a LAM (Mesoscale Model version 4, MM4). The results of a MM4 nested in a GCM illustrated that the small-scale meteorological fields at 70 x 70 km grid resolution, such as surface air temperature, precipitation, snow cover, and cloudiness, were much more realistic than that of the forcing GCM alone. Until 1996, many climate simulations were performed using a nested RCM in a GCM for at least one month as described in McGregor (1997).

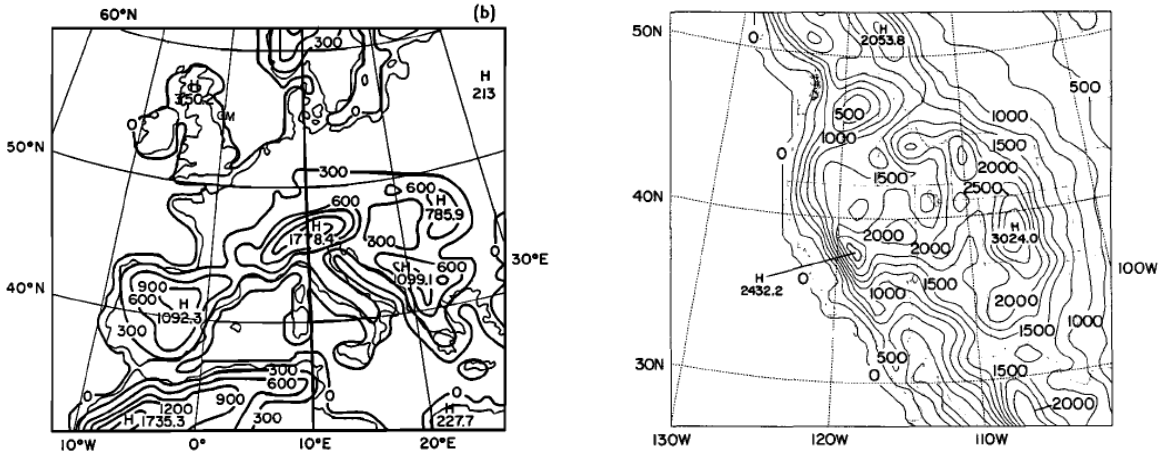

a) MM4 model topography over Europe (70 km x 70 km). Units are meters and the contour interval is 300 m (Giorgi *et al*., 1990)

b) MM4 model topography over US (60 km x 60 km). Units are meters and the contour interval is 250 m (Giorgi, 1990)

Figure 2.6: Domains with the one-way nesting MM4 in a GCM.

Rojas (2006) implemented a multiple nesting using the MM5 model. The initial and lateral boundary conditions to run this model were provided by the National Centre for Atmospheric Research (USA)/ National Centre for Environmental Prediction (NCEP-NCAR) for Southern South America (SSA) at a 6-hourly interval (Kalnay *et al*., 1996). The model resolution were configured at a grid size of 135 km

(domain 1), 45 km (domain 2) and 15 km (domain 3) (see Figure 2.7). The purpose of this work was to get the feedbacks from the smaller domain into the larger domain. The periods of simulation were used to run two five-month-long simulations (May-September 1997 and 1998) (Rojas, 2006). In comparison with the station precipitation and temperature data, the results showed a negative temperature bias and a positive precipitation bias of 2°C to 5°C and 40% to 80% respectively. Additionally, the model results at the highest resolution domain showed that there was a relationship between these biases and terrain and station elevation factors. Specifically, the smallest precipitation bias was at low-elevation stations and the largest positive bias was at high-elevation stations. The simulation results indicated that the observed meteorological fields (precipitation and temperature) were well simulated at the highest resolution domain after discarding precipitation above 1000 m. The study suggested that the large precipitation bias at high altitude needs to be carefully considered in the climate impact studies when using RCMs. In addition to this, horizontal grid of about 30km is sufficient to capture the important climatic processes at regional scale.

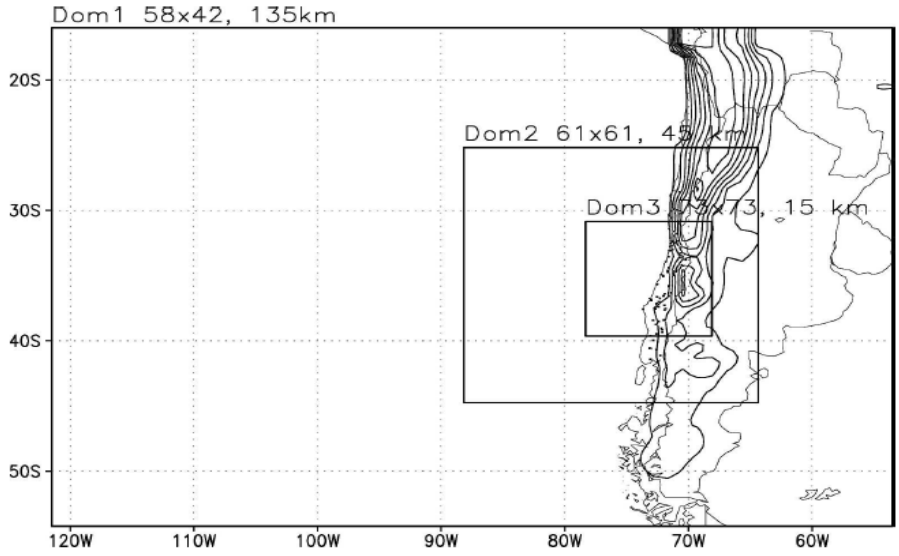

Figure 2.7: The MM5 model configuration: The domains and resolutions of three nested models. The dots represent the location of available station data (Rojas, 2006).

Using the Canadian Regional Climate Model (CRCM), climate reproductions and climate change projections are analysed for several decades of the present and future climate over North America. The simulation results from the embedded CRCM in the coupled Canadian General Circulation Model version 2 are satisfactory. Specially, they indicate a smaller positive bias for surface air temperature in winter in comparison with the GCM-driven simulation over northern regions (Plummer *et al*., 2006).

To be distinguished the one-way nesting, the two-way nesting technique refers to a substitution the coarse grids by the finer grids at the integration area where lie inside the fine grid. In this approach, the meteorological field information can be exchanged between parent and son grids in both directions (i.e., parent to son for the fine grid lateral boundary conditions and son to parent during the feedback). In other words, the exchange of information between the parent and the nest is considered to be bidirectional in the two-way nesting. Recently, this technique is implemented into

the Regional model (REMO) developed by the Max Planck Institute (MPI) in 1993 (Lorenz and Jacob, 2005). According to Lorenz and Jacob (2005), the nesting system is simultaneously run on both, the GCM and RCM, within a given system. During the simulation, a feedback is transformed to the GCM from the RCM at every GCM time step until the completion of the final simulation process (see Figure 2.8). The GCM provides the lateral boundary conditions (LBCs) for an RCM. Afterwards it also receives information on the effect of local interactions on a large scale from the RCM at every time step. The obtained results show a positive quality of RCM procedures without an increase in horizontal resolution. Alternatively, more than one son domain can be embedded in the parent domain as well.

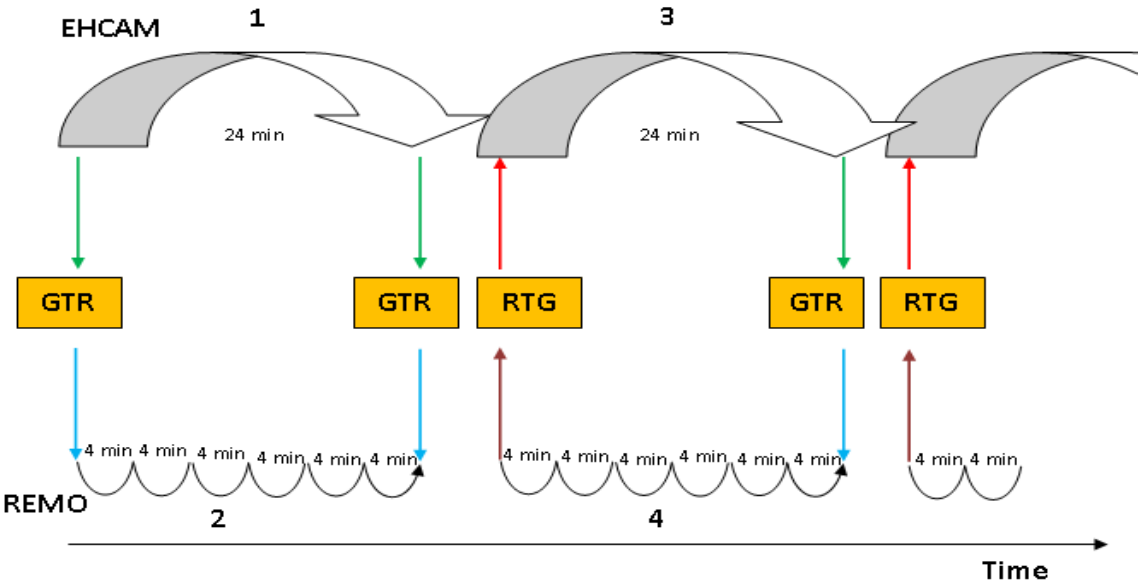

Figure 2.8: The two-way nested system; GTR: global to regional interpolation; RTG: regional to global aggregation (Lorenz and Jacob, 2005).

Presently, RCMs (e.g., RegCM, MM5, CCAM, REMO, CWRF, CRCM, HRCM, etc.) are able to reproduce well the regional and local climate in the past for most regions of the world. These results illustrate that RCMs play an important role in climate studies at regional and local scales. The horizontal resolution of RCMs amounts to 50 km or less. Aside from the TWN advantages RCMs in GCMs, it does have drawbacks. The first drawback is that errors in the meteorological fields of the GCMs may inflate inside the nested domain and become principal errors. A typical example for this is provided in Perkey and Maddox (1985), who show that a convective precipitation system can influence its large scale meteorological setting, which can then feedback to the mesoscale. The second point is that the RCMs can provide feedback to GCMs, but they also require the computing cost and can change the quality of the GCM's output. Moreover, using a two-way nesting system, the quality of GCM output could be modified.

To date, there are few experiments on the effectiveness of the two-way nesting approach. The main reason is seemingly computing resource cost. On the other hand, in the one-way nesting, large scale products are completed first, and available to be used by regional climate models which then compute small scale meteorological fields. One-way nesting is mostly used and the application of the two-way nesting technology for regional climate studies is an open question for the further projects.

An important consideration is that the performance of regional climate models also depends on lots of factors (i.e., domain choice, physical parameterization of subgrid scale processes, horizontal and vertical resolution, lateral boundary or buffer zone) as mentioned in the chapter 8 of the IPCC AR4 (IPCC, 2007), Rummukainen (2010), etc. It can be found in section 6.1 for further information on RegCM model performance as a typical example.

For the climate model uncertainty, there are several different classifications: i) forcing, ii) microscopic initial condition, iii) macroscopic initial condition and iv) model inadequacy (Stainforth *et al*., 2007a,b) or i) emission scenarios, ii) climate sensitivity, iii) natural variability, iv) climate feedbacks and 'surprises' and v) external forcing (Foley, 2010). An analysis focus on model uncertainties can be also found in the IPCC's reports (e.g, in the chapter 9 of the IPCC AR4). However, it is of great importance to state that global and regional climate models are considerably successful in providing the understanding of global climate changes when they are used for climate simulations and projections in the IPCC's reports.

2.1.2 Statistical downscaling

Recently, statistical downscaling methods or empirical downscaling methods have been drawn interest from scientists. They are useful tools to derive climate information from GCMs for the catchment and station-site scale. The principle of this method is to create a statistical link between the large scale and the local scale. In other words, the statistical downscaling method is the calculation of sub-grid scale climate information (predictands[8]) that are considered to be functions of large-scale predictors[9]

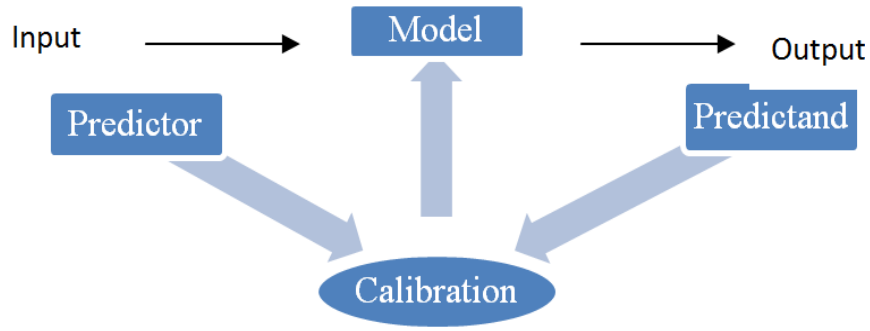

Figure 2.9: Scheme of the relationship between predictor and predictand in statistical downscaling (Benestad *et al*., 2007).

The calibration of statistical downscaling models requires both predictors and predictands. The model calculates the predictand (output) based the predictor (input), as shown in Figure 2.9. In theory, large-scale climate conditions may include climatic noise and local features. For instance, changes in solar radiation reaching the Earth or in large-scale circulations far-reaching affect the local

[8] The predictand is the output data of the statistical downscaling model, typically the small-scale variable representing temperature or rainfall at a weather/climate station.

[9] The predictor is the input data used in statistical models, typically a large-scale variable describing the circulation regime over a region

climate. Thus, there may exist an empirical relationship between the large-scale predictor and the local-scale predictand. Statistical downscaling of GCM data is carried out in two steps: First, the statistical relationship between large-scale predictors and local-scale predictands (e.g., precipitation and temperature) is derived from observed data. Afterwards, these relationships are used to reproduce or project local climatic parameters from a GCM. For the downscaling of climate variables, Wilby *et al*. (1998) assumed that the empirical relationships are stable at spatio-temporal scales. Three implicit assumptions, especially for climate change studies, are: (i) the predictors simulated by the GCMs are realistic, (ii) the statistical relationship between predictors and predictands is valid under future climatic conditions and (iii) the predictors fully typify the features of climate change (Hewitson and Crane, 1996). They are the key assumptions for the application of statistical downscaling methods (Wilby *et al*., 2004). According to Wilby *et al*. (2004), the useful guidelines for statistical downscaling are briefly presented in the following:

- Selection of a statistical downscaling method: This depends on the nature of the predictand. Normal distributed data (e.g., monthly mean temperature) do not require a complicated model, but a transfer function may be required for the heterogeneous variables in space and time, such as daily precipitation. A complex model requires a large amount of observational data.
- Selection of predictors: Meteorological fields that represent best the atmospheric circulation and climate change phenomena should be selected as predictors. The selection of predictors alters from region to region as mentioned in Anandhi *et al*. (2009).
- Performance of extreme events: Most statistical downscaling models have not been designed to simulate extreme events in a realistic way. In many cases, therefore, the performance of statistical downscaling models is only satisfactory for mean values.
- Nature domain under consideration (tropical regions): A strong variation of the relationship between predictors and predictands may occur within the annual cycle in tropical regions due to the strong ocean and atmosphere interactions.
- Feedbacks: The feedback processes of vegetation may come to play an important role in global climate change under a weak synoptic forcing. Additionally, anthropogenic forcing can potentially affect the fitting between the statistical models and the observational data.
- Application of statistical downscaling models: Statistical downscaling methods can be applied when the transfer function are stable over time (indicating a strong relationship between predictors and predictands). Before running any statistical downscaling model, it is necessary to handle the missing data and errors in observational data.

The advantages and disadvantages of statistical downscaling are mentioned for statistical downscaling in Wilby *et al*. (2004). The most important advantage of statistical downscaling is the low demand for computing resources and therefore a large “ensemble” allowance. The “ensemble” results are considered to be more reliable than the results of a single model. An overview of the advantages and disadvantages of statistical and dynamical downscaling methods is shown in Table 2.1.

Table 2.1: Advantages and disadvantages of statistical and dynamical downscaling methods.

	Advantages	Disadvantages
Statistical methods	- Low-cost and computationally efficient. - Provide point-scale climate information from global scale output. - Performance of multiple GCMs for ensembles and different emissions scenarios without time consuming. - Easily transferable to other regions.	- Require long-term and high-quality data for calibration. - Depend on choice of domain size, climate region, predictors and empirical transfer scheme. - Potential non-stationarity of the predictor and predictand relationship. - Depend on GCM boundary forcing. - Do not feedback into the host GCM.
Dynamical methods	- Dynamical physical processes simulation of meteorological fields at high resolution. - Simulation of a large, internally consistent set of atmospheric and surface variables.	- Require more computing resources than statistical downscaling methods. - Limited number of GCMs due to the required time. - Depend on choice of domain size, cloud/convection scheme, initial and boundary conditions.

Klein (1948) first carried out a statistical study about the relationship between 5-day precipitation and numerous features of the planetary wave train at 700 mb level over the Tennessee Valley during winter. The history of statistical downscaling is briefly described in Klein and Bloom (1987). In the early 1980s, statistical downscaling is pertained to as “Statistical Problem of climate inversion”. Kim *et al*. (1984) estimated the local distribution of climatic variables (i.e., monthly-averaged surface temperature and monthly total precipitation) for Oregon of USA when only a global scale value was given at a 500 x 500 km grid box. This value was considered as a sort of climate inversion problem (Kim *et al*., 1984). A dozen weather stations for a 30-year period were used over this grid box. The results showed that a diagnostic relation between large scale anomalies and local scale variables. Since the early 1970s, however, model output statistic (MOS) (Glahn and Lowry, 1972) and perfect prognosis (PP) (Klein *et al*., 1959) technologies have been applied in numerical weather prediction. Since then, many studies are conducted to investigate the link between large-scale and local-scale variables (Hewitson and Crane, 1996; Wilby and Wigley, 1997; Xu, 1999; Zorita and Von Storch, 1999; Giorgi *et al*., 2001; Fowler *et al*., 2007). In most cases, the linear methods-canonical correlation analysis (CCA) (Busuioc *et al*., 2008), multiple linear regression analysis (MLR) (Sachindra *et al*., 2013), singular value decomposition (SVD) (Yu *et al*., 2006), etc.-are applied to generate monthly and seasonal values. More details on CCA and SVD can be found in Bretherton *et al*., (1992). Several different methods (e.g. artificial neural networks (ANNs) (Harpham and Wilby, 2005), the analog method (Zorita and Von Storch, 1999) and self-organizing maps (SOM) (Yin, 2011), etc.) are developed for reproducing the relationship between large-scale and small-scale variables. A list of

different statistical downscaling methods applied to three predictands (i.e., temperature, precipitation and humidity) over the world can be found in Fowler *et al*. (2007). Statistical downscaling methods can be classified into three categories: weather classification schemes, regression models and weather generators (Wilby *et al*., 2004). Table 2.2 shows the advantages and disadvantages of different statistical downscaling methods.

Table 2.2: Advantages and disadvantages of different statistical downscaling methods (adapted from Wilby *et al*., 2004).

Methods	Advantages	Disadvantages	Main reference(s)
Regression methods	- Relatively easy to calibrate and fast to implement - Employ full range of available predictor variables	- Require normally distributed data - Poor representation of extreme events	Delta method (Hay *et al*., 2000) SVD (Yu *et al*., 2006) CCA (Busuioc *et al*., 2008) MLR (Sachindra *et al*., 2013)
Weather classification	- Yields physically interpretable between predictors and predictands variables - Can be applied to both normally and not normally distributed data	- Requires additional step of weather type classification - Requires large amount of data and computational resources - Inability to downscale GCM data that are outside the range of the historical data	Cluster analysis (Schoof and Pryor, 2001) Analog method (Zorita and Von Storch, 1999) ANN (Harpham and Wilby, 2005) SOM (Yin, 2011)
Weather generator	- Ability to simulate length of wet and dry periods -Provide a wide range of uncertainty analysis - Spatial interpolation to produce the weather data at new sites.	- Sensitive to missing or erroneous data in the calibration set - Only some weathers generators can check the coherency between multiple variables - Requires generation of multiple time series and statistical post-processing of result.s	Nonhomogeneous Hidden Markov Model (NHMM) (Hughes *et al*., 1997) LARS-WG (Semenov *et al*., 2002) Semenow *et al*., 1998

An alternative categorization for statistical downscaling is suggested by Rummukainen (1997) and later adapted by Maraun *et al*. (2010) who divide statistical downscaling into perfect prognosis (PP), model output statistics (MOS) and weather generators (WGs). In general, the PP comprises a base of regression and weather type. In this approach, the relationship between predictors and predictands is identified by using observed data. Contrary to this, MOS uses simulated predictors and observed predictands. According to this classification, statistical downscaling approaches are displayed in Figure 2.10. Reviews on statistical downscaling methods can be found in Wilby and Wigley (1997), Xu

(1999), Giorgi *et al*. (2001), Wilby *et al*. (2004), Benestad *et al*. (2007), Fowler *et al*. (2007) and Maraun *et al*. (2010).

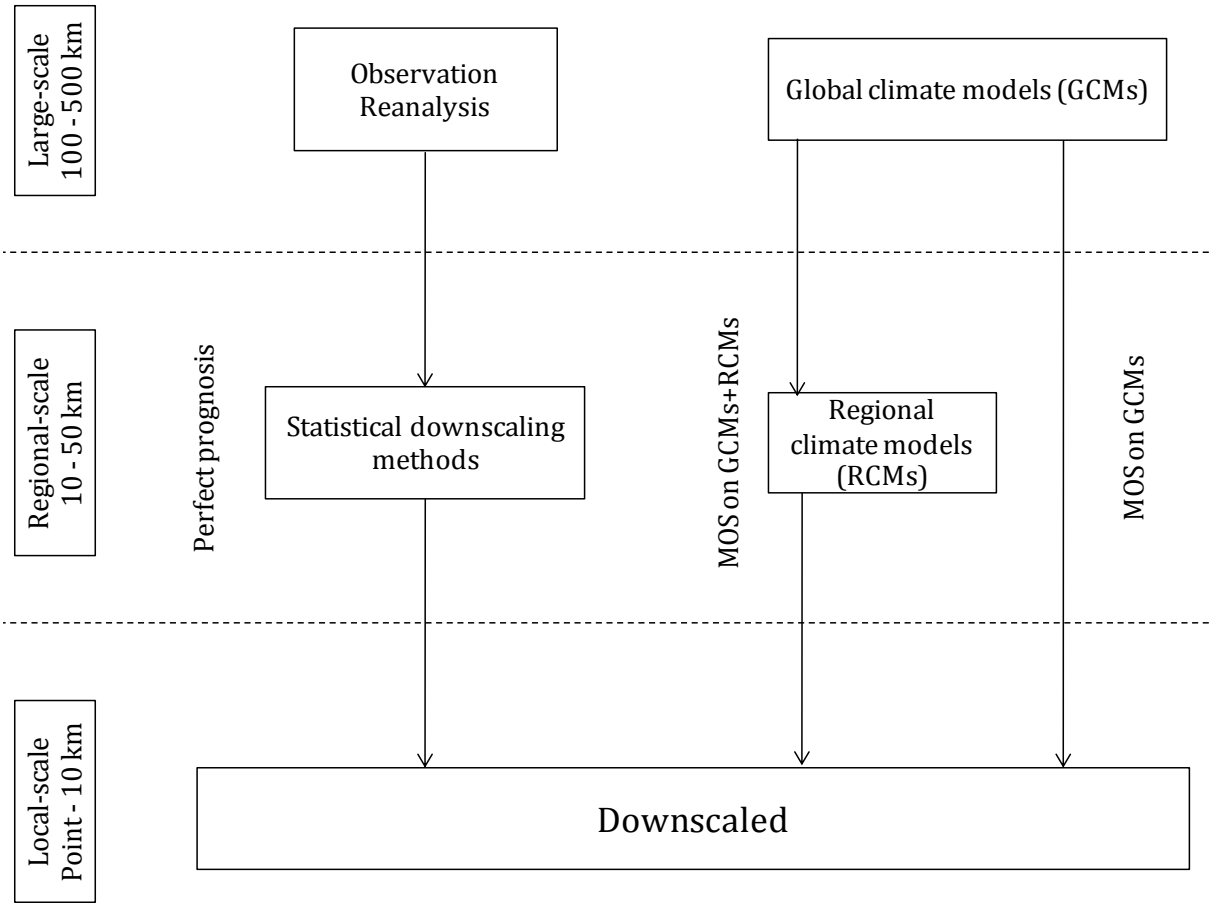

Figure 2.10: Approaches of statistical downscaling (adapted from Maraun *et al.*, 2010).

MOS can be applied directly to GCMs or RCMs. First, a dynamical downscaling method (DDM) is used to derive regional climate information from GCMs. The simulated results are then statistically downscaled to sub-grid scale information. Therefore, MOS can be considered as a two-step process.

So far, statistical downscaling is frequently applied when climate scenarios are required for individual locations at sub-grid scales due to the low computational efforts. Statistical downscaling offers a chance to run at multiple time slices due to the low demand for computational resources compared to dynamical downscaling. The low computational demand is because the statistical downscaling is only dependent on the transfer function, which can be developed using ANN (Harpham and Wilby, 2005), CCA (Busuioc *et al*., 2008) or other methods. Climate data can be downscaled at any time step (annual, seasonal, monthly, and daily, etc.). Historically, however, most of these functions are established at monthly, seasonal or annual temporal resolution for both the values of the predictors and the predictands rather than at daily or sub-daily time steps. What is more, the linear methods require normally distributed values of the predictors and the predictands. The weather generators methods can generate daily values, but they are sensitive to missing or erroneous data in the calibration set. The weather classification methods require large amounts of daily data to be analysed. The output of GCMs shows systematic error at the daily resolution. Thus, the development

of downscaling at a daily time step is a big challenge for most recent studies. It is also considered to be the key when setting up transfer functions for state-of-the-art downscaling models.

Enke and Spekat (1997) used the methods “classification” and “regression” to downscale global climate model outputs for seven climate variables (predictands) (e.g., daily maximum, minimum, mean temperature and sum of precipitation) at 52 German climate stations of the Deutsche Wetterdienst (DWD). In their study, the maximum number of predictors was limited to four for each predictand. Seemingly, the reason for this is the missing information or overfitting (see more discussion in Maraun *et al*., 2010).

Wilby *et al*. (1999) downscaled the daily climate data from the HadCM2 output for the Animas River sub-basin in the San Juan River basin, Colorado, USA using a statistical downscaling method. In the study, the three predictor variables (i.e., daily specific humidity, mean sea level pressure and 500 hPa geopotential height) were required to establish a stepwise regression model for each climatological season. The daily data of area-averaged three stations was used. Four predictands (wet day occurrence, wet day amounts, maximum and minimum temperatures) were selected to calibrate the model for the wet years during 1987 to 1995. The results illustrated that more than 80% of the variance in daily temperature and 30-45% of the variance in wet day amounts were explained by the stepwise regression model. In addition, downscaled information about wet days was closer to reality than it is for dry days and a better-performing model was obtained for spring and autumn.

Huth (1999) used stepwise regression, full regression, pointwise regression, singular value decomposition (SVD) and canonical correlation analysis (CCA) prefiltered the climate variables by principal component analysis (PCA) to downscale daily mean temperature for 39 stations in central Europe. The results pointed out that the pointwise regression method performed better than others do, followed by the other regressions and CCA.

Schoof and Pryor (2001) applied two different downscaling models, ANN and regression, to downscale four climate variables - maximum and minimum daily temperature, daily and monthly sum of precipitation - for Indianapolis, Indiana, USA. A 18-year time period was investigated. It was discovered that daily maximum temperature was well downscaled by the ANN approach. However, a poor simulation for daily precipitation was provided by both methods.

In general, most studies show that using statistical regression models, downscaled daily temperature is acceptable. It is recommended that before applying these models, the choice of predictors should be carefully investigated for each study region. For the daily precipitation predictand, it is big challenge to downscale to a small scale from a large-scale due to the increased unpredictability of precipitation at the station scale. Moreover, there is a lack of studies for Asia in general and the Southeast Asian region in particular as described in Fowler *et al*. (2007).

2.1.3 State of the art bias correction

Precipitation data with a daily or sub-daily temporal resolution is required for the analysis of climate change impacts on economic sectors, especially in agriculture and natural resources. Precipitation is the most important input variable for hydrological models, but an accurate quantification at the sub-

monthly temporal scale is challenging for meteorologists and hydrologists. This is especially the case for tropical regions, where the spatial distribution of surface temperature and air pressure is fairly uniform and the air mass is quite homogeneous (Krishnamurti *et al*., 2013). Additionally, the effects of local and mesoscale physical processes on terrestrial characteristics are more dominant than synoptic influences. Consequently, precipitation can change quickly due to convection processes. The simulation results of climate models show systematic biases caused by the limitation of spatial resolution, parameterization schemes, insufficient representation of thermodynamic processes, simplified physics and a lack of knowledge about climate system processes. In order to get the realistic climate information at high temporal resolution, climate model output needs to be post-processed by applying "bias correction". To date, studies on "bias correction" methods are conducted aiming to minimize these biases (Ines and Hansen, 2006; Piani *et al*., 2010a; Piani *et al*., 2010b; Dosio *et al*., 2012; Lafon *et al*., 2013). Among these approaches are statistical transformations that adjust the simulated historical data to observational data. Subsequently, these transformations are applied to adjust climate model outputs for future periods. The main advantages and disadvantages of applying bias correction to simulated climate data is described the following:

Advantages:

- It is relatively easy to compare the simulated and observed historical data and a transition into the future.
- The increase in expected variability for high resolution data can be calculated. Furthermore, as simulations for the future are corrected the same way like those for the present, they could directly be compared to the current climate state.
- It is possible to correct the simulated data in a way to get more detailed climate information. This helps to understand the impacts of climate change on natural sectors at small-scale that the change in variability of the data is not captured by a simple interpolation of the GCM data.

Disadvantages:

- An assumption made when applying any kind of bias correction is, that the bias in climate models is stable over time.
- The physical plausibility of the data could be demolished, even when adding the mean deviation from the observed data to the model output. For example, temperature might fall below zero degrees Celsius, whilst rainfall is not changed from liquid to solid state after the application of bias correction.
- The quality of the corrected simulation data strongly depends on the quality of the observational data and the output of the regional climate model.

Wood *et al*. (2004) evaluated the "bias correction and spatial disaggregation" method which is one of evaluated approaches for downscaling climate model outputs for a 20-year time period of climate simulations of the NCAR-DOE Parallel Climate Model (PCM) for past and near future, respectively. The main emphasis is to assess the ability of the different methods to adequately simulate climate variables used as input for hydrological models. The results showed a sufficient reproduction of the

climate variables from PCM and RCM outputs. The study stressed that PCM or RCM outputs are not suitable for the purpose of hydrological simulations without a bias correction step. Additionally, a different sensitivity of hydrological results derived from RCM (at 0.5 degree spatial resolution) and PCM (at T42 spatial resolution) to climate change is concluded. This refers a dependence of "bias correction" on a specific RCM model. In later studies, bias correction is directly applied to GCM outputs (Ines and Hansen, 2006); Piani *et al*., 2010a and Piani *et al*., 2010b).

Piani *et al*. (2010a) developed and applied a statistical bias correction technique to correct daily precipitation data for Europe using the output from the ECHAM5 global climate model and the EU project WATCH[10] (Harding and Warnaars, 2011). The original idea of this method is to apply a fitted histogram equalization function (a transfer function) to adjust the distribution of simulated data to the one of observed data (see Figure 2.11).

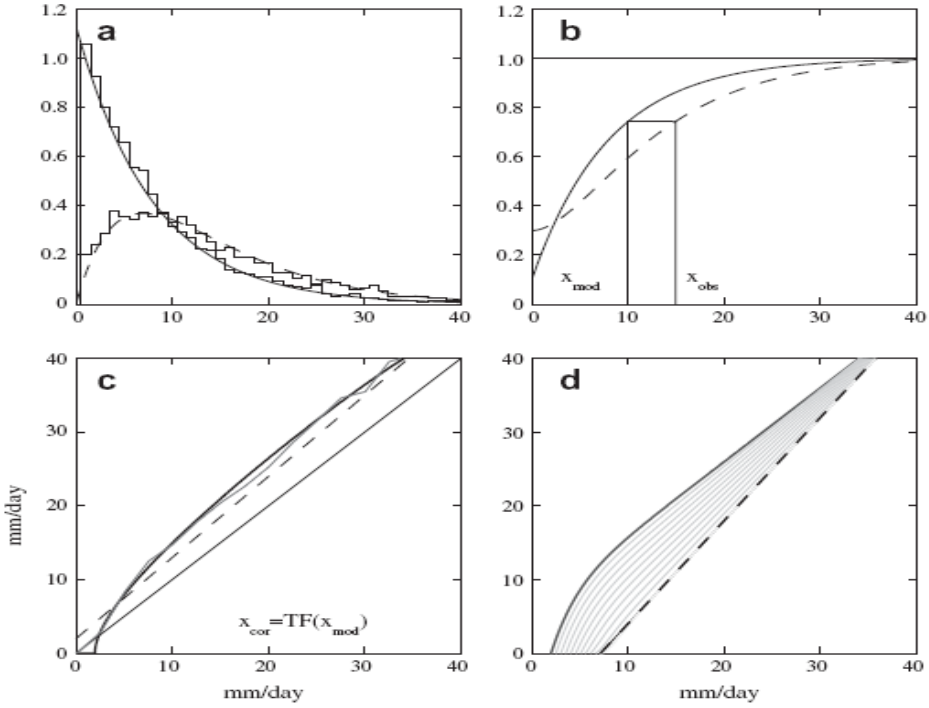

Figure 2.11: Representation of a transfer function method. (a) the simulated and observed daily precipitation histogram (continuous and dashed line respectively) fitted with gamma distributions. (b) CDFs obtained from the fitted PDFs in panel. (c) Transfer function derived from CDFs (continuous thick line) superimposed on "perfect" transfer function derived by re-sorting and plotting precipitation values directly (continues thin line). The linear fit to the "perfect" transfer function (dashed line) is shown. (d) Two examples of transfer functions: linear (dashed) and exponential with asymptote (continuous) along with relative transitional functions (copyright by Piani *et al*., 2010a).

The results indicated an effective improvement in some regions for both the mean and variance during a 10-year study period (1960-1969) (Piani *et al*., 2010a).

[10] WATer and global CHange

Although the bias correction approaches are a controversial subject in recent publications (Maraun, 2013; White and Toumi, 2013; Ehret *et al*., 2012, Teng *et al*., 2015), they are useful tools in water resources modelling (Piani *et al*., 2010a; Wood *et al*., 2004; Ines and Hansen, 2006). Before applying bias correction, it is strongly recommended to validate the method for the specific region, the climate model and the spatio-temporal resolution.

2.2 Evaluation of downscaling technologies

"Verification and validation of numerical models of natural systems is impossible."

Oreskes *et al*. (1994)

Although sensitive experiments are carefully investigated, there is no warrant for a passable computing model. The sources of uncertainty for a downscaling technology are the initial hypotheses, selection of parameters, etc. As mentioned in section 2.1, the ability of climate models to reproduce atmospheric processes varies from region to region. This is of particular importance when meteorological fields are simulated at local scale in this work. Therefore, it is important to assess the model performance for the region of interest. Consequently, the performance of RCMs is analysed and improved. Moreover, the quality of different climate models is compared. In other words, results of a climate model need to be carried out in comparison to observation data in order to define the stability, instability or significant difference of reproduction data. However, it is challenging to do this (Goose *et al.*, 2010). According to Goosse *et al.* (2010), the validation and verification processes of a climate model are depicted as shown in Figure 2.12. "Validation" stands for an establishment of truth, whilst "verification" stands for an establishment of legitimacy.

Many methods are carried out in weather and climate studies for the purpose of the evaluation of regional weather and climate models. Table 2.3 lists some major evaluation methods.

Table 2.3: Methods for the evaluation of numerical prediction model results.

Methods	Major reference(s)
Standard verification methods	Stanski *et al*. (1989)
Methods for dichotomous (yes/no) forecasts	Woodcock (1976), Stephenson (2000)
Methods for multi-category forecasts	Murphy and Winkler (1987), Murphy *et al*. (1989), Brooks and Doswell III (1996), Jolliffe and Stephenson (2012)
Methods for forecasts of continuous variables	Stanski *et al*. (1989), Jolliffe and Stephenson (2012)
Methods for probabilistic forecasts	Jolliffe and Stephenson (2012)
Field verification methods	Keil and Craig (2009)
Methods for probabilistic forecasts, including ensemble prediction systems	Wilson *et al*. (1999)

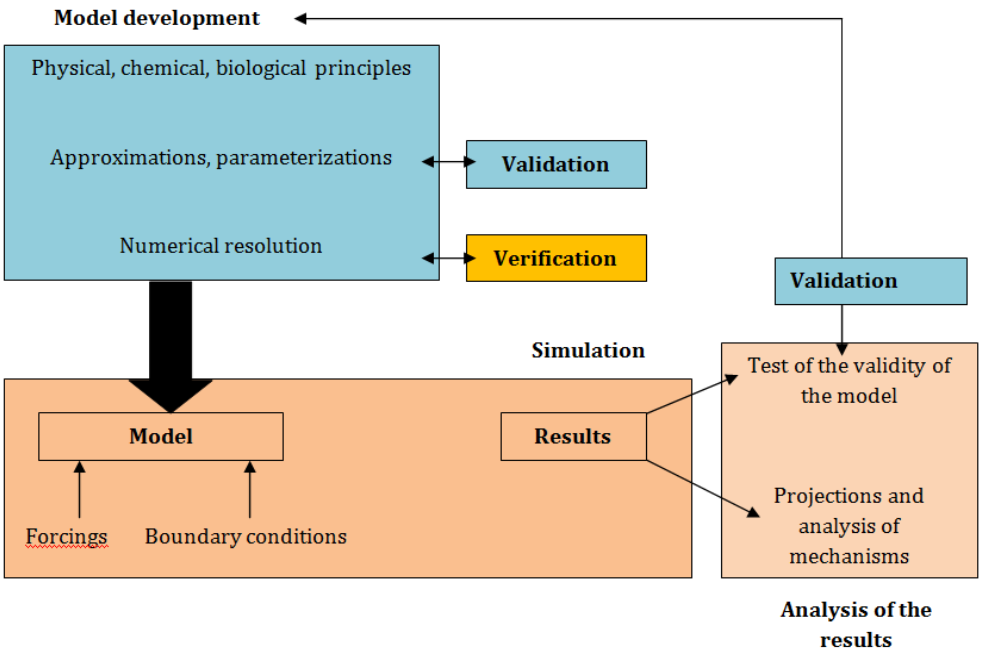

Figure 2.12: The validation and verification processes for a climate model (Goosse *et al.*, 2010).

In the whole work, the evaluation is carried out at the catchment scale using observed station-based data. The statistical evaluation indices standard deviation (SD), root mean square error (RMSE), bias and correlation coefficient shown in Table 2.4 are used to evaluate the performance of the climate model.

Table 2.4: Statistical evaluation indices.

Index	Formula	Range	Significance
SD	$SD = \sqrt{\frac{1}{N}\sum_{i=1}^{N}(F_i - \bar{F})^2}$	$0 < SD < \infty$ Perfect score: 0	Refer to the average forecast error.
RMSE	$RMSE = \sqrt{\frac{1}{N}\sum_{i=1}^{N}(F_i - O_i)^2}$	$0 \leq RMSE < \infty$ Perfect score: 0	Refer to the average magnitude of the forecast errors
Bias	$Bias = \frac{1}{N}\sum_{i=1}^{N}(F_i - O_i)$	$-\infty < Bias < \infty$ Perfect score: 0	Refer to the average forecast magnitude compared to the average observed magnitude.
Correlation coefficient	$r = \frac{\sum_1^N (F_i - \bar{F})(O_i - \bar{O})}{\sqrt{\sum_{i=1}^N (F_i - \bar{F})^2}\sqrt{\sum_{i=1}^N (O_i - \bar{O})^2}}$	$-1 \leq r \leq 1$ Perfect score: 1	Refer to the correlation of simulated and observed values

2.3 Hydrological models

2.3.1 Hydrological model classification

Hydrological models can be variously categorized. One of the classification methods introduced by Chow *et al*. (1988) is indicated in Figure 2.12. According to Chow *et al.* (1998), two types of models are widely classified: *physical* and *abstract* models. *Physical* models represent the real system with similar properties but on a reduced scale which is much easier to work with. *Abstract* models represent the system in mathematical form; the system operation links input and output variables with a set of equations. In most hydrological studies, a deterministic model is used. This kind of model can be further categorized as lumped, distributed or semi-distributed:

- Lumped models: These models assume homogenous conditions for the whole catchment, which means that model parameters do not vary spatially. Therefore, the hydrological processes are only evaluated at the outlet without explicitly accounting for the processes of individual sub-basins. This is considered to be the disadvantage of these models. An advantage of these models is their simplicity, what means that they do not require a powerful computing. Some examples of lumped models are SCS-CN based models, IHACRES[11] or WATBAL[12] model.
- Distributed models: These models require spatial information about various basin conditions such as soil types, land use and land cover and topography. Moreover, computational algorithms are added to estimate total runoff. The disadvantages of these models are that they require a large amount of input data and the relatively high computational costs due to the high degree of detail concerning physical processes. Models of this type are, for example, MIKE11/SHE, WATFLOOD or HYDROTEL.
- Semi-distributed models: This model type is a simplified form of distributed models. Parameters of semi-distributed models can partially vary in space by dividing the basin into a number of smaller sub-basins. The requirement for input data is less than for distributed models. In comparison with lumped models, their structure is more physically based. Typical models are SWAT, TOPMODEL or SWMM[13].

[11] Identification of unit Hydrographs And Component flows from Rainfall, Evaporation and Stream flow

[12] WATer BALance Model

[13] Storm Water Management Model

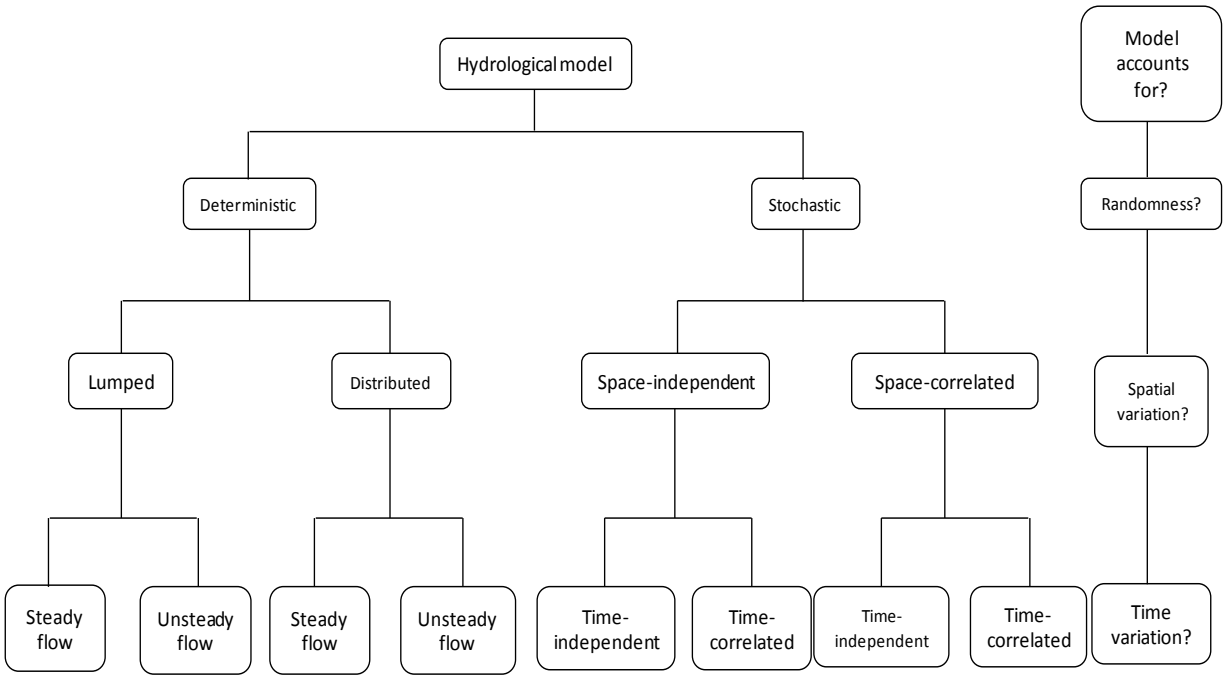

Figure 2.13: Classification scheme for hydrological models (Chow *et al*., 1988).

2.3.2 Choice of hydrological model

The selection of a (deterministic) hydrological model generally depends on the availability of hydrological and geometric components in relation with the water balance system. There exists large number of hydrological models. Some are briefly described in Table 2.3.

Table 2.5: Hydrological models.

Model	Category of hydrologic model	Short descriptions	Reference(s)
CREAMS	Distributed	The model is developed to simulate the impact of land management on water, sediment and nutrients. It is composed of three modules: hydrology, erosion and chemistry	Rudra *et al*. (1985)
HSPF	Distributed	HSPF is a comprehensive package for simulation of watershed hydrology and water quality for both conventional and toxic organic pollutants.	Chew *et al*. (1991)
ACRU	Distributed	ACRU is a multi-purpose, multi-level, integrated physical-conceptual model that is designed to simulate total evaporation, soil water and reservoir storages, land cover and abstraction impacts, snow water dynamics and stream flow at a daily time step	Kienzle and Schulze (1992)

SWAT	Semi-distributed	It is a river basin-scale model that is developed to quantify the impact of land management practices in large and complex watersheds	Rosenthal *et al*. (1995)
DHSVM	Distributed	It is a distributed hydrologic model that explicitly represents the effects of topography and vegetation on water fluxes through the landscape.	Nijssen *et al*. (1997)
SWIM	Semi-distributed	The SWIM model is based on two previously developed tools – SWAT and MATSALU.	Krysanova *et al*. (1998)
MIKE SHE	Distributed	It is an integrated hydrological modelling system for simulating surface water flow and groundwater flow. All terrestrial processes of the hydrologic cycle can be reproduced.	Boggild *et al*. (1999)
J2000	Distributed	The J2000 model is a distributed and process oriented distributed hydrological model for the simulation of mesoscale and macroscale catchments.	Krause (2002)
DWSM	Distributed	The DWSM is a physically based, event-based, distributed and unsteady rainfall-runoff, flood routing, soil/sediment erosion-transport-deposition, and agrochemical mixing-transport model.	Borah *et al*. (2004)

Within this study, however, the hydrological modelling system PANTA RHEI is selected. PANTA RHEI has been developed the hosting Leichtweiss Institute for Hydraulic Engineering and Water Resources (LWI), University of Braunschweig in collaboration with the Institute for Water Management IfW GmbH, Braunschweig (LWI-HYWAG and IFW, 2012). Reasons for selection are as follows:

(1) The model can be used to simulate both short-term periods (for single floods) using small time steps (e.g., 1 hour) and long-term periods (water balance) for the computation of the effects of climate change using small to large time steps (e.g., 1 day).

(2) It comprises modern programming techniques, a modular structure, database access, GIS[14] file import and a graphical interface with map access.
(3) It is a semi-distributed conceptual model: Information about the spatial variation of natural conditions can be processed with computational algorithms for each sub-catchment which is composed of hydrological units (hydrotopes).
(4) Results from PANTA RHEI can be displayed for all sub-catchments and nodes located along the rivers like reservoirs.
(5) A module for research-oriented water quality modelling is available.
(6) PANTA RHEI can be linked with other deterministic models for groundwater flow, hydrodynamic surface flow and reservoir operation. Hydrological outputs can thus be further investigated.

[14] Geographic Information System

3 SELECTION-DATA COLLECTION OF THE STUDY AREA: THI VAI RIVER CATCHMENT

The study catchment in this work, the Thi Vai catchment, is located southeast of Ho Chi Minh City of Vietnam. The catchment extends from 106.5°E to 107.2°E and from 10.3°N to 10.5°N in the coastal region, Southern Vietnam. It covers an area of approximately 500 km^2 and the three provincial administrative territories Ho Chi Minh, Ba Ria-Vung Tau and Dong Nai. The Thi Vai River catchment is a tributary to the Dong Nai River catchment which is the 3rd largest national river basin in Vietnam (see Figure 3.1).

The Thi Vai River catchment has been selected as a study area within the CLIENT Vietnam-Joint project Environmental and Water Protection Technologies of Coastal Zones in Vietnam (EWATEC-COAST) between German Ministry of Education and Research-BMBF and the Vietnam National University Ho Chi Minh City. This project is coordinated by the Department of Hydrology, Water Management and Water Protection at the Leichtweiss-Institute for Hydraulic Engineering and Water Resources (LWI), University of Braunschweig and the Institute for Environment and Resources (IER), Vietnam National University of Ho Chi Minh City. Results from this thesis will partly contribute to the joint research project.

3.1 Natural conditions of the study area

3.1.1 Topography

The catchment is characterized by relatively small topographical differences ranging from 10 m to 100 m above sea level in the east and northeast of river, to the highest peak of the Thi Vai mountain with an altitude of 462 m, located in Phu My Town, Tan Thanh District of Ba Ria-Vung Tau Province. In a small part in the northeast of the catchment elevation ranges from 100 to 300 m (see Figure 3.2). The large mangrove area Can Gio, located in the south of the Thi Vai catchment, is strongly affected by the semi diurnal tidal regime.

3.1.2 Climate

The complex climate of Vietnam is affected by the Asian monsoon system, geographical conditions, a cold high-pressure system over Siberia and the eastern sea (see more detail in section 4.2.1). A high base temperature and abundant sunshine duration are observed in Southern Vietnam. In this region, a tropical monsoon climate pattern dominates the regional climate regime. Therefore, climate in the Thi Vai catchment is strongly affected by this climate type with two distinguished seasons: rainy season and dry season. In this section, precipitation, temperature, atmosphere pressure, wind regimes, evaporation, humidity and sunshine duration obtained from the local meteorological stations and rain gauges (see section 3.3 and Appendix 2) are analysed at the catchment scale. This is fundamental to fully understand the climate regime and the observed changes in climate in the Thi Vai catchment described in chapter 5. The further analysis of climate factors that affect the regional climate regime will be presented in chapter 4.

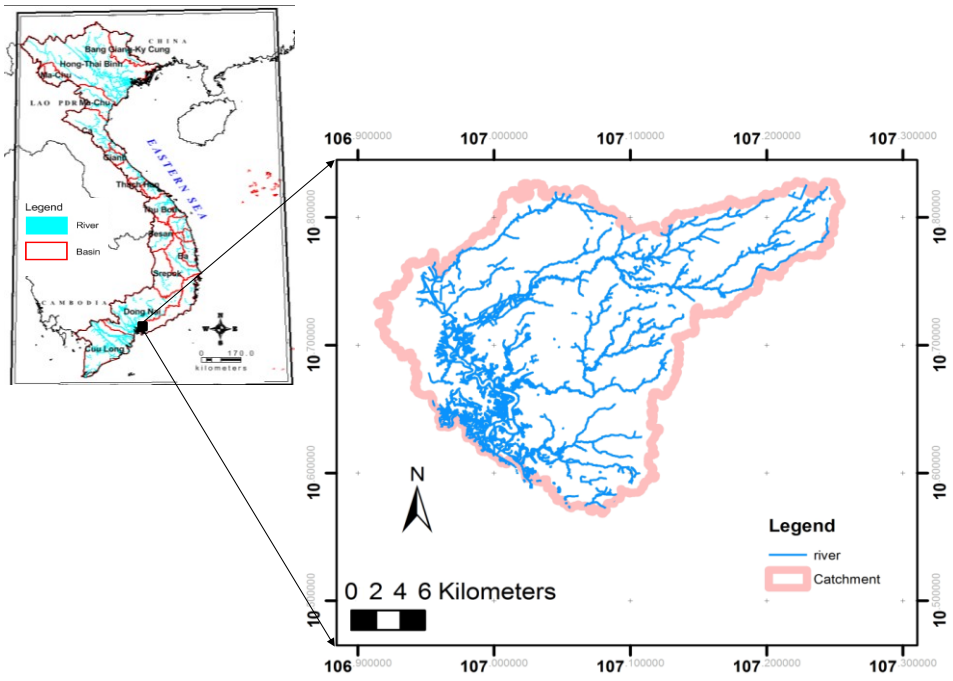

Figure 3.1: The study area river basin (*right*) in relation to the main river basin in Vietnam (*left).*

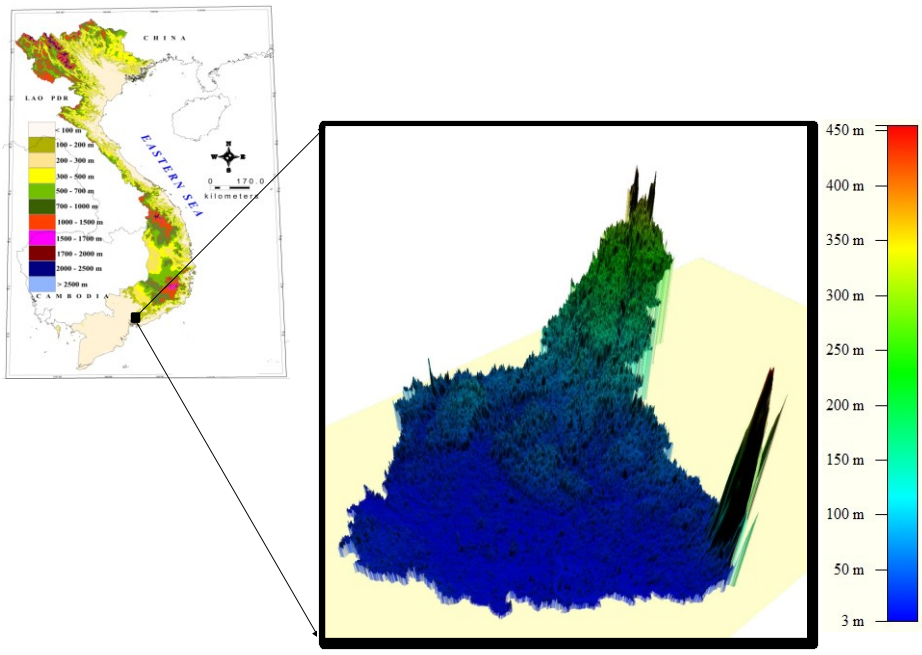

Figure 3.2: Topography of the study area (*right*) in relation to the Vietnam topography (*left*).

3.1.2.1 Precipitation

Precipitation plays a central role in the study of flood events. Table 3.1 shows a list of precipitation characteristics that are investigated at thirteen precipitation measuring stations during available periods (see Table 3.5). It is important to highlight that the available periods are investigated at stations as follows: Tan Son Hoa (1980-2013), Tam Thon Hiep (1981-2013), Can Gio (1980-2013), Vung Tau (1978-2013), Thong Nhat (1981-2010), Xuan Loc (1990-2010), Long Thanh (1978-2013),

Cam My (1981-2013), Hoc Mon (1980-2007), Bien Hoa (1978-2013), Binh Chanh (1982-2013), Nha Be (1992-2013) and Mac Dinh Chi (1980-2007). Further information on these stations can be found in section 3.3.1.1 and Appendix 2. The knowledge of precipitation features from this section is fundamental to study climate variability and change in the next chapters. The precipitation data is aggregated from the time scale of daily and hourly for available periods (see Table 3.5). A wet day is defined as a day with a precipitation amount of greater than or equal to 0.1 mm. Other features are defined in Appendix 6.

Table 3.1: Investigated precipitation characteristics.

Nr	Characteristics	Abbrev.	Nr.	Characteristics	Abbrev.
1	monthly rainfall	RRM	6	maximum 5-day rainfall amount	RX5day
2	seasonal rainfall	RRS	7	maximum 7-day rainfall amount	RX7day
3	annual rainfall	RRA	8	maximum consecutive wet days	MCWD
4	maximum 1-day rainfall amount	RX1day	9	maximum consecutive dry days	MCDD
5	maximum 3-day rainfall amount	RX3day	10	monthly wet days	MWD

The results from the analysis of precipitation at these stations show that the rainy season, which is defined as consecutive months with an average rainfall of over 100 mm, usually begins in May and ends in November. The dry season lasts from December to April. At some stations, the rainy season ends one month earlier and the dry season ends one month later (see Figure 3.3). The highest amount of monthly rainfall occurs from July to September.

The data at the four precipitation measuring stations that are located nearest to the catchment (Long Thanh, Cam My, Tam Thon Hiep and Thong Nhat) are analysed in detail in order to understand the precipitation variability and the available humidity source in the catchment (see Figure 3.4). At these stations, a large precipitation range (over 400 mm) is documented during the rainy season (seven months from May to November). The total precipitation from July to September contributes to almost 50% of the annual rainfall in the catchment.

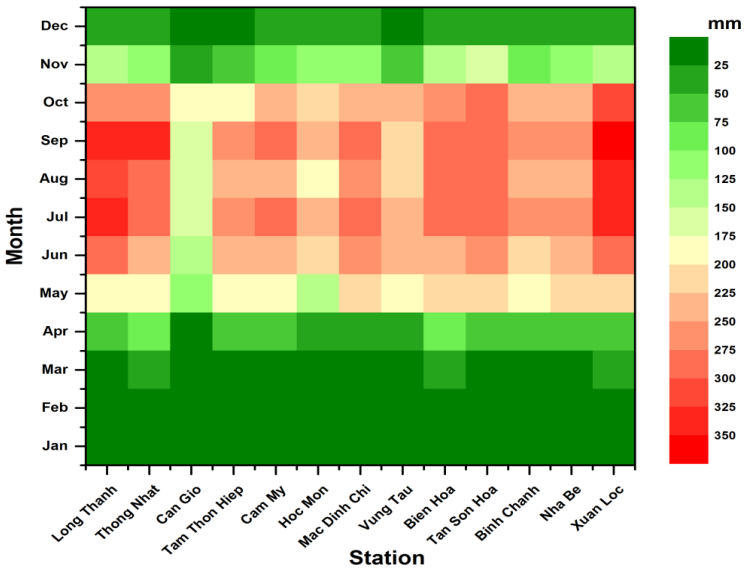

Figure 3.3: Monthly sum of rainfall at thirteen precipitation measuring stations.

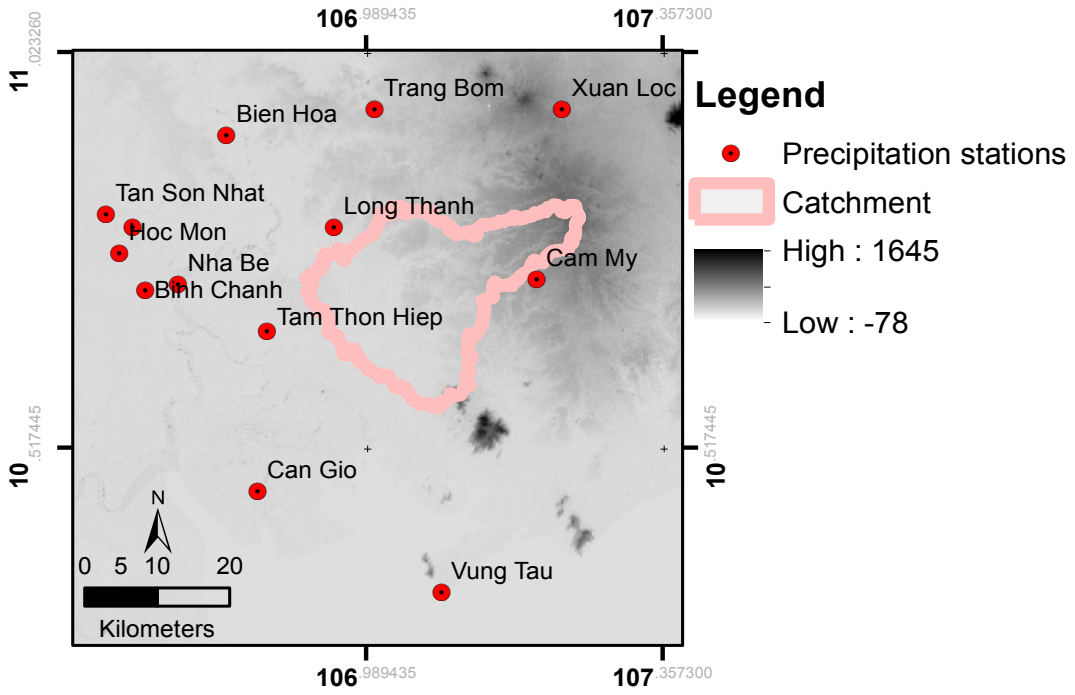

Figure 3.4: Map of precipitation measuring stations close to the Thai Vai catchment.

During the period 1978-2013 (36 years), the monthly rainfall at the observation station Long Thanh varies throughout the years. The highest amount of average monthly rainfall is observed in July (342 mm), contributing to 17.3% of annual rainfall, followed by September (16.5%) and August (15.2%). The lowest amount of average monthly rainfall (7.3 mm, equivalent to 0.4% of annual total) is recorded in February, followed by January (9.1 mm) with 0.5% and March (0.9%). The range of average monthly rainfall strongly patterns from January across December. The largest range of precipitation for the 36-years period is more than 500 mm in September, followed by October (470 mm) and July (458 mm). The lowest range is 60 mm in February, followed by January and March. Rainfall gradually increases from the month of January to July or September and then decreases. The total amount of rainfall during the rainy season contributes to about 93% of the annual rainfall (1983 mm) (see Figure 3.5).

For the observation station Cam My, the period from 1981 to 2013 (33 years) is analysed. At this station, the highest amount of average monthly rainfall is recorded in September (281.5 mm), contributing to 17.1% of annual rainfall, followed by July (17%), August (15%) and October (14.6 %). The lowest amount of average monthly rainfall (2.6 mm, equivalent to about 0.16% of annual total) is recorded in February , followed by January (5.9 mm) with 0.4% and March (0.8%). Rainfall gradually increases from the month of January to July or September and then decreases. The total amount of rainfall during the rainy season contributes to about 94% of the annual rainfall (1647 mm). Only within 3 months (from July to September), the averaged sum of rainfall contributes to about 50% of the annual rainfall at both Long Thanh and Cam My stations (see Figure 3.5).

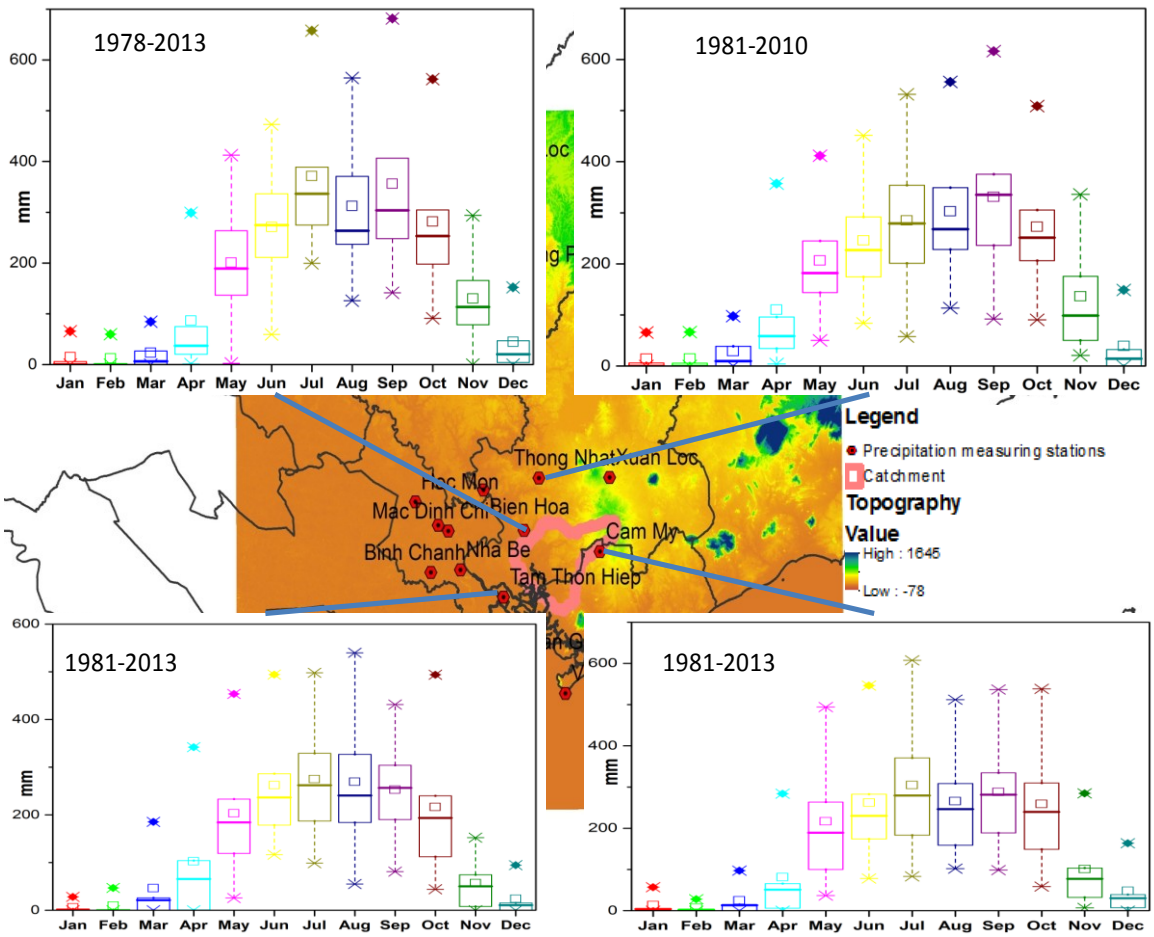

Figure 3.5: Box plot diagrams of precipitation at the stations Long Thanh, Cam My, Tam Thon Hiep and Thong Nhat.

Comparable with the above-described precipitation characteristics at the stations Long Thanh and Cam My, for the observation station Tam Thon Hiep during the 33-year period from 1981 to 2013, the average monthly rainfall in July contributed to 17.1% of annual rainfall (1531 mm per year), followed by September (16.8%). The lowest amount of average monthly rainfall is observed in February (1.5 mm, just equivalent to 0.1 % of annual total), followed by January (approximately 3 mm) with nearly 0.2 % of the annual amount of rainfall. The total amount of rainfall in the rainy season amounts to about 90% of annual rainfall (see Figure 3.5).

At the station Thong Nhat, the highest amount of average monthly rainfall is recorded in September (17.6% of annual rainfall of 1856 mm per year) during a 30-year period (1981-2010). In comparison with other stations (Long Thanh and Tam Thon Hiep), the highest rainfall is observed later in the year, in September, instead of July (see Figure 3.5). The lowest amount of average monthly rainfall is measured in February and January with more than 7 mm, which is equivalent to about 0.4 % of annual total rainfall.

The analysis of annual rainfall for 13 precipitation stations shows that the annual rainfall recorded in the 2000s is very abundant (over 2000 mm for most of the stations) (see Figure 3.6 *left*). This is a result of the La Nina event 1999-2000. The reason for this is that over Southeast Asian in general and

Southern Vietnam in particular could have wet or very wet conditions during the La Nina events (Nguyen, 2007; IMHEN[15] and UNDP[16], 2015). An amount of annual rainfall of more than 2500 mm is observed twice at the statins Bien Hoa and Xuan Loc and once at the stations Tan Son Hoa and Long Thanh. Among these stations, the highest annual rainfall (2871 mm) is measured at Long Thanh station in 1980. Generally, total annual rainfall is abundant during the given period at the stations Long Thanh and Xuan Loc.

The observed annual amount of precipitation at the stations located close to the coastline (Vung Tau, Can Gio and Tam Thon Hiep) is lower than it is at the other stations. At these coastal stations, the annual rainfall is less than about 1890 mm, except for in 1999 at the station Vung Tau and in 1990, in 2000 and in 2011 at Tam Thon Hiep station (see Figure 3.6 *left*). In the author's opinion, perhaps this shows that the effect of the monsoon circulation factor is more prevalent than the eastern wind factor (see section 4.2).

Figure 3.6 (*right*) shows spatial distribution of the average annual precipitation in the Thi Vai region. A heavy rainfall center is located in the northern part of the Thi Vai catchment. This is fully suitable in relation to the topography shape of the catchment, which partly contributes to observed precipitation amount. A decreasing tendency in annual rainfall is found from the north to the south of the catchment. In west-east direction, the precipitation difference is small, which indicates a symmetrical distribution. In the transition area, which covers the whole catchment, annual rainfall amounts to about 1500 mm. Over the Thi Vai region, generally, the spatial distribution of precipitation is unsteadily documented.

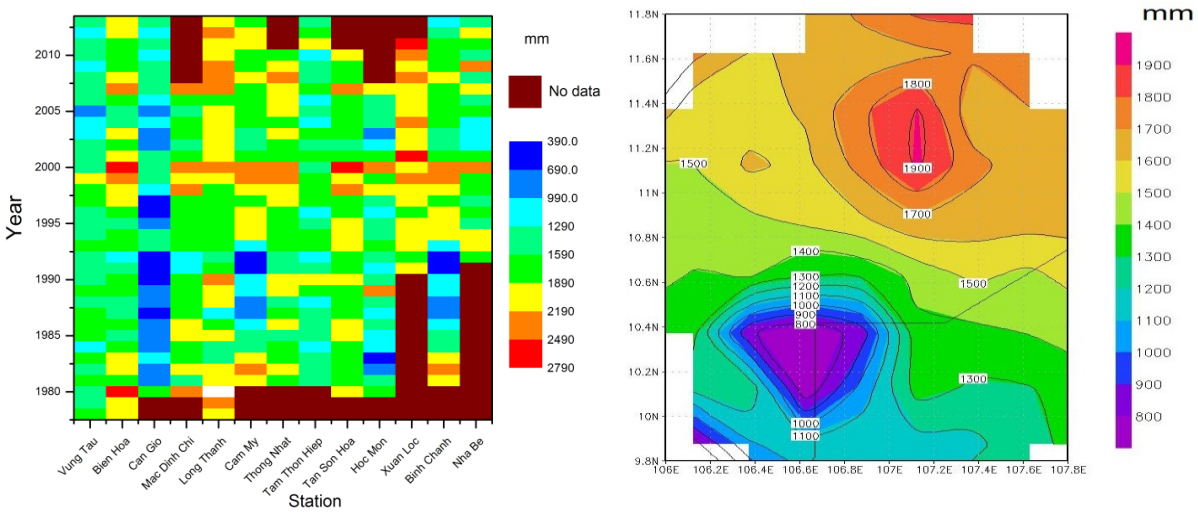

Figure 3.6: Annual precipitation distribution for 13 precipitation stations in time (*left*) and space (*right*).

The analysis of the maximum amount of rainfall for a one-, three-, five-, and seven-days period shows that the observed maximum seven-days rainfall amount (RX7day) is very heavy, especially at stations located in the Thi Vai river basin upstream (i.e., Xuan Loc and Thong Nhat stations). The maximum

[15] Institute of Meteorology, Hydrology and Environment

[16] United Nations Development Programme

value for RX7day is higher than 350 mm, up to 509 mm at Thong Nhat station, 442 mm at Xuan Loc station, and 432 mm at Long Thanh station. A small range of RX3day and RX5day is recorded at most stations out of 13 precipitation stations (see Table 3.2). However, a large range of RX5day and RX7day (more than 50 mm) is found at half of the considered stations (see Table 3.2). There is a peculiarly large leap between RX1day and RX3day (over 100 mm) at all stations.

Table 3.2: Values for RX1day, RX3day, RX5day and RX7day (mm) for 13 precipitation stations near the Thi Vai catchment.

Stations	Cam My	Long Thanh	Vung Tau	Bien Hoa	Xuan Loc	Tan Son Hoa	Mac Dinh Chi	Hoc Mon	Tam Thon Hiep	Can Gio	Binh Chanh	Nha Be	Thong Nhat
RX1day	169	226.5	271.4	194.5	246.7	162.2	174	142	162	173.7	169	196.1	241.7
RX3day	324	307.2	279.6	302.3	313.7	248.3	238.3	227.8	278.3	181.5	323.8	257.5	429.3
RX5day	347	350.2	287.3	336	375.2	287.8	310.4	253.8	311.6	199.2	347.3	262.1	453.4
RX7day	367	432.2	379.1	364.2	442.2	334.6	316.3	266.1	363.4	210.2	366.7	361.9	508.9

Table 3.3 shows the values for MCWD, MCDD and MWD for 13 precipitation stations near the Thi Vai catchment. The MCDD is relatively high (about 30% the days of the year). There are no big differences for MCWD, MCDD and MWD between the stations. The highest value of MCDD is observed at Hoc Mon station (154 days), followed by Can Gio station (147 days) and Tam Thon Hiep station (132 days). The highest value of MCWD is observed at the stations Cam My, Binh Chanh and Long Thanh with a value of 49 days, which is about 13% of the year.

Table 3.3: MCWD, MCDD and MWD for 13 precipitation stations near the Thi Vai catchment (days).

Stations	Cam My	Long Thanh	Vung Tau	Bien Hoa	Xuan Loc	Tan Son Hoa	Mac Dinh Chi	Hoc Mon	Tam Thon Hiep	Can Gio	Binh Chanh	Nha Be	Thong Nhat
MCWD	49	49	24	41	34	25	22	24	23	22	49	17	34
MCDD	126	114	135	117	105	122	123	154	132	147	126	123	111
MWD	15.5	17.8	16.7	17.2	25.7	16.8	15.5	11.9	11.7	11.8	13	12.5	14.9

On average from 13 precipitation stations near the catchment, more than 92 % of the annual precipitation amount falls during the rainy season. The highest amount of average monthly rainfall usually occurs in September or July with a total average of more than 250 mm. The observed maximum monthly rainfall at the stations Long Thanh, Tam Thon Hiep and Thong Nhat is more than 600mm. It is to be observed that the highest amount and range of average monthly precipitation do usually not occur at the same time of the year. Contrary to this, the lowest amount and range of average monthly rainfall usually appear at the same time of the year. The rainy and the dry season extend over 7-month period (from May to November) and the 5-month period (from December to April of the following year) respectively. The heavy rainfall centre is located in the north of the Thi Vai catchment, whereas there is a decreasing tendency of rainfall towards the south of river and the

coast. The monsoon system strongly influences the climate in the catchment. Monsoon effects are more important than the effect of eastern sea wind. The locality of precipitation features is also elaborated over the catchment.

3.1.2.2 Temperature

Figure 3.7 shows the variability of monthly temperature at the meteorological observation stations Bien Hoa, Vung Tau, Xuan Loc and Tan Son Hoa during the different period. The analysis of the temperature records at four stations near the catchment shows an abundant base temperature. The hottest month of the year is observed in April or May with an average temperature of about 29 °C. At the Xuan Loc station, temperature is lower due to orographical effects. In January, the coolest monthly temperature can be less than 25 °C. The period of temperature observations is seen in Figure 3.7. In general, the annual variability of temperature has a parabolic shape with the highest point in April or May and a gently slope to both sides. The highest monthly temperature can reach more than 31 °C (see Figure 3.7).

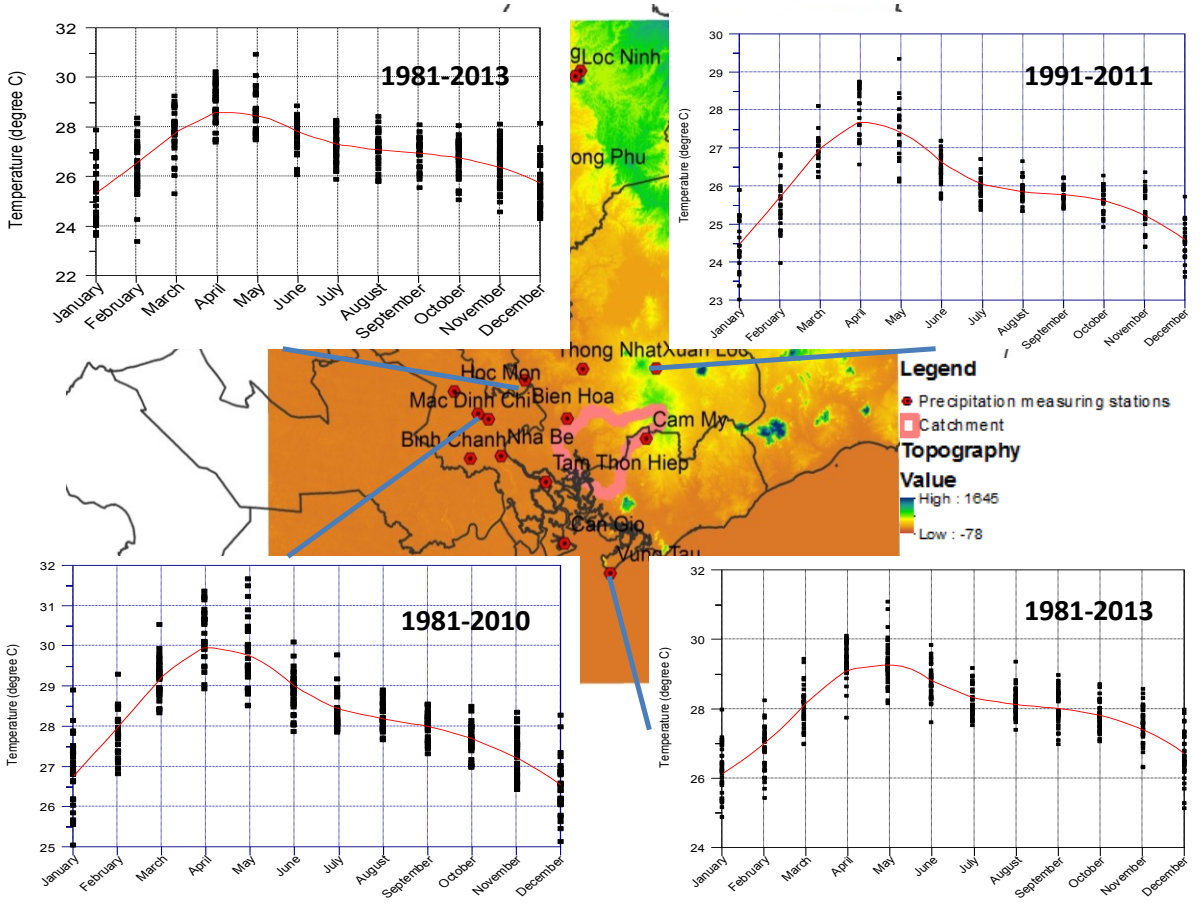

Figure 3.7: Variability of monthly temperature at the observation stations Bien Hoa, Vung Tau, Xuan Loc and Tan Son Hoa during the different period.

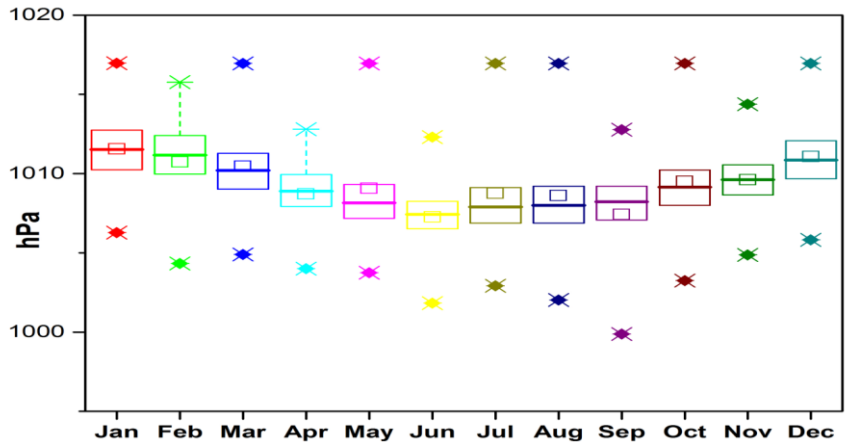

Figure 3.8: Atmospheric pressure at Vung Tau station during 1979-2010.

3.1.2.3 Atmospheric pressure

Figure 3.8 shows the variability of atmospheric pressure at Vung Tau meteorological station during 1979-2010. It is to be observed that atmospheric pressure slightly varies throughout the year. The minimum monthly value of about 1000 hPa coincides with maximum monthly rainfall in September. Maximum monthly value can reach up to 1018 hPa. During the rainy season, the values for atmosphere pressure are usually below 1010 hPa, whereas higher values are recorded during the dry season. The average atmospheric pressure is the lowest in June when it amounts to 1007 hPa.

3.1.2.4 Wind regimes

Southern Vietnam is affected by the south-easterly winds, which originate from the Southern Indian Ocean and change their direction when passing the equator. They bring monsoon rains, high moisture and heavy clouds to Southern Vietnam from May to October or November. Furthermore, a nonhomogeneous variation of wind direction and speed is illustrated at observation stations throughout the year (see Figure 3.9). During the rainy season, south-westerly and west-south-westerly winds with an average speed of about 3 m/s at the stations Tan Son Nhat and Vung Tau are predominant. There is, however, a change of direction in the north of the catchment. The prevailing wind direction at Xuan Loc station is south-easterly, whereas the wind direction ranges from west-southwest to east-southeast at Tan Son Nhat station. This shows that there is a strong interaction between the eastern sea, the south-easterly monsoon and the complex topography. Contrary to this, the easterly and north-easterly winds are predominant during the dry season with an average speed that is lower than during the rainy season.

3.1.2.5 Evaporation

Figure 3.10 shows a variability of monthly evaporation per day at Vung Tau station during 1979-2013. As can be seen in Figure 3.10 that total annual evaporation amounts to almost 1200 mm. An average maximum daily value is recorded in February, March or April (over 4 mm). Daily minimum evaporation occurs in September or October (more than 2 mm). The highest value reaches over 10 mm/day from February through April. The lowest values can be less than 1 mm from April to December. The variability of evaporation is strongest in April (see Figure 3.10).

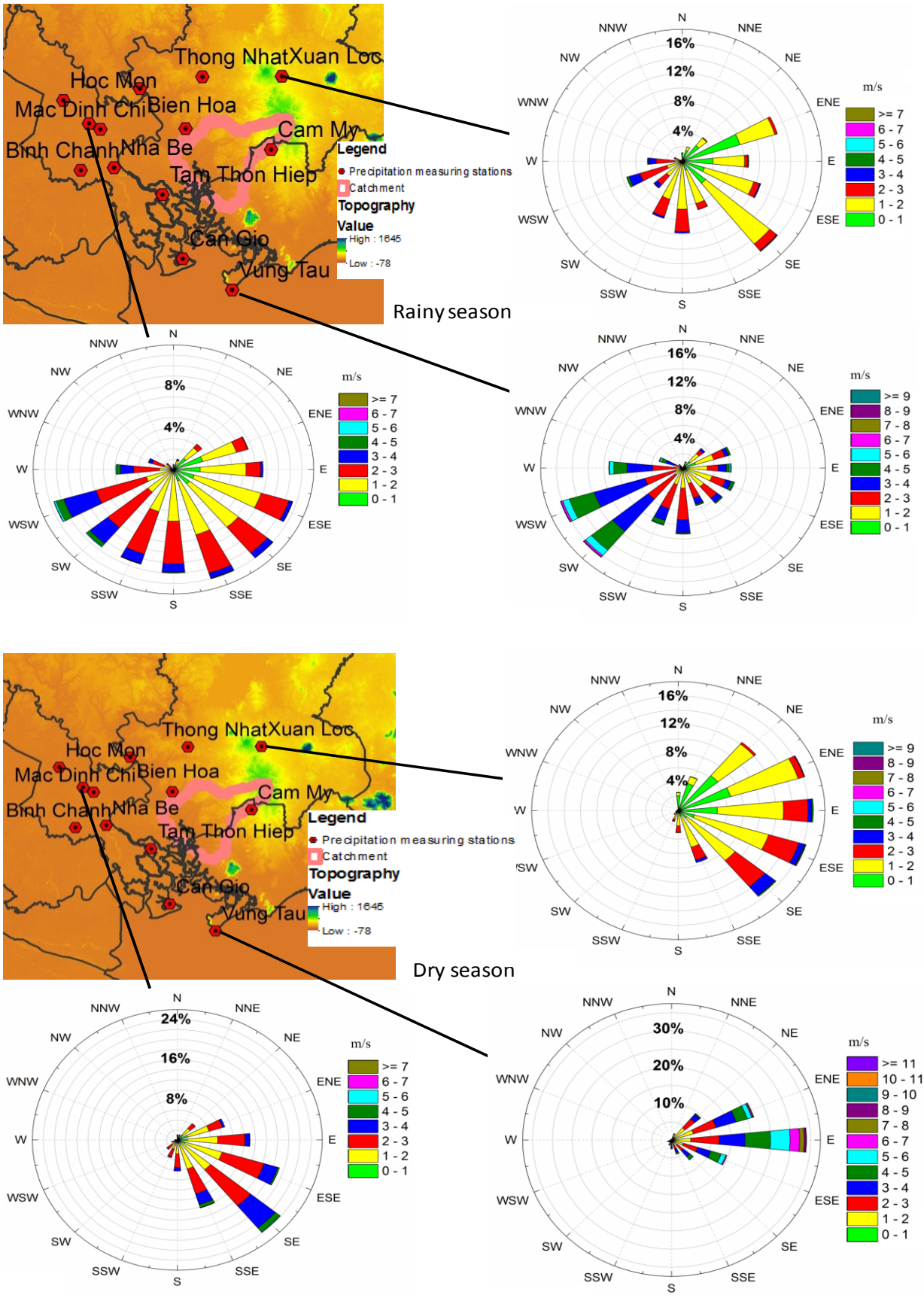

Figure 3.9: Windrose for the rainy season (*top*) and the dry season (*bottom*) at the stations Tan Son Nhat, Xuan Loc and Vung Tau. Cycle lines stand for the percent frequency of windrose. Different colours refer to wind speed (m/s).

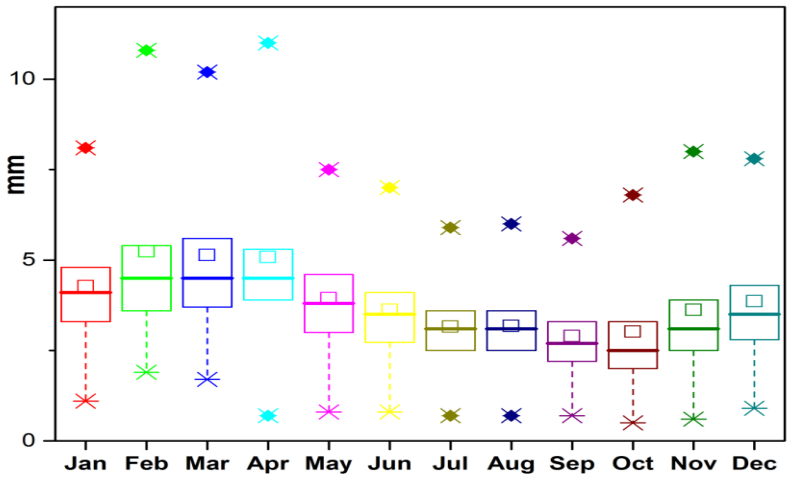

Figure 3.10: Variability of monthly evaporation per day at Vung Tau station during 1979-2013.

3.1.2.6 Humidity

Annual humidity ranges from about 75% to 85%. The highest value of daily humidity is recorded in October at Bien Hoa station (99% on 26/10/11993 and on 30/10/1987). Figure 3.11 shows a daily variability of humidity at Bien Hoa station. Generally, the relative humidity is significantly higher during the rainy season than during the dry season. Diurnally, the humidity amounts to maximum value at 7 am and falls to minimum value at 13-14 pm. This indicates an inversion relation between humidity and temperature.

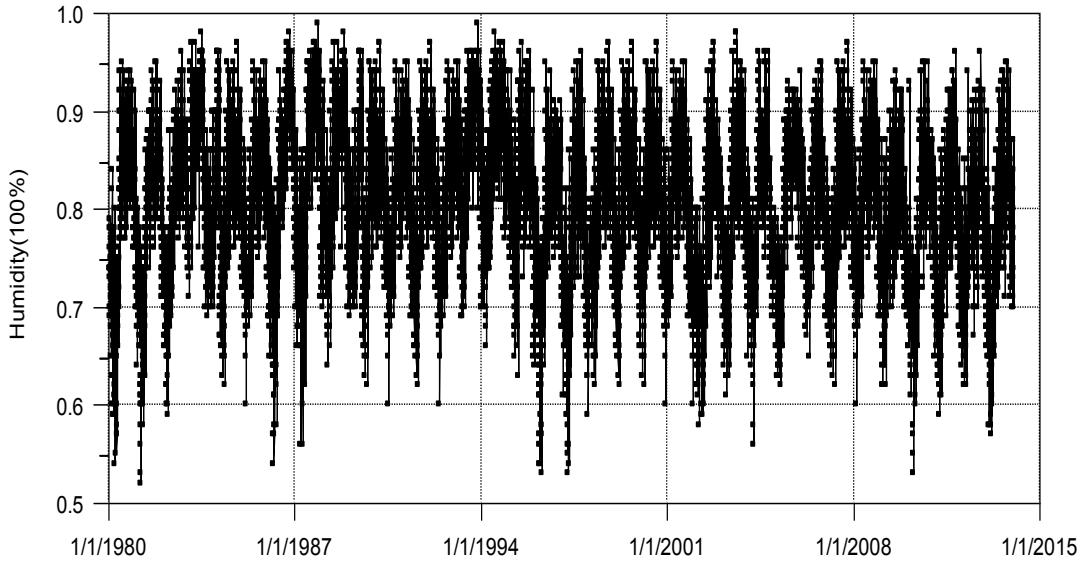

Figure 3.11: Daily variability of humidity at Bien Hoa station during the period 1980-2013.

3.1.2.7 Sunshine duration and solar radiation

The solar radiation regime is stable throughout the year. Total solar radiation is averagely about 128-186 W/m^2 for the areas Long Thanh District of Dong Nai province and Tan Thanh District of Ba Ria-Vung Tau province. An average daily sunshine duration of about 9.5 hours, occupying 56–66% out of the annual sum radiation is observed during the dry season. Total annual sunshine duration is 2640–2680 hours on average with an average daily value of 7.3 hours.

3.1.3 Land use and land cover

There are three main land use units in the catchment including paddy rice, perennial industrial tree and annual crop (see Figure 3.12).

3.1.4 Geology and soil texture

Figure 3.13 shows the main geological units in the Thi Vai river catchment. They are briefly described in the following:

- Q: Early Quaternary Period. The depth of this layer amounts to maximum of 15 m. The components are loam, pebble, grave, detrital shell and eluvi trail.
- N2-Q1: Upper Pliocen-Early Pleistocen. The maximum depth of this layer is from 10-15 m.
- Q1(2-3): Middle-Upper Pleistocen. The main component is loam clay and laterite clay. The maximum depth is 10 m.
- Q2: Holocen. The maximum layer is up to 30 m. The dominant components are clay and loam with botanic trails, grey- and loam-clay.

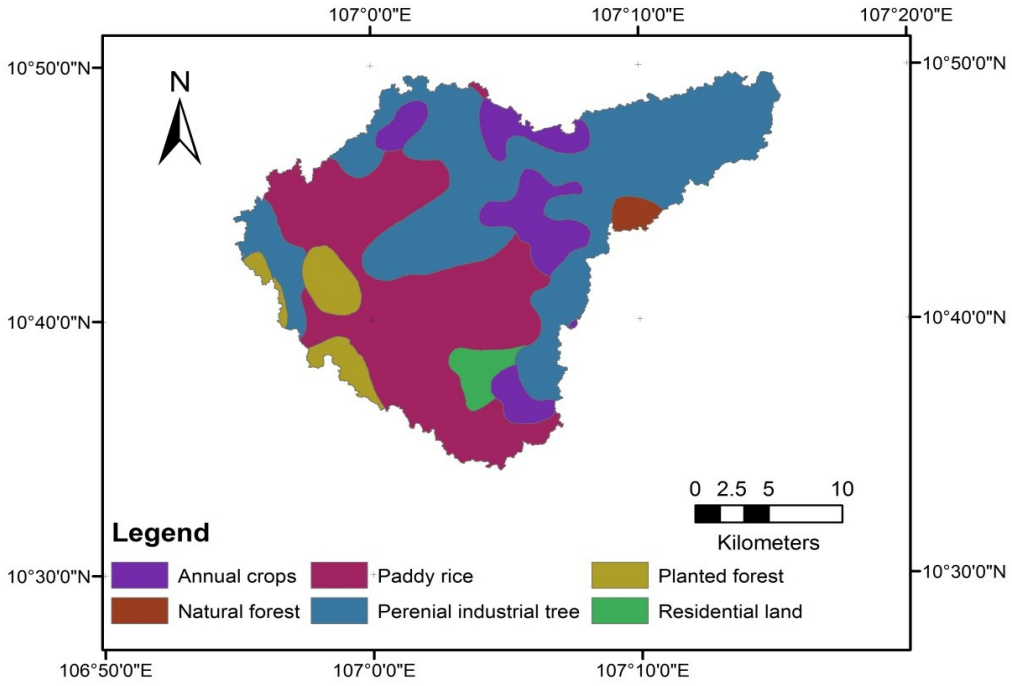

Figure 3.12: Land use and land cover units of Thi Vai River catchment (DONRE[17] and IER[18]).

The soils in the catchment are dominated by acidic soil types like acrisols (arenic acrisol, ferric acrisol, gleyic acrisol and plintic acrisol). Other important soil types are rhodic ferrasols and thionic fluvisols (see Figure 3.14).

[17] Dong Nai Department of Natural Resources and Environment

[18] Institute for Environment and Resources, Viet Nam National University HCMC

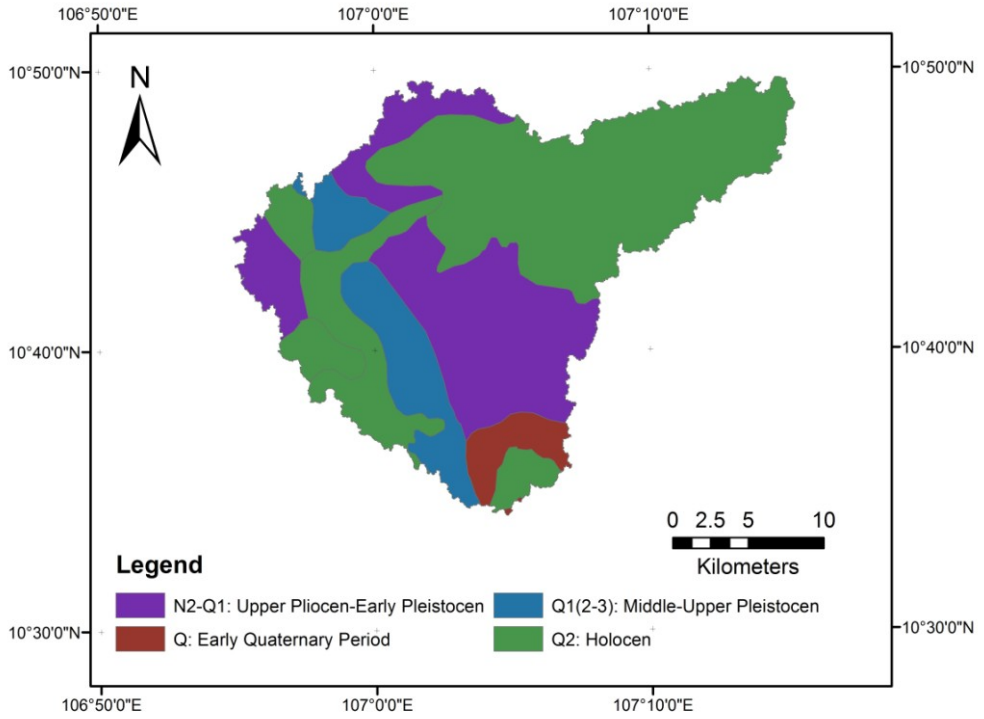

Figure 3.13: Geological map of Thi Vai catchment (DONRE and IER).

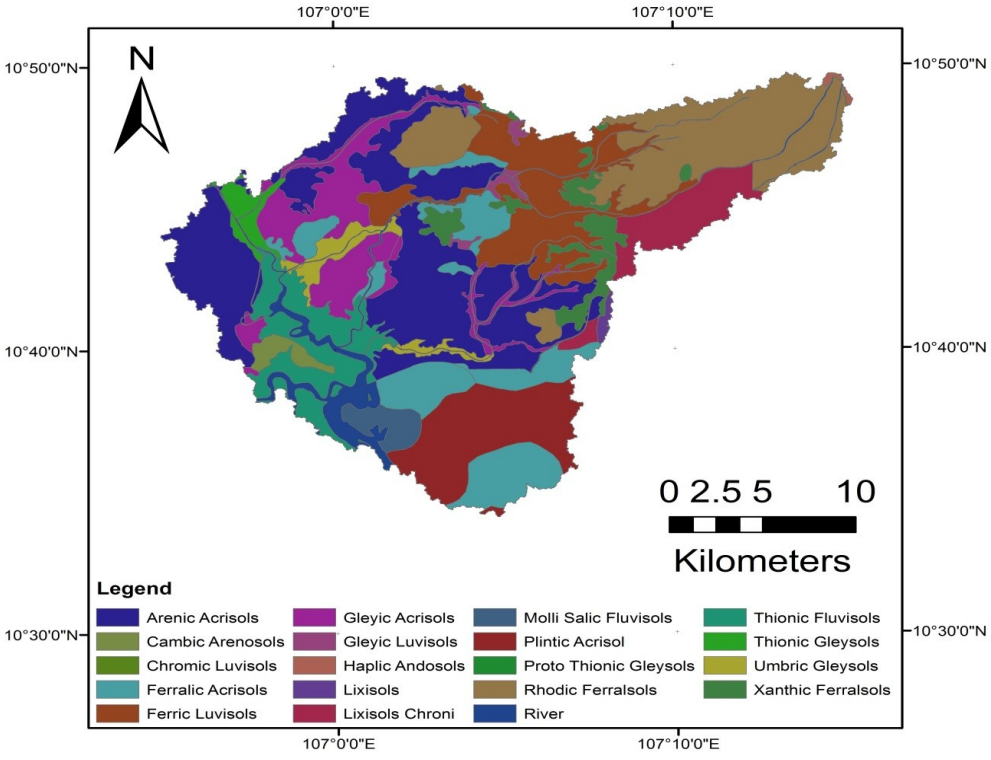

Figure 3.14: Soil map of the Thi Vai catchment (DONRE and IER).

3.1.5 Hydrological characteristics

The source of the Thi Vai River is the Bung Mon spring, located in the Long Thanh district which is part of the Dong Nai province. The river flows past the port Cai Mep in Tan Thanh district of Ba Ria-Vung Tau province, and finally flows into the Ganh Rai bay. It has a length of more than 40 km and

width of about 300 m in the upper part of the river and up to 900 m close to the mouth of the river. The tributaries of Thi Vai in the lower part of the river, such as Tac Nha Phuong and Go Gia are connected to the Sai Gon-Dong Nai river system. The Thi Vai river has three main tributaries: Bung Mon, Suoi Ca, and Cau Vac. It has four estuaries: Soc, Quyt, Nuoc Lon and Chan rivers. The Thi Vai River is affected by the semi diurnal tidal regime with a tidal range of approximately 1.4–4.0 m.

3.2 Socioeconomic conditions of the study area

3.2.1 Population

According to the statistical reports of Dong Nai, Ba Ria-Vung Tau and Ho Chi Minh Provinces (GSO, 2005), the total area of communes in the catchment is about 87688 ha with a population of more than 100 000 people and a population density of about 118 people per square kilometre.

Table 3.4: Population statistics (GSO, 2005).

Nr.	District	Commune/town	area (1000 ha)	population (1000 people)
1	Long Thanh	Long Phuoc	4.42	12.933
2		Phuoc Thai	1.72	15.794
3	Nhon Trach	Phuoc An	14.799	7.240
4		Long Tho	2.388	7.292
5	Tan Thanh	My Xuan	37.059	19.544
6		Phu My	3.1	14.687
7		Tan Phuoc	5.5	8.322
8		Phuoc Hoa	5.54	10.896
9	Can Gio	Thanh An	13.142	4.146
	Total		87.7	100.85

Almost all people along the Thi Vai River and its surrounding live on agriculture, salt production and fishing. Therefore, natural conditions strongly affect their life.

3.2.2 Socioeconomic conditions

The Thi Vai has a convenient location for only geographical connections, but functional connections. These connections between Cai Mep-Thi Vai area and Ba Ria-Vung Tau Province is especially effective, cost reducing and a good use of loading and unloading capacity as well as increasing competitive ability of Vietnam's seaports (IPC, 2014). According to the IPC's report (IPC, 2014), the deep-water ports nowadays mostly concentrate on the Thi Vai river area with many industrial parks along the river.

The aquaculture sector is another traditional economic sector in this area. However, the aquaculture production tends to decrease in recent years because of environmental pollution, especially water pollution from the industrial zones.

3.3 Data collection

3.3.1 Station data

3.3.1.1 Meteorological data

Local weather variables are obtained from the Vietnam HydroMetorological Data Centre (VHMDC) for more than 30 rain gauges and meteorological stations located in Southern Vietnam. However, thirteen precipitation measuring stations that are closest to study basin (see Table 3.5) are selected for further analysis in this study. Further information on weather variables at these stations can be found in Appendix 2. A map of these precipitation measuring stations is displayed in Figure 3.4. The records cover a period of more than 30 years (1981 to 2013). Although a longer time period would have been preferable, this is impossible due as gauges are not installed before 1981 or are destructed. Most gauges are installed after 1981. Some pictures of meteorological stations are shown in Figure 3.15. The elevation of these stations is displayed in Table 3.5. The weather data is carefully validated (as presented in chapter 5).

Table 3.5: Lists of the precipitation measuring stations.

Nr.	Station	Station code	Coordinates		Elevation (m a.s.l)	Period	Note
			Latitude (N)	Longitude (E)			
1	Tan Son Hoa	489000	10°49’	106°40’	5	1980-2013	MS
2	Vung Tau	489030	10°22’	107°05’	4.1	1978-2013	MS
3	Long Thanh	30901006	10°27	106°33	41	1978-2013	RG
4	Can Gio	30906007	10°14’	106°35’	9	1980-2013	RG
5	Bien Hoa	48896	10°34’	106°29	13	1978-2013	MS
6	Tam Thon Hiep	30906022	10°40	106°52	4	1981-2013	RG
7	Cam My	30901004	10°51	107°09	145	1981-2013	RG
8	Thong Nhat	30901013	10°57	107°00	61	1981-2010	RG
9	Nha Be	30906015	10°40’	106°44’	9	1992-2013	RG
10	Binh Chanh	30906004	10°44’	106°44’	9	1981-2013	RG
11	Xuan Loc	30901016	10°57’	107°14’	190	1990-2010	MS
12	Hoc Mon	30906010	10°46’	106°41’	8	1980-2007	RG
13	Mac Dinh Chi	30906014	10°48’	106°42’	6	1980-2007	RG

Note: MS: Meteorological station and RG: Rain gauge

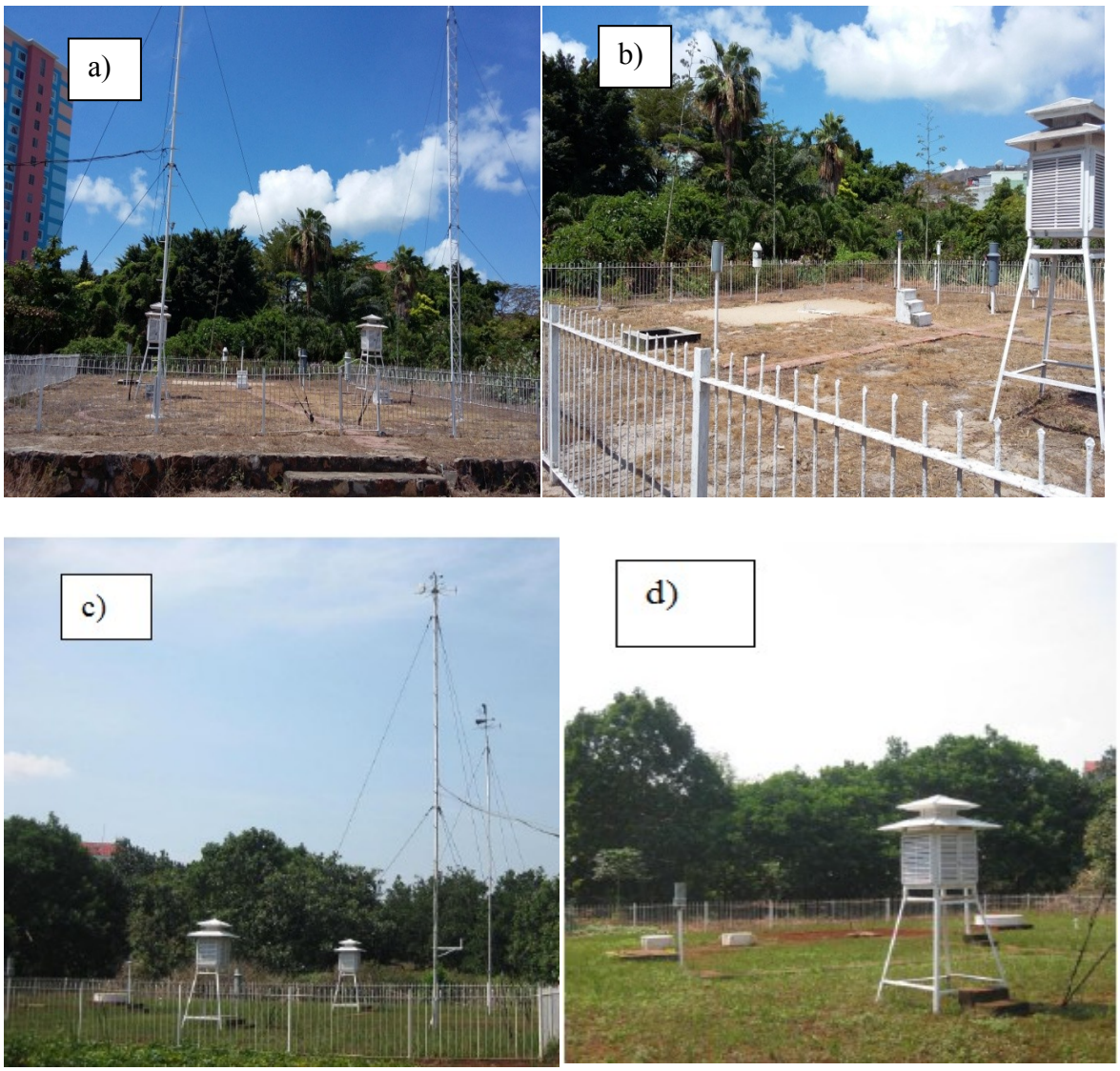

Figure 3.15: Meteorological station: Vung Tau station (a-b) and Xuan Loc station (c-d).

3.3.1.2 Discharge data

The installation of the measuring stations in the Thi Vai catchment was completely performed by the Leichtweiss-Institute, University of Braunschweig, Germany, in March 2013 within the joint German-Vietnamese research Project EWATEC-COAST. This means that the discharge data collection and availability of this work is only representative for over one year. The discharge data is obtained from the three hydrometric measurement stations Binh Son, Cau Vac and Suoi Ca at the inflow of tributaries (see Figure 3.16). The installed monitoring system in the catchment is described in more in the "EWATEC-COAST" project (Meon *et al*., 2014). In this work, a brief description of the observed discharge data is given. The time step of 15 minutes at each station is automatically installed. Two main criteria for the installation of these measuring stations are, that the main tributaries are unaffected by tidal influences and can easily be accessed. The location of the discharge stations is shown in Figure 3.16. Data for the period from July to August 2013 at the Suoi Ca station is missing because the station is stolen. In this study, these discharge data and precipitation data produced from a regional climate model at a three-hour interval step are aggregated to a daily time step.

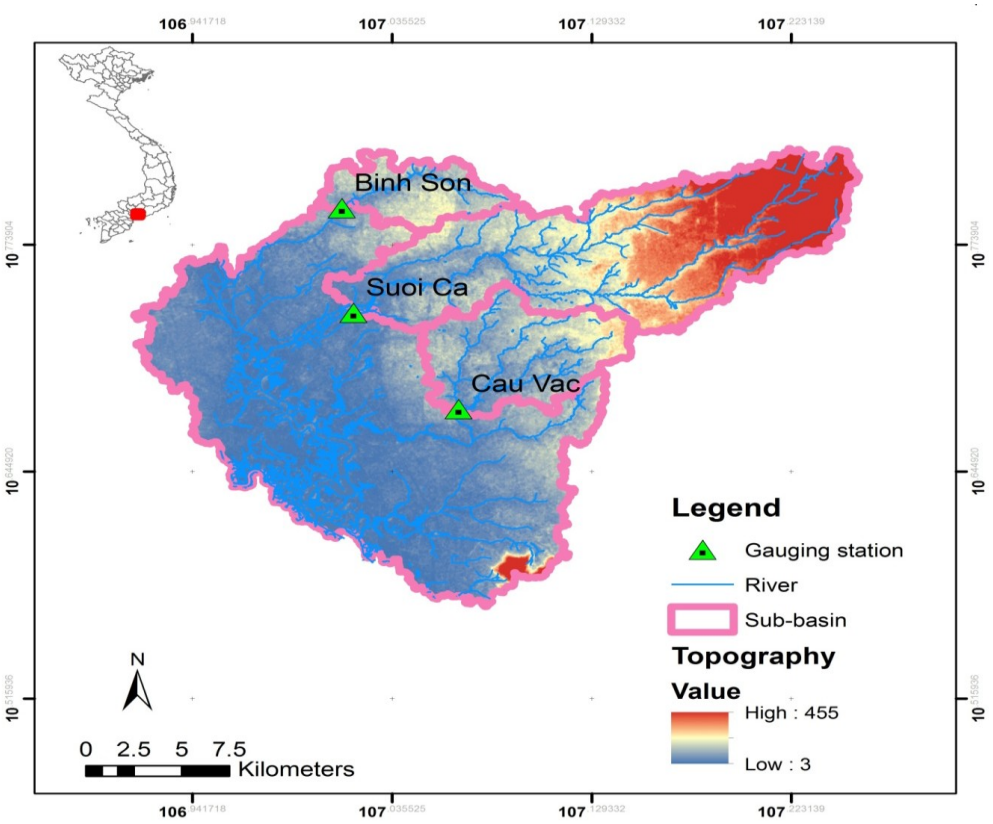

Figure 3.16: Monitoring locations for discharge in the Thi Vai river catchment.

3.3.2 Raster datasets for meteorological data fields

The gridded meteorological metadata are obtained from the World Meteorological Organization (WMO) and the National Aeronautics and Space Administration (NASA). The following data is analysed in this study: Climatic Research Unit (CRU), ERA-Interim, Global Precipitation Climatology Centre (GPCC), Asian Precipitation-Highly-Resolved Observational Data Integration Towards Evaluation (Apthrodite) and Tropical Rainfall Measuring Mission (TRMM).

- **Climatic Research Unit Time-Series**

Established in 1972, the Climatic Research Unit (CRU) at the University of the East Anglia (UEA) is reconstructed the measured data for climate data over land areas as much of a globe scale as possible. These datasets currently have a resolution of 0.5^{o} x 0.5^{o} latitude/longitude degrees. They are developed from the observed data from over 4 000 weather stations around the world (Harris *et al*., 2014). Almost all these weather stations are exchanged via the National Meteorological Services (NMSs) under the WMO's sponsorship; the data from these stations are exchanged via the CLIMAT network, which is part of the WMO Global Telecommunications System (GTS). In the early 1980s, many of the original datasets are published in decadal data publications entitled 'World Weather Records, WWR'. They also publish data from the National Climatic Data Centre in Asheville, North Carolina, USA. Both the gridded datasets and the station data archived have evolved over the years.

The latest versions of CRU datasets are available via the British Atmospheric Data Centre (BADC) consisting of CRU TS 3.00, CRU TS 3.10, CRU TS 3.20, CRU TS 3.21 and CRU TS 3.22 for the period 1901-2006, 1901-2009, 1901-2011, 1901-2012 and 1901-2013 respectively. The CRU TS is monthly

gridded data based on daily values; the ASCII and NetCDF files are available for various parameters such as mean temperature and radiation.

- **ERA-Interim**

This is a third generation reanalysis of the global atmosphere, initiated in 2006 to reproduce the previous reanalysis the European Centre for Medium-Range Weather Forecasts (ECMWF with the main objective to improve the ERA-40. The ERA-40 (1957-2002) is a second-generation reanalysis. The term "ERA" refers to the computerised weather data from the European Centre for Medium-Range Weather Forecasts. The "reanalysis" stands for a method that creates a comprehensive picture of the state of the Earth system on a four-dimensional grid. Generally, this method is a combination of weather prediction model and observations to produce gridded datasets of many meteorological fields (e.g., temperature or precipitation) at a high resolution of temporal. The products created with this method are known as reanalysis data (more detailed in WMO-Nr. 100, 2010). The ERA-Interim atmospheric model and reanalysis system are configured for (1) a spatial resolution of 60 levels in the vertical with the top level at the 0.1 hPa, (2) T255 spherical-harmonic representation for the basic dynamical fields and (3) a reduced Gaussian grid with a horizontal resolution of approximately 0.7 degrees latitude/longitude for surface and other grid-point fields (Dee *et al*., 2011).

- **Global Precipitation Climatology Centre**

The GPCC Full Data Reanalysis Product Version 6 (GPCC v6) is generated in December 2011 and is a new extended product version using the new GPCC climatology as analysis background. It covers the period from 1901 to 2010 based on a variety of data sources from about 10 000 to more than 47 000 climate stations and sets for the global land surface. These metadata sources are distributed by the NMSs under the WMO's sponsorship via the WMO GTS. Besides this, other available global and regional collections of climate data (e.g., the Global Historical Climatology Network (GHCN) and CRU) are integrated in the GPCC data base. These datasets are merged by the Deutscher Wetterdienst (DWD), the National Meteorological Service of Germany. The GPCC v6 has a horizontal resolution of 0.5°, 1.0° and 2.5° (Schneider *et al*., 2011).

- **Tropical Rainfall Measuring Mission**

The TRMM is a joint space mission between the NASA and Japan's National Space Development Agency with the purpose of monitoring and studying the precipitation over tropical and subtropical regions and the associated release of energy. The following instruments are used: TRMM Microwave Imager (TRMM TMI), the TRMM Precipitation Radar (TRMM PR), Clouds and Earths Radiant Energy System, Visible Infrared Scanner and Lightning Imaging Sensor. Among these devices, the main instruments for precipitation estimation are TMI and PR. These data is processed using in an algorithm in order to obtain the TRMM Combined Instrument calibration data set (TRMM 2B31) for the TRMM Multi-satellite Precipitation Analysis (TMPA), the TMPA 3B43 monthly precipitation and the TMPA 3B42 daily and sub-daily (3 hourly), which are probably the most relevant TRMM-related products. These products are available for the period 1998-present with a spatial resolution of 0.25° resolution and are used in this study. A recommendation for using the newest version 7 is also suggested (Huffman and Bolvin, 2013).

- **Asian Precipitation-Highly-Resolved Observational Data Integration Towards Evaluation**

Since 2006, daily high-resolution grids of precipitation are produced for the entire Asia within APHRODITE's Water Resources project, which is conducted by the Research Institute for Humanity and Nature (RIHN) and the Meteorological Research Institute of the Japan Meteorological Agency (MRI/JMA). The datasets cover the period 1951-2007. Data is based on a rain gauge observational network. The density of the rain gauges network is of higher density over the Himalayas, South and Southeast Asia and mountainous areas in the Middle East. The number of gauges varies between 5 000 and 12 000 and is therefore two and four times higher than those that are considered by WMO GTS (Yatagai *et al*., 2012).

- **CGCM3**

The version of CGCM3 is the third generation coupled global climate model, which is the latest AOGCM version produced at the Canadian Centre for Climate Modeling and Analysis and is used in the IPCC AR4. In comparison with the previous version CGCM2 or CGCM1, it has been substantially improved regarding the atmospheric component Atmospheric Canadian GCM, version 3 (AGCM3) (Jeong *et al*., 2012). Within this component, the process for the treatment of energy and moisture fluxes at the land surface (Verseghy *et al*., 1993), a new treatment of water vapor transport (Boer, 1995) and of the penetrative mass flux scheme within cumulus parameterization are considered (Zhang and McFarlane, 1995). CGCM3 has two versions with different resolutions: the T47 version has 31 levels in the vertical and provides a surface grid resolution of roughly 3.75 x 3.75 degrees latitude/longitude and the T63 version, which provides a spatial resolution of roughly 2.8 x 2.8 degrees latitude/longitude (Flato, 2005).

Table 3.6: Strengths and weaknesses of different gridded meteorological datasets.

Data	Strengths	Weaknesses
CRU	All data is merged into a consistent format from a variety of sources with various variables. Values for the variables evapotranspiration, diurnal temperature range, number of rain days and frost were estimated using the station data.	The data set is not strictly homogenous. The number of stations used for interpolation is less than the one used for GPCC
ERA-Interim	Multiple variables are available at high spatio-temporal resolution. The low-frequency variability is improved in comparison with ERA-40. The stratospheric circulation is ameliorated in comparison with ERA-40.	The intensity of the water cycle is too high over the oceans. In the Arctic: positive biases in temperature and humidity below 850hPA compared to radiosondes; does not capture low-level inversions.
GPCC	The large number of stations used; Higher density of gauge network compared to GHCN.	Variable number of stations per grid over time can be a major source of inhomogeneity.

		The climate products are not updated, but the monitoring products are frequently updated.
TRMM	The precipitation is estimated at high spatio-temporal resolution since 1998. It is a useful data source for the validation of the spatio-temporal distribution of rainfall characteristics in climate models.	The translating algorithms are complex. In regions of intense convection over land and in higher latitudes, the precipitation radar algorithm underestimates precipitation.
Aphrodite	The density of the station network is fine and the data is of good quality.	Station network changes in time. Lack of observation data (e.g., in India).

The global scale datasets are provided by the third version of the Canadian Centre for Climate Modelling and Analysis (CCCma) Coupled Global Climate Model (CGCM3) (Flato, 2005). In this study, CGCM3 T47 with a spatial resolution of roughly 3.75 degrees of Gauss grid and 31 levels in the vertical is used. The resolution over the oceans is roughly 1.8 degree with 29 levels in the vertical.

Table 3.7: Characteristics of the gridded datasets used in this study

Data name	Data type	Data source	Geographic coverage	Data format	Spatial resolution	Temporal interval	Temporal coverage	Note
TRMM3B42 V7	Satellite precipitation	NASA	50°S-50°N; 180°W-180°E	HDF	0.25°	1/1/1998; ongoing update	3-hourly	A joint U.S- Japan satellite mission
TRMM3B43 V7	Satellite precipitation	NASA	50°S-50°N; 180°W-180°E	HDF	0.25°	1/1/1998; ongoing update	Monthly	A joint U.S - Japan satellite mission
ERA-Interim	Global reanalysis	ECMWF	90°N-90°S; 180°E-180°W	GRIB, NetCDF	~0.7°	1/1979-7/2013; ongoing updates	6-hourly	It has much improved in comparison with ERA-40 e.g., higher spatial and temporal resolution, implementation of stratospheric circulation and low-frequency variability.
Aphrodite	Gauge-Sat Obs	RIHN/ MRI/JMA	60°E-150°E; 15°S-55°N	NetCDF	0.25°	1951-2007	Daily	The products interpolate the ratio of daily precipitation to daily climatology.
CRU TS 3.21	Global	BADC	All land areas (excluding Antarctica)	ASCII, NetCDF	0.5°	1901-2012	monthly	The dataset is not strictly homogeneous although many of the input data have been homogenized.
GPCC	Global	DWD	90°N-90°S; 180°E-180°W	ASCII, NetCDF	0.5°	1901-2010	monthly	The accuracy of GPCC products mainly depends on the spatial density of the stations used.

4 GLOBAL AND LOCAL CLIMATE CHANGE

4.1 Overview of climate change

This section is very important for basic understanding of global climate change. In the frame of this work, however, just a brief overview of the information dealing with global climate change are given.

4.1.1 Understanding climate, climate variability and climate change

4.1.1.1 Climate

Climate is defined as the statistical characteristics of certain variables such as temperature, precipitation, solar radiation and wind over a period, which ranges from months to millions of years. The weather refers to the state of atmosphere over a short period, which ranges from day to day or near future. According to the WMO's reports (WMO-No. 49 and WMO-No. 100), a period of 30 years is considered as the classical climate period.

The climate of a given region depends on the main factors such as geographical conditions, solar radiation and atmosphere circulations. Geographical conditions, such as elevation and geographical location determine amount of solar radiation that is absorbed and converted into changes in temperature. The unequal distribution of heat in the atmosphere results in large-scale airflows, also called the atmospheric circulation, which effect the reproduction of heat and moisture.

4.1.1.2 Climate variability

A variation in the statistical properties (e.g., standard deviations) of the climate outside individual weather events on all spatio-temporal scales is defined as climate variability. This term indicates the deviations of climatic statistics over a given period in comparison with long-term statistics for the same calendar period. Natural internal factors within the climate system like ENSO as well as natural or anthropogenic external factors such as changes in solar radiation and volcanism can cause a variability of the climate.

4.1.1.3 Climate change

Climate change is a change in the state of earth's climate system, including atmosphere, hydrosphere, biosphere, geosphere and cryosphere in present time and future due to natural variability, with the sun being the most important factor (see Figure 4.1) and anthropogenic activities. This definition differs from the one of the United Nations Framework Convention on Climate Change (UNFCCC) which states, that climate change is directly or indirectly caused by human activities that change the composition of the global atmosphere and that is in addition to natural climate variability observed in the same period.

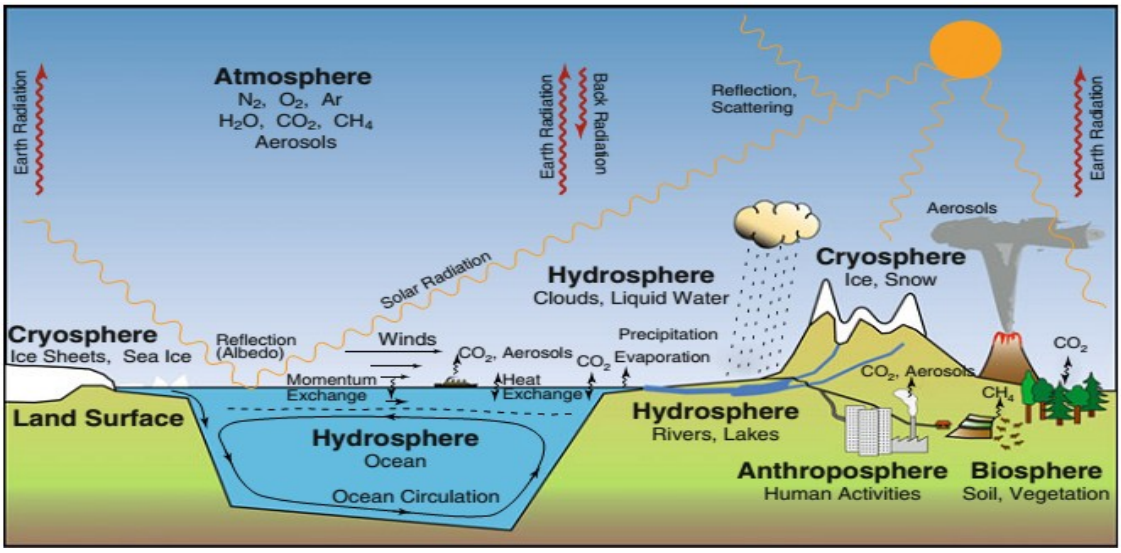

Figure 4.1: Schematic view of the components of the global climate system, their processes and interactions (Stocker, 2011).

4.1.2 Observed changes in climate on a global scale

Changes in climate variables can affect both the quantity and quality of fresh water, ecosystems, animal behaviours and human health. Until now, changes in the frequency and intensity of precipitation and an increase in the frequency of tropical cyclones, floods, droughts, and heat waves at many places over the world have been observed. Furthermore, significant changes in glaciers and sea level have become important scientific topics for climate change studies (Roer *et al*.**,** 2008).

4.1.2.1 Observed changes in temperature

It is well known that the temperature is the most important climate variable. It determines the thermal radiation circulation from the Earth and affects all climate variables. For example, the temperature difference between regions leads to the movement of wind and pressure fields; Extreme temperatures directly influence human health, physical processes of evapotranspiration or atmospheric convection movements. In the context of changing in climate, the behaviour of the climate system is changing not only on a global but also on a regional and even local scale. Hence, temperature is in the focus of almost all climate projects. Thus far, there is an increasing trend for temperature values on a global scale since the late 19th century. Over the period 1961-1999, surface temperature has increased about 0.6 °C. During 1951-2012, the warming trend amounts to up to 0.72 °C and about 0.89 °C over the period 1901-2012 (IPCC, 2013). According to the report of IPCC (IPCC, 2007) the hottest years in the 1990s coincided with the effect of El Nino events. However, these events are substituted by the 2000s in the latest report IPCC AR5 (IPCC, 2013). On the other hand, the coolest years coincided with elongated La Nina events in the years 2000 and 2008. The global warming trend has been detected for two different periods: from the early 1920s to the mid-1940s and since the mid-1970s. In comparison with the period 1906-2005 (see Figure 4.2), the warming trend per decade during 1956-2005 (0.10 to 0.16^{o}C) is approximately twice as high.

On a global scale, many research projects on changes in climatic variability put the focus on a specific region, because the variability is different for each region For example, the interannual variability of

seasonal temperature anomalies in entire North American has slightly increased during the period 1974 to 1993 in comparison with the period 1954 to 1973, whereas large increase was found in central North America (Parker *et al*., 1994). The result of a complete investigation of maximum and minimum daily temperature over China, the United States and the Soviet Union for the past 50 to 100 years is that intra-monthly temperature variability decreased (Michaels *et al*., 1998). The changes in temperature are observed for other regions, such as Australia and New Zealand (Plummer *et al*., 1999), Canada (Bonsal *et al*., 2001), northern and central Europe (Heino *et al*., 1999), Southeast Asia and South Pacific Region (Manton *et al*., 2001) and central England (Jones *et al*., 1999). In Europe, the warmest year since the beginning of observations in the 1500s is measured in 2014 (Blunden and Arndt, 2015), before that the hottest year is 2003 (Luterbacher *et al*., 2004).

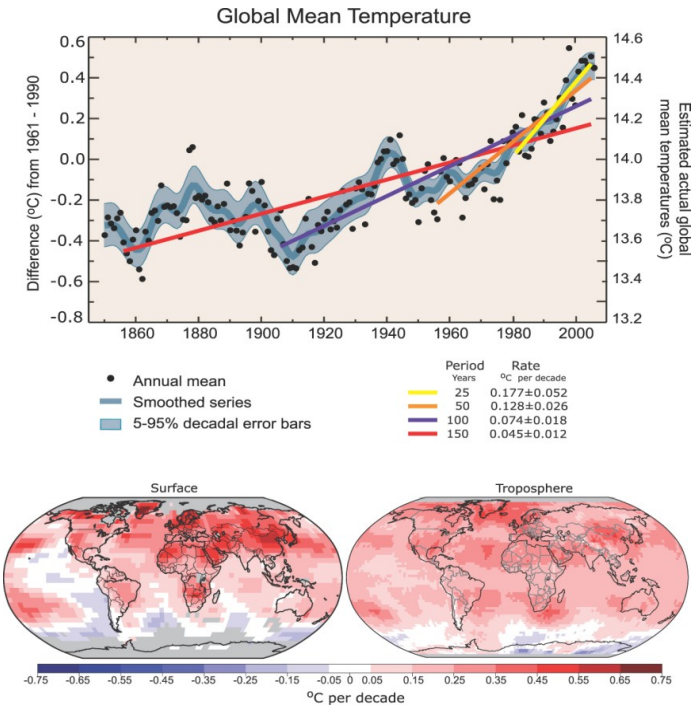

Figure 4.2: Anomalies of global annual mean temperatures. Annual global mean temperatures (*black dots*) with linear fits to the data. The left hand axis stands for the temperature anomalies relative to the 1961-1990 average and the right hand axis refers to estimated actual temperatures, both in degree C. Linear trends are shown for the 25 (yellow), 50 (orange), 100 (magenta) and 150 years (red) (*top*). Patterns of linear global temperature trends over the period 1979 to 2005 estimated at the surface (left) and for the troposphere from satellite records (right). Grey shows areas with incomplete data (*bottom*) (IPCC, 2007).

4.1.2.2 Observed changes in precipitation

Precipitation plays a key role in the water cycle, in defining the local climatic conditions and in ecosystems. It is also an important input parameter for most of the water resource management and hydrologic models. A variety of precipitation characteristics (e.g., intensity, duration, frequency and wet days) has a significant impact on economic sectors, especially in agriculture, and on natural resources. Under global warming, precipitation has been drawing much attention by scientists. Many

previous studies about changes in precipitation were performed for different time periods and regions as described by Bradley *et al*. (1987), Diaz *et al*. (1989), Schönwiese *et al*. (1990), Schönwiese (1994) and Busuioc and Storch (1996). Regional analyses in the Soviet Union (Gruza *et al*., 1999), the United States (Karl and Knight, 1998), Japan (Iwashima *et al*., 1993), Zwitzerland (Frei and Schär, 2001), China (Yafeng *et al*., 2003), Australia (Suppiah and Hennessy, 1995) and Canada (Stone *et al*., 2000) demonstrated that changes in precipitation have been continuously occurring under different behaviours. In the Northern hemisphere, for instance, precipitation drops as rain more often than as snow. During the years 1901 to 2005, annual precipitation has increased in most parts of North America and Canada. This is found by analysing the interpolated data of GHCN that have a resolution of 5^{o} x 5^{o} latitude/longitude degrees. Based on the data of GHCN and CRU, changes in annual precipitation for different regions worldwide were precisely analysed (see Figure 4.3).

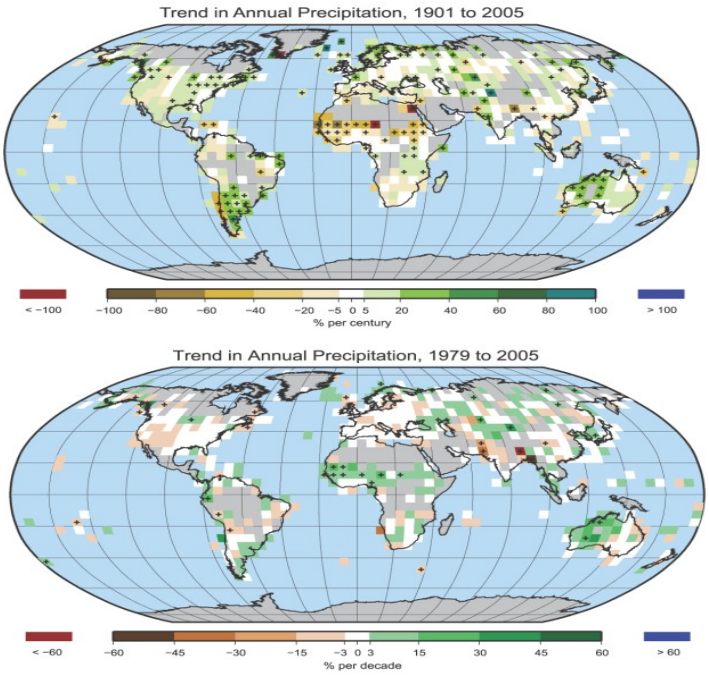

Figure 4.3: Trend of annual land precipitation in different parts of the world for 1901 to 2005 (top, % per century) and 1979 to 2005 (bottom, % per decade). The percentage is based on the means for the 1961 to 1990 period. Areas in grey have insufficient data to produce reliable trends. The minimum number of years required to calculate a trend value is 66 for 1901 to 2005 and 18 for 1979 to 2005. An annual value is complete for a given year if all 12 monthly percentage anomaly values are present. Black + marks indicate trends significant at the 5% level (IPCC, 2007).

4.1.2.3 Observed changes in other climate variables

The constituents of cryosphere, glaciers, ice-sheets, sea ice, snow cover, frozen ground and freshwater ice are important factors in the earth's climate system. They play a major role in the control on the physical, biological and social environment. A variety of interactions and feedbacks within the cryospheric system can also perturb the state of the climate. Of course, the observed spatio-temporal patterns of these components significantly contribute to the changes in climate on a

global scale. Within global climate-related observations, they are also considered as key variables for detecting changes in climate. In chapter 4 of the IPCC AR5 (IPCC, 2013) observed changes are described in detail. Compared to the period 1992-2001, for example, the rate of ice loss from the Greenland ice sheet has averagely increased by 181 Gt per year during the period 2002-2011. The decreasing rate of the Arctic amounts to 11.5±2.1% per decade during 1979-2012. Strong ice losses are found in different decades from the beginning of the measurements in 1946 (1946-1965, 1966-1985 and 1986-2005) equivalent to a slowing down, moderate mass loss and speeding up of ice loss (see Figure 4.4).

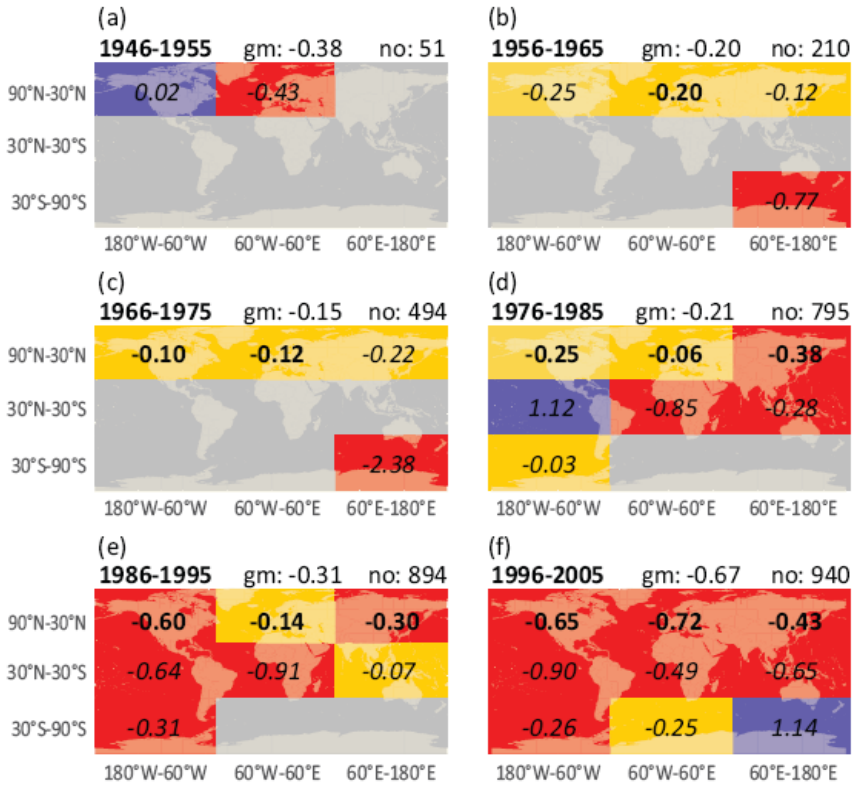

Figure 4.4: a-f. Spatio-temporal patterns of changes in glacier mass. The average annual mass balance for nine sectors of the globe over the different periods (a) 1946-1955, (b) 1956-1965, (c) 1966-1975, (d) 1976-1985, (e) 1986-1995, and (f) 1996-2005. The unit is meter water equivalent (m w.e). Grey: no data available, blue: positive balances, orange and red: ice losses up to 0.25 m w.e and above. Average decadal mass balance values based on less than 100 observations (marked in italics) are less representative for the entire sector. For each decade, the global mean (gm) annual mass balance in m w.e. and the number of observations (no) are indicated, taken from (Roer *et al.*, 2008).

4.2 Climate change in Vietnam

4.2.1 Major climate factors in Vietnam

The geographical characteristics of Vietnam are its long, narrow shape with the maximum width in the Red River Delta (~600 km) and the minimum width in Quang Binh province (50 km) as well as its extended coastline of over 15 degrees of latitude (Nguyen and Nguyen, 2004). The factor of eastern

sea climate has significant effects on the climate in Vietnam. Moreover, it is completely located within the intertropical zone; the climate in Vietnam has both tropical and monsoon characteristics. These factors play an important role in the differentiation the various climate regions in the country.

Solar radiation

According to Nguyen et al. (1992) and Nguyen and Nguyen (2004), the solar radiation absorption in Vietnam is determined by the intertropical solar regime. The sun reaches its zenith over the country twice a year (between mid-April to the summer solstice for the first time and between the summer solstice and the end of August for the second time). For the whole country, total sunshine duration per year is about 4300-4500 hours. The solar radiation potential can amount up to 267-290 W/m^2/year in case of a clear sky (higher than 40-60% under normal conditions in which the cloud covers a part of the sky). In southern Vietnam over 162 W/m^2 of the total solar radiation is absorbed under normal conditions. This results in a high annual temperature. The total amount of solar radiation depends on elevation and latitude (higher over lower latitude regions and lower at higher elevation areas).

General circulations

Vietnam territory is located in the tropics where the distribution of surface temperature and pressure is fairly uniform and the air mass is relatively homogeneous. The effects of local and mesoscale physical processes on terrestrial characteristics are more dominant than synoptic influences (COMET, 2016). For instance, precipitation and surface temperature can change quickly due to convection processes and sea breezes. The tropical convection processes are organized into mesoscale and even microscale with a range of scales in space and time such as thunderstorms (1-10 km, hour), mesoscale convection systems (100-500 km, day), synoptic-scale super clusters (1000-4000 km, week) and the Madden–Julian Oscillation (~10000 km, weeks to months). Moreover, the strong effects of extratropical cyclones during the winter can push cold fronts into subtropical and tropical regions. As a result, the temperature can drop a few degrees; heavy rainfall, strong winds and severe weather events can occur as well (Nguyen et al., 1992 and Nguyen and Nguyen, 2004). Another important parameter of the Vietnamese climate, which brings heavy rainfall, is the monsoon regime. Traditionally, “monsoon” term refers to an apparent seasonal shift of prevailing surface wind direction between summer and winter. Over the tropical regions, the monsoon regime can generate monsoon depressions, monsoon gyres and tropical cyclones. Figure 4.5 depicts that Southern Vietnam is completely located within in an impacted-region by monsoon winds. Within this region, the frequency of prevailing wind directions for both January and July is greater than 60% (Khromov, 1957). This indicates that the climate regime in general and particularly the climate variability in the study area are strongly dominated by monsoon regimes. Additionally, it is noticeable that over 90% local summer precipitation of the annual total is analysed from the observational data (see section 3.1.2.1). This figure is much higher than 55% local summer precipitation of the annual total as illustrated by Wang *et al*. (2011) by using the GPCC data over the study area. Based on a series of hourly and daily precipitation at the thirteen stations around the catchment (see Figure 3.4), the extreme heavy rainfall events (higher than 50 mm/day) are strongly localized (data not shown). Even if the distance between the precipitation measuring stations is not so far (~5 km), the recorded

precipitation is extremely difference. So, in the author's opinion, this could refer to strong locality of weather and climate regime on the catchment.

Nguyen et al. (1992) showed that in the north of Vietnam the winter season is cold which results from polar air pushed to the low latitudes of tropical region due to winter monsoon. In January, temperature can drop down 4-5 ^{o}C below the average value for the latitude from the 16th parallel northward. In the mountains with an elevation of more than 1500 m above sea level, temperature may reduce to 10 ^{o}C during the winter months. The range of temperature fluctuation from the 16th parallel northward is higher (over 6 and even 12-14 ^{o}C in the mountain places) than that in the southern plain of Vietnam (only 3-4 ^{o}C).

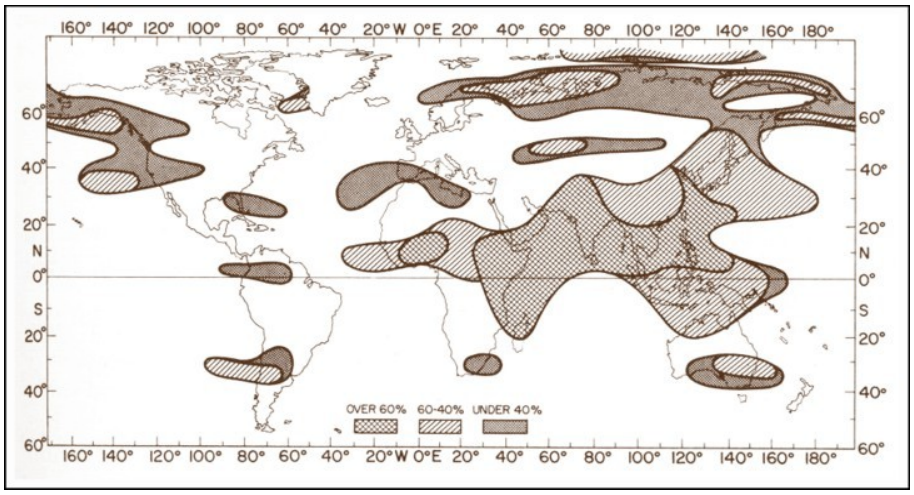

Figure 4.5: The monsoon regions of the world are classified by Khromov (1957). The prevailing wind directions for monsoon regions are under 40%, 40-60% and over 60% (Khromov, 1957).

The monsoon regime and the landscape patterns are the main factors for the differences in the climate regions in Vietnam. Unlike a cold winter season in the north, in the south and central highlands of Vietnam there are two distinct seasons: rainy and dry season. Besides this, there is a change in the rainy season in the east of Truong Son area and a drizzle season in the Red River Delta and in the north of central Vietnam. The effects of the monsoon, generally, are unstable due to the wide fluctuations in annual climate in Vietnam (Nguyen et al., 1992).

Furthermore, the tropical cyclones (TCs) in the Western Pacific strongly affect the moisture and heat regimes in Vietnam and cause extreme weather events like very heavy rainfall. Vietnam is located in the core regions of TCs with a share of 33% of the total number of global TCs (Tran, 2003). In this study, data for a 54-year period (1960-2013)[19] illustrates that the average number of TCs per year in the northwest pacific (NWP) region is 31 cyclones. More than 30% of these (9.5 cyclones) cross the coast of Vietnam (see green colour line in Figure 4.6b). During the period 1960-2013, a total of 1702 tropical cycles were recorded, among these were 934 super typhoons (wind speed more than 118.5 km/hour), 536 tropical storms (wind speed 63-117 km/hour) and 232 tropical depressions (wind speed less than 61 km/hour). Over the 54-year period, the highest number of TCs was observed in

[19] The database is obtained and summarized from the International Best Track Archive for Climate Stewardship and the Joint Typhoon Warning Center by the author.

the 1960s, followed by 1990s, whereas the 1980s showed a decreasing trend. An increasing trend was found over the 20-year period between the 1970s and the 2000s for both TCs Vietnam and TCs in NWP. Over a recent 13-year period (2000-2013), there is a reversal tendency of TCs in Vietnam (increasing trend) and TCs in NWP (decreasing trend). Figure 4.6a shows that normally, the TCs in the north occur earlier in the year, while those in the south occur later. Most TCs appear in August and September. The reason for this is due to the coincidental tendency of the Inter Tropical Convergence Zone (ITCZ) and TCs path related to southerly trade winds and high pressure centre in the Western Pacific. The least number of TCs occurs in January, February and March due to the effects of winter monsoon and polar air masses. Over Binh Thuan-Ca Mau territorial water (see Figure 4.7); however, there is a change in the time of occurrence of TC paths in the recent years. The TCs always appear between October and December, but there is one TC occurring in Vung Tau in Jan 2010 and another one in March 2012 with the strong intensity. There is a decreasing trend in TCs NWP as well as TCs Vietnam but there is a difference in the quantity, intensity and occurring time.

Oceanic air masses

The Vietnamese climate is dominated by tropical and oceanic air mass conditions. The air masses transfer the moisture from the sea to the land. Consequently, the climate in Vietnam is characterized by high precipitation and humidity. The annual average of relative humidity can reach 90% with an annual rainfall higher than 1500 mm in many regions (Nguyen and Nguyen, 2004). In the study area, for example, the annual rainfall is about 1600 mm.

In total, the interactions of the three major factors of climate, geographical characteristics, solar radiation and atmospheric circulations, determine the complexity of the Vietnamese climate regions. Furthermore, the interaction intensity of air masses in the process of controlling or replacing one another is a challenge for meteorologists and climatologists.

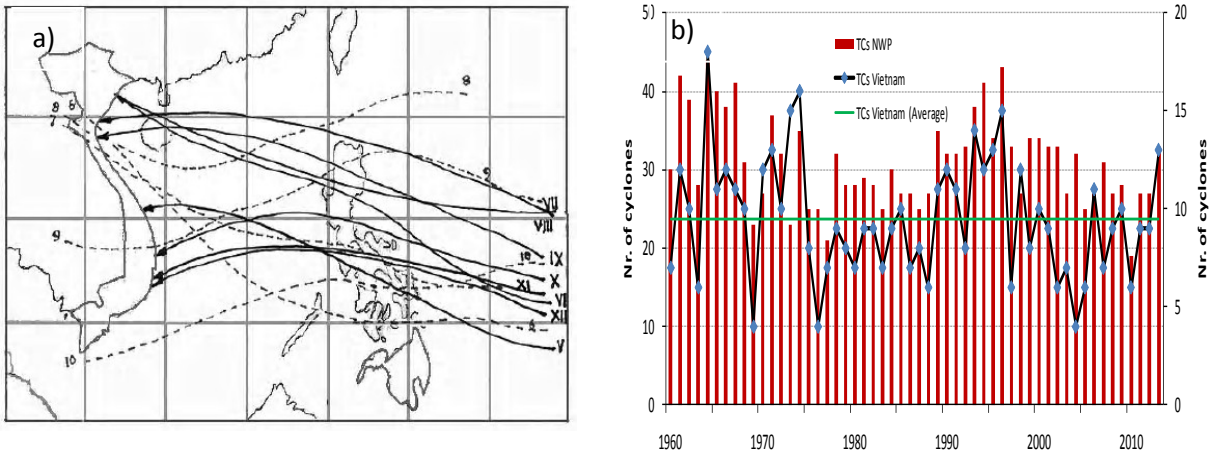

Figure 4.6: a) Average position of tropical cyclones (solid line) and ITCZ (dash line). The roman numbers refer to the month of the year (Hydrometeorology Atlas of Vietnam, 1994) and b) Average number of tropical clones per year in the northwest pacific (TCs NWP) region and Vietnam (TCs Vietnam) during 1960-2013. Green colour line refers to annual number of tropical cyclones that cross the coast of Viet Nam from the Vietnam Eastern Sea.

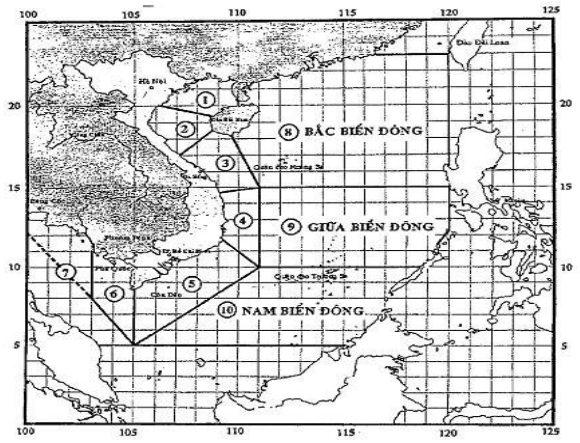

a) Vietnam territorial waters, taken from decision No 46/2014/QĐ-TTg dated August 15, 2014.

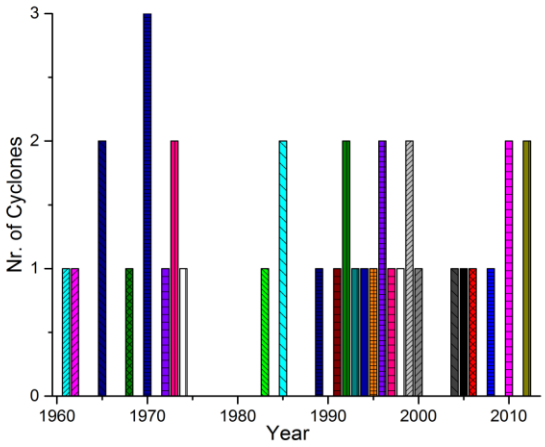

b) The number of TCs landed Binh Thuan-Ca Mau territorial water of Vietnam (1960-2013).

Figure 4.7: a) Vietnam territorial waters and b) the number of TCs landed Binh Thuan-Ca Mau region. Note: 1) North of Tonkin Gulf, 2) South of Tonkin Gulf, 3) Quang Tri-Quang Ngai, 4) Binh Dinh-Ninh Thuan, 5) Binh Thuan-Ca Mau, 6) Ca Mau-Kien Giang, 7) Thai Lan Gulf, 8) North of eastern sea, 9) Center of eastern sea and 10) South of eastern sea.

4.2.2 Climate change projects

On a global scale, the reports of IPCC are the ones that received most attention. Important milestones are the IPCC FAR (IPCC, 1990), IPCC SAR (IPCC, 1995), IPCC TAR (IPCC, 2001), IPCC AR4 (IPCC, 2007) and IPCC AR5 (IPCC, 2013). On the regional scale, South-eastern Asia it is paid much attention to in the ADB's climate change projects. In Vietnam, climate change scenarios are firstly published in 1994 in the ADB's report on changes in climate in Asia (MONRE, 2009). Nguyen *et al*. (1992) described the potential socio-economic effects of climate change on Vietnam. Although these results are just preliminary investigations, the sectors affected by climate change are identified (e.g., energy-environment interactions, human health, the mangrove ecosystem, the coastal zone and agriculture) (Nguyen *et al*., 1992). The most important milestones of time history regarding climate change scenarios produced for Vietnam are: (i) in 1994, (ii) 1998, (iii) 2009, (iv) 2012 and (v) 2015 coming up (see more in Appendix 7). Furthermore, individual scientists such as Nguyen (2007) and Tan *et al*. (2010) significantly contribute to the study results of climate change in Vietnam. According to the IPCC AR4 (IPCC, 2007), the mean annual temperature increased by 0.27 °C for the period 1961-1980 in comparison with the period 1895-1980. An increasing trend in annual rainfall in the northern part of Vietnam and a decreasing trend in the southern part are observed since the 1960s.

Tran (2011) investigated the relationship between summer monsoon and climate change. The data for latitude wind speed at 850 mb during the period 1950-2010 obtained from the NCAR/NCEP was used to investigate the variability of summer monsoon features in Vietnam. The results revealed that some of summer monsoon characteristics were changed: The time of the first and last summer monsoon day, the duration and rhythm of summer monsoon and the intensity of wind, but any conclusions made in this study were correlation based according to the SCSSM index (Tran, 2011).

The results of a study about the correlations between climate change and atmospheric flows show a translucence variation in Southeastern Asia, but it is obvious that monsoon rainfall varies under climate change in Southeastern Asia. Moreover, the intensity of intermittent flooding of some areas during the monsoon season is observed (Loo *et al*., 2014).

According to Nguyen (2009), the number of hot days during 1991-2000 has significantly increased in comparison with prior decades, especially in the southern and central parts of Vietnam. The study of the temperature trend for the four seasons during 1960-2007 revealed an increase in temperature of about 0.1 to 0.4, 0.04 to 0.17, 0.1 to 0.18, and 0.1 to 0.15 ^{o}C per decade in winter, spring, summer and autumn, respectively (Nguyen *et al*., 2010).

The reports on climate change published by the Ministry of Natural Resources and Environment of Vietnam (MONRE) described the changes in climate for different climate regions in Vietnam (see Table 4.1) for the past and the future under climate change scenarios (MONRE, 2009; MONRE, 2012a; MONRE, 2012b). In the most recent projects the coastal regions of Vietnam are in the main focus (Meon *et al.*, 2014; Nguyen *et al*., 2014).

Table 4.1: Changes in temperature and precipitation during 1960-2009 for climate regions in Vietnam (MONRE, 2012a).

Climate regions	Temperature (^{o}C)			Precipitation (%)		
	January	July	Year	Nov-Apr	May-Oct	Year
Northwest	1.4	0.5	0.5	6	-6	-2
Northeast	1.5	0.3	0.6	0	-9	-7
Red river delta	1.4	0.5	0.6	0	-13	-11
North central coast	1.3	0.5	0.5	4	-5	-3
South central coast	0.6	0.5	0.3	20	20	20
Central highlands	0.9	0.4	0.6	19	9	11
South region	0.8	0.4	0.6	27	6	9

4.2.3 Impacts of climate change in Vietnam

4.2.3.1 Overview of climate change impacts

It is well known that the impacts of climate change have been broadly occurring and potentially affecting many sectors of human life as well as natural disasters on spatial and temporal scales. In the agriculture field, for instance, the two deltas of the Mekong and Red River, two key rice and agricultural producing areas in Vietnam, are considered to be severely affected by climate change (MONRE, 2008). Thus, it is of great importance to identify changes in climate as well as its impacts on Vietnam. According to the National strategy on climate change presented by the Prime Minister of Vietnam in 2011, climate change impacts cause costs of about 1.5% GDP per year. Moreover, tropical cyclones, floods, flash floods, landsides, droughts, saltwater intrusions and other calamities have done significant damage to human life and assets and have resulted in more than 9500 deaths and missing persons cases during the 10 years (2001-2010). Additionally, the sea level may rise by about 75 cm to 1m by the end of the 21st century in comparison with the baseline period of the 20 years

(1980-1999)[20]. With an increase of the sea level by 1m, roughly 40% of the Mekong Delta, 11% of the Red River Delta and 3% of the coastal provinces will be inundated. In addition to this, about 10 to 12% of Vietnam's population would be directly affected. It would also cause a loss of 10% of the GDP.

The overall perspective of the impacts of climate change on main sectors include the field of natural resources, agriculture and forestry, energy, health, aquiculture, environment and tourism. The level of vulnerability is different for each sector and region. Table 4.2 shows the climate change impacts and vulnerabilities by region.

Table 4.2: Impacts of climate change on sectors and vulnerability objects (MONRE, 2011).

Regions	Impacts of climate change	Impacted sectors due to climate change	Vulnerable population
Coastal and islands regions	(1) Sea level rise (2) more frequent tropical cyclones (3) increase in the number of flood and landside events (central regions).	(1) Agriculture and food security (2) aquaculture (3) transportation (4) construction and development of infrastructure for urban and rural areas (5) environment, water resources and diversity (6) health and other social issues (7) business services, commerce and tourism.	(1) Poor farmers and fishermen in coastal regions (2) elderly people, woman and children.
Delta regions	(1)Sea level rise (2) more frequent tropical cyclones (3)more floods and landslides (north regions) (4) saltwater intrusion.	(1) Agriculture and food security (2) aquaculture (3) industry (4) transportation (5) construction and development of infrastructure for urban and rural areas (6) environment, water resources and diversity. (7) health and other social issues (8) business services, commerce and tourism.	(1) Elderly people, women and children.
Mountains and midlands	(1) More floods and landside events (2) increase in extreme weather events (3) increase in temperature and	(1) Food security (2) transportation (3) environment, water resources and diversity (4) health and other social issues	(1) Dwellers on mountains, especially ethnic minorities (2) Elderly people, women

[20] http://chinhphu.vn/portal/page/portal/English/strategies/strategiesdetails%3FcategoryId%3D30%26articleId%3D10051283

	drought (highland, north mountain and central regions)		and children
Urban	(1) Sea level rise (2) higher frequency of tropical cyclones (3) more flood and inundated events (4) increase in temperature	(1) Industry (2) transportation (3) construction and development of infrastructure for urban and rural regions (4) environment, Water resourcesand diversity (5) health and other social issues (6) business services, commerce and tourism (7) energy	(1) Poor people (2) elderly people, women and children(3) immigrants

4.2.3.2 Impacts of climate change on surface water resources

Water resources are a key for human life. It is, however, also a big challenge for Vietnam due to issues of quantity and quality, especially the effects of natural disasters such as floods or flash floods under a global warming. Vietnam has a dense river network of 2360 rivers with a length of over 10 km, comprising 15 large river systems with a catchment area of more than 2500 km^2. The total area of all international catchments within and outside Vietnam is close to 1.2 million km^2 (WB, 2003). The largest river systems are Red River, Thai Binh, Bang Giang-Ky Cung, Ma, Thu Bon-Vu Gia, Ba, Lam, Dong Nai and Cuu Long. The annual water availability in Vietnam amounts to about 835 billion cubic meters. Two thirds of Vietnam's water resources originate from neighbouring countries; the rest falls as rain on the country's territory. There is a shortage of water during dry season months (6-7 months), when only 15 to 30% of the total amount of the water resources is available.

This deficiency is a result of the uneven distribution of annual rainfall (about 1960 mm) in Vietnam. The issues of water resource availability for different regions in Vietnam are presented in detail in the report of the World Bank (WB, 2003). The floods, flash floods, severe seasonal droughts and low river flow during prolonged dry season are highlighted for south central coast region. Until now, the changes in temperature and precipitation are continuing. Thus, it is of utmost importance to assess the impacts of global warming on water resources. The impacts of climate change on water resources of major river catchments are presented in Table 4.3. Results are projected for future under a medium climate change scenario B2 in comparison with the baseline period 1980-1999 (see Table 4.3).

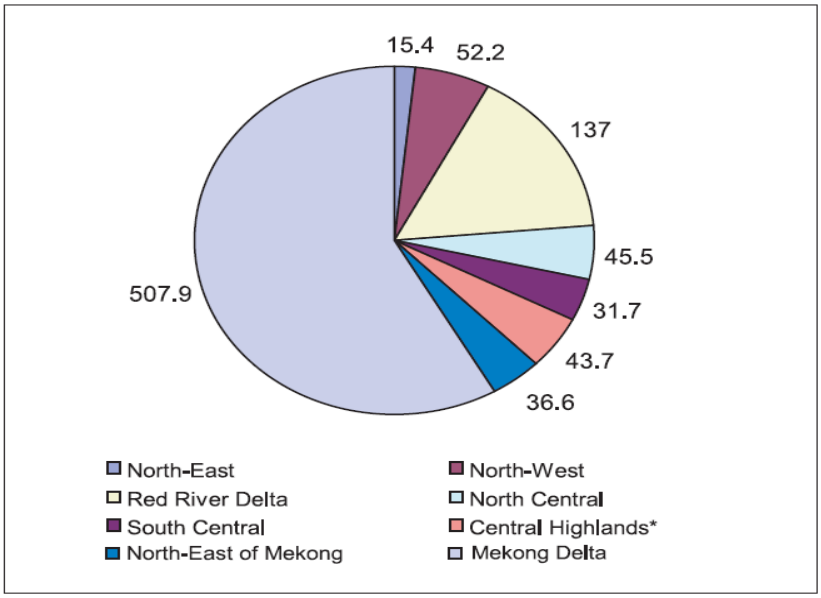

Figure 4.8: River run-off per Region (billion m^3/year) (WB, 2003).

Table 4.3: Changes in water resources in major river catchments (%) caused by climate change a medium climate change scenario B2 in comparison with the baseline period 1980-1999 (Nguyen *et al.*, 2010).

Catchments	wet season stream flows			dry season stream flows			annual stream flows		
	2020	2060	2100	2020	2060	2100	2020	2060	2100
Ky Cung	+4.1	+11.9	+18.3	-8.9	-12.4	-15.0	+1.3	+6.6	+10.9
Red River	+8.2	+12.0	+15.1	+10.4	+14.6	+18.0	+8.9	+12.8	+16.0
Ca	+2.8	+9.0	+14.1	+1.8	+5.6	+8.7	+2.3	+7.3	+11.5
Ba	+2.7	+8.0	+12.4	-2.8	-6.4	-9.3	+2.7	+5.6	+8.9
Thu Bon	+1.47	+6.56	+11.0	-6.7	-9.7	-12.2	-0.72	+2.22	+4.8
Se San	+0.84	+1.98	+2.97	+1.43	+0.34	-0.53	+1.06	+1.36	+1.66
Dong Nai	+1.9	+1.9	+1.9	-21.8	-22.2	-22.5	-4.6	-4.7	-4.8

4.3 Selection of a climate change scenario for the Thi Vai river catchment

The greenhouse gases (GHGs) emission is the main cause for the changes of the current and future climate such as global warming and melting ice at the poles of the earth. Since 1996, different emission scenarios have been developed to project future climate change based on different assumptions about the driving forces such as socio-economic and technological development and other factors. In the IPCC TAR and IPCC AR4, the Special Report on Emissions Scenarios (SRES) was the basis for projections for future changes in climate. These emission scenarios consist of 40

different scenarios (for 35 of them, data about a range of gases needed for climate models, is provided) organized into families. In the SRES, four major families of emission scenarios including A1, A2, B1 and B2 are designated as "makers". These scenario families are briefly described as follows:

A1 scenario: The A1 scenario family is subdivided into three groups that describe the changing trend of technology in energy systems: energy sources from fossil products (nonrenewable or fossil intensive) (A1FI), non-fossil energy sources (A1T) or a balance across all sources (A1B).

A2 scenario: This scenario describes a world uneven. Developing countries insignificantly affected developing countries. Population growth is continuously expected. Economic development is regionally oriented rather than a global change. Technological changes are more fragmented and slower than other storylines.

B1 scenario: It has global population peaking in the mid-21st century and declining thereafter as in the A1 scenario family. Economic structures are focused on a service and information technology with an introduction of clean and resource-efficient technologies. It aims at global solutions to ensure a sustainable environmental development and protection.

B2 scenario: This scenario depicts an increasing global population, but does not peak in the mid-21st century. Emphasis is on local solutions to addressing economic, social and environmental sustainability. Economic development is less rapid than in the B1 and A1 but with more diverse technological change than in the A1 and B1 storylines.

Table 4.4: Overview of greenhouse gasses (GHGs), ozone precursors and sulfur emissions for the SRES scenario groups by the year 2100. Numbers are for the four markers and (in brackets) for the range across all scenarios from the same scenario group (standardized emissions) (IPCC, 2007).

Scenario	CO2 (GtC)	CH4 (MtCH4)	N2O (MtN)	HFC, PFC, SF6 (MtC equiv.)	CO (Mt CO)	NMVOCs (Mt)	NOx (MtN)	SOx (MtS)
A1B	13.5 (13.5- 17.9)	289 (289- 640)	7.0 (5.8- 17.2)	824 combined	1663 (1080- 2532)	193 (133- 552)	40.2 (40.2- 77.0)	27.6 (27.6- 71.2)
A1C	(25.9- 36.7)	(392- 693)	(6.1- 16.2)	same as in A1	(2298- 3766)	(167- 373)	(63.3 - 151.4)	(26.9- 83.3)
A1G	(28.2- 30.8)	(289- 735)	(5.9- 16.6)	same as in A1	(3260- 3666)	(192- 484)	(39.9 - 132.7)	(27.4- 40.5)
A1T	(4.3- 9.1)	(274- 291)	(4.8- 5.4)	same as in A1	(1520- 2077)	(114 -128)	(28.1- 39.9)	(20.2- 27.4)
A2	29.1 (19.6- 34.5)	889 (549- 1069)	16.5 (8.1- 19.3)	1096 combined	2325 (776- 2646)	342 (169- 342)	109.2 (70.9- 110.0)	60.3 (60.3- 92.9)
B1	4.2 (2.7- 10.4)	236 (236- 579)	5.7 (5.3- 20.2)	386 combined	363 (363- 1871)	87 (58- 349)	18.7 (16.0- 35.0)	24.9 (11.4- 24.9)
B2	13.3 (10.8- 21.8)	597 (465- 613)	6.9 (6.9- 18.1)	839 combined	2002 (661- 2002)	170 (130- 304)	61.2 (34.5- 76.5)	47.9 (33.3- 47.9)

In the IPCC AR5 (IPCC, 2013), the updated emission scenarios are the Representative Concentration Pathways (RCPs) (i.e., RCP2.6, RCP4.5, RCP6 and RCP8.5). As pointed out by van Vuuren *et al*. (2011),

the “representative” refers to a large set of scenarios within each RCPs. The “concentration pathway” stands for full-integrated scenarios. According to IPCC (2013), the four RCPs are four greenhouse gas concentration, not emission trajectories. The selection of these RCPs is based on their total radiative forcing pathway and level by 2100. The four RCPs, RCP2.6, RCP4.5, RCP6 and RCP8.5, are named according to a possible range of radiative forcing values in the year 2100 (i.e, from +2.6 to 8.5 W/m^2) relative to pre-industrial levels.

The selection of scenarios, which are further analysed for a specific region, as well as the baseline period depends on the purpose of study and the socio-economic circumstances. The climate change scenarios for Vietnam were developed based on the released climate change scenarios of the Intergovernmental Panel on Climate Change. To be more precise, the Minister of Natural Resource and Environment, Vietnam officially approved three climate change scenarios of A1F1 (High emission scenario), B2 (Medium emission scenario) and B1 (Low emission scenario) in June 2009. Based on these scenarios, change for temperature and rainfall were simulated for seven climate regions in Vietnam with the baseline period 1980–1999 (MONRE, 2009), updated in 2012 (MONRE, 2012). In this study, the SRES A1B scenario was used to project changes in climate. This scenario belongs to the A1 scenario family and is used to assess climate change impacts on hydrological characteristics for the future in the Thi Vai River catchment.

5 ANALYSIS OF OBSERVATIONAL DATA

The weather datasets at a global scale play an extremely important role in analysing the climate system behaviours. These datasets, which are provided by terrestrial weather stations, radars, weather balloons, satellites as well as measuring instruments on aircrafts, ships and buoys (see Figure 5.1), are also an essential resource for understanding the variability and change in climate. By using the WMO GTS[21] system, the metadata have been exchanged and analysed in different projects. Thus, the understanding of weather and climate has been more detailed.

To date, challenges in handling observational data is local changes in station location and land use, measurement errors and the decision on filling missing records. The quality of hydro-meteorological data is always a key to the success of a climate impact project. In a typical set of data, there are two main types of errors: random and systematic errors. The random errors may arise from the measuring devices or the environmental circumstances that are unpredictable or unknown during the experiment. Whereas the systematic error may occur because of insufficient handling of the measuring devices or a system failure.

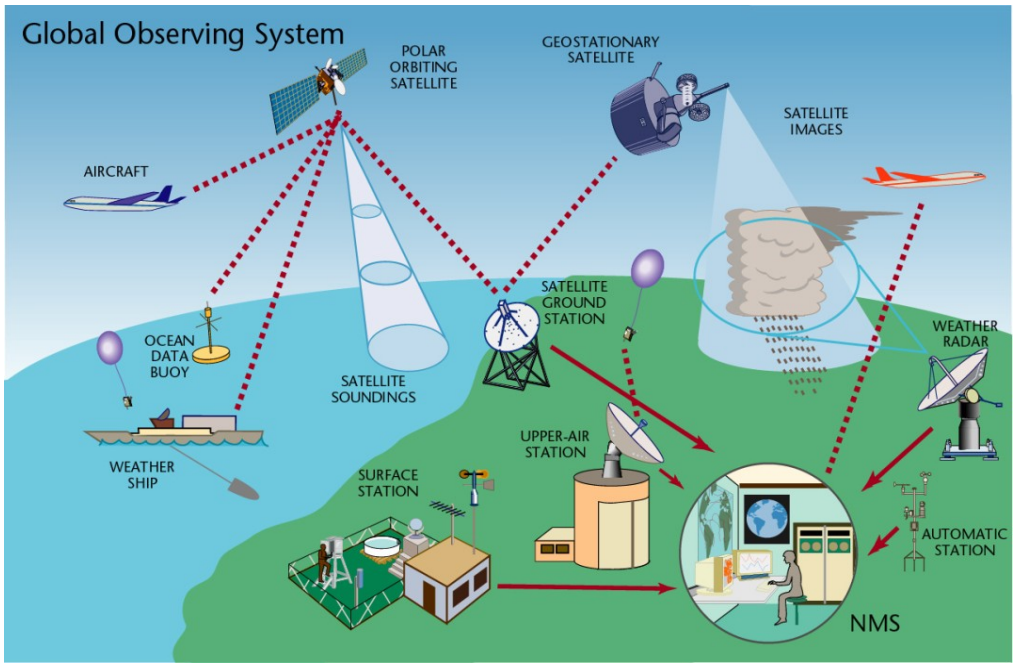

Figure 5.1: An illustration of the instruments that comprise the WMO Global Observing System (WMO-No. 1069).

To ensure a high quality of the obtained datasets, all terrestrial meteorological data is checked and processed in this study, focusing on the precipitation and temperature variables. The following analysis steps are carried out:

[21] The Global Telecommunication System (GTS) is defined as: The co-ordinated global system of telecommunication facilities and arrangements for the rapid collection, exchange and distribution of observations and processed information within the framework of the World Weather Watch (https://www.wmo.int/pages/prog/www/TEM/index_en.html)

- Checking observational data limits (i.e., upper and lower warning levels) for a period that is as long as possible: The aim of this work is to identify the suspicious and missing data. These limits are calculated as follows:

  Upper warning level = mean + 3*(standard deviation)

  Lower warning level = mean - 3*(standard deviation)

  After calculating, the plot of the yearly values shows the upper and lower warning levels. Values are marked if they are extremely higher or lower than other observations in the climatological statistical series at the same station or extremely higher or lower than other values at the neighbouring stations. This approach is also used in Phan (2010).
- The detected suspicious and missing records are checked against the obtained data. The data from satellite cloud images from the Japan Meteorological Agency and radiosonde data at Tan Son Hoa station are also used as the references. The detected missing records are estimated and filled by the average value for that station or for the neighbouring stations in case that the average annual precipitation for the station differed from the one of stations used for interpolation by less than 10%. Alternatively, following a suggestion from the handbook of hydrology (ASCE, 1996), the method of normal ratio (see section 5.1.1) is applied. During the processing, however, the highest priority is to maintain the original records.
- Checking for inconsistency of records by the double mass curve method: In order to ensure that the detected trends are not caused by a change in the gauge location or the observational methods, the observational data is checked by the double mass curve method. The principle of this method is that when each recorded datum comes to the same parent population, it will be consistent.
- Homogeneous tests for the detection of trends: The homogeneity of observed datasets is tested for the detection of trends in order to determine whether or not in the past there were changes in climate in the Thi Vai River catchment.
- Areal observational data estimation: One of the research objects is to downscale the global climate variables to the small basin scale. However, precipitation measuring stations are not available within the catchment. Thus, the main purpose of interpolation procedures is to provide climate data information for the Thi Vai river catchment.

5.1 Estimation of missing precipitation records

5.1.1 Introduction to research methods

In hydrological and meteorological studies, many methods for estimating the missing values are developed, such as linear or multi regression, arithmetic average or distance power. In the handbook of hydrology, however, it is recommended to apply the inverse distance weighting and normal-ratio methods. The arithmetic average is used in this study if the average annual precipitation of the station under consideration differs from those of the interpolation stations by less than 10%. Otherwise, the normal-ratio method is applied.

Arithmetic Average Method: This method estimates the missing precipitation based on the arithmetic average value from the same stations in this case study. It is given as:

$$P_{ijk} = \frac{\sum_{l=1}^{N-x} P_{ijl}}{N-x} \quad (5.1)$$

where:

P_{ijk} is missing precipitation record on the i^{th} day of j^{th} month of k^{th} year

N is the number of years in the period under consideration

x is the number of missing data (of years)

Normal-ratio Method: The idea of this method is to estimate the missing values as the weighted average of edging stations in a relationship of the following form:

$$P_x = \frac{1}{N} \sum_{i=1}^{N} \frac{N_x}{N_i} P_i \quad (5.2)$$

where:

P_x is the missing precipitation for the 'x' station [mm]

P_i is the precipitation at the i^{th} station for the same period [mm]

N_x is the annual precipitation for the 'x' station [mm]

N_i is the annual rain for the i^{th} station [mm]

N is number of rain gauges [-]

$N_x/(N*N_i)$ is normalized weight [-]

5.1.2 Analysis results

Considering thirteen rain gauges, the missing precipitation records at the stations Binh Chanh and Cam My are filled. At Cam My station, the original data show missing precipitation records from Sep 1, 1982 to Sep 15, 1982 during a 33-year period (1981-2013) (see Figure 5.2). These records are filled based on the Equation 5.1. The result (i.e., for 1/9/1982) is given in Table 5.1.

Table 5.1: Estimation of daily precipitation at Cam My station by arithmetic average method.

	Observational precipitation on the 1st September at Cam My station (mm)								Estimated precipitation (mm)
Year/value	1981	1983	1984	1985	1986	1987	1988	1989	7.3
	3.7	0	17.6	0	0	0	0	0	
	1990	1991	1992	1993	1994	1995	1996	1997	
	0	0	0	11.4	12.8	45	28.6	0	
	1998	1999	2000	2001	2002	2003	2004	2005	
	2.1	9.3	0	0	0	0	44.3	0	
	2006	2007	2008	2009	2010	2011	2012	2013	
	3.4	0	0	24	21.3	0	0	9.4	

At Binh Chanh station, the percentage of the missing data is approximately 6% for the 34-year of 1980-2013 (see Figure 5.2). The analysis of four precipitation measurement stations shows a high

correlation coefficient on a monthly scale and a moderate one on a daily scale (see Table 5.2). The shorter the distance between two stations, the higher is the correlation coefficient. The long-term averages of observed annual rainfall at Binh Chanh, Tan Son Hoa, Mac Dinh Chi and Hoc Mon are 1579, 1911, 1782, and 1441 mm respectively. In comparison with annual rainfall at Binh Chanh station, the rainfall at the other stations differs by about 21 (Tan Son Hoa), 12.8 (Mac Dinh Chi) and 8.8% (Hoc Mon). Thus, the amount of precipitation at Tan Son Hoa and Mac Dinh Chi stations are used to estimate the missing precipitation records for Binh Chanh station by the normal ratio method based on Equation 5.2. As mentioned in the previous chapters, precipitation characteristics (e.g., wet days or intensity) are unevenly in space and time in tropical region in general and southern Vietnam in particular. The closest precipitation measuring station from the Cam My station are remarkably far (about 30 km), whereas the distance from Binh Chanh station to the closest station is not far (about 3 km) (see Figure 3.4). This is considered to be one of reasons to select two different methods for two different stations.

Table 5.2: Correlation coefficients between precipitation measurement stations Binh Chanh (BC), Tan Son Hoa (TSH), Mac Dinh Chi (MDC) and Hoc Mon (HM).

Stations	On daily scale				On monthly scale			
	BC	TSH	MDC	HM	BC	TSH	MDC	HM
BC	1				1			
TSH	0.44	1			0.82	1		
MDC	0.45	0.78	1		0.83	0.93	1	
HM	0.36	0.48	0.43	1	0.78	0.84	0.83	1

The normalized weights for Tan Son Hoa (TSH) and Mac Dinh Chi (MDC) stations are 0.413 and 0.443 respectively. The estimated precipitation is tabulated in Table 5.3.

Table 5.3: Estimation of daily precipitation at Binh Chanh station by normal ratio method.

Date	Observed rainfall (mm)		Estimated rainfall at Binh Chanh (mm) Weights		Date	Observed rainfall (mm)		Estimated rainfall at Binh Chanh (mm) Weights	
	MDC	TSH	0.443	0.413		MDC	TSH	0.443	0.413
4/1/1985	0	0.1	0.0		4/16/1985	0	0.1	0.0	
4/2/1985	0	0	0.0		4/17/1985	0	28.9	6.0	
4/3/1985	0	0	0.0		4/18/1985	5.6	2.8	1.8	
4/4/1985	0	0	0.0		4/19/1985	0	0.2	0.0	
4/5/1985	0	0	0.0		4/20/1985	1.9	0.6	0.5	
4/6/1985	0	0	0.0		4/21/1985	2.4	0	0.5	
4/7/1985	0	0	0.0		4/22/1985	16.9	21.9	8.3	
4/8/1985	0	0	0.0		4/23/1985	39.2	28.9	14.7	
4/9/1985	0	0	0.0		4/24/1985	0.7	0.2	0.2	
4/10/1985	0	0	0.0		4/25/1985	25.5	21.6	10.1	
4/11/1985	0	0	0.0		4/26/1985	14.8	1.6	3.6	

4/12/1985	0	0	0.0	4/27/1985	50.6	42.2	19.9
4/13/1985	0	0	0.0	4/28/1985	1	0	0.2
4/14/1985	0	0	0.0	4/29/1985	22.8	44.7	14.3
4/15/1985	0	0	0.0	4/30/1985	50.4	29.4	17.2

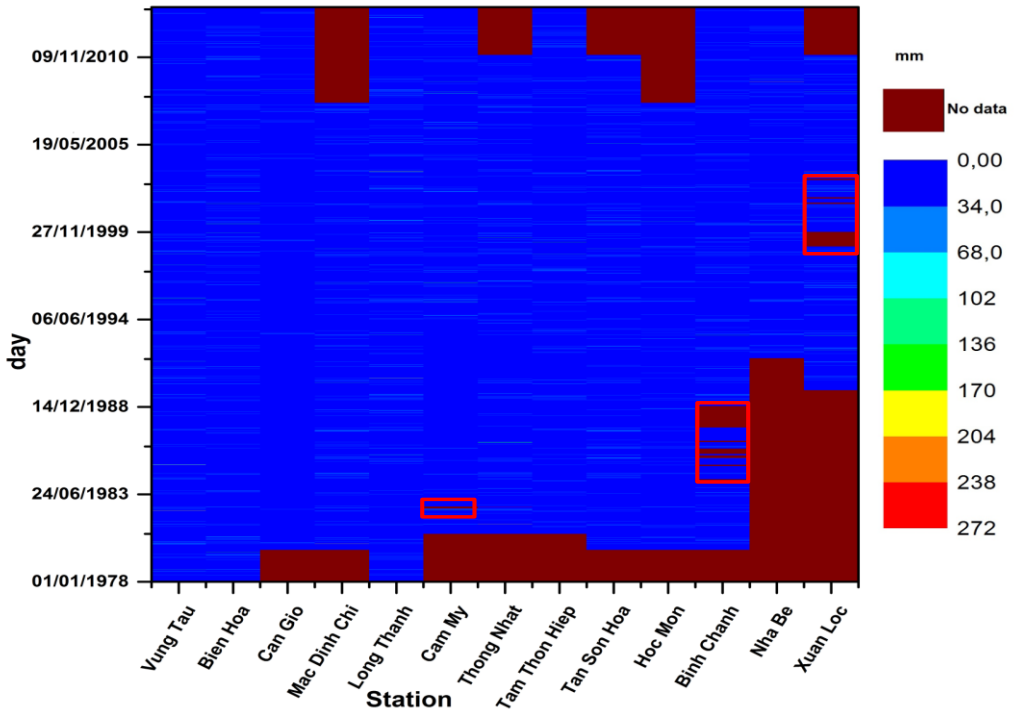

Figure 5.2: Missing observational daily precipitation before gap filling (red boxes).

5.2 Double mass curve

5.2.1 Introduction

The double mass curve is a plot of the accumulated rainfall data for a specific station against the mean of the cumulative rainfall for a group of surrounding stations. This method is widely used to analyse hydro-meteorological data in order to identify whether it is needed to adjust the data because of local changes such as a change in the gauge location or surrounding conditions. If any changes in a series of observational data is identified, precipitation records are corrected by the coefficients computed from the double mass curve. The corrected precipitation is estimated by the multiplication of the observational value with a correction factor α as shown in the following equation:

$$P_c = P_o \frac{M_c}{M_o} = P_o \alpha \tag{5.3}$$

where:

P_c is the corrected precipitation [mm]

P_o is the observed precipitation [mm]

M_c is corrected slope of the double mass curve [-]

M_o is original slope of the mass curve [-]

5.2.2 Analysis results

The stations in the study area are divided into three groups based on their spatial location. The first group includes three stations (Tam Thon Hiep, Can Gio, and Vung Tau). The second group contains five stations (Bien Hoa, Thong Nhat, Long Thanh, Xuan Loc, and Cam My). The stations Hoc Mon, Tan Son Hoa, Mac Dinh Chi, Nha Be and Binh Chanh belong to the third group. Aggregated to an annual time step, the double mass plot between the accumulated values for the test station and those for the station groups is drawn for the available periods for each station after gap filling. The double mass curves for some stations and the corresponding groups are shown in Figure 5.3. The breakpoints refer to a change in the observed rainfall amount (e.g., see Figure 5.3b). The other rainfall measurement stations are also analysed and there is no considerable break in the slope of the curves. This indicates that there is no inconsistency in the station data.

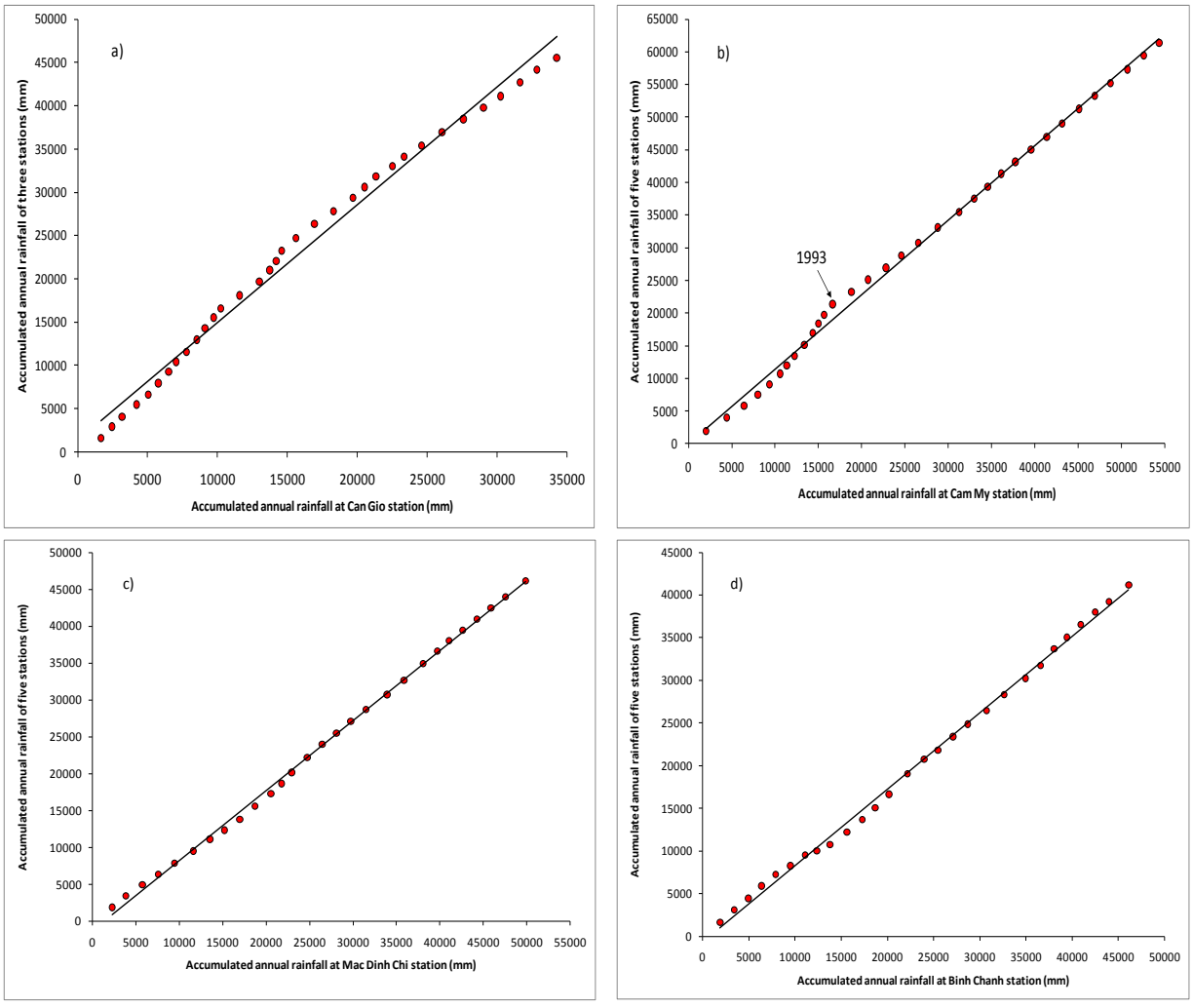

Figure 5.3: Double mass curves for the rainfall at the stations a) Can Gio, b) Cam My, c) Mac Dinh Chi and d) Binh Chanh.

As observed in Figure 5.3b, there is a significant change in the amount of observed rainfall in 1993 at Cam My station. These breakpoints are also found at the other stations (see Figure 5.3a-b). An analysis and checking are conducted for the detected inconsistency of precipitation records, but do not find any local changes like the gauge location. Thus, it can be concluded that the observational data at the four stations before and after the breakpoints is only caused by a change in observed precipitation series. Moreover, as mentioned earlier, the highest priority is to maintain the original records; therefore, no adjustment of the rainfall time series is made.

5.3 Homogeneous tests for the detection of trends

5.3.1 Introduction to research methods

5.3.1.1 Mann-Kendall test

The Mann-Kendall (MK) test (Mann, 1945; Kendall, 1948) is used for the detection of trends in this study. The advantage of this test is that the results for identifying a trend are not affected by the magnitude of extreme values as it is the case for the different tests of regression or correlation. The replacement of rank among all the data in the sample for the value of each data is considered as a key of this method (Basseville and Nikiforov, 1993; Yue and Wang, 2004; Gocic and Trajkovic, 2013). The MK test statistics, represented by the parameter S, is briefly presented in the following:

Let x_1, x_2, …, x_n denote n data points where x_j represents the data point at time j. Each data value is compared to all other data values in ordered time series. The test parameter, S, is calculated as the sum of the sign(.) function for all data values with an assumed initial value of S = 0. Based on the difference in subsequent values, this function returns 1 for a positive and 1 for a negative argument. On other words, S is 1 or -1 when a value is higher and lower than the one of the previous time step respectively. If there is no difference in subsequent values, S is constant. An expression of S is given by:

$$S = \sum_{k}^{n-1} \sum_{j=k+1}^{n} \operatorname{sign}(x_j - x_k) \tag{5.4}$$

where:

n is the number of data points

x_j and x_k are the data values in the time series j and k and

$$\operatorname{sign}(x_j - x_k) = \begin{cases} +1 & \text{if } x_j - x_k > 0 \\ 0 & \text{if } x_j - x_k = 0 \\ -1 & \text{if } x_j - x_k < 0 \end{cases} \tag{5.5}$$

A positive value of S refers to an increasing trend. Conversely, a negative value of S refers to a decreasing trend. The strength of the trend is proportional to the absolute value of S. The null hypothesis H_o assumes that there is no trend (S = 0) in the data series. The alternative hypothesis H_1

assumes that there is an upward or downward trend. Instead of calculating the test parameter S, the test procedure can be computed by a normal approximation test Z_{MK} in case of a sample size of more than 10 values:

The variance of S is calculated by:

$$\mathrm{Var(S)} = \frac{\mathrm{n(n-1)(2n+5)} - \sum_{\mathrm{t=1}}^{\mathrm{g}} \mathrm{t_i(t_i-1)(2t_i+5)}}{18} \tag{5.6}$$

$$\mathrm{Z_{MK}} = \begin{cases} \dfrac{\mathrm{S-1}}{\sqrt{\mathrm{Var(S)}}} & \text{if } \mathrm{S} > 0 \\ 0 & \text{if } \mathrm{S} = 0 \\ \dfrac{\mathrm{S-1}}{\sqrt{\mathrm{Var(S)}}} & \text{if } \mathrm{S} < 0 \end{cases} \tag{5.7}$$

where:

n is the sample size

g is the number of tied groups. A tied group is a set of the sample data with the same values

t_i represents the number of data points in the i^{th} group.

In the case that the computed probability S is greater than the specific significance level α, H_o is rejected;The data series shows an increasing trend if Z_{MK} is positive and a decreasing trend if Z_{MK} is negative. There is no trend if the computed probability S is less than the level of significance (H_o is accepted). Within this study, the three different significance levels α 0.01, 0.05 and 0.1 are used to carry out the MK test. At the α significance levels 0.01, 0.05 and 0.1, the null hypothesis is rejected if $|\mathrm{Z_{MK}}| > 2.576, 1.96$ and 1.645 respectively.

5.3.1.2 Sen-Theil slope estimator

In order to calculate the strength of a trend (Q), the Sen's nonparametric method (Sen, 1968) has been applied. It is estimated by the slope of all data pairs (N = n(n-1)/2) as the following formula:

$$\mathrm{Q_i} = \frac{\mathrm{x_j - x_k}}{\mathrm{j-k}} \text{ for } \mathrm{i} = 1, \mathrm{N} \tag{5.8}$$

where:

Q is slope between the data points x_j and x_k

x_j and x_k are the data values at time j and k (j>k) respectively,

j is time after time k

The Sen's slope estimator is computed by the median slope as:

$$Q_{med} = \begin{cases} Q_{\left[\frac{N+1}{2}\right]} & \text{if N is odd} \\ \frac{Q_{\left[\frac{N}{2}\right]} + Q_{\left[\frac{N+2}{2}\right]}}{2} & \text{if N is even} \end{cases} \quad (5.9)$$

where:

N is the number of calculated slopes

To estimate the confidence limits for the nonparameter slope estimator Q_{med}, the upper (L_{uper}) and lower (L_{lower}) limits are computed as the following:

$$L_{upper} = (N + C_\alpha)/2 \quad (5.10)$$

$$L_{lower} = (N - C_\alpha)/2 \quad (5.11)$$

$$C_\alpha = Z_{MK(1-\alpha/2)}[Var(S)]^{1/2} \quad (5.12)$$

where:

$Z_{MK(1-\alpha/2)}$ is the 100*(1 - α/2) percentile of the standard normal distribution. The true slope at 100*(1- α) % confidence interval is given by:

$$L_{lower} \leq Q_{med} \leq L_{upper} \quad (5.13)$$

To estimate the nonparametric intercept coefficient (B) (Helsel and Hirsch, 1992) of the assumed linear trend, the following formula is used:

$$B = X_{med} - Q_{med} * T_{med} \quad (5.14)$$

where:

X_{med} is median of the n measurements x_1, …, x_n

T_{med} is median of the n times t_1, …, t_n

Q_{med} is the nonparametric slope estimate.

Autocorrelation effect

Von Storch and Navarra (1995), Pilon *et al*. (2002) and Yue and Wang (2004) show that the test results are significantly affected by the autocorrelation when the nonparametric tests are applied for the time series data. To overcome these problems, Von Storch and Navarra (1995) proposed to pre-whiten the time series data before applying nonparametric tests to detect trends. So, all of the rainfall time series data within this study was firstly examined for the presence of an autocorrelation coefficient (r_1) at the three significance levels of 0.1, 0.05 and 0.01 using the two-tailed test. The r_1 coefficient is computed by:

$$r_1 = \frac{\sum_{i=1}^{n-1}(x_i - \bar{x})(x_{i+1} - \bar{x})}{\sum_{i=1}^{n}(x_i - \bar{x})^2} \quad (5.15)$$

where $\bar{x} = \sum_{i=1}^{n} x_i$ is the mean of all values

The autocorrelation coefficient value at a given confidence interval depends on one-tailed or two-tailed test. In this study, the two-tailed test was tested against the H_o at the three significant levels of 0.1, 0.05 and 0.01. According to Anderson (1942), the probability limits on the correlogram are described in the following:

$$r_1(90\%) = \frac{-1 \pm 1.645\sqrt{n-2}}{n-1} \quad (5.16)$$

$$r_1(95\%) = \frac{-1 \pm 1.96\sqrt{n-2}}{n-1} \quad (5.17)$$

$$r_1(99\%) = \frac{-1 \pm 2.576\sqrt{n-2}}{n-1} \quad (5.18)$$

Where n is the sample size.

The time series data is serially correlates if the computed value r_1 lies between the upper and lower limits of the confidence interval; the method of pre-whitening (Yue *et al*., 2002) was applied to eliminate the serial correlation effect for both the MK test and the Sen's slope. Contrarily, the MK test and the Sen's slope were directly applied to the original series data.

5.3.1.3 Cumulative sum charts

To identify abrupt changes in a climate series, cumulative sum charts (CuSum) (Efron and Tibshirani, 1994) is a useful approach. This method is briefly described as the follows:

Let x_1, x_2, …, x_n represent n data points. The cumulative sums S_0, S_1, S_2, … S_n are calculated by these steps:

(1) Calculate the average of sample data ($\bar{x}$),

(2) Set the cumulative sum at zero $S_0 = 0$,

(3) Calculate the other cumulative sums: $S_i = S_{i-1} + (xi - \bar{x})$, for i = 1, .., n.

The cumulative sum will always be positive with an upward slope if the calculated values are above the average value. In contrast, if the calculated values are below average value, the cumulative sum will always be negative with a downward slope during a given period. Thus, change points exist if there is a change in the shade of graph.

5.3.2 Analysis results

5.3.2.1 Temperature

The monthly mean temperature is analysed for the detection of trends for four meteorological stations (Bien Hoa, Vung Tau, Tan Son Hoa, and Xuan Loc). The MK test results show an upward trend for the entire region with different magnitudes and significances. Table 5.4 shows that a positive trend is detected at the stations Bien Hoa (0.2 ^{o}C/10 years; significance: 0.1) and Vung Tau (0.14 ^{o}C/10 years; significance: 0.01). At a significant level of 0.05, the MK test shows an upward trend for the station Xuan Loc (0.1 ^{o}C/10 years). There is an increasing trend of temperature for the station Tan Son Hoa (0.04 ^{o}C/10 years), but it is not significant.

Table 5.4: MK test for temperature at observation stations.

Station	Period	test Z	^{o}C/year	%/year	Significance
Bien Hoa	1981-2013	3.81	0.02	0.07	0.1
Tan Son Hoa	1981-2010	1.15	0.004	0.012	no significance
Vung Tau	1981-2013	4.11	0.014	0.048	0.01
Xuan Loc	1990-2011	2.18	0.01	0.036	0.05

The results from the analysis of abrupt changes (i.e., Vung Tau and Bien Hoa stations) are displayed in Figure 5.4. As can be seen in Figure 5.4, a change point is found in Oct 1998 at Vung Tau station. A change point is also identified around Jan 1990 at the station Bien Hoa.

5.3.2.2 Precipitation

The precipitation characteristics (previously mentioned in chapter 3) are analysed in this section for thirteen precipitation measurement stations during the observed period. The statistical MK test is conducted for the distinct period (see Table 5.5). The analyses of precipitation characteristics are presented in two groups; the first group includes data at the monthly (RRM), seasonal (RRS) and annual (RRA) scale and the second group includes about the results for the maximum consecutive wet (MCWD) and dry days (MCDD), the amount of wet days per month (MWD) and the maximum rainfall amount for 1-day (RX1day), 3-days (RX3day), 5-days (RX5day) and 7-days (RX7day).

Analysis of RRM, RRS and RRA

Figure 5.5 shows different trends with different significance levels for different stations for RRM, RRS and RRA. A decreasing trend for rainfall can be seen for most stations in June and August, followed by July. A significant increasing trend of rainfall is observed in March, followed by Jan, Feb, and May. It is noteworthy that half of the stations show a trend that is not significant. In other words, the trend is not significant for all significance levels for RRM, RRS and RRA. In general, a significant upward trend is observed for the dry season and a negative trend for the rainy season. Figure 5.5 shows the

spatial distribution of precipitation measuring stations and the observed trends at different significant levels during the given period. In order to get the strength of the consistent trend (Q), Sen's slope estimator was calculated at different time scales.

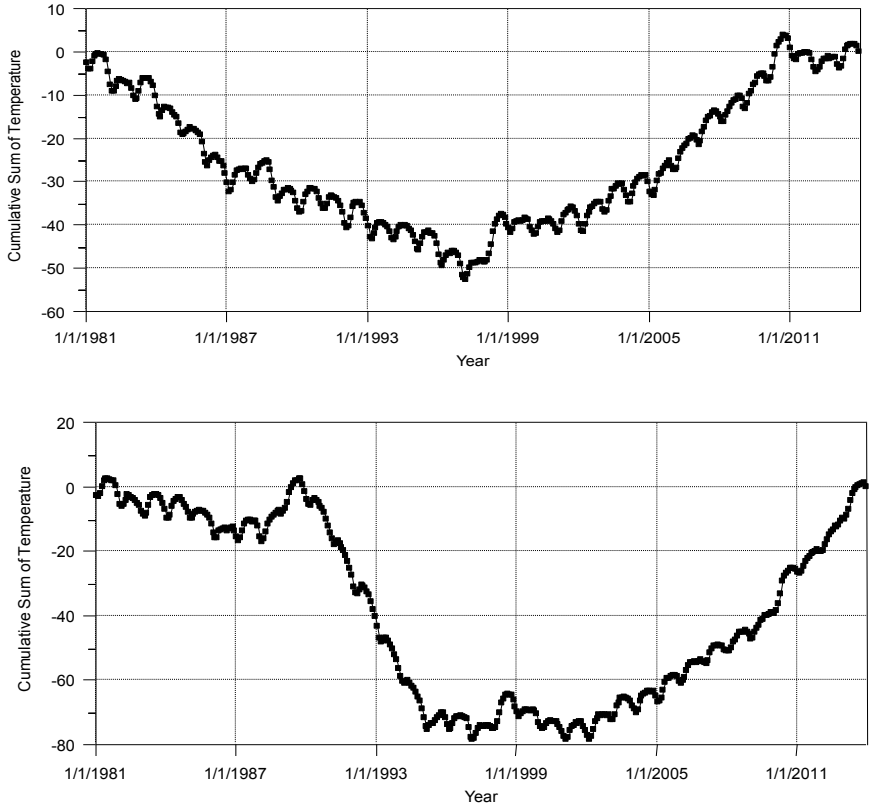

Figure 5.4: Cumulative Sum charts for mean temperature at the stations Vung Tau (*top*) and Bien Hoa (*bottom*) during 1981-2013.

Table 5.5: Results of Sen's slope for monthly and annual precipitation.

Stations	Bien Hoa	Cam My	Hoc Mon	Long Thanh	Mac Dinh Chi	Thong Nhat	Tan Son Hoa	Vung Tau	Can Gio	Tam Thon Hiep	Xuan Loc	Binh Chanh	Nha Be
Jan	0.06	0.00	0.00	0.00	0.00	0.00	-0.04	0.01	0.00	0.00	0.01	0.00	0.00
Feb	0.00	0.00	0.00	0.00	0.00	0.00	0.00	0.00	0.00	0.00	0.00	0.00	0.00
Mar	0.46	0.00	0.00	0.30	0.00	0.17	0.03	0.00	0.00	0.00	0.95	0.18	0.00
Apr	0.42	0.28	0.45	0.06	0.19	0.10	0.37	0.43	0.60	1.02	-0.48	0.37	-0.07
May	1.58	4.98	2.32	1.67	2.56	2.58	4.05	-0.91	3.20	2.33	6.00	4.42	1.93
Jun	-0.42	0.05	1.61	-2.22	-3.37	1.98	-4.50	-2.26	-0.72	-1.48	-2.66	-1.43	-5.59
Jul	2.65	7.47	0.85	2.92	-4.76	4.37	-2.99	-2.80	0.94	-0.05	0.59	3.90	-2.37
Aug	-0.65	-0.46	2.86	-0.90	-2.14	-0.07	0.95	-1.17	2.26	-2.44	1.01	-1.14	-4.51
Sep	-1.85	4.72	2.42	0.55	0.36	-1.37	-0.82	-1.08	2.17	-1.30	5.08	1.70	2.88
Oct	-0.41	1.43	5.57	0.05	-1.07	1.73	1.46	-1.28	3.75	0.71	1.25	1.20	-1.06
Nov	-1.30	0.37	0.12	2.28	-1.65	-0.93	0.51	0.11	1.03	0.18	4.36	0.74	1.94
Dec	0.09	-0.36	0.37	0.08	0.82	0.13	0.29	0.03	0.05	0.00	0.00	-0.35	-0.35
Annual	3.39	13.46	16.69	10.32	-7.81	9.47	-0.32	-7.02	18.36	1.39	18.19	2.63	-5.90

As shown in Table 5.5 and Table 5.6, the strongest increasing trend for annual precipitation is observed at the stations Can Gio, Xuan Loc, Hoc Mon and Cam My. The maximum downward trend for monthly precipitation was detected at the station Nha Be (5.59 mm in June during 22 years), followed by Mac Dinh Chi (4.76 mm in July during 28 years) and Vung Tau (2.8 mm in July during 36 years). The maximum upward trend in monthly precipitation is observed at the station Cam My (7.47 mm in July during 33 years), followed by Hoc Mon (5.57 mm in October during 28 years).

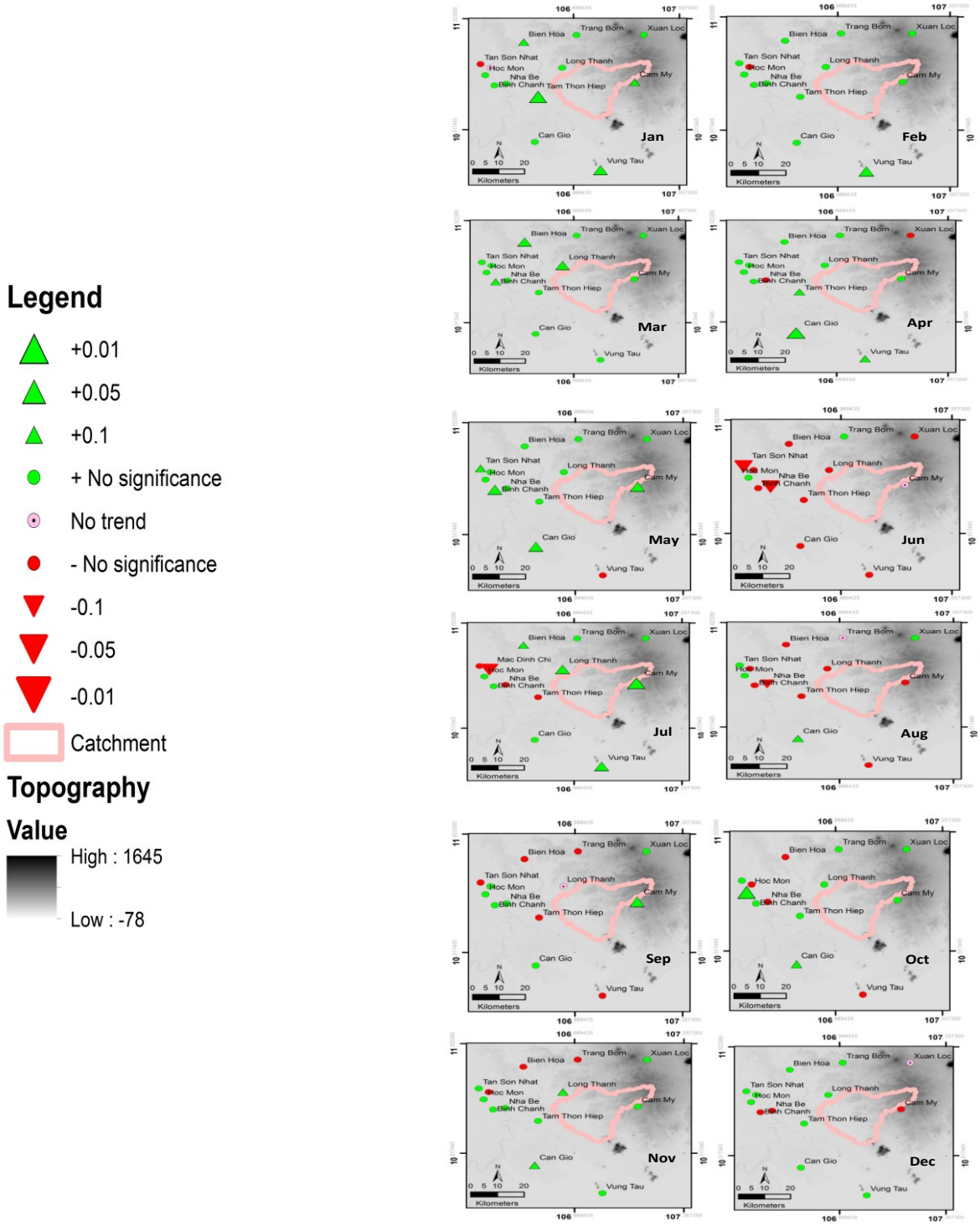

Figure 5.5: Spatial distribution of monthly precipitation trends with the results of the MK test at the significant levels 0.1, 0.05 and 0.01 (red colour refers to a decreasing trend, green colour refers to an increasing trend and rose dot cycle refers to no trend).

Similar to the monthly precipitation analysis, both positive and negative trends can be found for different stations for the different seasons (see Table 5.6). During the rainy season, the strongest negative trend is observed at the stations Nha Be (9.36 mm) and Vung Tau (8.3 mm) per one rainy season, whereas the strongest positive trend is seen at the stations Xuan Loc (15.4 mm), Hoc Mon (12.84 mm), Can Gio (15.2 mm) and Mac Dinh Chi (15.2 mm). In the months of dry season, a positive trend is recorded at all the stations (see Figure 5.5). Significant positive trends at considerable confidence intervals are found at the stations Long Thanh, Xuan Loc, Can Gio and Hoc Mon. A significant negative trend is only detected for Vung Tau station. Figure 5.6 shows the spatial distribution of seasonal and annual precipitation trends at different significant levels.

Table 5.6: Results of statistical tests for seasonal and annual precipitation.

Station	Characteristics	Maximum value	Minimum value	Mean	MK test	Sen's slope	Range
Tan Son Hoa	annual	2662.9	1321	1910.7	-0.1	-0.32	1341.9
	rainy season	2307.8	1165.9	1778.6	-0.81	-3.62	1141.9
	dry season	515.8	1.4	135.2	1.03	2.02	514.4
Vung Tau	annual	1970.8	930.6	1478.2	-2.65	-7.01	1040.2
	rainy season	1661.5	849.6	1345.0	-2.76	-8.3	811.9
	dry season	535.7	7.2	130.6	0.96	1.1	528.5
Long Thanh	annual	2870.9	1260.6	1983.2	2.06	10.32	1610.3
	rainy season	2725.7	1180.0	1843.7	1.51	8.18	1545.7
	dry season	522.7	4.7	141.3	0.71	1.34	518
Can Gio	annual	1672	395.1	1008.3	2.58	18.36	1276.9
	rainy season	1625.8	387.2	923.5	2.25	15.2	1238.6
	dry season	337	0.1	81.1	2.31	3.14	336.9
Bien Hoa	annual	2679.2	1230.1	1860.2	0.62	3.38	1449.1
	rainy season	2494.1	1200.9	1702.1	-0.02	-0.19	1293.2
	dry season	621.3	10.1	160	1.7	2.9	611.2
Tam Thon Hiep	annual	2115	1197.5	1530.4	0.23	1.38	917.5
	rainy season	1830.8	1065.7	1373.9	-0.29	-1.33	765.1
	dry season	583.9	26.7	156.7	0.6	0.88	557.2
Cam My	annual	2460.6	624.3	1646.9	0.97	13.4	1836.3
	rainy season	2145.4	571.1	1466.5	0.91	11.17	1574.3
	dry season	725.9	17.1	181.8	0.55	0.9	708.8
Thong Nhat	annual	2394.7	1307.4	1856	1.82	9.47	1087.3
	rainy season	2163.6	1249.9	1710.9	1.6	6.58	913.7
	dry season	623	12.6	145.9	0.28	0.81	610.4
Nha Be	annual	2405.9	1102	1708.7	-0.28	-5.9	1303.9
	rainy season	2032.9	1090.8	1554.6	-0.79	-9.36	942.1
	dry season	578	15.3	160.1	0.39	2.07	562.7
Binh Chanh	annual	2396.0	456.4	1505.3	0.17	2.62	1939.6
	rainy season	2160.1	402.2.1	1283.1	-0.07	-1.67	1757.9
	dry season	742.6	17.7	225.4	0.74	1.28	724.9
Xuan Loc	annual	2645	1677.6	2141.2	2.14	18.2	967.4
	rainy season	2431.1	1553.8	1982.3	1.72	15.4	877.3
	dry season	399.8	27	164.8	0.9	4.05	372.8
Hoc Mon	annual	2269.2	533.7	1440.9	1.68	16.68	1735.5
	rainy season	2032.6	533.7	1329.9	1.4	12.84	1498.9
	dry season	480.4	0	112	1.04	2.14	480.4
Mac Dinh Chi	annual	2431	1147	1782.1	-1.32	-7.8	1284
	rainy season	2316.4	1121.0	1672.8	2.25	15.2	1195.4
	dry season	473.2	0	111.6	1.23	2.52	473.2

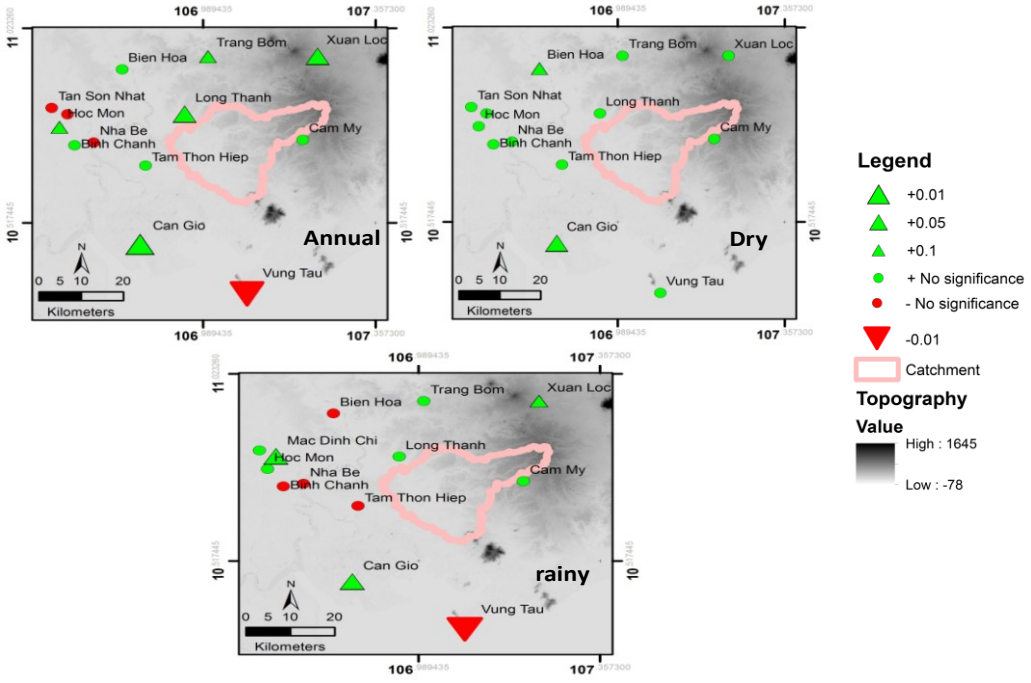

Figure 5.6: Spatial distribution of seasonal and annual precipitation trends with statistical tests at different significant levels 0.1, 0.05 and 0.01 (red colour refers to a decreasing trend and green colour refers to an increasing trend).

Analysis of other rainfall characteristics

Similar to the precipitation characteristics, both positive and negative trends can be found for different stations and significance levels for MWD on a monthly and annual time scale (see Appendix 1). The strongest positive and negative trends are found at the station Binh Chanh (Z_{MK} = 3.73) with a significance level of 0.01 in May and at the station Tan Son Hoa (Z_{MK} = −2.85) with a significance level of 0.05 in June. An increasing trend is seen at almost all stations except for Bien Hoa. The increasing trend for almost all stations shows a good fit of the trend for monthly rainfall amount (see Figure 5.5). The strongest trend for MWD is found for the stations Thong Nhat (0.38 days) in July, Binh Chanh (0.33 days) and XL (0.32 day) in May.

On the annual scale, a decreasing trend for MCDD was observed for all stations with the highest value for the MK test at the station Vung Tau (Z_{MK} = −2.93), followed by Long Thanh (Z_{MK} = −2.69). In contrast, an increasing trend for MWDD is found at almost all stations. A significant positive trend is seen at the station Can Gio for RX1day, RX3day, RX5day and RX7day, whereas a negative trends for these parameters are detected at the stations Vung Tau and Mac Dinh Chi (see Appendix 1).

Climate variability is investigated at a local scale discarding the effects of serial correlation of the time series. The analysis of monthly, seasonal and annual precipitation showed a decreasing trend for August and June and a decreasing trend for the amount of rainfall in the rainy season except for an increasing trend in May. During the dry season, an increasing trend is observed at all the stations

for given significance levels. The strength of the positive or negative trend varies from station to station.

Both positive and negative trends are observed at most stations for the maximum one-, three-, five- and seven-day rainfall amount at different significance level as illustrated in Appendix 1. This is similar to the analysis results of MCWD and MCDD, which show a significant positive trend at the stations Hoc Mon and Thong Nhat for MCWD and a significant negative trend at the stations Vung Tau, Long Thanh, Bien Hoa and Binh Chanh for MCDD.

Figure 5.7 shows the direction changes in the trend of rainfall that can be found for some gauges. The abrupt change in the slope in the first parabola for the stations Long Thanh and Cam My indicates a linear upward trend. A linear downward trend with an abrupt change in the slope is recorded for the other stations. As shown in Figure 5.7, there are at least two change points in the time series of the four stations that are closest to the catchment.

a)

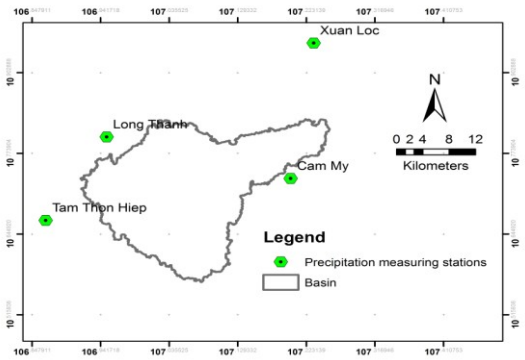

b)

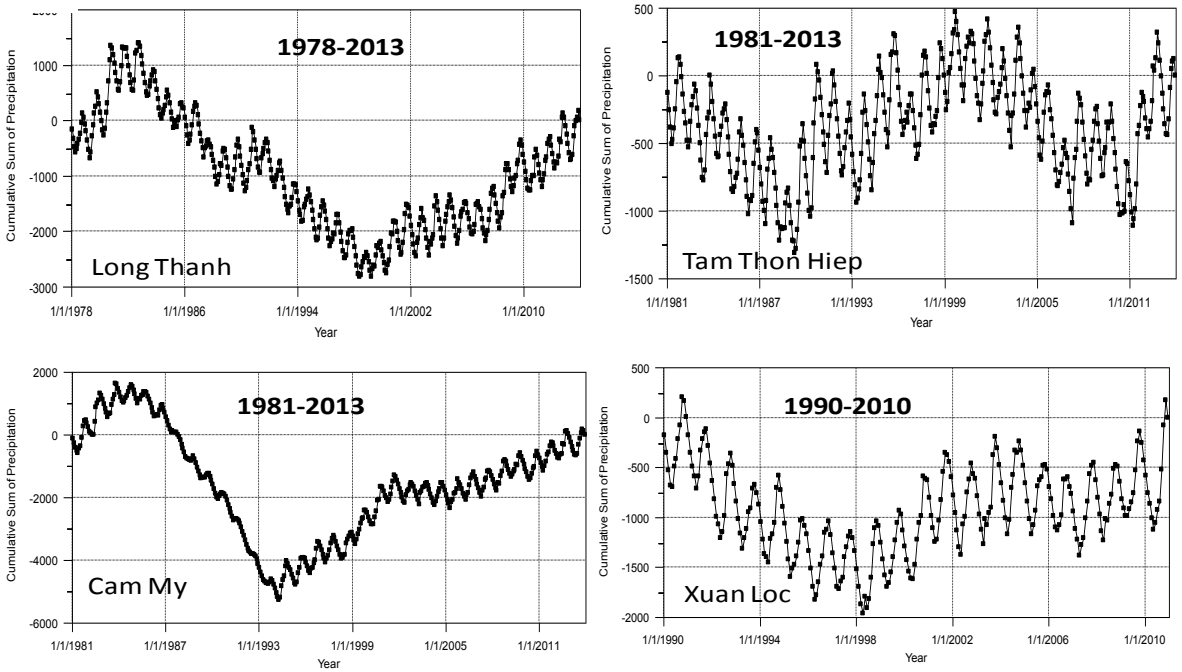

Figure 5.7: a) Map of considered precipitation stations and b) Cumulative Sum charts for daily precipitation at the four stations during different period.

5.4 Spatial interpolation

5.4.1 Introduction to research methods

Several technologies of interpolation have been broadly applied to generate spatial continuous data of precipitation based on observational rain gauges data (Cressie, 1990; Journel and Deutsch, 1992; Goovaerts, 1997; Webster and Oliver, 2007; Chiles and Delfiner, 2009; Matheron, 1971). Generally, spatial interpolation methods estimate a regionalized value for unsampled points based on the formula:

$$R = \sum_{i=1}^{n} \omega_i R_i \tag{5.19}$$

where:

R is the interpolated value

R_i is the observed value at point i

n is the total number of observed points

ω_i is the weight contributing to the interpolation at station i.

The difference between the interpolation methods is the way of estimating the weights that are used in the interpolation.

5.4.1.1 Cressman

Cressman (1959) described a method that is widely used to interpolate meteorological data. The idea of this method is to calculate the value for a grid point by the weighted average depending only on the distance between the grid point and the location of the precipitation measuring stations. This factor is called an “influence radius - R”. The smaller the R value is, the more the interpolated values correspond with the observed values. The value of R can be changed to adjust the weights. To perform the Cressman interpolation, a background field obtained from a numerical model is required to define the grid cells. In this thesis, the background field of precipitation obtained from the Tropical Rainfall Measuring Mission 3B43 v7 (TRMMv7) (Huffman and Bolvin, 2013) is selected. The “influence radius” factor has been carefully examined. The weighting function is given by:

$$\omega_i = \frac{(R^2 - r_i^2)}{(R^2 + r_i^2)}, \text{for } r^2 \leq R^2 \tag{5.20}$$

$$\omega_i = 0, \text{for } r^2 > R^2 \tag{5.21}$$

where:

r_i is the distance between the observation station to the grid point

R is the radius of influence.

5.4.1.2 Ordinary kriging

The term “Kriging” was originally used in the late 1950s (Matheron, 1962). With the development of different kriging versions in geostatistics, the term “kriging family” has been introduced by Cressie (1990) and further developed by Goovaerts (1997). The core concept of the “kriging family” is that each sample is assigned with a different weight according to the spatial correlation among the sample points and the estimated error is minimized. The values at unknown points are estimated based on known points at given sites (Isaaks and Srivastava, 1989). The estimator of all versions of kriging is defined by Goovaerts (1997). The aim of all types of kriging is to determine the kriging weight and to minimize the variance of the estimator with the unbiasedness constraint (Isaaks and Srivastava, 1989; Goovaerts, 1997; Hengl, 2007). Ordinary kriging (OK) is often associated with the “best linear unbiased estimator” because (1) its estimations are weighted linear combinations of the available data and (2) it tries to define the mean residual equal to zero and minimises the variance of the errors. A more detailed description of this postulation can be found in Goovaerts (1997), Stein (1999), Isaaks and Srivastava (1989) and Webster and Oliver (2007).

5.4.1.3 Regression kriging

In the regression kriging (RK) version, the best unbiased linear prediction (BULP) for spatial data is implemented. The value of the target variables at specific sites is modelled as the sum of the deterministic and stochastic component (Goovaerts, 1997; Hengl *et al*., 2007). RK is a combination of the regression that is used to fit the explanatory variation and simple kriging with an expected value of 0 is used to fit the residuals (Hengl *et al*., 2007).

$$\hat{z}(s_o) = \hat{m}(s_o) + \hat{e}(s_o) = \sum_{k=0}^{p} \hat{\beta}_k . q_k(s_o) + \sum_{i=0}^{n} \lambda_i . e(s_i) \quad (5.22)$$

where:

$\hat{m}(s_o)$ is the fitted drift or deterministic part

$\hat{e}(s_o)$ is the interpolated residual

$\hat{\beta}_k$ are estimated drift model coefficients

λ_i are kriging weights determined by the spatial dependence structure of the residual

$e(s_i)$ is the residual at location s_i.

The coefficients $\hat{\beta}_k$ is estimated from the sample by some fitting method, e.g., ordinary least squares (OLS) or, optimally, using generalized least squares (GLS):

$$\hat{\beta}_{GLS} = (q^T . C^{-1} . q)^{-1} . q^T . C^{-1} . z \quad (5.23)$$

where:

$\hat{\beta}_{GLS}$ is the vector of estimated regression coefficients

C is the covariance matrix of the residuals

q is a matrix of predictors at the sampling locations

z is the vector of measured values of the target variable.

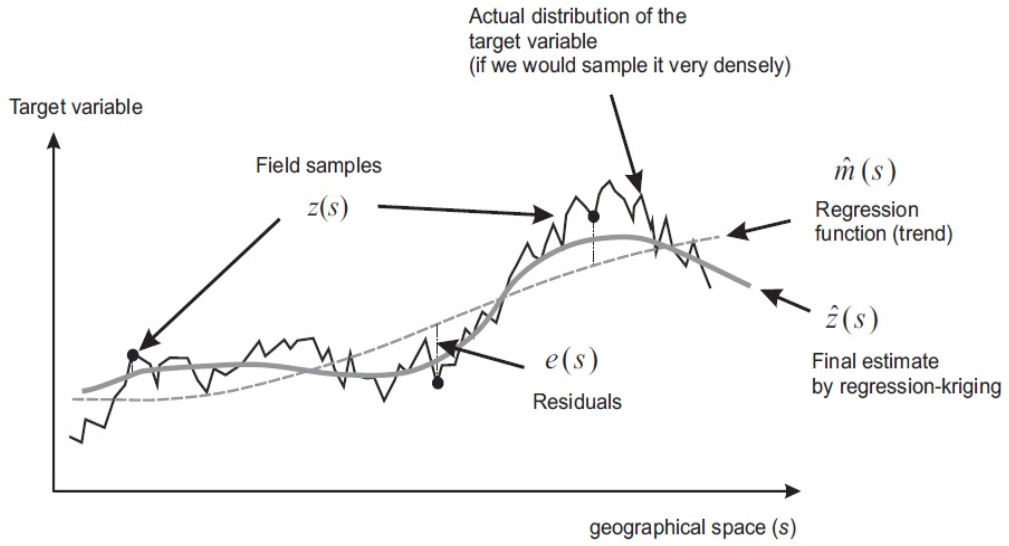

Figure 5.8: A schematic example of regression kriging: fitting a vertical cross-section with assumed distribution of an environmental variable in horizontal space (Hengl, 2007).

5.4.1.4 Dual kriging

Dual kriging (DuK) is a global interpolator within the "kriging family". The key of this method is to estimate the covariance values instead of data values (Goovaerts, 1997). The kriging linear system can be solved by the DuK method to interpolate all points. Thus, the computational costs are significantly effective for a large amount of meteorological values, that is interpolated (Goovaerts, 1997). An assumption is that the correction weights associated to the data values only depend on the distance. A further discussion can be found in Echaabi *et al*. (1995).

5.4.1.5 Inverse distance weighting

The main idea of this method to estimate unknown values based on a linear combination of surrounding observational data. During the interpolation, the sample points are weighted with the inverse proportion of the distance between the observation and the interpolated points. The weighting function is given as Equation 5.24. A more detailed description of the IDW can be found in Tomczak (1998), Lam (1983) and Hengl (2007).

$$\omega_i = \frac{\frac{1}{d_i^P}}{\sum_{i=1}^{n} \frac{1}{d_i^P}} \tag{5.24}$$

where:

d_i is distance between observation and interpolated point

p is a coefficient that is used to adjust the weights

n is the number of sampled points used for the estimate.

When p is zero, the inverse distance weighting method (IDW) is referred to as “moving average” method (Laslett *et al*., 1987; Hosseini *et al*., 1993). When p is 1, IDW is a “linear interpolation”, when p is not equal to 1 it is a “weighted moving average” (Burrough *et al*., 1998).

5.4.2 Analysis results

Results from the various interpolation technologies are validated at different spatio-temporal scales. In space, the accuracy of these methods is validated by the comparison of the values with the TRMM and the Apthrodite raster databases. In time, the time series of daily precipitation for the rainy season from May to November 2013 at the station Long Thanh located within the interpolated area is used for the validation.

The interpolated results at the grid cell that is nearest to the Long Thanh station are used for the comparison with the station data. A low root-mean-square deviation (approximately 15) and a moderately high correlation coefficient (about 0.6) show that the performance of these methods is satisfactory (see Figure 5.9), but the technology of IDW interpolation shows the best performance. Therefore, the IDW interpolation approach is selected within this study. The poor performance of “kriging family” could be caused by the limited number of stations.

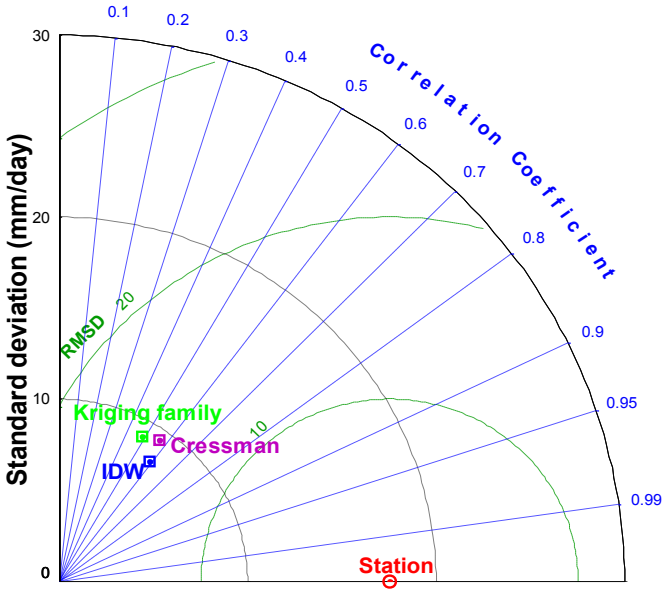

Figure 5.9: Taylor diagram displaying a statistical comparison of observations with interpolation methods of precipitation over the Thi Vai River catchment from May to November 2013 (Taylor, 2001). Black dashed lines indicate the standard deviation (mm/day). Green dashed lines indicate the root-mean-square deviation (mm/day). Blue dashed lines indicate the correlation coefficient.

The interpolation methods are validated on the spatial scale by comparing the interpolated heavy or light rainfall centres with those of the raster databases for a specific period. Experiments are carried out for observed events of extreme precipitation or drizzle days. Figure 5.10 shows the spatial distribution of precipitation for 31/8/1998 that is produced from different data sources (e.g., gridded data or station data). This day is chosen because of the availability of both raster datasets, TRMM and Apthrodite.

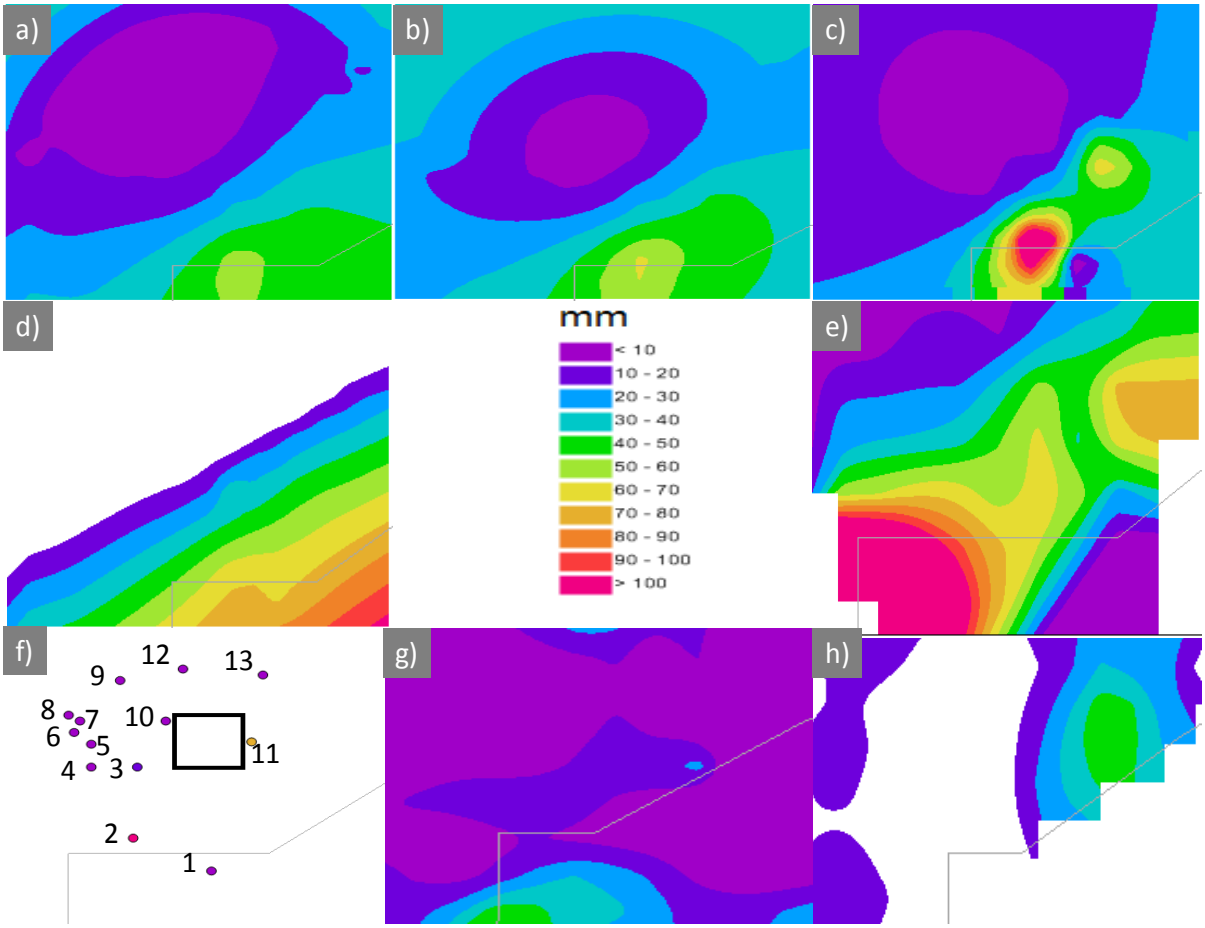

Figure 5.10: Spatial distribution of precipitation (mm/day) over the Thi Vai catchment from various interpolation technologies: a) Dual kriging, b) Ordinary kriging, c) Inverse distance weighting, d) Regression kriging, e) Cressman in comparison to f) station data and the raster datasets g) TRMM 3B42 and h) Apthrodite on 31/8/1998. ***Note: Lines indicate coastline boundary, square indicates Thi Vai area. Precipitation measuring stations (1) Vung Tau, (2) Can Gio, (3) Tam Thon Hiep, (4) Nha Be, (5) Binh Chanh, (6) Hoc Mon, (7) Mac Dinh Chi, (8) Tan Son Nhat, (9) Bien Hoa, (10) Long Thanh, (11) Cam My, (12) Thong Nhat and (13) Xuan Loc.***

6 IMPROVEMENT OF DYNAMIC-STATISTICAL DOWNSCALING TECHNOLOGY IN CLIMATE CHANGE STUDIES

6.1 The dynamical downscaling model: An introduction of the RegCM model

The Regional Climate Model RegCM was first developed in 1989 and labeled as RegCM version 1 (RegCM1) at the International Centre for Theoretical Physics (ICTP). Since then, it has been improved through the different model versions in 1993 (RegCM2), 1999 (RegCM2.5), 2006 (RegCM3), 2010 (RegCM4) and in RegCM5 in the near future (Giorgi and Anyah, 2012). The RegCM model is a very flexible model that is widely applied for climate studies for worldwide climate projections for the past, the present and the future.

"*Regional climate modeling is truly something in which NCAR has been a pioneer. When we started, nobody had done it before. Now most major laboratories, worldwide, and many smaller institutes, including some in developing countries, are doing it. The approach is one of the centerpieces of programs such as START (the Global Change System for Analysis, Research, and Training) that are aimed at fostering climate system research in developing countries.*"

Bob Henson (1997)

Table 6.1: The development of the RegCM model versions.

	RegCM1	RegCM2	RegCM2.5	RegCM3	RegCM4
Primary references	Dickinson *et al.* (1989) Giorgi and Bates (1989)	Giorgi *et al.* (1993a,b)	Giorgi and Shields (1999); Pal *et al.* (2000)		
Dynamics	Anthes *et al.* (1987)	Hydrostatic (Grell *et al.*, 1994)	Hydrostatic (Grell *et al.*, 1994)	Hydrostatic (Grell *et al.*, 1994)	Hydrostatic (Giorgi *et al.*, 1993a)
Radiative transfer	CCM1 (Kiehl *et al.*, 1987)	CCM2 (Briegleb, 1992)	CCM3 (Kiehl *et al.*, 1996)	CCM3 (Kiehl *et al.*, 1996)	CCM3 (Kiehl *et al.*, 1996)
Boundary layer	Deardorff (1972)	Holtslag *et al.* (1990)	Holtslag *et al.* (1990)	Holtslag *et al.* (1990)	Holtslag (Holtslag *et al.*, 1990); UW-PBL (Bretherton *et al.*, 2004)
Land surface	BATS 1e (Dickinson *et al.*, 1986)	BATS 1e (Dickinson *et al.*, 1993)	BATS 1e (Dickinson *et al.*, 1993)	SUBBATS (Giorgi *et al.*, 2003a)	BATS (Dickinson *et al.*, 1993); Sub-grid BATS (Giorgi *et al.*, 2003); CLM (Steiner *et al.*, 2009)
Convective precipitation	Anthes (1977)	Grell (1993); Anthes (1977)	Zhang and MacFarlane (1995); Grell (1993)	MIT (Emanuel, 1991); Anthes–Kuo (1977); Grell (1993)	Simplified Kuo (Anthes *et al.*, 1987); Grell (1993); MIT (Emanuel and Zivkovic-Rothman, 1999); Tiedtke (1989)

Resolvable precipitation	Implicit (Giorgi and Bates, 1989)	Explicit (Hsie et al., 1984)	SIMEX (Giorgi and Shields, 1999)	SUBEX (Pal *et al.*, 2000)	SUBEX (Pal *et al.*, 2000)
Ocean fluxes	Not available	Not available	Not available	BATS (Dickinson *et al.*, 1993); Zeng (Zeng *et al.*, 1998)	BATS (Dickinson *et al.*, 1993); Zeng (Zeng *et al.*, 1998); Diurnal sea surface temperature (Zeng and Beljaars, 2005)
Interactive aerosols	Not available	Not available	Qian and Giorgi (1999)	Solmon *et al.* (2006) Zakey *et al.* (2006)	Organic and black carbon, SO4 (Solmon *et al.*, 2006); Dust (Zakey *et al.*, 2006); Sea salt (Zakey *et al.*, 2008)
Interactive lake	Not available	Not available	Not available	Not available	1D diffusion or convection (Hostetler *et al.*, 1993)
Tropical band	Not available	Not available	Not available	Not available	Coppola *et al.* (2012)
Coupled ocean	Not available	Not available	Not available	Not available	MIT (Artale *et al.*, 2010); ROMS (Ratnam *et al.*, 2009)

By using the RegCM2, Giorgi *et al.* (1993) simulated climate variables such as precipitation, temperature, moisture and cloudiness. The model simulations showed that both boundary layer parameterization and radiative transfer formulation schemes significantly affected the results for Europe. Additionally, the results implied that these features could be reproduced better when using Grell scheme instead of using Kuo scheme (Giorgi *et al.*, 1993). Further information about these schemes can be found in section 6.3.2.2, Grell (1993) and Kuo (1974).

Reboita *et al.* (2014) used the RegCM3 to simulate the climate variables air temperature, precipitation and the monsoon for South America. The model was nested in the GCMs HadCM3 and ECHAM5. Three time-slices: present (1960-1990), near- (2010-2040) and far-future (2070-2100) were considered. The results from nested RegCM3 in HadCM3 significantly differed from those obtained by the nested RegCM3 in ECHAM5. This indicated that the LBCs from global models played a significant role in simulating climate fields.

Diallo *et al.* (2014) forced RegCM4 with the version 4.0 of the Community Atmosphere Model (CAM4) (grid resolution at 1^o x 1^o). In this study, climate simulations were performed for a period of 20 years at a resolution of 25 km x 25 km over Southern Africa. The climatic fields (i.e., precipitation, 2 m temperature (mean, minimum and maximum) and large-scale circulation) were well reproduced. Because of the higher resolution, the results from the nested RegCM4 in CAM4 were better than those from CAM4 without a nesting RCM.

In Vietnam, the RegCM3 version has been widely applied for climate studies. Kieu *et al*. (2000) used this system to perform climate simulations for precipitation over Vietnam. The performance of model simulations was satisfactory. This model was also used to reproduce meteorological fields for Vietnam for two months (11/1999 and 10/2003), in which the highest floods were recorded in Central Vietnam (Nguyen and Le, 2004). The results showed that heavy precipitation centers could be

reproduced by the RegCM model. However, when comparing the results to measured data, the bias was relatively large. The temperature simulations for Central and Southern Vietnam were better than those for Northern Vietnam. The sensitivity of topography and land surface conditions to the simulation of atmosphere-land surface interaction processes by RegCM2 was tested by Phan (2005). It is illustrated that the simulation results for explicit and latent fluxes, precipitation amount and intensity, convective and non-convective precipitation ratio are strongly sensitive to changes in land surface conditions. RegCM3 was coupled with four convection precipitation schemes (Kuo, Grell-AS74, Grell-FC80 and Mit-Emanuel) to simulate climate parameters (temperature and precipitation) during 1996-1998 (Phan and Ho, 2008). The study showed that RegCM3 configured with the Mit-Emanuel and Grell-AS74 schemes performed better than the configurations with the other schemes. A large number of climate projects using RegCM were also reported by the following authors: Phan (2008), Phan (2010), Phan *et al.* (2009), Nguyen and Le (2004), Kieu et al. (2000), etc.

From all those studies, it can be concluded, that the RegCM model can well reproduce the climate of different parts of the world including Vietnam. Nevertheless, the quality of climate simulations strongly depends upon: (1) the selected domain, (2) the analyzed model variable, (3) the LBCs from the GCM or the global reanalysis, (4) the parameterization schemes and (5) the resolution. Therefore, it is an extremely important step to design and set up these factors before running the model.

"*Regional models may add value to global model results, but improvements depend essentially on the kind of application, experimental setup, analyzed model variable, and location.*"

Feseret *et al*. (2011)

6.2 The dynamical downscaling model RegCM4: Description and model setup

6.2.1 Model description

The RegCM model code, which was first developed by Dickinson *et al.* (1989), was used for regional climate modeling. The dynamical structure of RegCM consists of the hydrostatic version of the MM5, which was developed at the National Center of Atmosphere Research (NCAR) and the Penn State University (PSU). Since the main tasks of this study is to simulate climate variables under a climate change scenario for a small basin, the RegCM4 model (version 4.1.1), which is a compressible, hydrostatic, sigma-p vertical coordinate and limited area model, has been chosen and applied. In comparison with other regional climate models like PRECIS or REMO, RegCM4 has several advantages: (1) convection schemes with closure options are implemented; (2) it is an open-source model and (3) it is flexible with respect to the driving global climate models (Elguindi *et al.*, 2011). Furthermore, it allows to perform dynamical downscaling from global scale to local scale at high resolution. A brief description of the dynamical equations and the physical parameterization schemes is given in Elguindi *et al.* (2011) (see also in the Appendices 3 and 4). A detailed documentation of the model, the source code and the development of different versions as well as further information are

freely available on the Internet[22]. In RegCM, a dimensionless σ coordinate is used to define the height levels.

$$\sigma = \frac{(p - p_t)}{(p_s - p_t)} \tag{6.1}$$

where:

p is the pressure (Pa)

p_t is a specified constant top pressure (Pa)

p_s is the surface pressure (Pa)

The scalars (T, q, p, etc.) are defined at the center of the grid box, while the eastward (u) and northward (v) velocity components are collocated at the corners as shown in Figure 6.1 right.

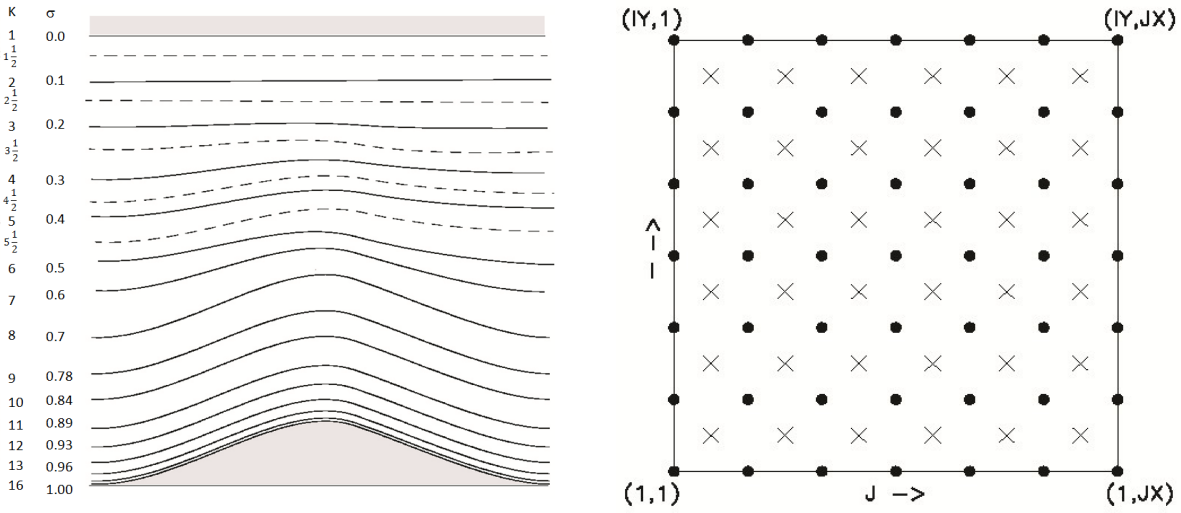

Figure 6.1: The vertical structure with 16 layers as an example. Dashed lines indicate half-sigma levels and solid lines indicate full-sigma levels (left). The structure of horizontal staggering B-grid (right) (Elguindi *et al.*, 2011).

6.2.2 Model setup

In this study, RegCM4 is run with 18 vertical levels including 6 levels of planetary boundary layer (Holtslag *et al.*, 1990). The convection precipitation scheme of Emanuel (1991) is configured in RegCM4. The selection of this scheme is because several schemes (e.g., Grell, Kuo, Emanuel and Tiedtke) were tested for some months and years in random before the scheme Emanuel is selected and configured. Grell (Grell, 1993) and Kuo (Kuo, 1974) schemes are categorized as deep convection schemes, whilst Emanuel (Emanuel, 1991) and Tiedtke (Tiedtke, 1989) schemes belong to shallow convection schemes. A deep convection scheme refers to a description of convective phenomena that strongly develop in the vertical over a wide span of the troposphere, whilst shallow convection denotes at a smaller and weaker level in the vertical. A further perspective of these convective schemes can be found in Grell (1993), Kuo (1974), Emanuel (1991), Tiedtke (1989), Houze (1993), Warner (2010) and Stensrud (2007).The results showed that the RegCM4 configured with the Kuo,

[22] https://gforge.ictp.it/gf/project/regcm

Grell and Tiedtke schemes largely underestimated the amount of precipitation during rainy season in comparison with the gridded and station data, especially for the small domain. Although the model configured with these schemes performed better than the configurations with the Emanual scheme during dry season, precipitation is mostly recorded in rainy season over a small catchment like the Thi Vai (see section 3.1). Within this work, the sensitivity tests are not main purpose; hence, the results of model performance with the schemes Kuo, Grell and Tiedtke are not shown. For the deep convective parameterization schemes, in the latest recent study for the CORDEX-SEA[23] Domain, Neng Liew et al. (2015) also suggested that the model RegCM4 should be configured with the Emanuel MIT convective scheme. However, the sensitivity tests of this configuration have not been implemented for a small domain. The relaxation exponential technique with the size of 15 grid points is performed based on the recommendations from Elguindi *et al*. (2011), Skamarock *et al*. (2005), Grell *et al*. (1994) and Warner (2010). A large buffer zone size is to ascertain a greater consistency of large scale forcings. For Vietnam domain, the sensitivity tests on the buffer zone parameter can be found in Luong (2010). The radiation scheme of the National Center of Atmosphere Research (NCAR) Community Climate Model (CCM3) (Kiehl *et al.*, 1996) is used. The physical parameterization schemes of climate models play an essential role for the quality of the results because they are very sensitive to changes in model variables (Stensrud, 2007). For this reason, the Biosphere-Atmosphere Transfer (BATS) version 1E (Dickinson *et al.*, 1993) as well as the Community Land Model version 3.5 (CLM 3.5) (Oleson and Dai, 2004) are configured into RegCM4. The purpose of BATS is to determine the fraction of incident solar radiation, whilst the CLM is the land surface model developed by the NCAR as part of the Community Climate System Model (CCSM). More details in these schemes are presented in Appendix 4. In case the model is configured with BATS, named as RCM_BATS. Another is named as RCM_CLM as illustrated in Table 6.2.

No less important than the physical parameterization schemes, the domain size is considered the key to discard the effect of boundaries. It is necessary that the domain is large enough to contain all relevant forcings and natural processes in the atmosphere. Furthermore, the domain should be large enough for the simulation of the development of atmosphere circulations. For the downscaling to a local scale, the resolution should be high enough to capture local physical processes. However, a higher resolution requires higher computing costs and the stability of climate simulations may be lower. As a high proportion of the precipitation amount over the South of Vietnam is convective precipitation, the use of a fine spatial resolution may capture the precipitation intensity better. Therefore, the model was configured with three self-nesting steps of 60, 25 and 10 km horizontal resolutions (see Figure 6.3) centered at 13.5^{o}N and 106^{o}E with more than 120 grid points in West-East and South-North direction for the first domain. The performance of self-nesting steps is not available for CLM 3.5 within the RegCM system.

Due to the advantages of the ERA-interim reanalysis dataset (see Chapter 3 for further details), this is used to reduce the influence of systematic biases on RegCM4 outputs. Thus, the RegCM4 is forced by the ERA-interim reanalysis data, which provides the initial and boundary conditions for a 30-year

[23] CORDEX-Southeast Asia

period (1981-2010). The purpose of this work is to validate the capability of the RegCM4 model to simulate the climate variables. For the climate projections, four simulations are performed with RegCM4 (see Table 6.1), forced by CGCM3 as a global circulation model which is the third version of the Coupled Global Climate Model (CGCM3) (Flato, 2005), developed by the Canadian Centre for Climate Modelling and Analysis (CCCma). Three time slices, a historical period (1961-1990), a present period (1981-2010) and a far-future period (2071-2100), are considered for each set of the projections. The emission scenario for the future period is the SRES A1B scenario. The CGCM3 T47 with a spatial resolution of roughly 3.75 degrees of the Gauss grid and 31 vertical levels is selected. The ocean resolution is roughly 1.8 degree with 29 vertical levels. The CGCM3 data is freely available. At the resolution of 1 x 1 degree, data of sea surface temperature obtained from the Global Ice Coverage and Sea surface Temperature (GISST) is used to generate the Initial and boundary conditions for the model. In addition, the obtained data of topography and land use with a resolution of 30 seconds from the United State Geological Survey is used for the model to create the terrain files on a particular domain.

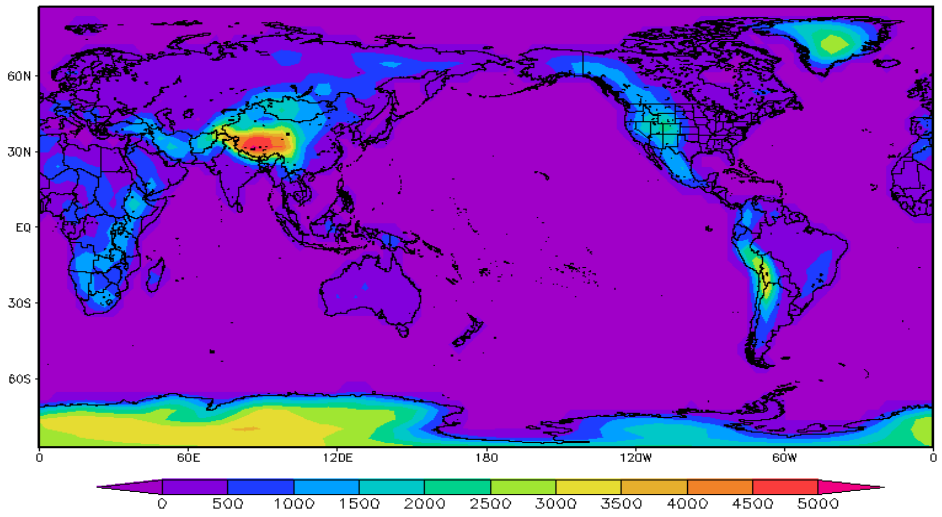

Figure 6.2: Topographic map of global domain from CGCM3 (m).

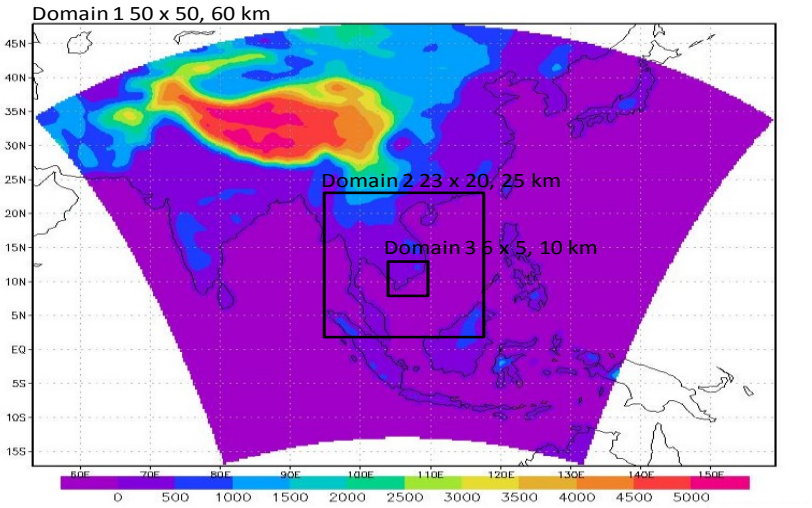

Figure 6.3: Topographic map of the domains with 30-seconds resolution from RegCM4 (m). The domain size (latitude x longitude) and resolution of different domains are also presented.

Table 6.2 shows the experimental configuration design of land surface schemes, domains and resolutions into the model. For time slices of the past 1961-1990 and the far future 2071-2100, the model is driven by CGCM3 T47. The remaining time slice of the present 1981-2010, the model is forced by ERA-Interim reanalysis data.

Table 6.2: Experimental configuration design of land surface schemes, domains and resolutions.

Nr.	Name of experiment	Land surface schemes	Domain	Resolution	Location	Period of time
1	RCM_BAT60	BATS	50^{o} x 50^{o}	60 km x 60 km	80E-130E; 15S-35N	1981-2010 1961-1990 2071-2100
2	RCM_CLM60	CLM	50^{o} x 50^{o}	60 km x 60 km	80E-130E; 15S-35N	1981-2010 1961-1990 2071-2100
3	RCM_BAT25	BATS	23^{o} x 20^{o}	25 km x 25 km	95E-118E; 2N-22N	1981-2010 1961-1990 2071-2100
4	RCM_BAT10	BATS	6^{o} x 5^{o}	10 km x 10 km	103E-109E; 8N-13N	1981-2010 1961-1990 2071-2100

Within this work, all simulations are performed on the supercomputer cluster of the Faculty of Architecture, Civil Engineering and Environmental Sciences at the TU Braunschweig[24]. The cluster consists of 184 Nodes with eight cores for each node (2x184 = 368 2.6GHz Intel X5550 Quad processors) and a total of 2.2 TBytes memory. The individual nodes are connected by a so-called Infiniband network with 20 Gbit/s to each other.

6.3 Analysis and evaluation of model results

To evaluate the performance of RegCM4 model simulations in all cases, results of the RegCM4 forced by ERA-Interim reanalysis data (RCM4/ERA-Interim), outputs are compared to the datasets constructed from different sources consisting of ERA-Interim reanalysis (Dee *et al.*, 2011), CRU TS3.21 (Jones and Harris, 2013), TRMM 3B42 v7 and TRMM 3B43 v7 (Huffman and Bolvin, 2013), GPCC (Schneider *et al.*, 2014), Apthrodite (Yatagai *et al.*, 2012). A special emphasis is put on the comparison with station data in the catchment that are aggregated from a daily and hourly time step. The results of downscaled temperature data is compared to the driving ERA-Interim data, CRU TS3.21 and observed station values. The downscaled precipitation results are evaluated by comparing them to TRMM 3B42 v7, TRMM 3B43 v7, GPCC and Apthrodite data as well as to observed station values. The technology of bilinear interpolation is used to transform the gridded datasets into the model grid. For the CRU TS3.21 data, only non-ocean grid-cells are considered. For the comparison of the simulation outputs and the station data, the model bias is calculated from the

[24] www.tu-braunsweig.de/hpc-fk3/luwig/hardware

daily, monthly, seasonal and annual area-averages for the catchment scale, named as TV domain and for the regional scale, named as SV domain. The TV domain is covered the area of 106.5^{o}E to 107.2^{o}E and 10.3^{o}N to 10.5^{o}N. The SV domain covers by the border of 9.5 to 11.8^{o}N and 104 to 108^{o}E. Four simulations are carried out, but the analysis in this study focuses on the finest resolution of 10 km x 10 km. The two variables of mean temperature and precipitation are analysed and validated.

6.3.1 Temperature

6.3.1.1 Spatial variability in surface air temperature

Figure 6.4a-d shows the seasonal surface air temperature biases of the output of the RegCM4 model, which is driven by the ERA-Interim data, for autumn (SON), winter (DJF), summer (JJA) and spring (MAM) compared to the CRU TS3.21 and ERA-Interim data for the period 1981-2010. Here, the variability of four climatological seasons are displayed, but the two climatological seasons winter and summer are given priority in the analysis (see Figures 6.4a-b, 6.5 and 6.6).

Over the SV domain, both observational datasets and model simulations indicate a similar pattern for surface air temperature. The downscaled temperature is generally lower than the one of CRU TS3.21 and ERA-Interim. These differences tend to become larger from east to west. For all four seasons, a warm bias is seen over several parts of the domain in comparison with the driving ERA-Interim data. Contrary to this, a cold bias was found over almost all parts of the domain with respect to the CRU TS3.21 data. The ERA-Interim mean temperature is significantly lower than the CRU TS3.21 temperature. The temperature bias is regionally different. The areas with the coldest bias are located in high elevation parts. A cold bias in winter that amounts up to -5 ^{o}C is identified particularly over the west (see Figure 6.4a).

Interestingly, over the TV domain, as compared to driving data ERA-Interim, RCM4/ERA-Interim simulations show that the seasonal temperature is overestimated. An underestimation is seen with respect to the CRU TS3.21 data in all cases. This also reflects that the CRU TS3.21 data constructed from observation data has a higher base temperature than the driving data ERA-Interim. In winter, RCM4/ERA-Interim simulations compared to the CRU TS3.21 data show a cold bias between -1.5 to -1 ^{o}C (see Figure 6.4a left). In contrast, a warm bias about 1 ^{o}C is identified in comparison with the ERA-Interim (see Figure 6.4a right). The difference between RCM4/ERA-Interim and ERA-Interim presents the difference between the downscaled data by RCM4 forced by the driving data ERA-Interim and the driving data ERA-Interim (see more in chapter 3). In summer, RCM4/ERA-Interim output shows a warm bias up to 1.5 ^{o}C compared to ERA-Interim (see Figure 6.4b right). A cold bias up to -1.5 ^{o}C, however, is recorded with respect to CRU (see Figure 6.4b left).

RCM4/ERA-Interim and CRU TS 3.21	RCM4/ERA-Interim and ERA-Interim	RCM4/ERA-Interim and Station

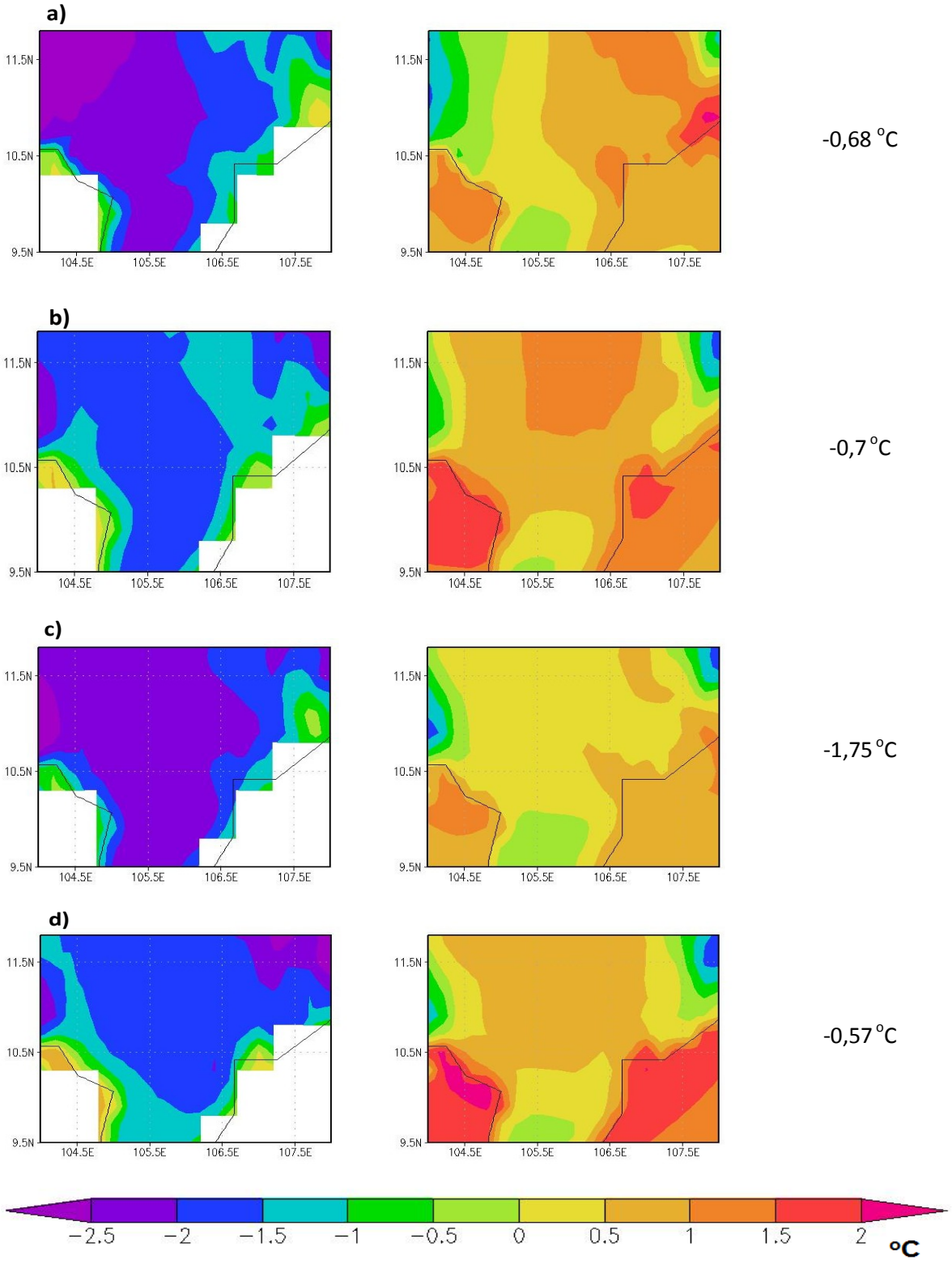

Figure 6.4: Spatial distribution of temperature biases in mean (1981-2010) (°C) for four seasons a) DJF, b) JJA, c) MAM and d) SON.

In comparison with the station data over the TV domain, the bias amounts to -0.57 in autumn, -0.68 in winter, -0.7 in summer and -1.75 °C in spring. The correlation coefficient between the simulated and the observed temperature time series is high for each season (see Table 6.3). This implies that the model is able to reproduce well the observed temperature, especially in summer and autumn. In these seasons, the results are most reliable. In contrast, the simulated winter precipitation is poorer as the simulated precipitation amount is too low.

Table 6.3: Correlation coefficient between the simulated and observed temperature in the period 1981-2010.

Seasons	RCM4/ERA-Interim and CRU TS3.21	RCM4/ERA-Interim and ERA-Interim	RCM4/ERA-Interim and OBS
Winter	0.59	0.66	0.65
Spring	0.87	0.81	0.82
Summer	0.87	0.83	0.89
Autumn	0.84	0.84	0.85

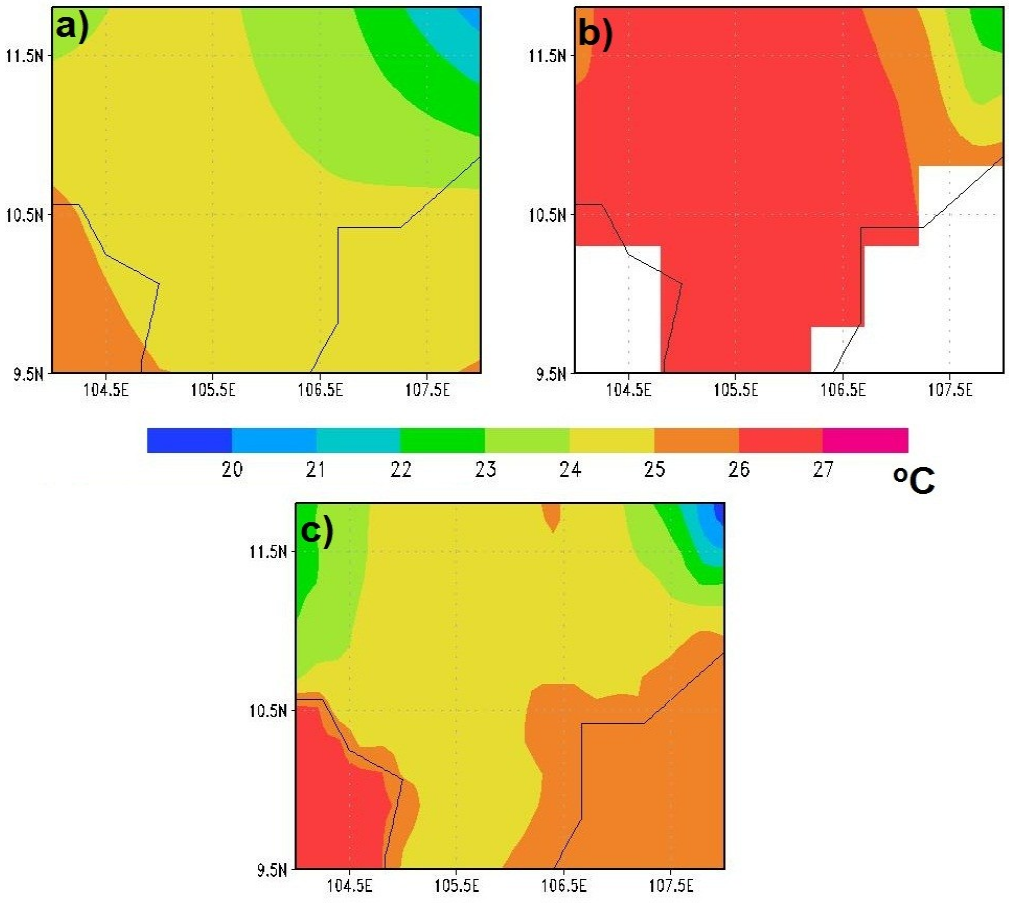

Figure 6.5: Averaged (1981-2010) air temperature in DJF for (a) ERA-Interim, (b) CRU and (c) RCM4/ERA-Interim (°C).

Figure 6.5 presents the seasonal surface air temperature in winter for the driving data ERA-Interim, CRU TS3.21 and RCM4/ERA-Interim. CRU TS3.21, ERA-Interim and RCM4/ERA-Interim show a similar

spatial pattern, but the ERA-Interim mean temperature is lower than the one of CRU TS3.21. In winter, the temperature simulated by RCM4/ERA-Interim amounts to about 25.5 °C on average. The mean air temperature in summer is shown in Figure 6.6. There is a considerable difference in the spatial pattern of CRU TS3.21 and ERA-Interim. However, the spatial pattern of RCM4/ERA-Interim temperature is similar to the one of CRU TS3.21. In summer, the simulated temperature over the TV domain amounts to 27.5 °C.

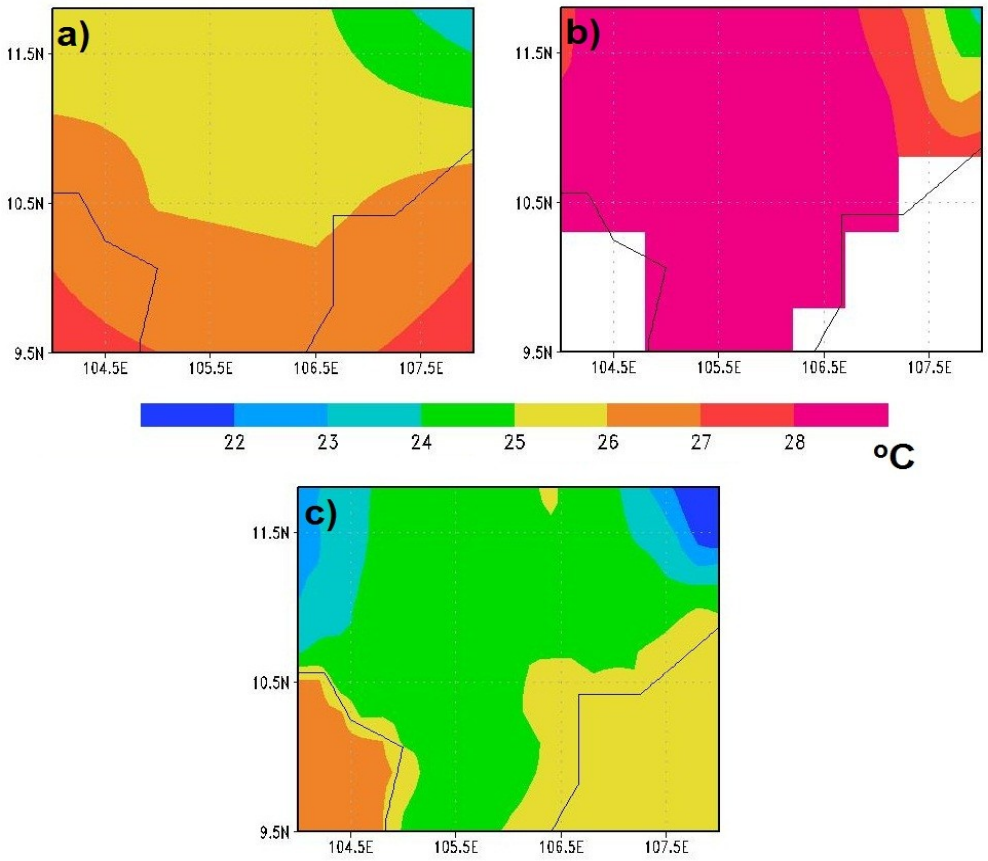

Figure 6.6: Averaged (1981-2010) air temperature in JJA for (a) ERA-Interim, (b) CRU and (c) RCM4/ERA-Interim (°C).

The analysis of the results shows that RCM4/ERA-Interim reproduces seasonal temperature for winter, autumn and summer adequately but spring. As shown in Figure 6.4, the locations of the coldest centers in the SV domain are well simulated for individual seasons. A cold bias in all seasons is seen when comparing RCM4/ERA-Interim output with CRU TS3.21. Inversely, RCM4/ERA-Interim output in comparison with ERA-Interim show a warm bias in four seasons.

6.3.1.2 Daily variability of surface air temperature

The investigation of the daily temperature profile by latitude for a band of longitude (106.5-107.2°E) during 1981-2010 of the driving data ERA-Interim illustrates that the daily temperature over the whole domain during the winter days could reach about 24.4 °C. The range of values for the different latitudes is the largest from the days of March to May (see Figure 6.7 left). In comparison with this reanalysis database, results from RCM4/ERA-Interim show a positive bias during this time. The daily

temperature profile by longitude for a band of latitude (10.3-10.5°N) shows that within the domain of 106.5°E-107.2°E, the largest temperature range for the different longitude is recorded during the months March to June (see Figure 6.8). During that period, the temperature could reach over 27.4 °C (see Figure 6.7 right). The Figures 6.7 and 6.8 indicate that the daily temperature gradient is nearly 1.2 °C/°Latitude during March to July and is much stronger than the one of longitudinal temperature variation.

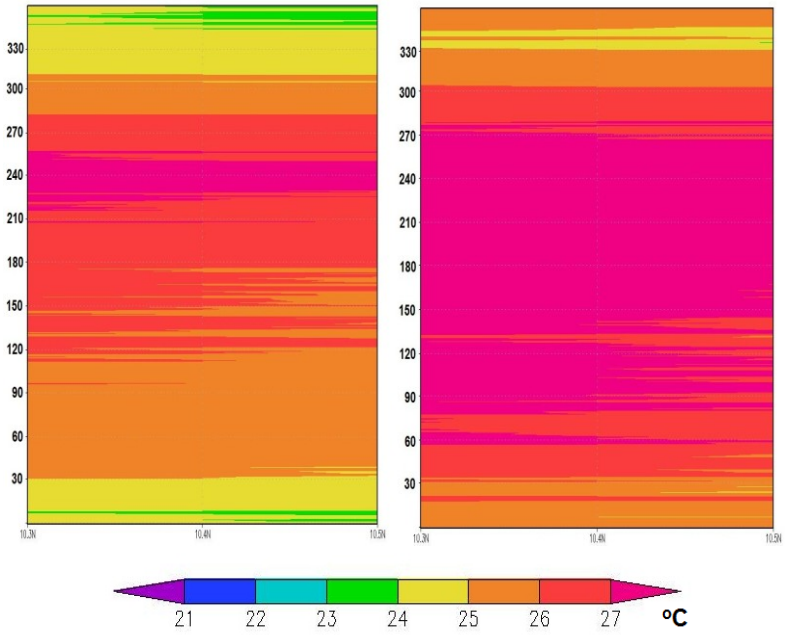

Figure 6.7: Latitude-time plots of daily temperature of the driving data ERA-Interim (left) and RCM4/ERA-Interim (right) during 1981-2010. The vertical axis indicates Time/day and the horizontal axis indicates Latitude/degrees (°C).

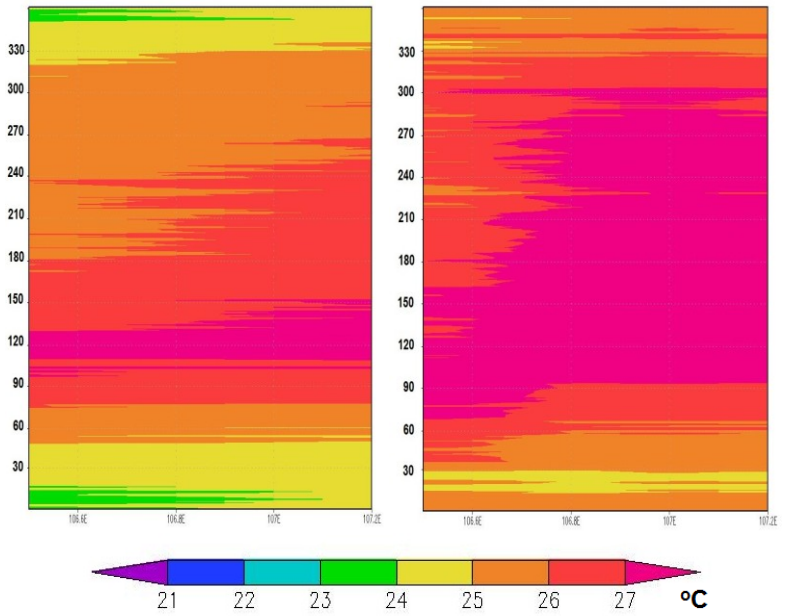

Figure 6.8: Longitude-time plots of daily temperature of the driving data ERA-Interim (left) and RCM4/ERA-Interim (right) during 1981-2010. The vertical axis indicates Time/day and the horizontal axis indicates Longitude/degrees (°C).

6.3.1.3 Variability in surface air temperature on the temporal scale

Figure 6.9 presents the monthly average temperature in the Thi Vai river catchment during the period 1981-2010. The analysis of surface air temperature data from different sources illustrates that there is a similar course of the year for temperature over the catchment. The surface air temperature measured at the stations is the warmest in April (over 29 ^{o}C). The station temperature is higher than the one of the other datasets for the whole year. The lowest monthly mean value of surface air temperature is observed in January (25.8 ^{o}C), followed by December (25.9 ^{o}C). The RCM4/ERA-Interim simulation of surface temperature is closer to the station data than the one of the driving ERA-Interim data, but shows a higher bias than the one of CRU TS3.21. It can be concluded that the CRU TS3.21 is more reliable than the driving ERA-Interim data.

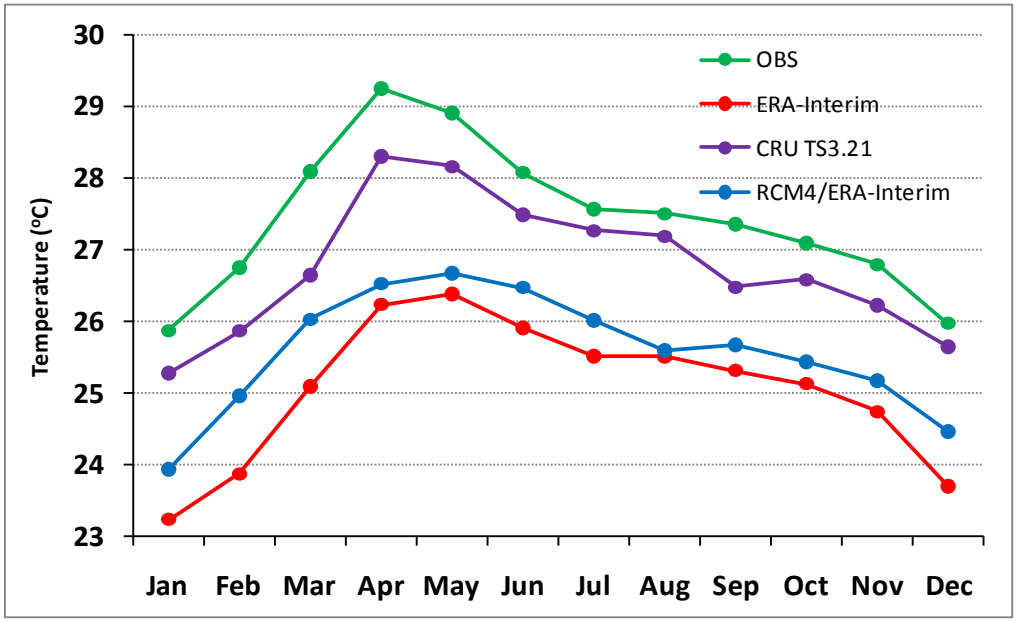

Figure 6.9: Monthly (1981-2010) surface air temperature over the Thi Vai basin.

The Taylor diagrams[25] (Taylor, 2001), which contain complex statistical information including standard deviation, correlation coefficient and root mean square deviation (RMSD) is used to evaluate the performance of RCM4/ERA-Interim simulations at the annual time scale. The simulated data is compared to station data. In terms of temperature, the results show a root-mean-square deviation of approximately 0.5 and a standard deviation that is similar for both station data and simulated values (see Figure 6.10), which indicates, that the simulation is good. The reason for this might be the use of ERA-Interim as driving data, which is highly related to the station data. Compared to the station data, the correlation coefficient of ERA-Interim, CRU TS3.21 and simulation results of RCM4/ERA-Interim is poor. The reason for this might be a lack of observational station used to create the gridded data ERA-Interim and CRU TS3.21 over the SV domain or effects of local geographical conditions.

[25] Taylor diagrams provide a concise statistical summary of how well patterns match each other in terms of their correlation, their root-mean-square difference and the ratio of their variances.

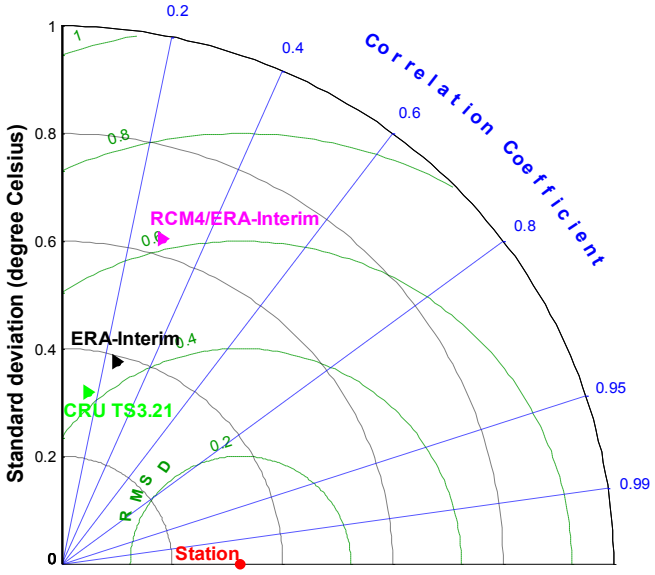

Figure 6.10: Taylor diagram for the performance of temperature simulation at the annual scale for the period 1981-2010 (RMSD is the abbreviation of root-mean-square deviation).

6.3.2 Precipitation

The performance of RCM4/ERA-Interim at the seasonal and monthly scale is evaluated by the gridded datasets TRMM 3B43 v7, GPCC and Aphrodite. The TRMM 3B42 v7 and Aphrodite data is used to evaluate the simulations of daily precipitation. Different periods are available for TRMM 3B43 v7 and TRMM 3B42 v7 (1998-2010), for GPCC (1981-2010) and Aphrodite (1981-2007). It is noteworthy that these different periods are used to analyse the performance of model simulations at different spatio-temporal scales in the period 1981-2010. The first step is to identify the differences between station data and the data from Aphrodite and TRMM.

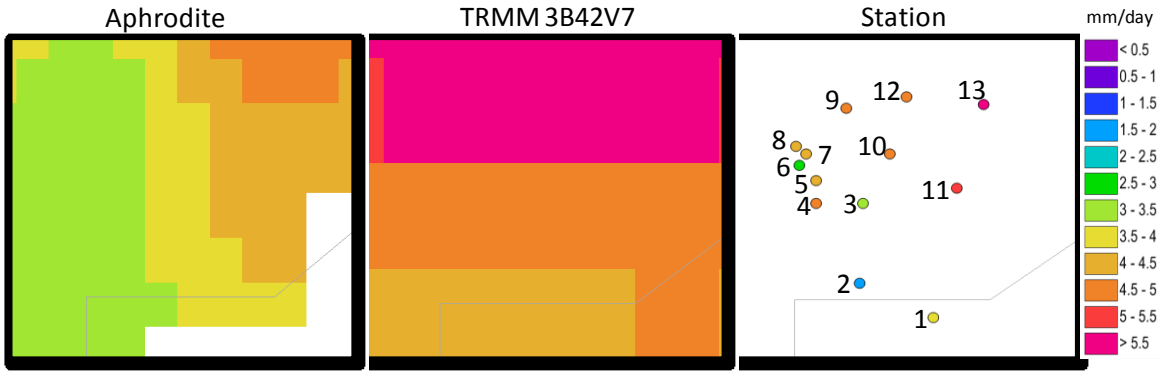

Figure 6.11: Spatial distribution of average daily precipitation (mm/day) for Aphrodite (1981-2007), TRMM 3B42V7 (1998-2010) and station data (1981-2010). Stations (1) Vung Tau, (2) Can Gio, (3) Tam Thon Hiep, (4) Nha Be, (5) Binh Chanh, (6) Hoc Mon, (7) Mac Dinh Chi, (8) Tan Son Nhat, (9) Bien Hoa, (10) Long Thanh, (11) Cam My, (12) Thong Nhat and (13) Xuan Loc.

Figure 6.11 shows that the spatial pattern of station data, Aphrodite and TRMM for precipitation is similar to some extent. All these data, a heavy rainfall center is well represented in the north of

domain of interest. As compared to other data, however, a light rainfall center can be identified from the station data in the south of the domain of interest. Precipitation obtained from Aphrodite shows a higher amount of precipitation (approximately 1 mm/day) than the station data over the TV domain. The precipitation obtained from TRMM is up to more than 1 mm/day higher than the one from the station data. Ignoring the role of algorithms applied to create the TRMM and Aphrodite data (see more in Huffman and Bolvin, 2013; Yatagai *et al.*, 2012), the reason for this could be the development of convective flows within the tropical regions in general and Southern Vietnam in particular. Explication for this is that these flows strongly develop in the vertical with a strong vertical velocity at a small scale in the horizontal. The convective precipitation, which is produced from these convective flows, has a high rainfall rate. This is a main reason, contributing to the inaccuracy in the radar data (more detailed in Houze, 1993; Houze, 1997; WMO-Nr. 8, 2008). Consequently, the precipitation data obtained by radars and satellites as TRMM is higher or lower according to the water content in clouds (see chapter 3). A fragile performance of TRMM on coastal areas with high elevation is pointed out by Chen *et al.*, 2013. Additionally, the limitation of the rain gauges over Vietnam used for reproducing the gridded precipitation data is a reason of this issue. The potential uncertainties of precipitation model from the RCM4/ERA-Interim will be analysed in the following subsections.

6.3.2.1 Spatial variability of precipitation

The comparisons of seasonal mean precipitation for the four seasons winter, spring, summer and autumn of RCM4/ERA-Interim with the observational datasets Aphrodite, GPCC and TRMM during the period from 1981 to 2010 are shown in Figure 6.12a-d. The analysis focuses on the seasons MAM, JJA and SON, because more than 95% of the annual rainfall amount falls in these times of the year (see Figures 6.12b-d, 6.13, 6.14 and 6.15).

Figure 6.12 indicates a similar pattern for the difference in precipitation over the displayed domain when comparing RCM4/ERA-Interim results with Aphrodite, GPCC and TRMM. In general, the downscaled precipitation tends to overestimate precipitation. These differences show a bias from west to east. During all seasons, wet biases are identified over the whole domain, but the largest biases are found in high elevation regions. The largest wet bias is found in JJA, followed by SON. The bias for the Aphrodite data is larger than the one for other datasets. This implies that there is a significant difference in the simulations of mean precipitation between the datasets Aphrodite, GPCC and TRMM. A small absolute bias is seen in winter for all datasets. The reason for this is that the observed amount of rainfall in winter is relatively small.

As is illustrated over the TV domain, it can be concluded that RCM4/ERA-Interim successfully reproduces the precipitation distribution. In the northern part of the catchment, with complex orographic effects of mountain peaks higher than 1500 m, the bias tends to enlarge. The RCM4/ERA-Interim simulations reproduce the spatial rainfall pattern of the observational datasets, but the simulated results overestimate the amount of rainfall by 2-16 mm/day. The reconstruction of the rainfall amount in winter is better than that in other seasons, especially in the Coastal zone (~1 mm/day). The driest bias is identified in MAM, followed by DJF (see Figure 6.12a-b).

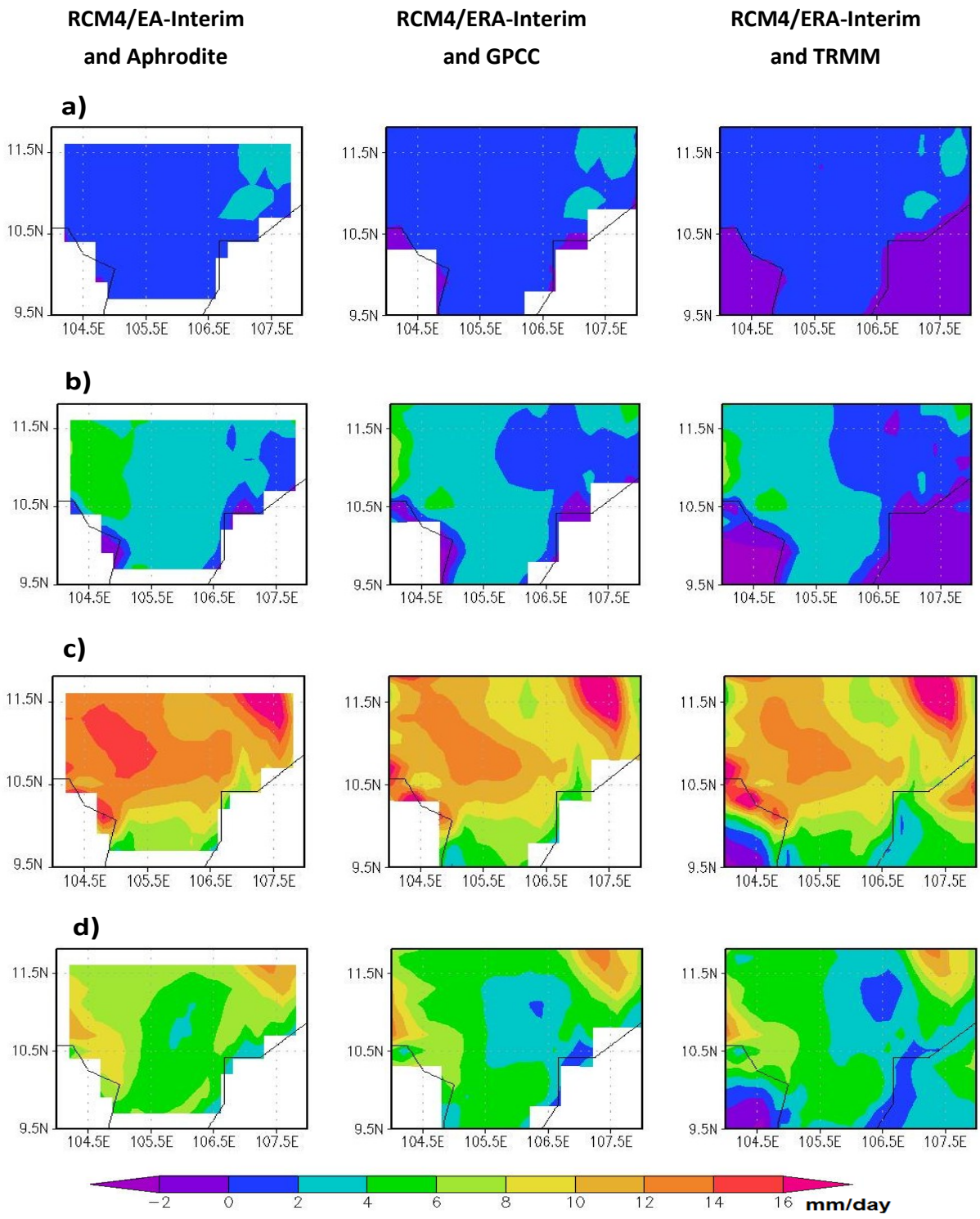

Figure 6.12: Spatial distribution of precipitation bias (mm/day) for four seasons a) DJF, b) MAM, c) JJA and d) SON in the SV domain.

Over the Thi Vai river catchment, seasonal precipitation mainly depends on the monsoon onset. The seasonal precipitation of the datasets Aphrodite, GPCC, TRMM and RCM4/ERA-Interim are shown in Figures 6.13-15. For spring (MAM) a precipitation amount of up to 7-8 mm/day is shown by TRMM and RCM4/ERA-Interim (see Figure 6.13), whereas it is only 1-3 mm/day by Aphrodite and GPCC. Figure 6.13 shows similar values and spatial patterns of MAM mean precipitation over the domain of

interest. Over the north of far from the Thi Vai catchment, however, the average spring precipitation during the period 1981-2010 for RCM4/ERA-Interim is higher than 9 mm/day.

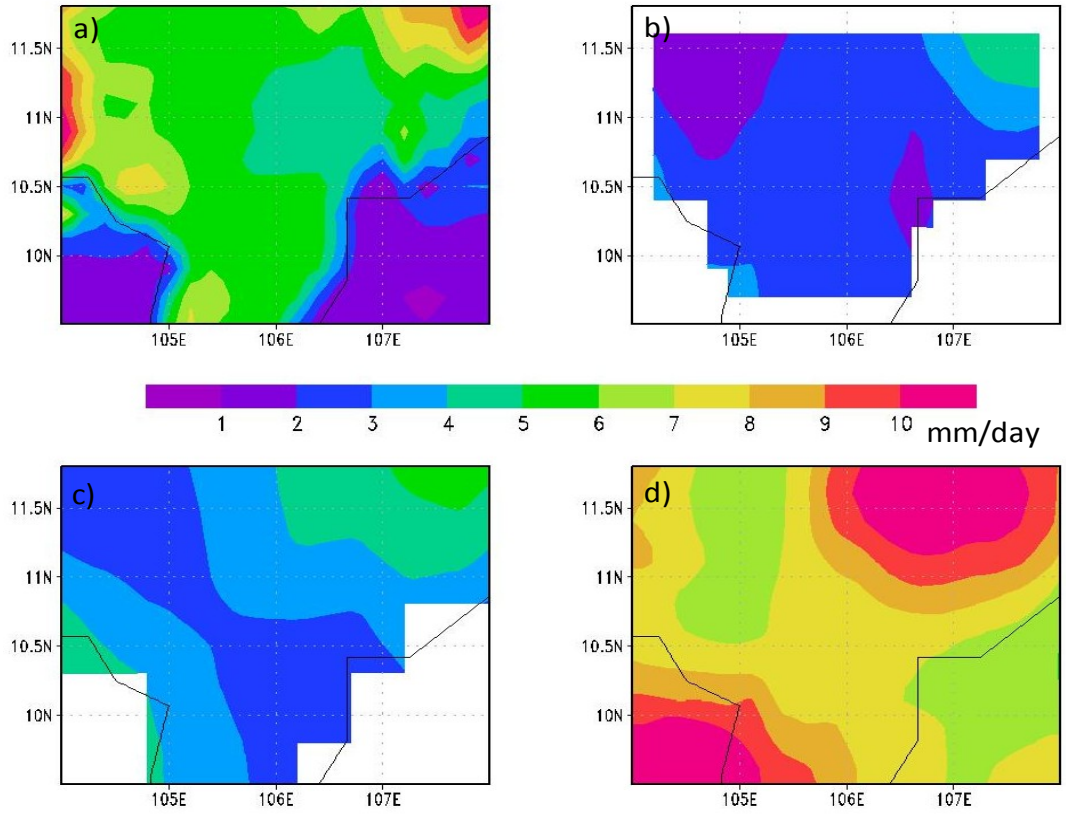

Figure 6.13: Average precipitation in MAM for (a) RCM4/ERA-Interim, (b) Apthrodite, (c) GPCC and (d) TRMM (mm/day).

Figure 6.14 presents the summer monsoon precipitation for observations (Apthrodite, GPCC and TRMM) and RCM4/ERA-Interim simulations for the period 1981-2010. The observed precipitation amounts up to 10 mm/day, whereas the RCM4/ERA-Interim simulation precipitation is up to more than 20 mm/day. There is no considerable spatial difference between Apthrodite, GPCC and TRMM. All these data exhibit a similar spatial pattern of summer precipitation (see Figure 6.14). Contrary to this, there is a reasonable difference between Apthrodite, GPCC, TRMM and RCM4/ERA-Interim simulations in autumn (see Figure 6.15). As it is illustrated in Figures 6.14-6.15 the seasonal precipitation of the Aphrodite data is close to that of the GPCC data, but significantly different from those of TRMM and RCM4/ERA-Interim. The precipitation of the RCM4/ERA-Interim simulation is up to about 14 mm/day, whereas TRMM is drier.

Systematic biases depend on the choice of the parameterization schemes. The different schemes lead to different performances. The results show that the choice of convection precipitation scheme of Emanuel tends to produce the overestimative seasonal mean precipitation.

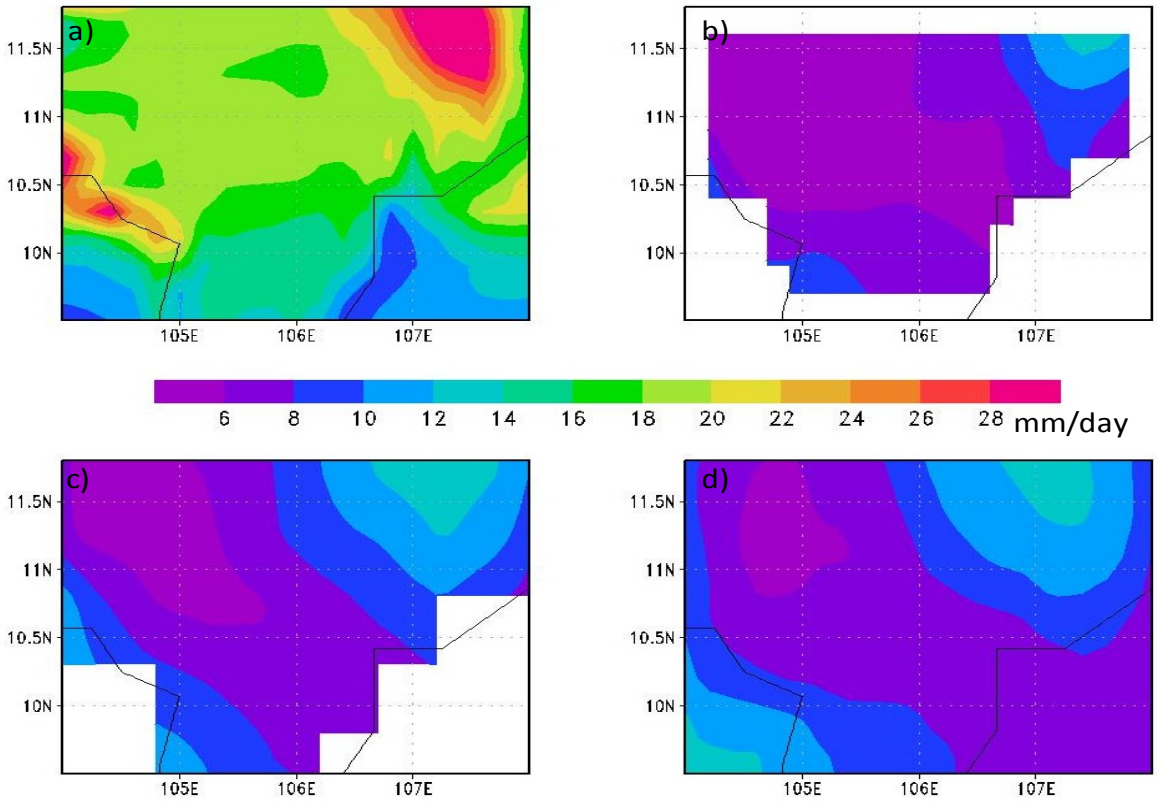

Figure 6.14: Average precipitation in JJA for (a) RCM4/ERA-Interim, (b) Apthrodite, (c) GPCC and (d) TRMM (mm/day).

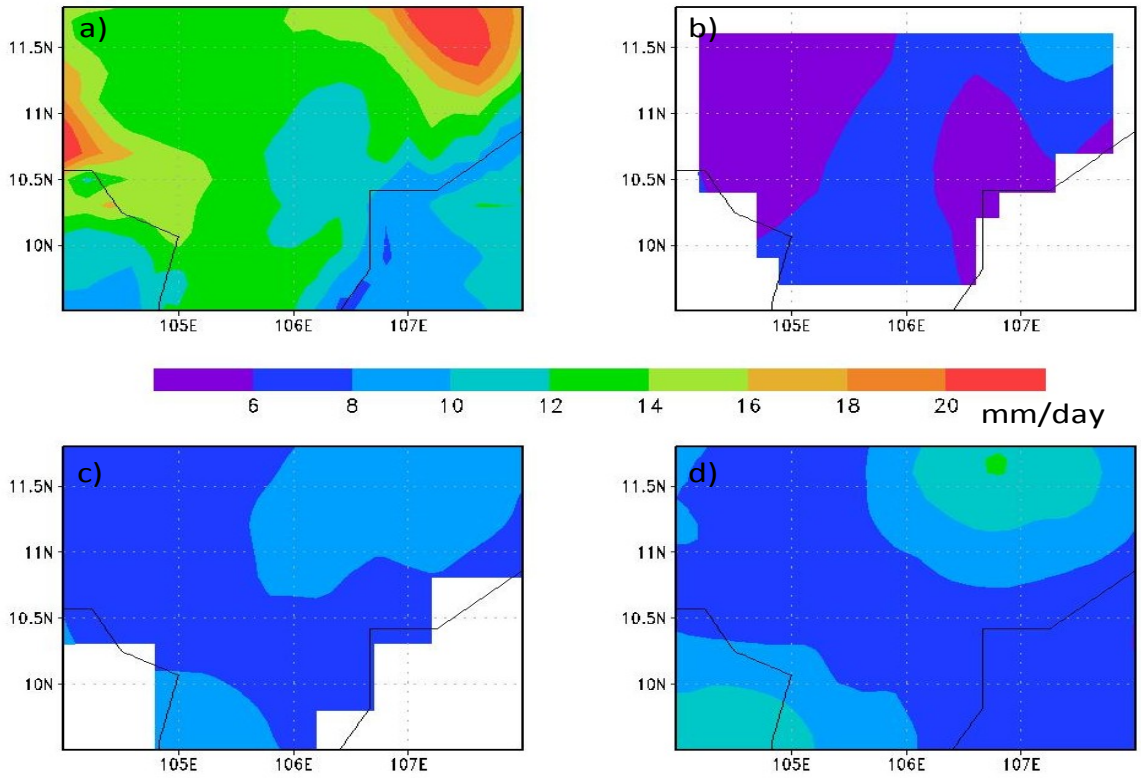

Figure 6.15: Average precipitation in SON for (a) Apthrodite, (b) GPCC, (c) TRMM and (d) RCM4/ERA-Interim (mm/day).

6.3.2.2 Daily variability of precipitation

The analysis of the daily precipitation profile in space and time illustrates that the daily precipitation over the domain of interest in winter is negligible. Precipitation mainly occurs from May to November (from the 120th to 300th day) for both observed and simulated data (see Figure 6.16). The simulated precipitation from RCM4/ERA-Interim is two times higher than the observed precipitation from Aphrodite and TRMM (see Figure 6.16). As illustrated in Figure 6.16, the daily precipitation from RCM4/ERA-Interim can amount to more than 100 mm/day in summer. This is again caused by the cumulus convective scheme Emanuel which is used in this study. Within this study, The Emanuel convective scheme tends to produce higher precipitation over land compared other schemes (Grell, Kuo or Tiedtke). This partly represents a consistent with the previous studies (e.g., Nguyen *et al*., 2012; Ho, 2008). A typical example for this is that Nguyen *et al*. (2012) showed that the simulated precipitation is drier (50 - 100 mm/month) and wetter (100 - 200 mm/month) for the Vietnam's territory in comparison with the CRU data when the model RegCM3 was configured with the schemes Kuo and Emanuel, respectively. It is noteworthy that these tests were implemented using the NNRP2 reanalysis dataset as the initial and boundary conditions for a 10-year period during summer (from April to October).

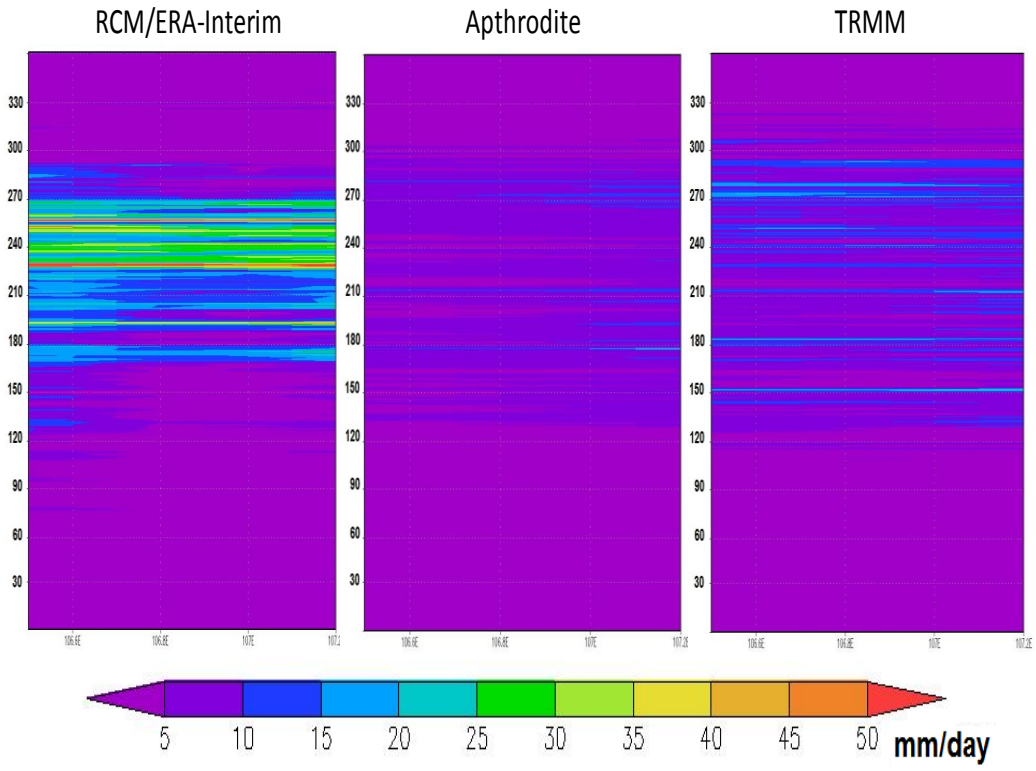

Figure 6.16: Longitude-time contour plots of daily precipitation for a band of latitude 10.3^{o}N-10.5^{o}N. The vertical axis indicates Time/day and the horizontal axis indicates Longitude/degrees (mm/day).

Furthermore, the distribution of daily precipitation (see Figure 6.17) depicts that the model poorly reproduces the number of days with a precipitation between 5 and 10 mm/day. The days with a precipitation amount of less than 5 mm/day are well simulated. However, the simulation of extreme values is poor.

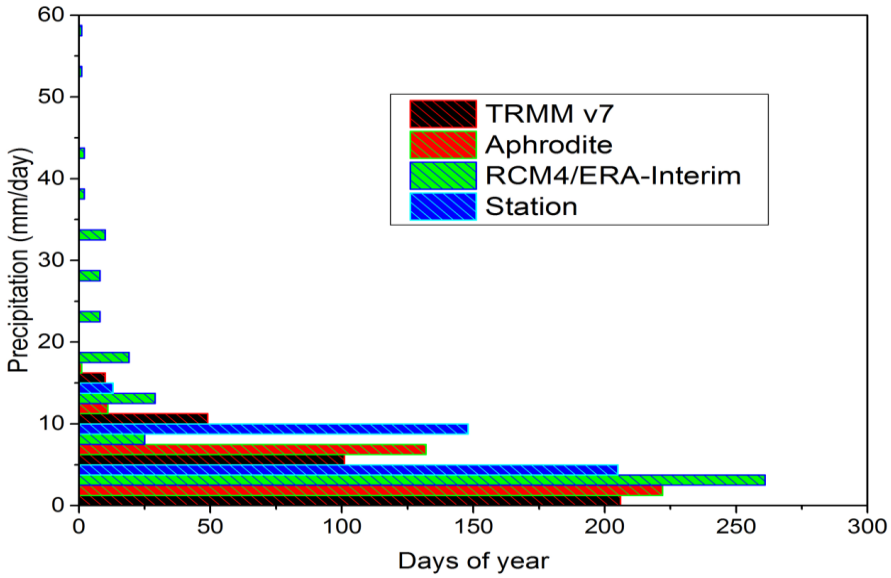

Figure 6.17: Distribution of daily precipitation over Thi Vai catchment.

6.3.2.3 Temporal variability in precipitation

Figure 6.18 shows the precipitation of different data sources over the Thi Vai basin. RCM4/ERA-Interim greatly overestimated the summer precipitation and slightly underestimated the precipitation of April, May, November and October when comparing to the station data. This shows that the summer precipitation is not reproduced well over the Thi Vai basin by RCM4/ERA-Interim. The simulated precipitation is overestimated by more than 200 mm/month.

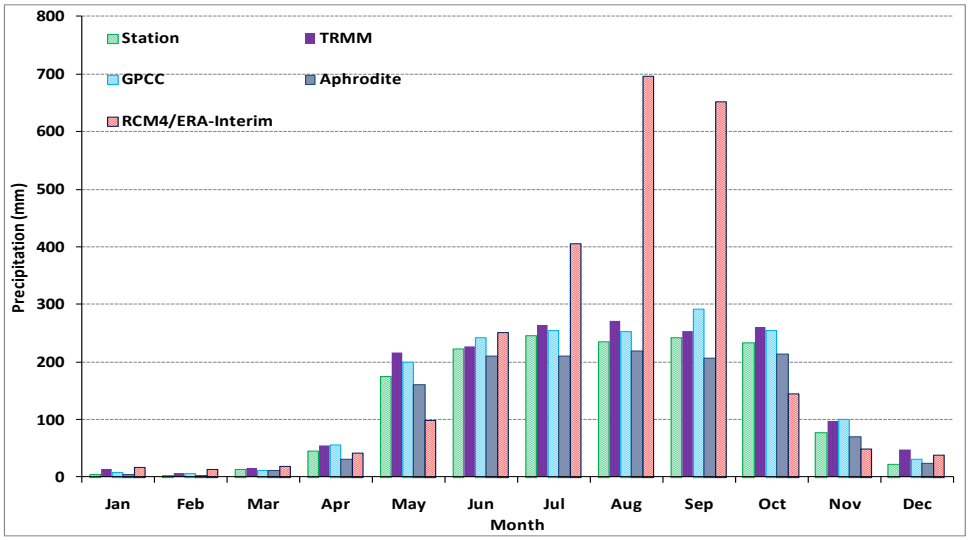

Figure 6.18: Monthly precipitation over the Thi Vai basin.

Compared to the station data, Figure 6.19 shows a large root-mean-square deviation (RMSD) for the simulation of monthly precipitation simulations by RCM4/ERA-Interim. This reflects the high degree of complexity of the spatial pattern of precipitation in this area. This is expected due to the higher signal to noise ratio of the precipitation simulation at a high spatial resolution.

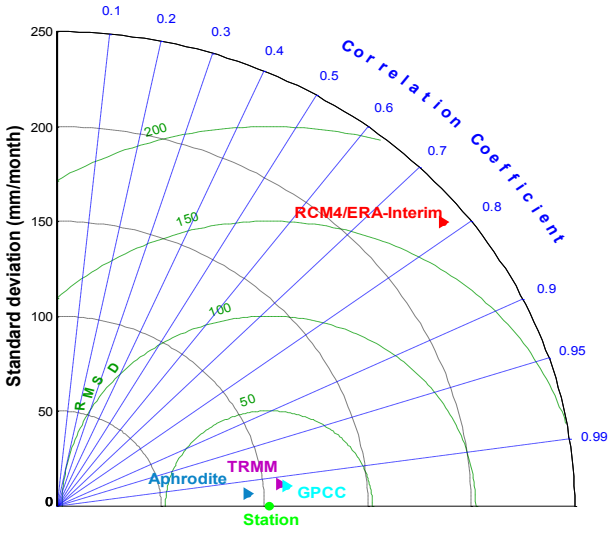

Figure 6.19: Performance of rainfall simulations over the domain of interest at the monthly scale (RMSD is the abbreviation of root-mean-square deviation).

6.4 Statistical downscaling technology for an improvement of climate simulations

The model performance for climate simulations by dynamical downscaling technology using RegCM4 shows a weakness in simulating temperature and precipitation at the daily scale, as there is a large bias compared to station data. As the main purpose of this study is to quantify the climate change impacts on flood events, approaches of statistical downscaling and bias correction were adapted and developed to improve RCM4/ERA-Interim outputs with a focus on the climate variables temperature and precipitation, respectively. After that the approaches are applied for climate simulations for past and far-future periods. The highlight point is that the outputs from RCM_BAT and RCM_CLM are considered to be predictors for the statistical downscaling approach in case of temperature variable. For precipitation variable, a bias correction approach (so-called Two Step Model-TSM) is developed to diminish the bias from dynamical downscaling model outputs. This method uses distributions of gamma with two parameters and weibull to correct the frequency and intensity of daily precipitation directly aggregated from regional climate model RegCM4 output. All nine grid point values from the RCM4/ERA-Interim outputs (see Figure 6.20) were used for defining a grid-averaged value. A correction of climate variables at the daily scale was carried out by a statistical downscaling technology for these grids.

6.4.1 Model Output Statistic for the “correction” of daily temperature

6.4.1.1 General description

A method of MOS (Klein *et al.*, 1959; Glahn and Lowry, 1972; Marzban *et al.*, 2006) was initially used as a stochastic downscaling approach for the post-processing of GCM output. The fundamental idea of this method is to identify the empirical relationships between large-scale predictors (GCMs output) and local scale predictands. One of the most important steps in statistical downscaling in

general and for the MOS method in particular is the identification of appropriate predictor variables, as they strongly influence the downscaling results. Based on an existent relationship between the predictors and the predictands, any variable can be chosen as predictors. As a rule, however, the selected predictors have a strong correlation with the predictands. Moreover, the over-fitting and decrease states in the predictive power could be loaded if too many predictors are taken into account (see more discusion in Maraun *et al.*, 2010). Hence, the quantity of the selected variables in this study is limited to get enough information of the empirical relationships between predictands and predictors. The large-scale predictors are selected from the RCM4/ERA-Interim outputs. The downscaling is carried out at the daily time step. A non-parametric stepwise predictor identification analysis is performed to identify sets of significant atmospheric predictors. Table 6.4 provides the list of atmospheric predictors identified as significant for this approach.

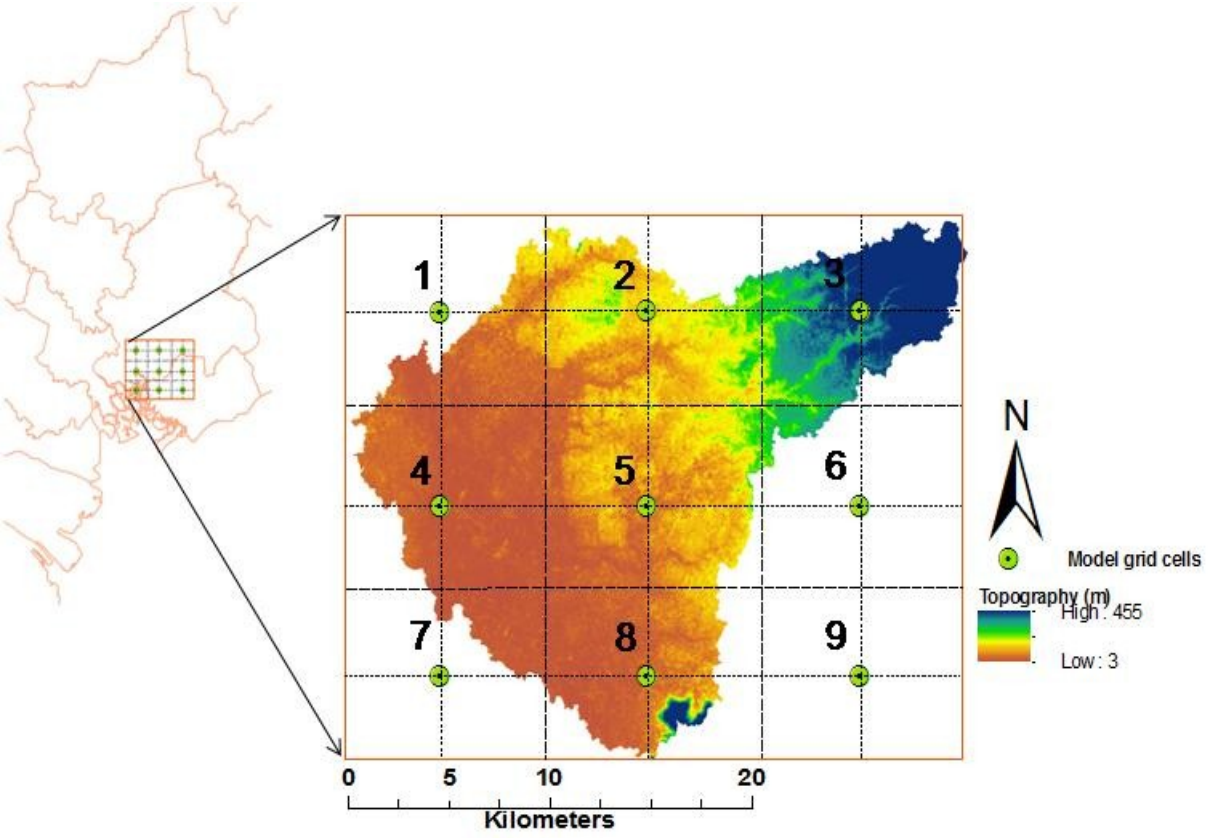

Figure 6.20: Grid cells of the domain of interest.

Table 6.4: Large-scale predictor variables for the "correction" of daily temperature.

Nr.	Predictor variables	Abbreviation	Source
1	maximum temperature	t2maxclm	RCM_CLM60
2	mean temperature	t2m	RCM_BAT10
3	velocity	vgl	RCM_BAT10
4	atmospheric pressure	ps	RCM_BAT10
5	evaportranspiration	evp	RCM_BAT10

6.4.1.2 Results

A good linear regression (see Figure 6.21) between observed and downscaled temperature data from station and model data, respectively indicates that MOS method is well fitted to the RCM4/ERA-Interim output. On average, the coefficient of determination increases from 0.5 to approximately 0.88. This proves that the combination of MOS and RCM4/ERA-Interim is an effective approach for simulating daily mean temperature. The bias of the simulated daily mean temperature reduces to nearly ±2 °C/day from ±5 °C/day. Furthermore, the regression line of the downscaled data with MOS fitted much better to the perfect line than the RCM4/ERA-Interim without MOS. Without MOS the data shows a warm bias in daily mean temperature for the values of lower than about 27 °C (see Figure 6.21a). Contrary to this, a cold bias existed for higher temperatures (see Figure 6.21a). After applying MOS, just a small warm bias is seen in daily mean temperature for values below 25 °C (see Figure 6.21b).

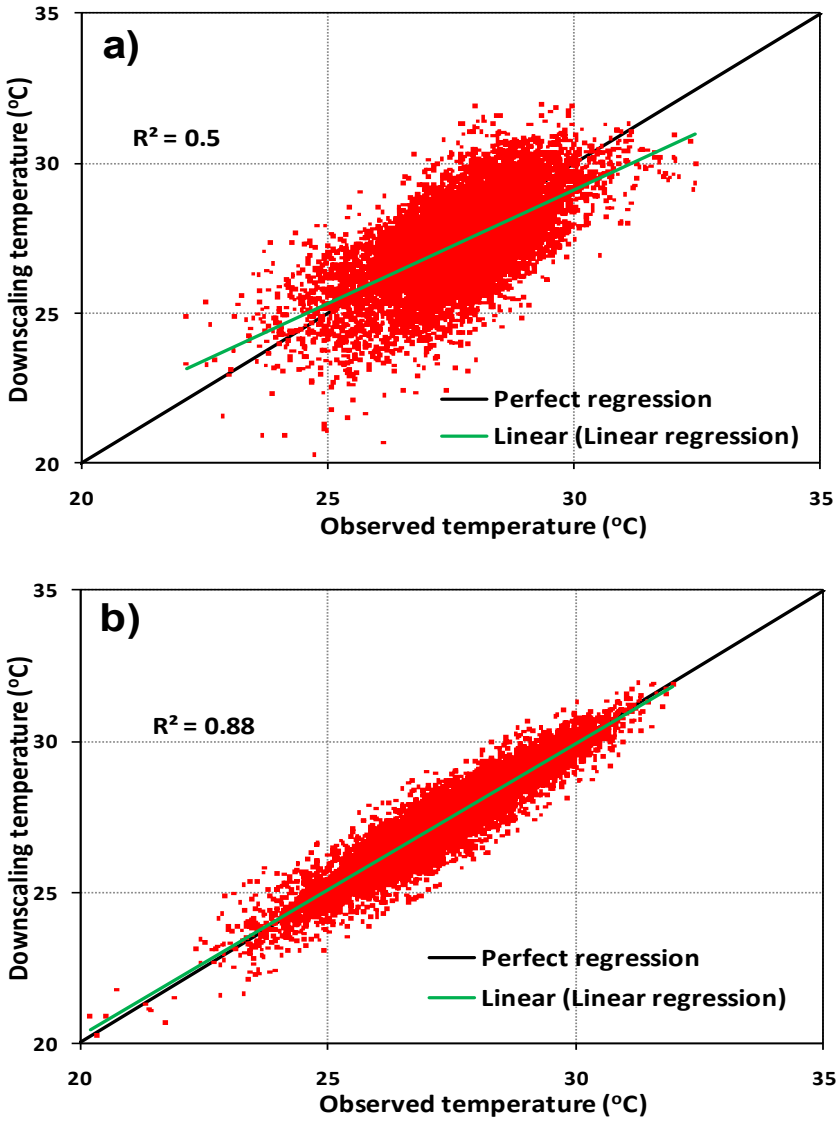

Figure 6.21: Relationship between observed and downscaled daily temperature (°C) for RCM-outputs (a) without applying MOS and (b) with the application of MOS.

6.4.2 Development of a Two Step Model for the "correction" of daily precipitation

6.4.2.1 General description

The principal idea of this method is to separate the precipitation processes into two parts: a model for the occurrence of wet days and another model for precipitation amount on wet days. This approach is called the Two-Step Model (TSM). In the first step, the distribution of Weibull (Weibull, 1951) is fitted to the distribution of the observed precipitation. For this, only the values greater than a threshold value are taken into account. Within this study, a threshold value of 0.1 mm is used for the identification of wet days in the station data time series for the period 1981-2010. The form of the Weibull distribution is the following:

$$F(x) = 1 - \exp\left[-\left(\frac{x}{b}\right)^{c}\right] \tag{6.2}$$

where:

b is the scale parameter (b > 0)

c is the shape parameter (c > 0)

The estimation of Weibull parameters is carried out using the method of least-square estimation of logarithmic transformation. These parameters are calculated separately for each month and for all nine grid cells. A threshold for the simulated wet days is identified from the RCM4/ERA-Interim daily precipitation series aggregated from the time step of three hours. The number of values that exceed the threshold in the simulated time series matches the number of wet days in the observed series. The threshold for the simulation is calculated using an assumption proposed by Michelangeli *et al.* (2009). This assumption is based on the relationship function between large scale and local scale values. The application of this relationship to calculate the threshold value for large-scale daily precipitation series can be expressed as:

$$x_m = F_m^{-1}\left(F_{obs}(x_{obs})\right) \tag{6.3}$$

where:

x_{obs} is local scale data

x_m is large scale data

F_m^{-1} is the inverse function of F_m

The F_m^{-1} function can be found by using the method of inverse transformation. The subscript denotes large-scale data and local scale data.

In the second step of the TSM, Chin and Miler (1980) pointed out that there is no dependence of distribution of daily precipitation on the preceding weather circumstances except for the winter season in the northwestern Pacific. Five distribution models for precipitation amount were also examined in the Western Pacific (Chapman, 1994). So, although many distributions were widely

studied for different areas over the world, studies in the domain of interest with its complex local climate have not been carried out so far. In previous researches, a number of distribution functions for precipitation amounts were investigated (Jones *et al.*, 1972; Woolhiser and Roldán, 1982; Ines and Hansen, 2006; Piani *et al.*, 2010a). These studies revealed that the distribution of the observational daily precipitation can be well approximated by the gamma distribution with two parameters. This distribution has a closed form of inverse distribution function. For the second step, thus, the gamma distribution with two parameters is used to correct the downscaled amount of precipitation for the previously identified wet days. The large-scale amount of precipitation above the identified threshold is carried out separately for each month by the two-parameter gamma distribution. Three datasets are manipulated in the above described way; the baseline from RegCM4 driven by GCM data from 1961 to 1990, RCM4/ERA-Interim from 1981 to 2010 and projected from RegCM4 driven by GCM data from 2071 to 2100. An assumption of the gamma distribution with two parameters has been held in these datasets. The form of the probability density function is calculated the following:

$$f(x) = \frac{\beta^{-\alpha} x^{\alpha-1}}{\Gamma(\alpha)} \exp\left(\frac{-x}{\beta}\right) \qquad \alpha, \beta, x > 0 \qquad (6.4)$$

where:

α and β denote the shape and scale parameter, respectively

x represents the daily precipitation amount

$\Gamma(\alpha)$ is the gamma function evaluated at α

In Equation 6.4, the amount of daily precipitation x (mm/day) is defined as product of the mean intensity on wet days when precipitation exceeds 0.1 mm. This means that the days with an amount of precipitation less than 0.1 mm were excluded in the calculation. First, the observed and simulated values for daily precipitation on wet days were fitted separately to the two-parameter gamma distribution with the cumulative density function of gamma distribution (see Equation 6.5).

$$F(x; \alpha, \beta) = \frac{1}{\beta^{\alpha}\Gamma(\alpha)} \int_{\tilde{x}}^{x} t^{\alpha-1} \exp\left(\frac{-t}{\beta}\right) dt \alpha, \beta, x > 0 \qquad (6.5)$$

The level of positive skew is determined by the shape parameter (α), whereas the scale parameter (β) determines the spread of values. According to Geng *et al.* (1986) and to Schuol and Abbaspour (2007), the gamma parameters can be estimated by experimental formulas. Alternatively, they can be estimated by the method of moments (Aksoy, 2000). However, the study of Wilks (2006) illustrated that the method of moments can provide particularly poor results for the case that the shape parameter is very low. Teng *et al.* (2015) showed that in comparison with other methods (e.g., Piani *et al.*, 2010a), the method of maximum-likelihood estimation can provide more accurate results. Thus, to avoid estimated values for the parameters alpha and beta that are below zero and enlarge the accuracy, the method of maximum-likelihood was used to determine these parameters (see Appendix 5). After the estimation of these parameters, the rainfall intensity was corrected by

matching the distribution of RCM4/ERA-Interim to the observed one for each month at all nine grid cells. The corrected rainfall on a wet day i can be calculated as:

$$x_{cor} = F_{obs}^{-1}\left(F_m(x_m)\right) \quad (6.6)$$

where F_{obs}^{-1} is the inverse function of F_{obs}

The simulated values below a threshold value were assigned a value of zero.

6.4.2.2 Results

Over the domain of interest, the interpolated station data at the resolution of 10 x 10 km has been used to evaluate the performance of TSM for the correction of the daily precipitation, produced from RCM4/ERA-Interim at all nine grid cells. As presented in Figure 6.22 the corrected results for the amount of precipitation are very powerful. When applying TSM, the corrected precipitation amount is closer to the observational data during the rainy season, especially from August to November for all grid cells. During these months, the daily biases fall down to about 2 mm/day from more than 10 mm/day at the first to third grid cells (see Figure 6.22). At these grid cells, the daily precipitation biases significantly reduce during the remaining months. This proves that the large biases from uncorrected simulations have been removed by the application of TSM. Although this correction method has been carried out for all nine grid cells, in this part of the work only grid1 cell is considered for a detailed analysis.

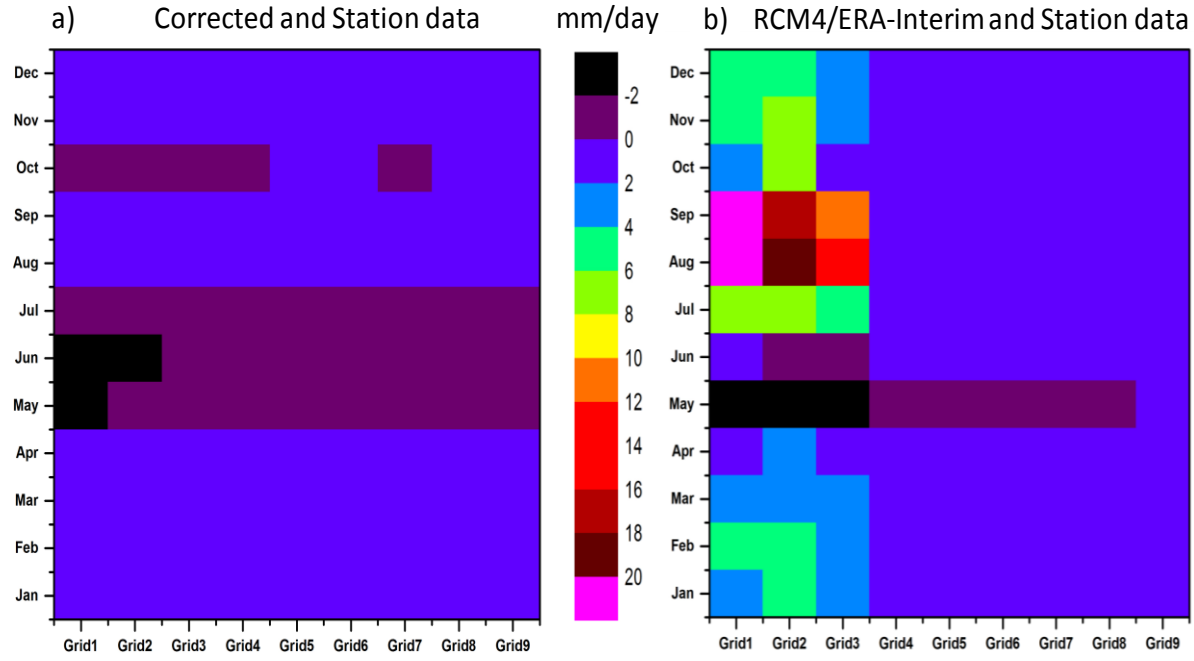

Figure 6.22: Daily precipitation intensity bias for RCM4/ERA-Interim outputs compared to interpolated station data a) with the application of TSM and b) without applying TSM for the period 1981-2010. The vertical axis denotes the time of month and the horizontal axis denotes the number of grid cells.

For the cell grid1 (see Figure 6.20), the data without the application of TSM (uncorrected data) shows an overestimation of the sum of monthly rainfall. A large positive bias for monthly values is found,

except for June. With the bias correction, the precipitation amount drops down from nearly 30 mm/day to over 5 mm/day during August to November (see Figure 6.23). A weakness of this method is the poor correction of both frequency of wet days and rainfall intensity in wintertime. A reason for this might be the overestimation of simulated rainfall values higher than the threshold value. In this study, the value of 0.1 mm is defined as a threshold because it is a standard wet day threshold in some previous studies. Using the same value could make it easier to compare the results. In the further analysis, this value will be investigated to ascertain the best suitable value for the Thi Vai basin. The analysis of observation data shows that most of the annual amount of precipitation falls between May and November. During winter in the period 1981-2010, the total amount of monthly rainfall is negligible with a value of less than 25 mm/month (see Figure 6.23). After applying the TSM, the monthly rainfall amount simulated by RCM4/ERA-Interim falls down from about 100 to less than 50 mm/month in winter.

The cumulative distribution graph (see Figure 6.24) shows the effects of TSM on the distribution of simulated precipitation in August. It can be seen from the graph that the extreme precipitation events of RCM4/ERA-Interim simulations are eliminated.

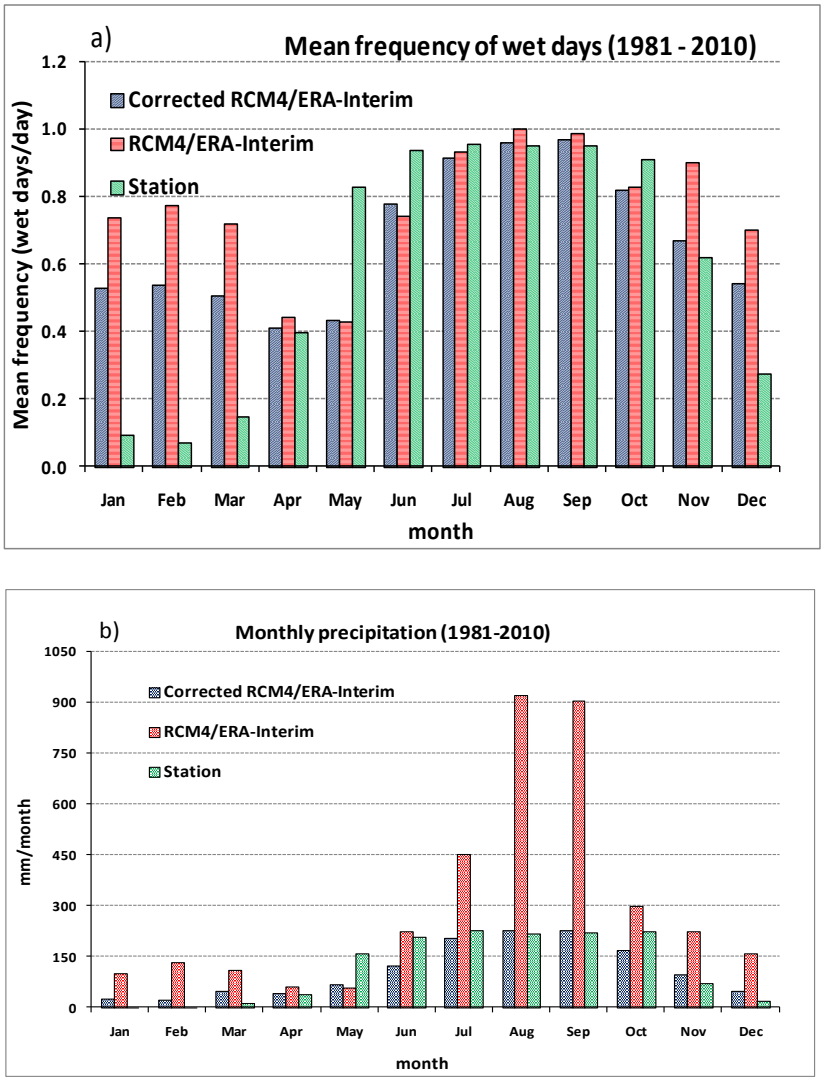

Figure 6.23: Performance of TSM at grid1 cell: (a) corrected number of wet days, (b) corrected monthly precipitation intensity.

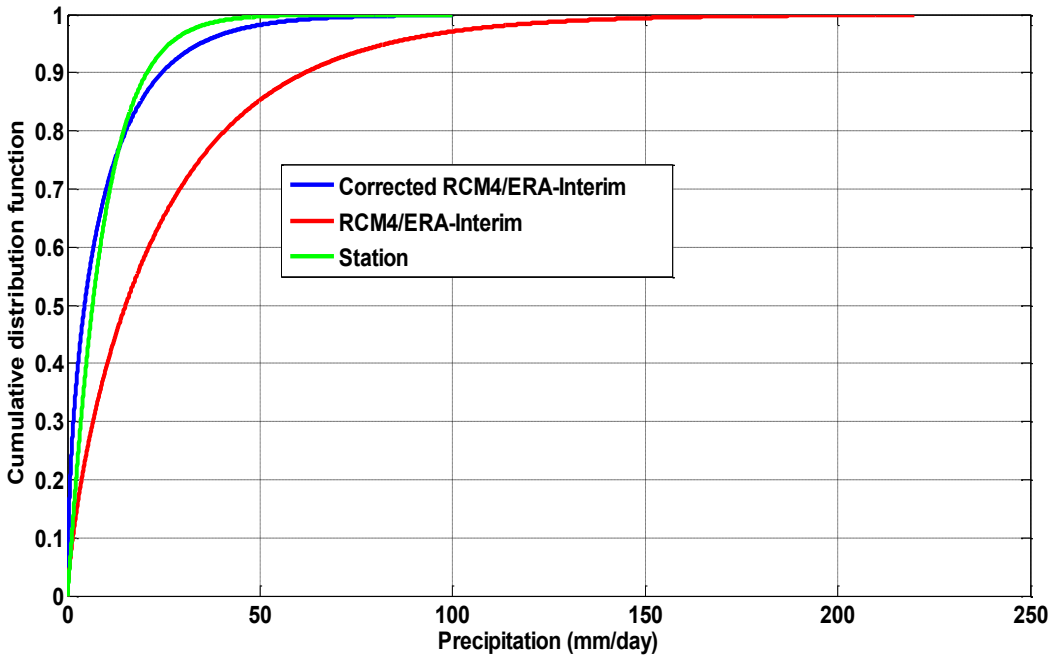

Figure 6.24: Cumulative distribution of station data, RCM4/ERA-Interim and corrected RCM4/ERA-Interim precipitation at grid1 cell in August for the period 1981-2010.

Compared to the observed data, the correction results of wet day frequency is poor for most grid cells. This is expected by the selection of the threshold value. Both wet day frequency and precipitation intensity is well performed by the application of TSM to RCM4/ERA-Interim during rainy season (May to November) when more than 92% of the annual rainfall amount is recorded over this area.

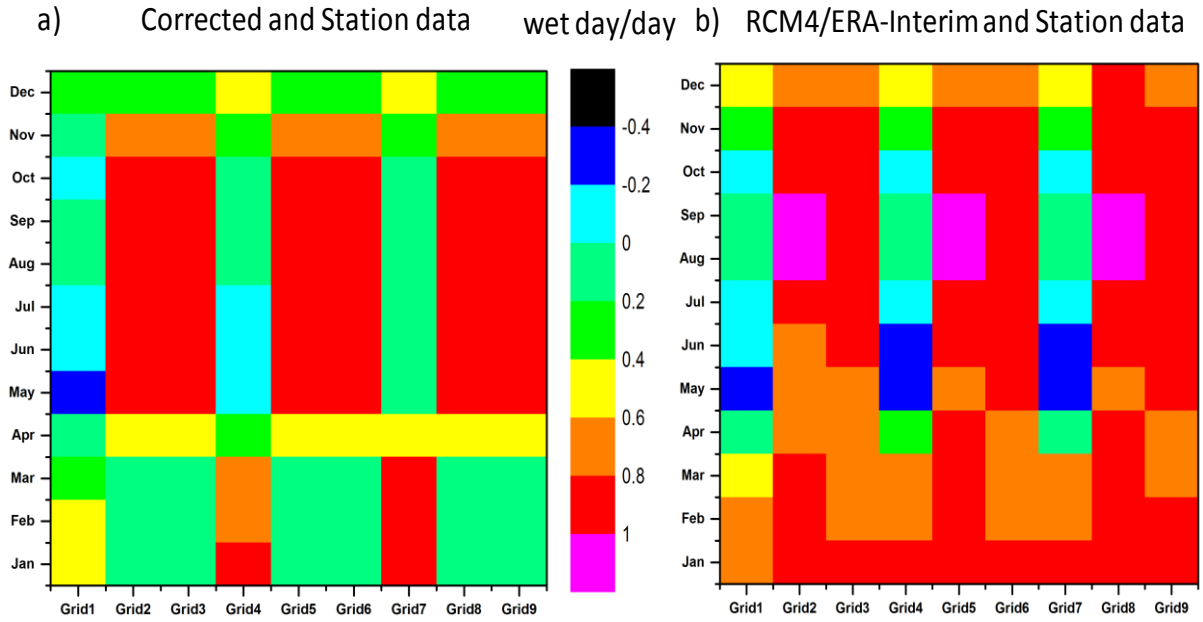

Figure 6.25: Wet day frequency bias between RCM4/ERA-Interim output and observed data a) without applying TSM and b) with the application of TSM to the RCM4/ERA-Interim output.

6.5 Climate change signals using the combined technology of dynamic-statistical downscaling

For the purpose of projecting future changes of temperature and precipitation over the Thi Vai river catchment, the climate change signal is defined as the changes in climate variables (P: precipitation and T: temperature) for the future period 2071-2100 under the A1B emission scenario in comparison with the baseline period 1961-1990 as follows:

$$\Delta T = T_{2071\text{-}2100} - T_{1961\text{-}1990} \quad (6.5)$$

$$\Delta P = P_{2071\text{-}2100} - P_{1961\text{-}1990} \quad (6.6)$$

6.5.1 Climate Change signals in precipitation

Figure 6.26 provides information on the seasonal precipitation change signals and the absolute values of projected precipitation. In summer, the projected change of average daily precipitation over the study area amounts to around 1mm/day for the decades 2081-2090 and 2091-2100 (see Figure 6.26a). Over the whole period 2071-2100, an increase in the projected precipitation up to over 0.8 mm/day is illustrated in Figure 6.26a. Compared to other decades, the projected change of daily precipitation is lower with over 0.4 mm/day in the first decade in 2071-2100. In spring (MAM), a slight increase in daily precipitation up to about 0.7 mm/day is projected for the period 2071-2080. Other periods 2081-2090, 2091-2100 and 2071-2100, however, a slight decrease in daily precipitation around -0.4 mm/day is documented (see Figure 6.26a). As illustrated in Figure 6.26a, there is a similar tendency of projected change in daily precipitation during four seasons between the different periods 2081-2090, 2091-2100 and 2071-2100. A dissimilar tendency of this change is pointed out during winter and spring for the decade 2071-2080 in comparison with other periods (see Figure 6.26a). In general, the change signals in precipitation are not clear over the period 2071-2100 in winter and spring. The strongest signal in the projected precipitation change is in summer and in autumn (over ±0.8 mm/day) for the periods 2081-2090, 2091-2100, 2071-2100 and for the periods 2071-2080, 2091-2100, respectively. The projected absolute precipitation values are shown in Figure 6.26b. It can be seen from the graph that a summer precipitation of approximately 16 mm/day is projected, followed by spring (nearly 8 mm/day). The lowest projected precipitation is over 1 mm/day in winter.

To get an accurate picture of the variation in changes in precipitation over a period of 30 years from 2071 to 2100 compared to the period from 1961-1990, the projected changes and absolute values of monthly precipitation are produced (see Figure 6.27). For the first decade from 2071-2080, the changes in daily precipitation range from about -1.0 to 2.5 mm/day. During 2091-2100, the projections for the changes range between below -2.0 and over 1.5 mm/day (see Figure 6.27a).

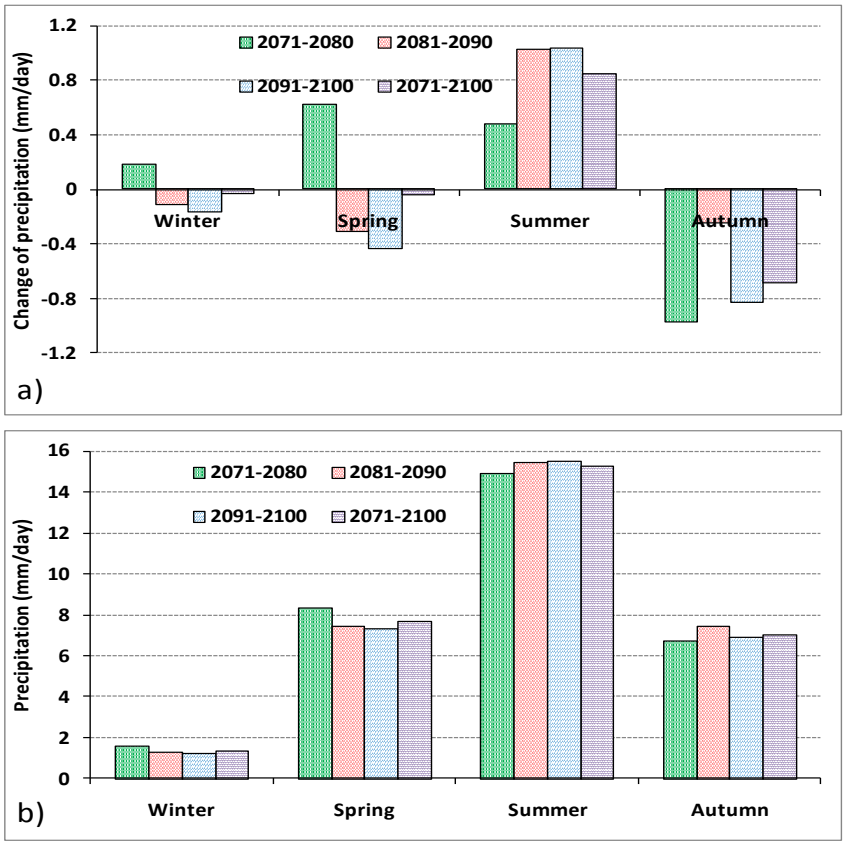

Figure 6.26: a) Projected changes of seasonal precipitation over the Thi Vai River basin for the period 2071-2100 compared to 1961-1990 and b) projected absolute precipitation for the four seasons under the SRES A1B scenario.

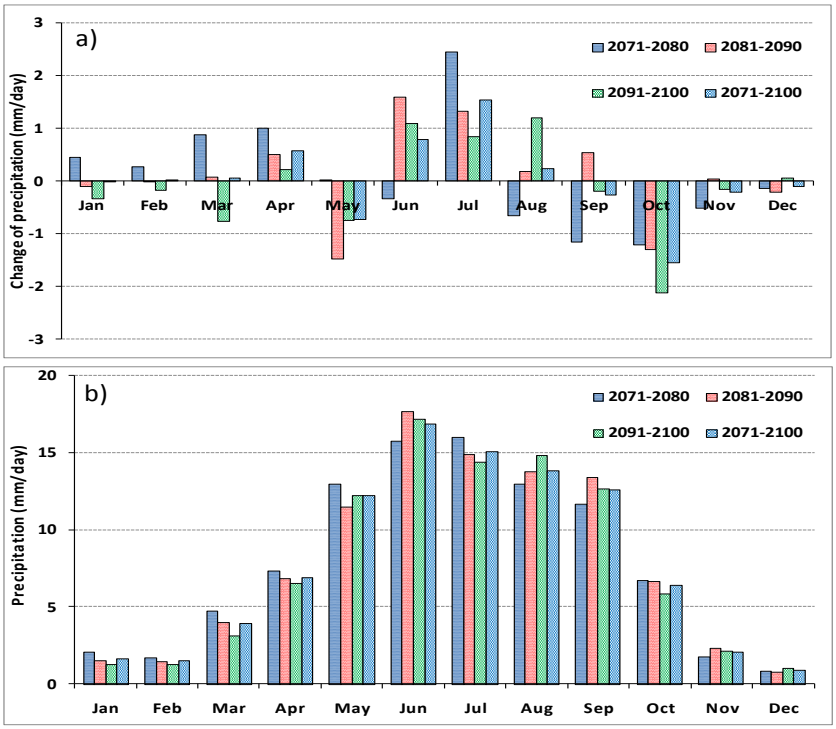

Figure 6.27: a) Projected changes of monthly precipitation over the Thi Vai River basin for the period 2071-2100 compared to 1961-1990 and b) projected absolute precipitation for each decade from 2071-2100 under the SRES A1B scenario.

Figure 6.27a exhibits the projected changes of mean monthly precipitation in the basin. Generally, there is a similar tendency for change is mean precipitation for all decades. During the period 2071-2100, on a monthly basis, the amount of average increase in precipitation is highest in July (about 1.5 mm/day), followed by June (approximately 1 mm/day). The largest decrease in average precipitation is projected for October (nearly minus 1.5 mm/day), followed by May (over 0.5 mm/day). At the end of the 21st century, the largest decrease of precipitation is projected for October (well over 2 mm/day). Monthly projected absolute precipitation for each decade from 2071-2100 is displayed in Figure 6.27b. As illustrated in Figure 6.27b, the largest precipitation is projected for June (over 15 mm/day) for the periods 2081-2090, 2091-2100 and 2071-2100. In the decade 2071-2080, the largest precipitation is projected for July (over 16 mm/day). It is noteworthy that total monthly projected precipitation values of over 100 mm/month begins in March and ends in October.

6.5.2 Climate change signals in temperature

Figure 6.28 shows the projected changes of seasonal and annual temperature change and the projected absolute values for temperature. In winter, the mean daily temperature is projected to increase by approximately 2.8 ^{o}C. In spring, the seasonal temperature may increase by over 3.2^{o}C. The greatest increase is projected in spring, the lowest in summer. In summer, the simulation shows an increase of seasonal temperature of approximately 3 ^{o}C. In autumn, the seasonal temperature is projected to increase by about 3 ^{o}C. The spring temperature is projected to amount approximately 30 ^{o}C, followed by summer (above 29 ^{o}C).The smallest projected temperature is over 28 ^{o}C in winter (see Figure 6.28b) during 2071-2100. At annual scale, temperature is projected to increase by more than 3 ^{o}C.

The projected absolute temperature value is the smallest in winter and highest in spring in a given decade. The tendency of these values amounts to higher values in order of decades 2071-2080, 2081-2090 and 2091-2100 (see Figure 6.28b).

Figure 6.29 exhibits the projected changes in the mean monthly temperature in the basin for the period 2071-2100 compared to 1961-1990. There is a similar tendency of mean temperature between different decades, except for in the first decade (2071-2080). During the whole period 2071-2100, the projected increase in temperature is the greatest in May (about 3.5 ^{o}C) and November (over 3 ^{o}C), followed by December, April, and June (around 3 ^{o}C), while the warming for the other months is less. The greatest value of projected increase in temperature is documented in May, followed by November for the decades 2081-2090 and 2091-2100. Contrary to this, the projected increase in temperature is the greatest in June, followed by October for the decade 2071-2080 (see Figure 6.29a). The net result is fairer winter temperatures and increased spring temperatures. At the end of the 21st century, the temperature reaches the first peak in April and the second one in May (around 31 ^{o}C and over 30.5 ^{o}C, respectively). The lowest temperature is projected for January, followed by December (over 26.5 ^{o}C and just above 27 ^{o}C, respectively).

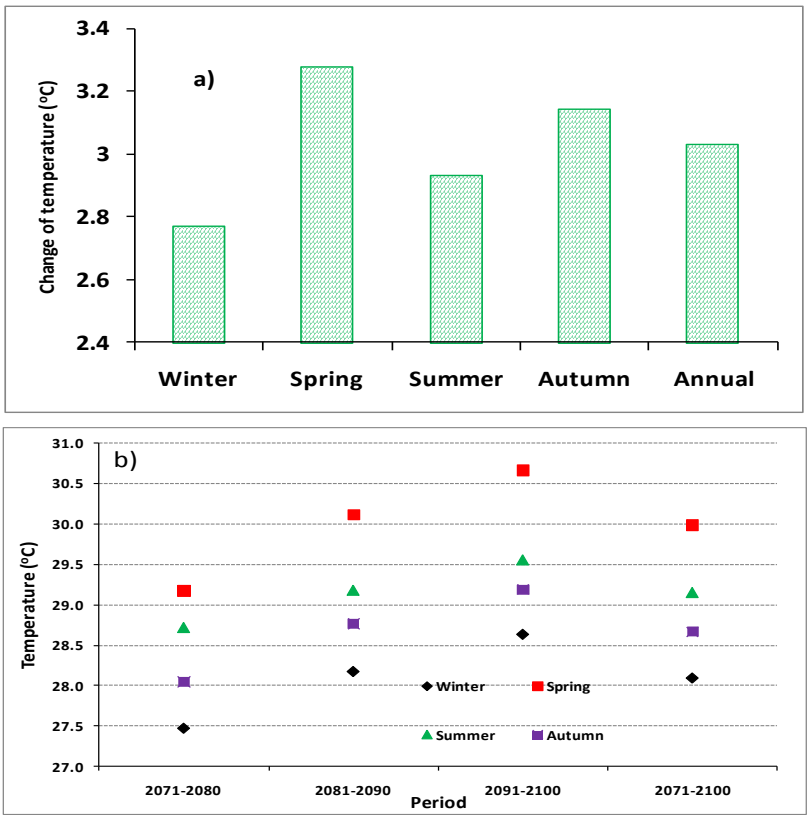

Figure 6.28: a) Projected changes of seasonal temperature over the Thi Vai River basin for the period 2071-2100 compared to 1961-1990 and b) projected absolute temperature values for the decades in 2071-2100 under the SRES A1B scenario (°C).

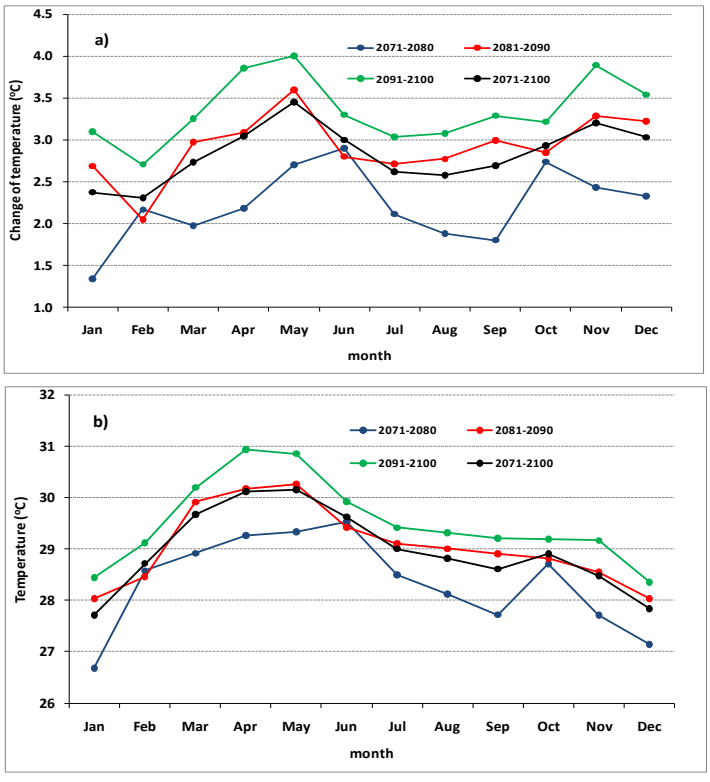

Figure 6.29: a) Monthly temperature difference for the decades 2071-2100 compared to 1961-1990 and b) projected absolute temperature for the decades in 2071-2100 under the SRES A1B scenario (°C).

In summary, the projected climate change signal is very clear in case of temperature. In case of precipitation, however, this signal is not clear in winter and spring. In summer and autumn, wetter conditions and drier conditions are projected compared to the late 20th century, respectively. These projected opposite are an indicator for only small changes in the precipitation over the entire Thi Vai region as documented in chapters 3 and 5.

7 POTENTIAL CLIMATE CHANGE IMPACTS ON STREAM FLOW

To investigate the potential climate change impacts on stream flow, the combination of meteorological and hydrological modeling is applied. The focus in this chapter is on hydrological modeling using the outputs of dynamic-statistical downscaling as input. The simulations of the hydrological model and the impacts of climate change on hydrological characteristic will be analysed for the future period 2071-2100.

7.1 The hydrological model PANTA RHEI

As a long tradition of the development and application of hydrological models at the Department of Hydrology, Water Management and Water Protection (HYWAG) of the Leichtweiss Institute of Hydraulic Engineering (LWI) at the TU Braunschweig, the hydrological model system PANTA RHEI has been developed and applied since 2006 in collaboration with the Institute for Water Management IfW GmbH, Braunschweig. PANTA RHEI is based on the preceding model system NAXOS (Riedel, 2004). It has been written in C++.

PANTA RHEI is a deterministic, semi-distributed, hydrological model system with a vector based GIS-interface (Riedel et al., 2011). The three hydrological processes of (1) the formation of runoff consisting of precipitation, interception, infiltration and percolation, (2) the concentration of runoff consisting of surface runoff, interflow and baseflow and (3) the routing of flow are the main processes in PANTA RHEI as shown in Figure 7.1.

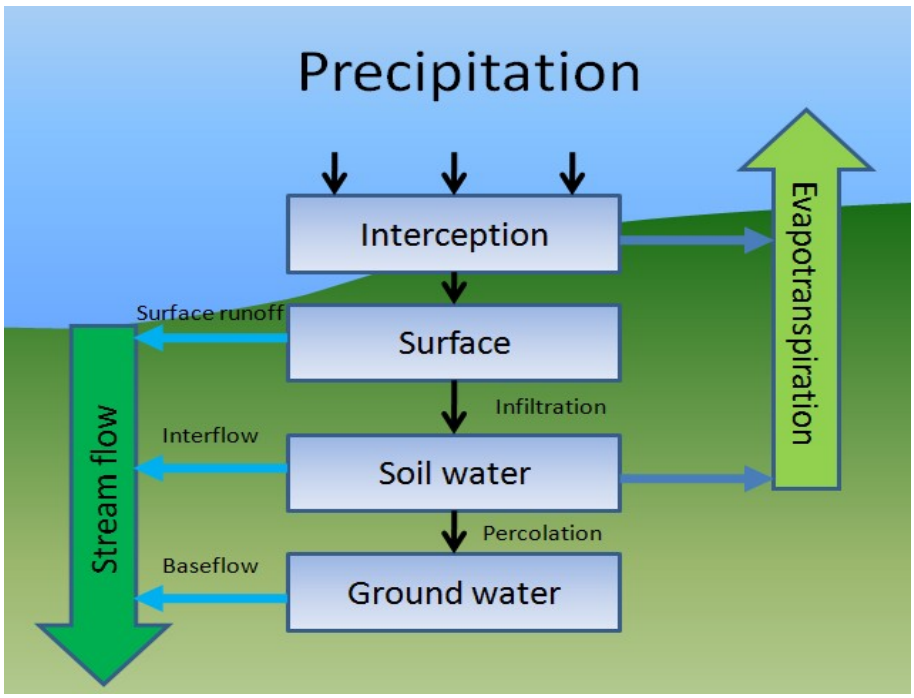

Figure 7.1: Main hydrological processes.

The application of PANTA RHEI requires spatial data for topography, land use and soil types as input. As part of the pre-processing, the catchment is divided into a number of sub-catchments based on

the river network and the topography. A further subdivision of each sub-catchment is defined by hydrotopes (or hydrological response units, HRUs) which are homogeneous in terms of their soil type and land use type. For each hydrotope, the hydrological processes of runoff formation and runoff concentration are calculated. Hydrological characteristics can be displayed for any sub-catchment. A modern graphical user interface allows to manage large amounts of data that are needed for the simulations as shown in Figure 7.2.

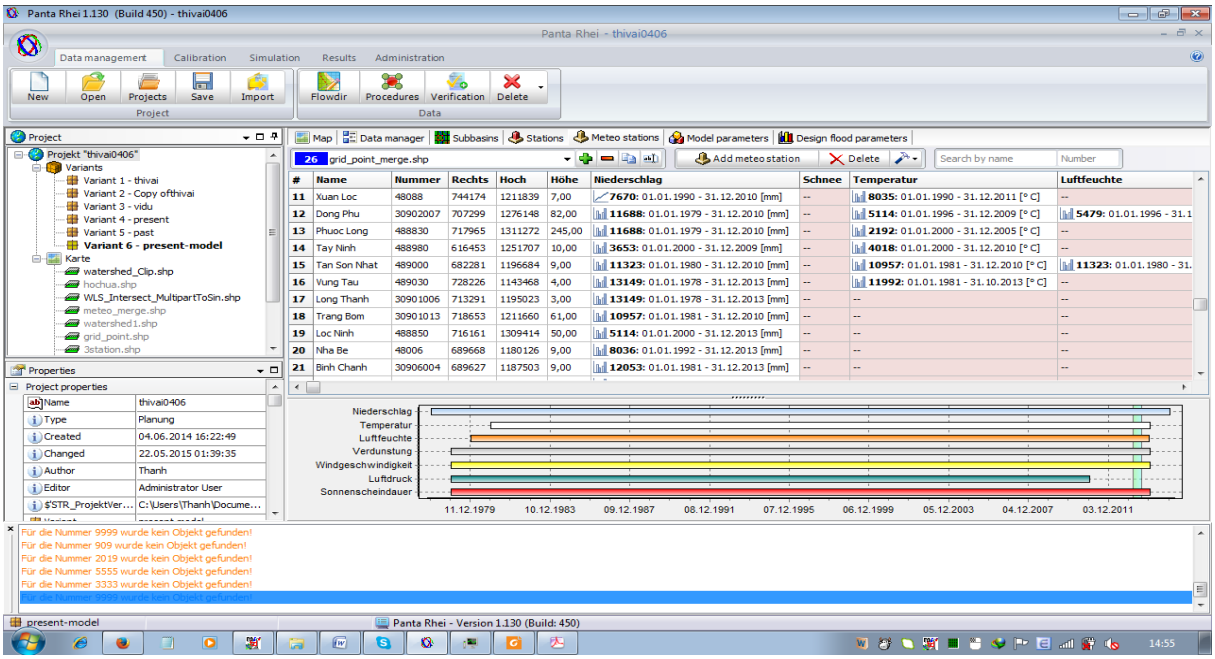

Figure 7.2: Screenshot of the windows in the tab "Meteorological stations" in PANTA RHEI.

The model system can be applied for hydrological planning of flood protection measure (event-based simulations), in research (climate change impacts on the water balance with long-term simulations) and for operational flood forecast (e.g., in Lower Saxony, Germany). The model is also successfully applied for international projects (Meon *et al*., 2014). PANTA RHEI outputs simulations can be used as input for other modelling systems, e.g., for hydrodynamic surface flow. Further developments and applications of PANTA RHEI can be found in Förster (2013), Förster *et al*. (2014), Kreye (2015) and Lorenz (2015).

7.2 Structure of the hydrological model PANTA RHEI

7.2.1 Evapotranspiration

The estimation of potential evapotranspiration is of great importance for climatological modeling as well as for hydrological modeling. It is defined as the maximum amount of water that evapotranspirates in a given climate from the vegetation that covers the whole ground and that is well supplied with water (WMO, 2008). PANTA RHEI provides several options for the estimation of potential evapotranspiration: Priestley-Taylor (Priestley and Taylor, 1972), Penman-Monteith (Monteith, 1965), etc. The choice of a method depends on the data availability. In this study, the

method of Penman-Monteith is used. At each time step and for each hydrotope, the potential evapotranspiration is calculated as follows:

$$ETP_{t,i} = \frac{1}{L} \cdot \frac{\Delta \cdot (R_N - G) + \rho \cdot c_p \cdot (e_s - e)/r_a}{\Delta + \gamma \cdot \left(1 + \frac{r_c}{r_a}\right)} \quad (7.1)$$

where:

R_N is the net radiation [W/m²]

G is the soil heat flux [W/m²]

(e_s - e) represents the vapour pressure deficit of the air [Pa]

r_a is aerodynamic resistance [s/m]

ρ_a is the mean air density at constant pressure [kg/m³]

L is enthalpy of evaporation [J/kg]

c_p is the specific heat of the air [J/(kg K)]

Δ represents the slope of the saturation vapour pressure temperature relationship [Pa/K]

γ is the psychrometric constant [Pa/K]

r_s is surface resistance [s/m]

7.2.2 Interception

In Horton (1919), precipitation interception is defined as precipitation which does not reach the soil. This component can be a small fraction of total evapotransspiration and is neglected in some models (Gerrits *et al.*, 2010). Swank (1968), however, stated that interception is a major hydrologic process that influences the quantity, timing and spatial distribution of water input and output in a catchment. This is due to the loss of from 10 to 35% of annual precipitation in forest interception studies in the United States (Kittredge, 1948; Zinke, 1967). Later, Savenije (2004) also showed that interception plays an important role in rainfall-runoff analysis because the intercepted amount of rainfall significantly contributes to the water balance budget. Because of the importance of this parameter, a storage balance module is used to simulate the interception process in PANTA RHEI.

7.2.3 Runoff formation

Generally, surface runoff is defined as all the waters that flow on the surface of the earth, including overland sheet flow and channel flow in rills, gullies, streams or rivers (ASCE, 1996). In order to simulate this process, a great variety of models has been developed by different authors. According to the report of WMO (1975), the differences between model simulations are quite small in comparison with deviations between measured and simulated stream flow. For the simulation of

surface runoff, the approach of SCS[26] that allows the direct calculation of the runoff volume has been widely applied in hydrological models due to the simplicity, predictability and stability (Ponce and Hawkins, 1996). This approach is based on the potential of soil to absorb a certain amount of moisture. It can be found in most hydrology textbooks or handbooks (SCS, 1972; Chow *et al.*, 1988). At the LWI of the TU Braunschweig, Riedel (2004) has developed a modified version of the SCS method. In the original version, the possible infiltration depends on the classified soil group and the land use type. It is calculated by using Equation 7.2. To get better time-dependent soil moisture in PANTA RHEI, however, the soil moisture-dependent curve number is calculated by the equations 7.3 and 7.4.

$$S = \frac{25400}{CN} - 254 \tag{7.2}$$

where:

S is potential maximum retention [mm]

CN is runoff curve number [-]

$$CN_{sm} = \begin{cases} \dfrac{1000}{\dfrac{1000}{CN} - \dfrac{rsm_{(t)}}{25.4}} & \text{for } CN < 100 \\ 100 & \text{for } CN \geq 100 \end{cases} \tag{7.3}$$

where:

CN_{sm} is the soil moisture-dependent curve number [-]

CN is the curve number of the soil moisture class II [-]

$$rsm_{(t)} = rsm_{(t-1)} + Neff_{(t)} - (Qtfl_{(t)} + QS_{(t)} + V_{(t)}) \tag{7.4}$$

where:

$rsm_{(t)}$ is relative soil moisture [mm]

$rsm_{(t-1)}$ is relative soil moisture from the previous time step [mm]

$Neff_{(t)}$ is direct runoff [mm]

$Qtfl_{(t)}$ is area runoff [mm]

$QS_{(t)}$ is saturation of the soil moisture through precipitation [mm]

$V_{(t)}$ is evaporation [mm]

[26] U. S. Soil Conservation Service.

7.2.4 Runoff concentration

PANTA RHEI provides a transfer function of single linear storage to simulate the runoff concentration process. This function is based on the assumption of a proportionality factor between the runoff of the reservoir and the actual storage content.

$$Q(t) = \frac{S(t)}{K} \tag{7.5}$$

where:

Q(t) is runoff at time step t [m³/s]

S(t) is storage content at time step t [m³]

K is proportionality factor [s]

Layers in the soil can be used to describe the runoff concentration process. In PANTA RHEI, up to four different soil storages are filled with different mean residence time through the process of runoff formation.

7.3 Model setup

In this work, the stream flow was calibrated at the stations Binh Son, Suoi Ca and Cau Vac (see Figure 3.15). The drainage areas are 29, 164.7 and 57.2 km^2 for the sub-catchments Binh Son, Suoi Ca and Cau Vac, respectively. An overview scheme of the application of the hydrological model PANTA RHEI for the case study area of the Thi Vai river basin is shown in Figure 7.3. Layers of land use, soil type and topography are separately given in chapter 3 in detail. The procedure includes the delineation of the watershed, the calibration and the simulation. The hydrotopes (or HRUs) were produced by overlapping the maps of sub-basins, land use and soil. Artificial structures like reservoirs or retention structures are not included in the watershed model due to the lack of data. The data of the sub-catchment areas were imported and handled directly via the GIS interface of PANTA RHEI (see Figure 7.2). Meteorological data is entered at one-day time step but PANTA RHEI internally calculates with a one-hour time step. During the calibration process, an adjustment of values for the model parameters was carefully performed to improve the results of discharge simulation, so that the simulated values are as close as possible to the observed ones. In comparison with measured data, these model parameters were adjusted until the simulation results are “sufficiently accurate” for the project goal. In this study, the procedures given in Table 7.1 were chosen for the simulation.

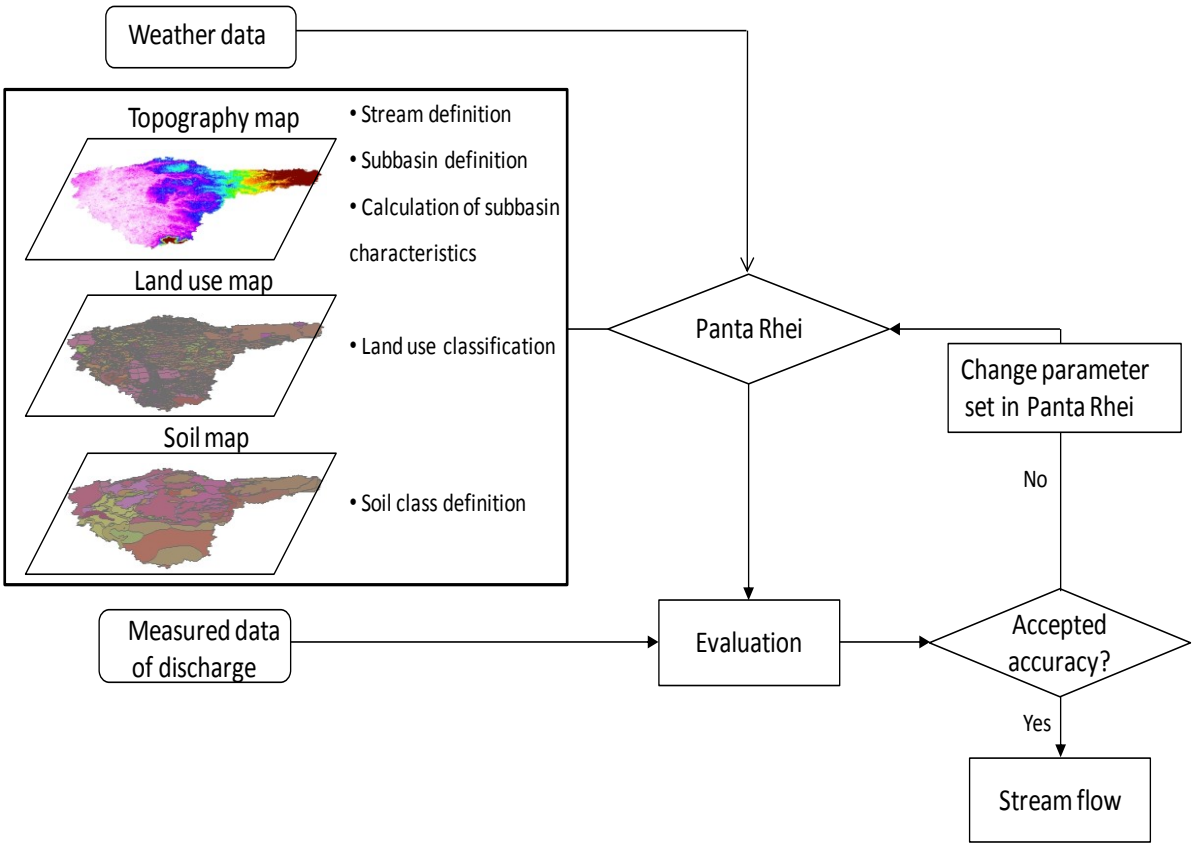

Figure 7.3: Flow chart of modeling stream flow in the Thi Vai river basin using PANTA RHEI.

Table 7.1: Selected procedures for water budget.

Process	Procedure description for water budget
Potential evapotranspiration	Penman-Monteith
Interception	(Standard) storage balance method
Runoff-formation, soil water	Extened SCS after Riedel (Riedel, 2004)
Concentration of runoff	4 linear storages
Base-flow	4 linear storages
Flow routing in river reaches	Linear storage function

The meteorological data at the five precipitation measuring stations Vung Tau, Bien Hoa, Long Thanh, Tam Thon Hiep and Cam My is used to calibrate the stream flow. The locations of these stations can be seen in Figure 3.4.

7.4 Evaluation of the model performance

Efficiency criteria are used to evaluate the performance of PANTA RHEI by comparing the simulated with the measured discharge data. Thus far, the Nash-Sutcliffe efficiency (NSE) (Nash and Sutcliffe, 1970) and the coefficient of determination (R^2) are the most frequently used criteria for evaluating the performance of hydrological models. If the value of R^2 and NSE is less than or close to zero, the model simulations are considered unacceptable. Alternatively, if the values approach one, the model simulations become perfect (see Table 7.2). These efficiency measures are very sensitive to the peak

flows but not so much to low flows. None of the efficiency criteria is perfectly suitable for all tested cases. As suggested by Krause *et al.* (2005), the Nash-Sutcliffe efficiency with logarithmic values ln(NSE) is added to expect a better quantification of the performance in different conditions (peak and low flows).

Table 7.2: Statistical evaluation indices.

Index	Formula	Range	Significant
ln(NSE)	$\ln(\mathrm{NSE}) = 1 - \frac{\sum_1^n (\ln O_i - \ln F_i)^2}{\sum_1^n (\ln O_i - \ln \bar{O})^2}$	$-\infty \le \ln(\mathrm{NSE}) < 1$ Perfect score: 1	Difference between the simulated and the observed values.
NSE	$\mathrm{NSE} = 1 - \frac{\sum_1^n (O_i - F_i)^2}{\sum_1^n (O_i - \bar{O})^2}$	$-\infty \le \mathrm{NSE} < 1$ Perfect score: 1	Difference between the simulated and the observed values.
Coefficient of determination	$R^2 = \left(\frac{\sum_1^n (F_i - \bar{F})(O_i - \bar{O})}{\sqrt{\sum_1^n (F_i - \bar{F})^2} \sqrt{\sum_1^n (O_i - \bar{O})^2}} \right)^2$	$0 \le R^2 \le 1$ Perfect score: 1	The correlation between the simulated values and the observed values.

The discharge data from 11/3/2013 to 31/12/2013 at Binh Son station and from 11/3/2013 to 31/5/2014 at the stations Cau Vac and Suoi Ca were used for the analysis and the calibration of PANTA RHEI. Figure 7.4 depicts the average daily measured and simulated discharge after the calibration.

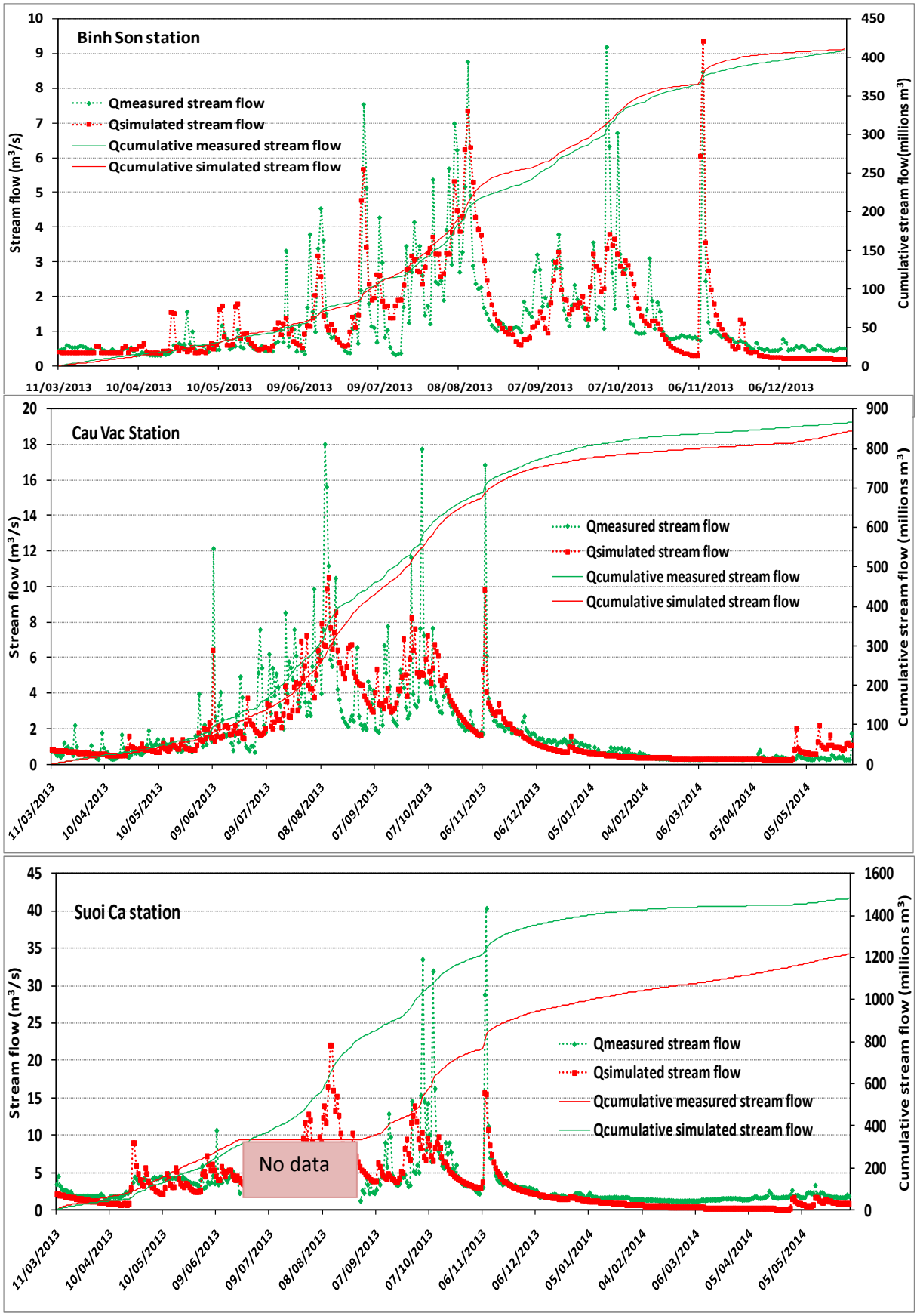

Figure 7.4: Hydrographs of simulated and measured discharge at the stations Binh Son, Cau Vac and Suoi Ca using the station data.

On the daily time step, R^2 and NSE are 0.6 and 0.6 for the station Cau Vac, 0.54 and 0.52 for the station Suoi Ca, and 0.63 and 0.61 for the station Binh Son, respectively. The ln(NSE) index for the daily data is 0.81 for Cau Vac, 0.05 for Suoi Ca and 0.58 for Binh Son. This implies that the discharge simulation at the stations Binh Son and Cau Vac well fitted to the measurement data for both peak and low flows, especially for low flows at the station Cau Vac. On the other hand, the low flow simulations are too hard for Suoi Ca. It needs to be considered that the indices for the statistical evaluation for Suoi Ca are calculated for a shorter period. The reason for this is that the data is not available for the period from 23/06/2013 to 28/8/2013. The coefficient of determination R^2 for all stations indicates that the model is able to explain at least 54 percent of the variability in the measured stream flow, which means a moderate agreement between observation and simulation. The events of single peak flows are well captured by the model. The visual inspection shows that the peak flows are often underestimated by the model. Figure 7.4a shows that the extreme events, except the one on 2/10/2013, are well captured by the model at the station Binh Son. At the other stations, the simulated peak flows, however, sometimes occur a day later than the observed peak flows (e.g., on 7/10/2013 at the station Cau Vac). The main reasons of this might be (1) the sparse density of rain gauges over Southern Vietnam, (2) insufficient rainfall data over the catchment, (3) the complex interaction of tropical climate patterns within this region (i.e., the local convective precipitation events). More importantly, hydropower dams located in upstream of the Dong Nai catchment (e.g., Dong Nai 3), weirs (e.g., Long An, Ba Ky), reservoirs (e.g., Binh Son, Cau Moi) and drain (e.g., Ong Keo) are not taken into account due to a sophisticated system. The location of these place-names can be found in DONRE (2015). According to Vu (2009), hydraulic characteristics (slope of water surface, morphology and roughness of river bed) are strongly affected by these factors. Therefore, there exists a potential deviation between measured and simulated flows (high and low flows). The sparse density of rain gauges and insufficient rainfall data over the catchment are a great source of uncertainty as precipitation is the most important input parameter for the hydrological model. Furthermore, the local conditions (e.g., convective processes) strongly influence the precipitation events and therefore the quality of the simulations of the hydrological model. Considering all model simulations, the statistical indices for the model efficiency indicate that the model could be calibrated satisfactorily.

As pointed out in the EWATEC-COAST project, the calibration results for the stream flow are very good (see Meon *et al*., 2014). In comparison with EWATEC-COAST results for calibration in the same period, the study results show a slight worse model performance. On the example of calibrated stream flow at Cau Vac station, the statistical indices R^2, NSE and ln(NSE) are 0.6, 0.6 and 0.81 for this study, but 0.73, 0.61 and 0.79 for the EWATEC-COAST project, respectively. The reasons for this are slightly different methods used for the processing of measured discharge and different configurations of PANTA RHEI between this study and the EWATEC-COAST project (see more Meon *et al*., 2014). For example, meteorological data is used at one-day time step in this study instead of step of one-hour in the EWATEC-COAST project. In this work, only terrestrial meteorological data is used after the steps of analysis and validation of obtained data as illustrated from the previous chapters, meanwhile the EWATEC-COAST project used the reproduced data from a combination of the

observational precipitation amount and distribution of precipitation obtained from the TRMM. The main objective of this study is to downscale climate variables from global to local scale and to develop a climate change impact scenario on water balance. Therefore, a slight difference is acceptable as the focus is on the analysis of projections for future stream flow under the climate change scenario SRES A1B.

In terms of the total amount of stream, the model simulations show a slight underestimation during the dry season and an overestimation in the rainy season at the stations Binh Son and Cau Vac. Contrary to this, an underestimation is seen during the considered period (11/3/2013 to 31/5/2014) at the station Suoi Ca. Although the peak flows are not accurately captured, the simulation results show a good match with the measured data (see Figure 7.4). When aggregating the daily data to monthly mean values, the simulation results for stream flow are good. Due to insufficient availability of measured data, an additional simulation of discharge is performed for the period between March 2008 and May 2009. The PANTA RHEI model parameters from the calibration and the climate data from the stations Vung Tau, Bien Hoa, Long Thanh, Tam Thon Hiep and Cam My were used. These simulated discharge data is considered to be the reference data. The purpose of this is to provide discharge information for the period when downscaled climate data is available for the period March 2008-May 2009. These climate data can be directly applied as input for PANTA RHEI by using the PANTA RHEI model parameters obtained by the calibration. However, this partly contributes to the errors of the model simulations. Thus, the reference data is used for the comparison with the simulated discharge, when using the downscaled climate data as input for PANTA RHEI. The aim of this work is to evaluate the performance of the hydrological model using the downscaled climate data. There are a couple of reasons for this approach:

- Reanalysis data for the downscaling cannot be obtained for the period from August 2013 to now. The reason for this is that only large meteorological centers over the world can create these reanalysis data with supercomputer systems.
- The similarity analyses to transfer the statistical indices (e.g., mean index of discharge) from neighbouring catchments into the study area are a useful approach. However, this is an extremely great challenge for medium and small sub-catchments in Southern Vietnam due to a sparse hydrometeorological network density. Therefore, in this study this approach is not considered.
- The period between March 2008 and May 2009 was chosen to ensure that the uncertainty in model parameters is minimized. At five precipitation measuring stations, the observed annual rainfall in this period is similar to the observed annual rainfall in the period between March 2013 and May 2014.

Another test of the combined hydrometeorological model performance is provided by analysis of the simulated daily stream flow with the RCM4/ERA-Interim data. Figure 7.5 shows that the stream flow simulation forced by the downscaled data on daily time scale is considerably good for Binh Son. The coefficient of determination R^2 for the station Binh Son indicates that the model driven by RCM4/ERA-Interim is able to explain 78 percent of the variability in the simulated stream flow, which means a very good agreement between the simulation with climate model data and the simulation

with station data. Contrary to this, a moderate to poor coincidence was seen for the stations Suoi Ca and Cau Vac. In comparison with the simulation forced by the downscaled data, the simulation forced by the station data performs better on the daily time scale for the stations Suoi Ca and Cau Vac. The ln(NSE) indices for the daily data is 0.54 for Cau Vac, 0.55 for Suoi Ca and 0.98 for Binh Son. This implies that the stream flow simulation fitted well to the reference data at all stations for low flows, especially for the low flows at the station Binh Son.

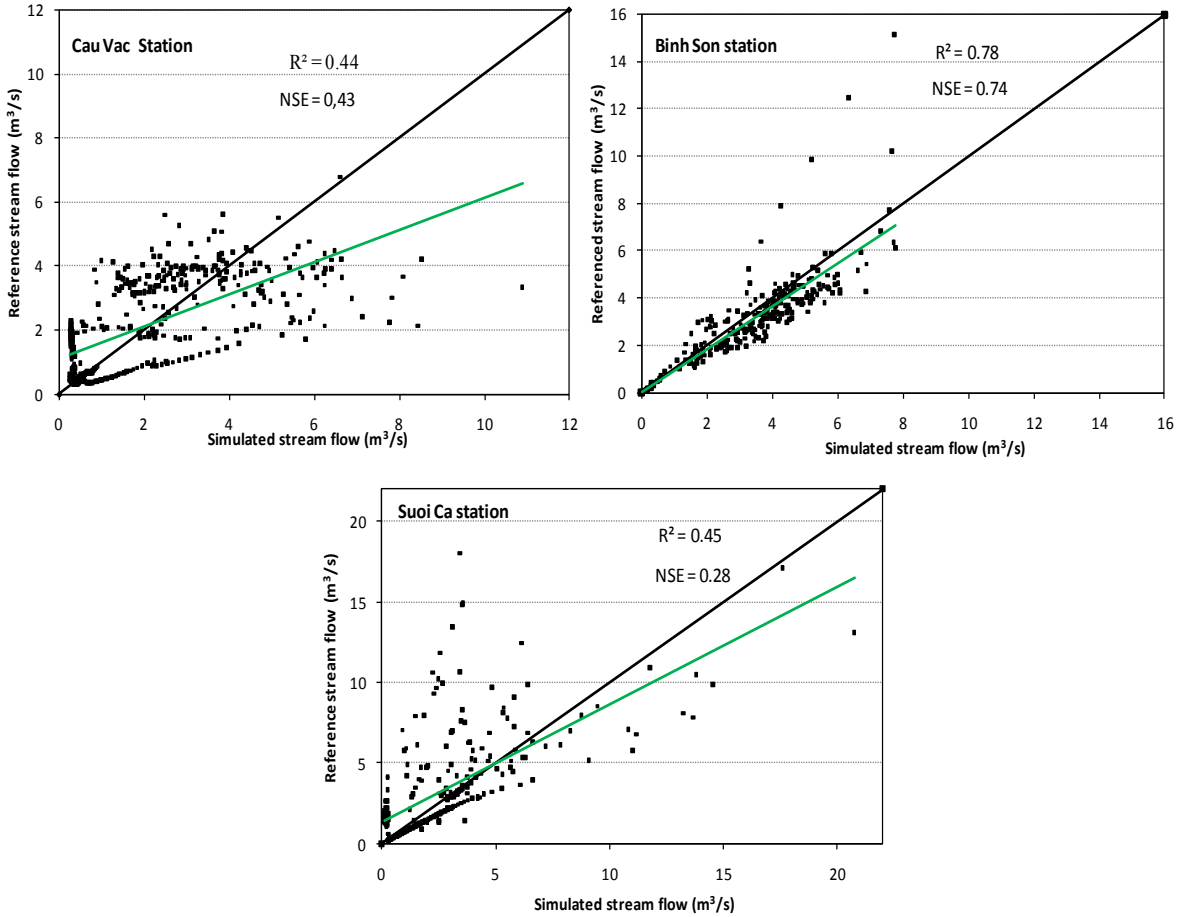

Figure 7.5: A comparison of reference stream flow using climate station data and daily stream flow simulated with downscaled climate data for the stations Binh Son, Suoi Ca and Cau Vac, 2008-2009. The solid green line refers to the linear regression between the two time series. The solid black line is the perfect regression.

7.5 Potential climate change impacts on stream flow

In this section, a focus analysis of potential climate change impacts on stream flow is carried out for the station Cau Vac with the drainage area of about 57 km^2. Furthermore, percentage changes in stream flow are presented for the Thi Vai catchment. The results for Thi Vai catchment are averagely calculated from the sub-catchments. The other stations Binh Son and Suoi Ca are analysed similarly. The results for these stations are given in Appendix 8.

7.5.1 Impacts on monthly stream flow

One of the objectives of this study is to analyse the potential future impacts of climate change on the water resources in the Thi Vai catchment. Therefore, the output of the dynamic-statistical downscaling models for rainfall and temperature were used as input data for the hydrological model PANTA RHEI in order to quantify the impacts of a changing climate on the stream flow in the Thi Vai catchment. The time series for the variables wind speed and atmospheric pressure are directly taken from the RCM4/CGCM3. Two periods were simulated: the baseline (1961-1990) and the future (2071-2100). For the simulation of the future the SRES A1B scenario was chosen.

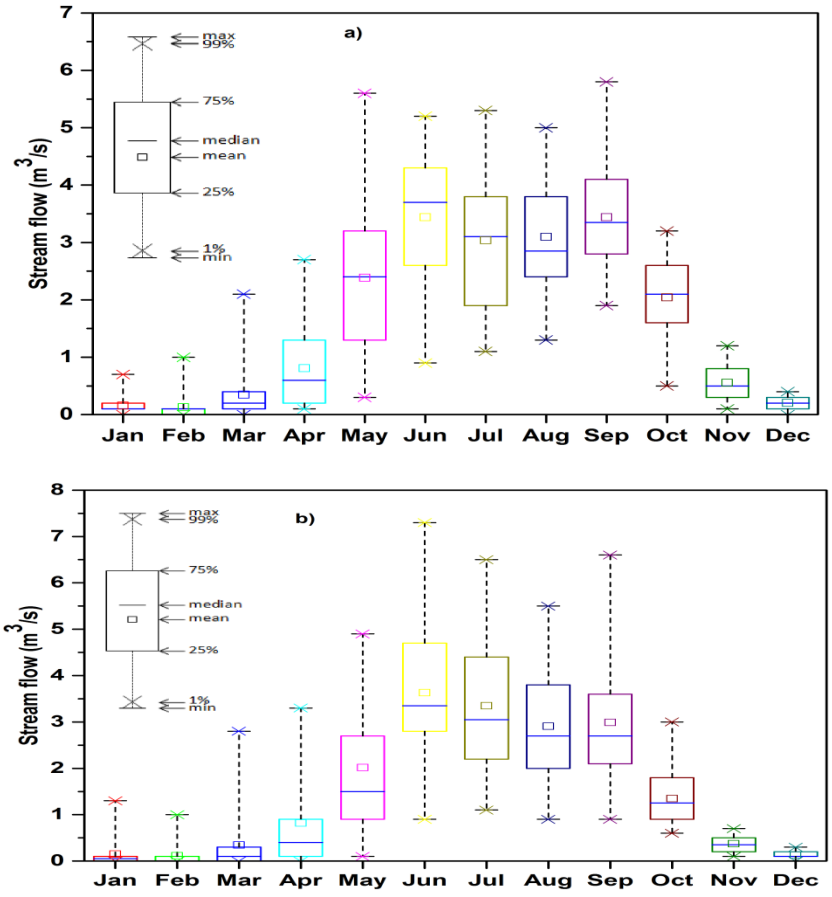

Figure 7.6: Simulated monthly stream flow for the baseline (1961-1990) (a) and the future (2071-2100) (b) periods for the station Cau Vac (m^3/s).

The simulated stream flow at the station Cau Vac for the baseline and the future periods are displayed in Figure 7.6. For the baseline period, the simulated monthly stream flow values is the strongest in September (nearly 6 m^3/s), followed by May (over 5.5 m^3/s) (see Figure 7.6a). Meanwhile, the projected monthly stream flow is the strongest in June (over 7 m^3/s) and July (over 6 m^3/s, followed by August (approximately 5.5 m^3/s) (see Figure 7.6b). In January and February, the simulated monthly stream flow values are mostly changed for both the baseline and the future periods (see Figure 7.6).

Figure 7.7 shows an overview of the simulated monthly stream flow difference for the future (2071-2100) and the baseline (1961-1990) periods for the station Cau Vac. The stream flow increases from

January, peaks in June or September and then decreases from October for both the baseline and the future periods. The simulated monthly stream flow values for the future period could reach up to 3.6 m^3/s in June. As can be seen from the graph, the simulated monthly stream flow for the future period is lower than that for the baseline period in consecutive five months (from August to December). Figure 7.7 shows a drier condition in six months of the year. Wetter conditions are projected during in June and July. Changes of stream flow in these months are very clear. Contrarily, the signals of changes in projected monthly stream flow are not clear in February and in January.

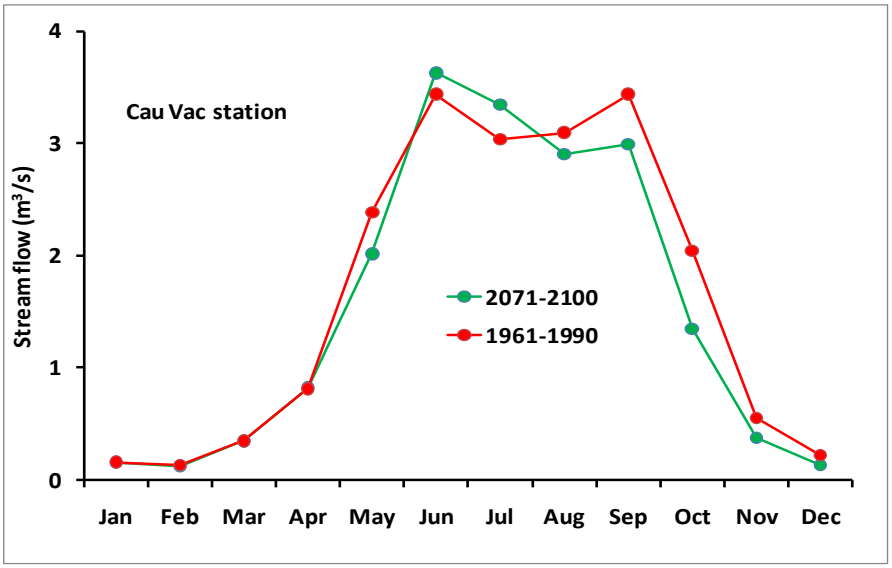

Figure 7.7: Simulated monthly stream flow for the base-line (1961-1990) and for the future (2071-2100) periods for the station Cau Vac (m^3/s).

The percentage change in monthly stream flow for the station Cau Vac is presented in Figure 7.8. Changes in temperature and precipitation have a great impact on changes in monthly stream flow at the station Cau Vac, especially for the three months from October to December. During these months, the changes in monthly stream flow are less than -30%, especially for December (less than -40%). However, an increase in stream flow is clearly pointed out in July (nearly +10%). It is noteworthy that no change is projected in March. Changes in monthly stream flow are very small in January and April (see Figure 7.8).

The percentage of change in monthly stream flow for the Thi Vai catchment is presented in Figure 7.9. During the months from October to December, the changes in monthly stream flow are very high (less than -40%). An increase and decrease in stream flow is very small in March, June and August (nearly ±5%, respectively). There is very small change in monthly stream flow in January (see Figure 7.9).

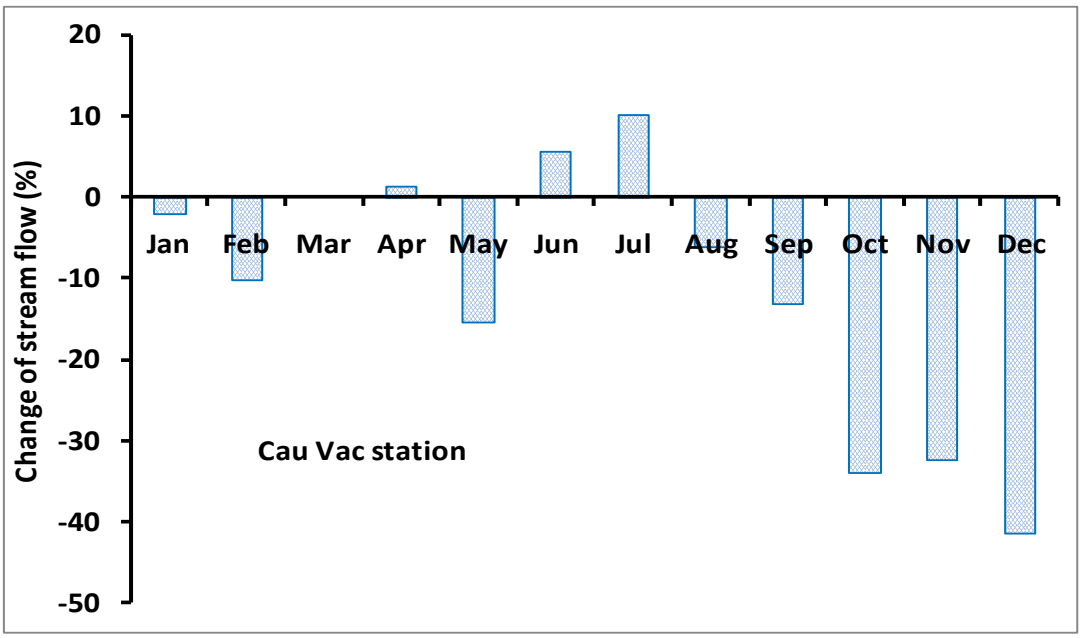

Figure 7.8: Projected monthly stream flow changes (2071-2100 compared to 1961-1990) for the station Cau Vac (%).

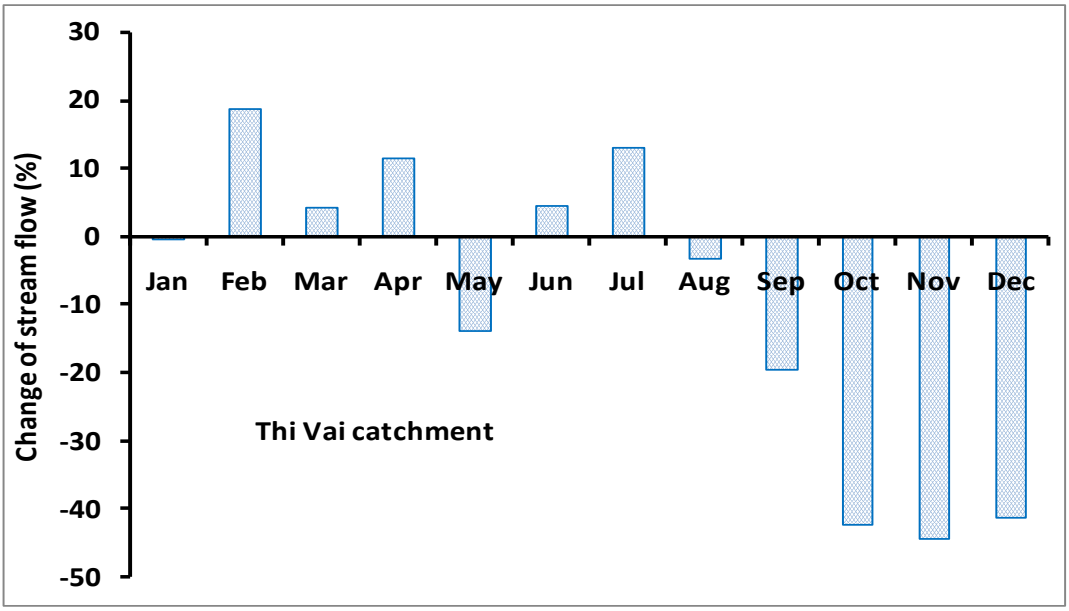

Figure 7.9: Projected changes in monthly stream flow (2071-2100 compared to 1961-1990) for the Thi Vai catchment Thi Vai (%).

7.5.2 Impacts on seasonal and annual stream flow

In this section, impacts of potential climate change on seasonal and annual stream flow are presented. The simulation results are interpreted at an aspect of seasonal classification (i.e., two seasons and four seasons). As described in chapters 3 and 6, two seasons are defined as follows: rainy season (May to November) and dry season (December to April). Four seasons are defined as follows: winter (December-January-February), spring (March-April-May), summer (June-July-August) and autumn (September-October-November). The reason for this work is to give a multi perspective of simulated stream flow in time. Moreover, the results from this work can be easily compared to

those of other studies because the simulated results are typically given at two and four seasons in a large number of climate change impact studies, especially in Vietnam.

Figure 7.10a shows the largest stream flow simulation in summer (over 3 m^3/s), followed by autumn (about 2 m^3/s) for the baseline period. For the future period, the largest stream flow projection is in summer (over 3 m^3/s), followed by autumn (nearly 1.5 m^3/s). The stream flow in winter is comparatively low for both the baseline and the future period.

In rainy season, stream flow simulations are relatively large for both the baseline and the future periods (see Figure 7.10b). In comparison with the baseline period, projected stream flow in the future is slightly lower in rainy season. In dry season, there are only small differences in stream flow simulations. On the annual time scale, stream flow could reach up to nearly 2 m^3/s in the baseline period, higher than that in the future period (see Figure 7.10b).

To assess the potential climate change impacts on stream flow, quantifications of changes in stream flow are the most important part. The reason for this is that percentage of changes in stream flow is a key to determine the overall availability of water in the catchment. In this study, the aggregated results of monthly value were analysed for two different seasons at the station Cau Vac. The percentage changes in seasonal and annual stream flow are calculated between the baseline (1961-1990) and the future (2071-2100) periods as shown in Figure 7.11. According to the calculated results, decrements of stream flow can be expected during winter, spring and autumn (see Figure 7.11a). Stream flow is projected to decrease by less than -20% in autumn, followed by nearly -20% in winter. This result indicates that the decrease in precipitation over the Thi Vai catchment under the SRES A1B scenario causes a shortage of water. The increased temperature significantly contributes to this deficiency due to evapotranspiration. Contrary to this, a slight increase in seasonal stream flow is projected in summer (about +3%) (see Figure 7.11a). The reason for this is that the increased precipitation from the climate change scenario SRES A1B lead to an increase in stream flow. So, the increased precipitation significantly offsets the loss of water due to evapotranspiration caused by the increased temperature over the sub-catchment under this scenario. In spring, stream flow is expected to decrease by around -10%. As analysed in chapter 6, the change in precipitation is very small in spring (see chapter 6). Therefore, the results show that even if the amount of precipitation only changes slightly, stream flow significantly changes when the air temperature rises. This shows that percentage change in stream flow is highly sensitive to the seasonal cycle in precipitation.

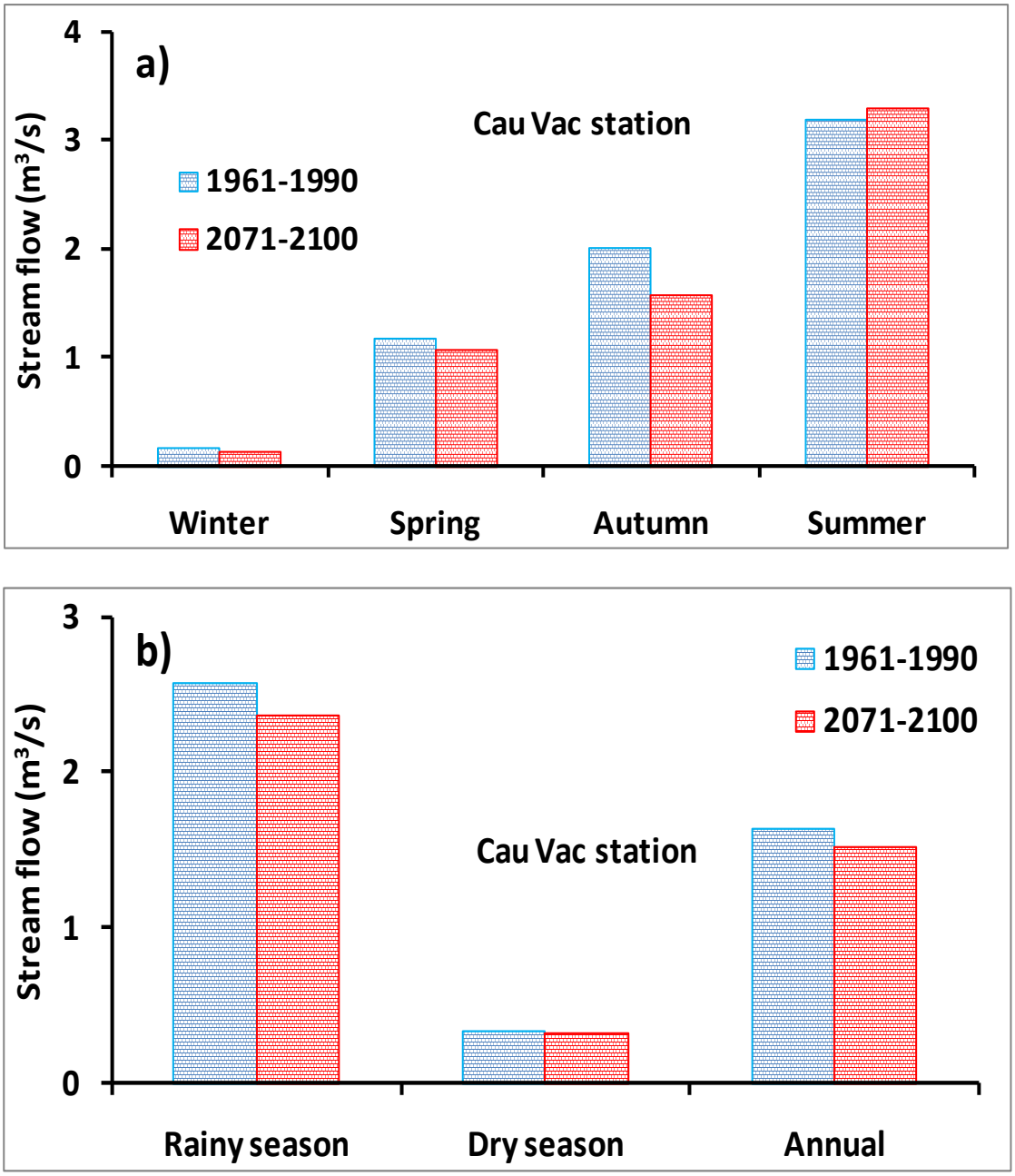

Figure 7.10: Simulated seasonal stream flow for the baseline (1961-1990) and the future (2071-2100) periods with (a) four seasons and (b) two seasons for the station Cau Vac (m^3/s).

Figure 7.11b shows an overview of projected percentage changes in stream flow during rainy and dry seasons and on annual scale. A moderate change in annual stream flow of around -7% is simulated is documented. Percentage changes in stream flow are greater in the rainy than in the dry season (less than -5%).

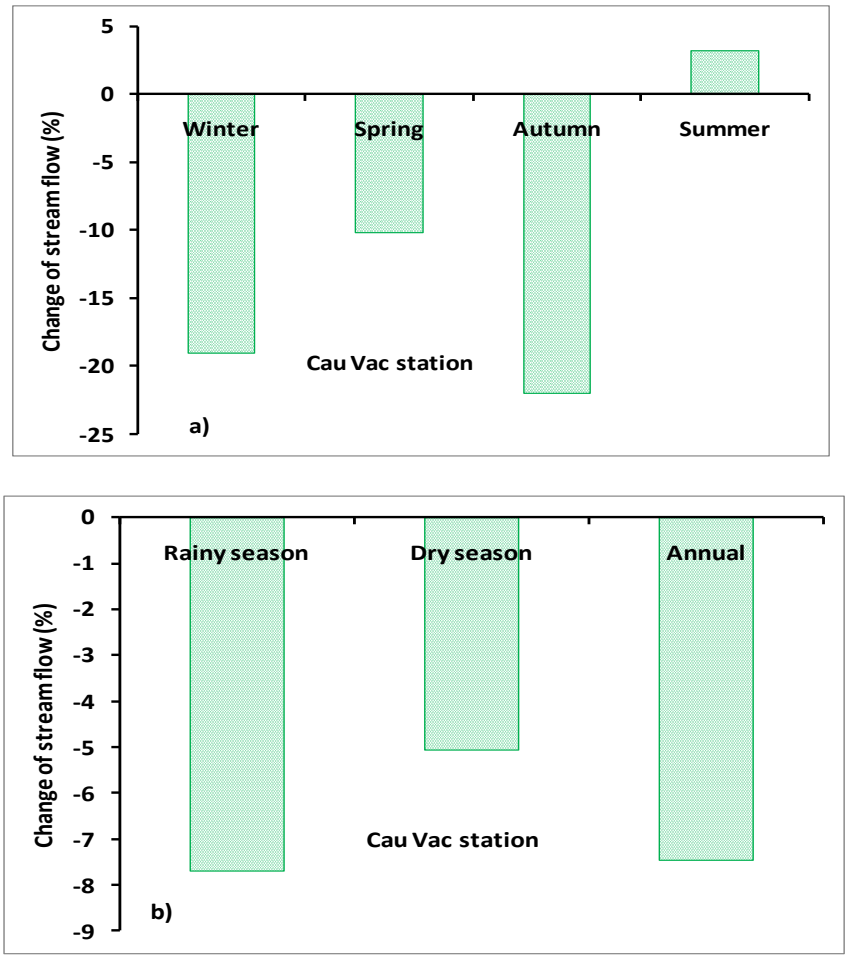

Figure 7.11: Projected changes in seasonal stream flow (2071-2100 compared to 1961-1990) for (a) four seasons and for (b) two seasons for the station Cau Vac (%).

Figure 7.12 shows the simulated changes in seasonal stream flow for the Thi Vai catchment. The greatest change is projected in autumn (less than -30%). Contrary to this, the potential change in stream flow is relatively small for the whole catchment in winter, spring and summer. A percentage change in stream flow of about -5% can be expected for winter and spring. In summer, an increase in stream flow by +5% was projected (see Figure 7.12a). The reason for this is directly related to the changes in precipitation. The local precipitation at the mountains in the North-Eastern Thi Vai catchment might contribute to this change.

The analysis of potential stream flow changes during the rainy and dry season (see Figure 7.12b) shows that a decrease in stream flow change is projected for the whole catchment during the rainy season (less than -6%). During the dry season hardly any change in stream flow can be identified (just over +2%). A decrease of nearly -6% in projected annual stream flow is calculated for the catchment Thi Vai (see Figure 7.12b).

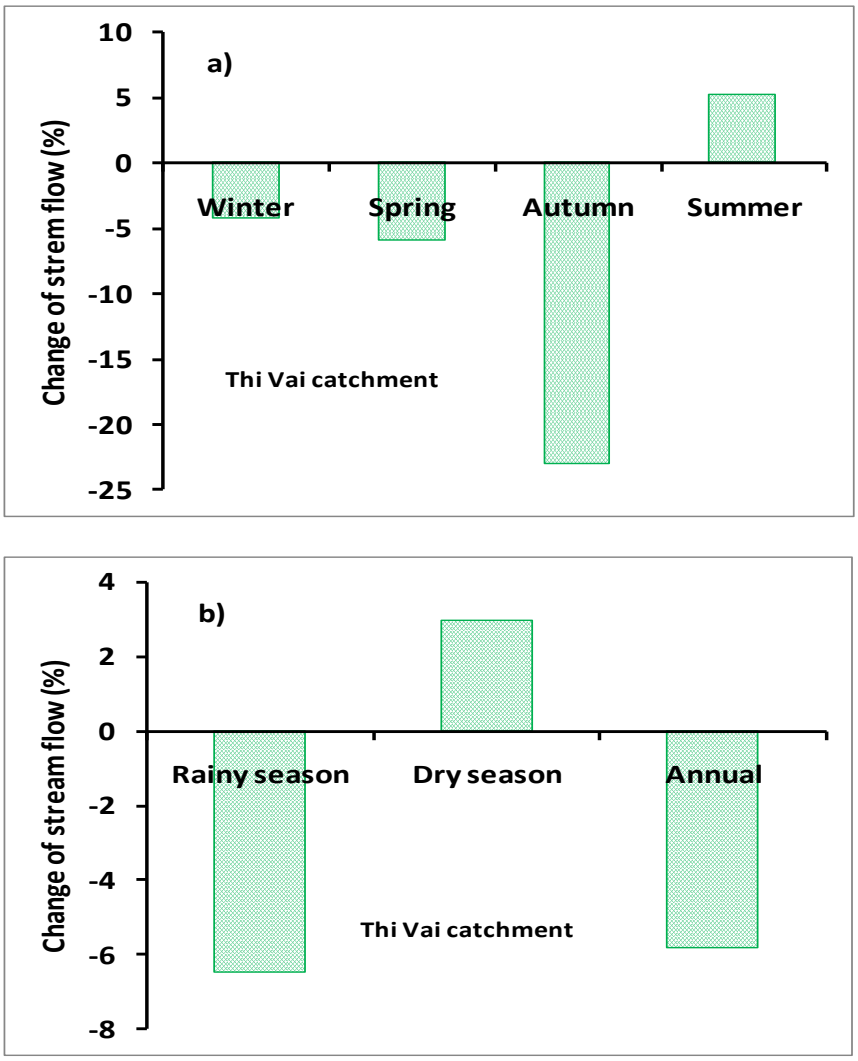

Figure 7.12: Projected changes in seasonal stream flow (2071-2100 compared to 1961-1990) for (a) four seasons and for (b) two seasons for the Thi Vai catchment Thi Vai (%).

7.5.3 Impacts on the day of year of stream flow

Climate change as well as its impacts, of course, can impossibly be detected from one day to the next, but in this study, impacts of potential climate change on the day of year of stream flow were analysed based on averaged day of year during 30 years in the past and future. This work is expected to identify climate change impacts on water, even if this is potentially uncertainty.

Figure 7.13 provides information on the projected stream flow for the future at the observation stations. On the daily scale, the peak flow is found at Binh Son on the 173rd day (3.65 m^3/s), at Cau Vac on the 181st day, (4.89 m^3/s) and at Suoi Ca on the 175th day (20.29 m^3/s). An increasing tendency of future stream flow from the first day of the year to about the 175th day is identified. From this time of the year until the 270th day, a slight fluctuation is detected. A decreasing tendency of future stream flow is simulated until the end of year.

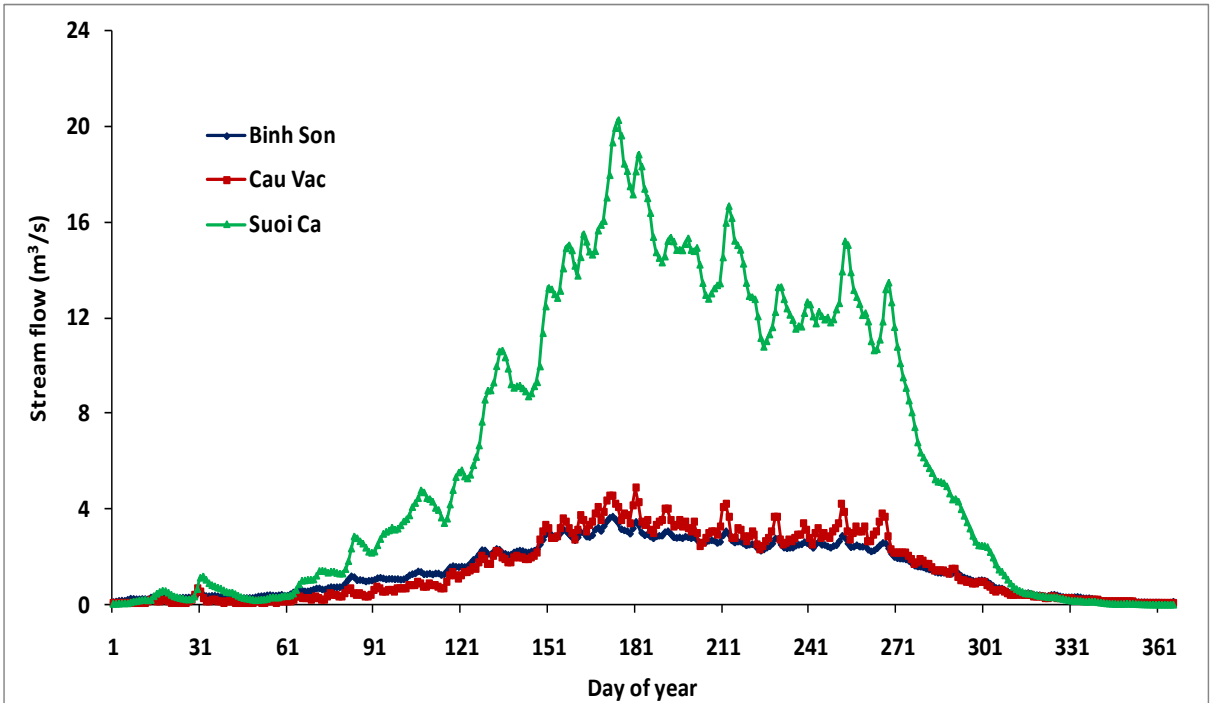

Figure 7.13: Projected stream flow for future (2071-2100) at the observation stations.

Figure 7.13 depicts percentage changes in the day of year of stream flow under potential climate change impacts over the whole catchment Thi Vai. On the daily scale, changes in stream flow could reach up to 100% as shown on the 31st day (see Figure 7.14). A decreasing tendency of future stream flow changes was consecutively seen from the 231st day to the 15th day in the following year.

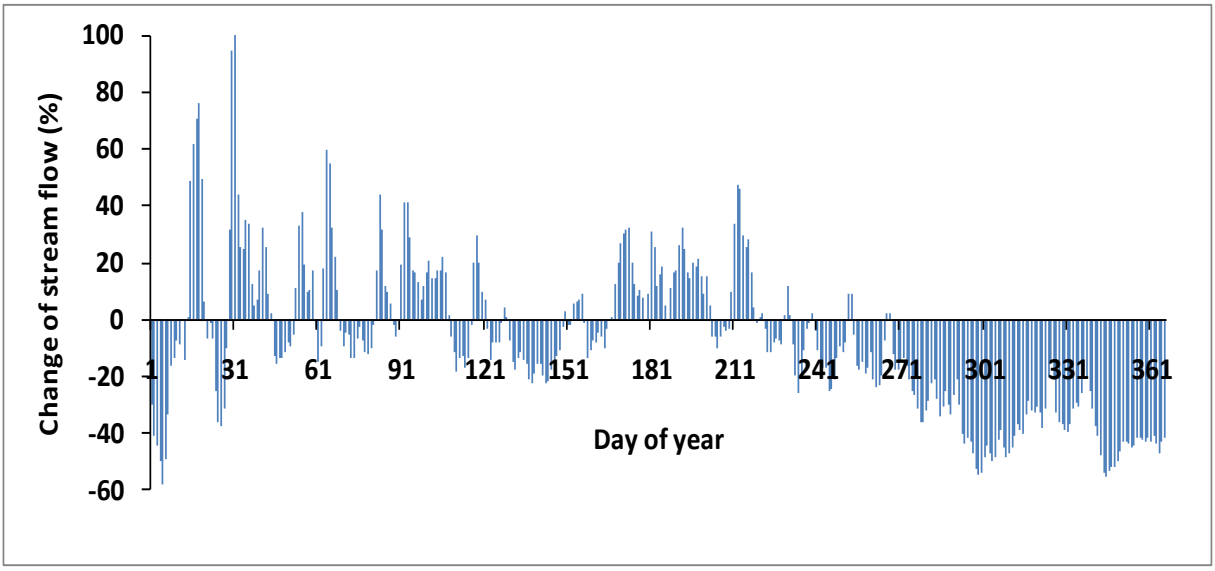

Figure 7.14: Projected diurnal stream flow changes (2071-2100 compared to 1961-1990) for the Thi Vai catchment (%).

In section 7.5 it is shown that mean monthly stream flow is projected to decrease in May, September and October at all stations. Slightly wetter conditions are projected for June and July at the station Binh Son. Changes in mean monthly stream flows strongly depend on monthly precipitation changes, whereas seasonal variability only modestly depends on seasonal precipitation changes.

In this chapter the potential changes of stream flow at daily to annual time scales for the future are analysed. The performance of the hydrological model PANTA RHEI for the Thi Vai catchment is also evaluated. The results of stream flow simulation were interpreted at an aspect of seasonal classification (i.e., two seasons and four seasons). This is a new perspective in comparison with the EWATEC-COAST project results where simulated changes in stream flow are only analysed for the dry, dry/wet, wet, and wet/dry seasons. It needs to be noted that not only the simulated stream flow but also the future period is different between the PhD study and the EWATEC-COAST project (e.g., far-future 2071-2100 and near-future 2046-2066 for the simulation period in PhD and EWATEC-COAST projects, respectively). So, it is hard to make a comparison between the PhD and EWATEC-COAST project results. The results of this study present a combination and supplement but independence with the EWATEC-COAST project. According to Meon *et al*. (2014), a decrease in stream flow is pointed out for near-future 2046-2066 during dry, wet and wet/dry seasons over the whole catchment. An increase in stream flow is seen in dry/wet season. Meanwhile, this work results illustrate a decrease in simulated changes in stream flown in rainy, spring, winter and autumn seasons for far-future 2071-2100 over the whole catchment. A slight increase in simulated changes in stream flow for far-future 2071-2100 is pointed out in dry and summer seasons.

8 STRATEGY FOR FUTURE ANALYSES OF THE REVERSE EFFECTS OF CHANGES IN THE WATER BALANCE ON THE OUTPUTS OF DOWNSCALING MODELS

8.1 Basic thoughts

It is well known that there are several natural factors which play an important role in controlling the global water cycle, for example temperature, precipitation, land use and vegetation. Changes in temperature and precipitation are the most important factors for changes in the atmospheric water cycle at various scales from local to global. Other factors, including changes in land use and vegetation are of special importance at regional scales. Although the characteristics of precipitation, temperature, land use and vegetation can vary considerably at even a scale of meters, the effects of their changes on the water cycle are hardly found at a small scale. To do this, detailed microclimatic investigations would be necessary. This could help to explain the relationship between atmosphere, biosphere and hydrosphere. Consequently, the interplay between these components could be analysed.

At a large scale, the natural factors mentioned above are key points to fully understand the processes of the water cycle. However, the single parameters interact with each other and it is difficult to study them in isolation. As an example, the water cycle is strongly controlled by changes in temperature and/or precipitation. Increasing precipitation could increase the amount of stream flow and cause extreme flood events or an increased water reservoir volume. So, if the interaction of these factors can be interpreted well, reverse effects of water balance changes on the meteorological variables (i.e., temperature and precipitation) would also be explainable. To date, however, to answer the question whether or not a change in temperature and/or precipitation is considered as a result of changes in hydrological variables (e.g., stream flow) is still one of the most challenging topics. The stream flow characteristics of a river in time and space depend on a lot of factors such as the hydrological characteristics of a river (e.g., slope, length of river) and meteorological characteristics (e.g., precipitation and temperature). It is presently impossible to simulate all two-way physical interaction processes, even the one-way simulation is challenging in detail. Therefore, in this study, a first suggestion for a strategy to investigate the reverse effects of water balance changes on meteorological variables (i.e., temperature, precipitation) is made. The main purpose is to explore feedbacks of hydrological and meteorological variables, because those processes help to understand the interactions of processes. So, firstly, understanding the concepts of feedback processes is essential. Feedback processes of the water cycle may cause changes in climate conditions (amplifying or suppressing). The feedback effects strongly depend on the response time of the feedback factor. For example, the response time of stream flow when temperature increases is very likely different from the one when there are changes in precipitation. Up to present, the concepts of feedbacks are described in detail in the IPCC's reports, Cess (1978), Hansen *et al* (1984), Jonathan (2003) and

Ruddiman (2007). Within this work, two feedback processes (temperature - stream flow and precipitation - stream flow) are investigated. There may exist a linear or non-linear relationship between temperature, precipitation and stream flow. The scientific questions are posed as follows: (1) In case increased or decreased temperature leads to changes in stream flow (increasing or decreasing), whether or not the potential changes in stream flow cause changes in temperature (increasing or decreasing) and (2) whether or not the potential changes in stream flow cause changes in precipitation (increasing or decreasing). To answer these questions, a large number of observational datasets is needed to validate and interpret the interactions within the climate models. After that, an integrated analysis of exchanged energy fluxes at land surface through the atmosphere boundary layer needs to be carried out. The aim of this work is to improve the understanding of land surface parameterization schemes within climate models. For the first question, changes in temperature (as cause) affect changes in stream flow (as response) via many sub-models in climate models (e.g., cloud, soil and vegetation). The course of this loop can occur, for an example, because an increased temperature causes an increase in water vapour in the atmosphere which then could lead to an increase in precipitation. Thus, stream flow increases or decreases depending on the atmospheric circulations at a large scale and/or local circulations. In turn, the increase in temperature can be greater or smaller depending on vegetation. So, there may exist a positive and/or negative feedback within the relationship between cause and response factors. For the second question, increased precipitation mostly causes an increase in stream flow and vice versa if an assumption of a closed system is made. Although this interaction depends on some other factors like surface vegetation, they directly influence each other in general. So, an existence of a positive feedback within the relationship between precipitation and stream flow is very likely. Therefore, additional tests of coupled atmosphere-land surface-vegetation models would be needed to investigate these feedback processes.

It is argued that the factor of changes in land use is considered to be a very important factor for climatic investigations. Another factor, human activities, would extremely be valuable due to its great effects on climate change as pointed out in many scientific documents (e.g., the IPCCs reports). However, the scientific problems dealing with the feedback processes in climate models would become more complex. Therefore, mathematical descriptions for coupling hydrological and atmospheric processes are very difficult. An attempt to keep the model as simple as possible stretches throughout the thoughts. Together with this strategy, three subsequent problems need to be maintained: (1) physical principles in nature, (2) obtaining extensive land use and land cover data and (3) minimizing the requirement of computing power. Probably, it would be less complex when feedback processes between temperature - precipitation - stream flow would operate within the climate system. In other words, using a climate model to investigate these relationships would be more efficient. Regarding stream flow processes, however, a great uncertainty of stream flow would be possible when land surface parameterization schemes of hydrological processes (i.e., infiltration, stream flow and evapotranspiration) could be modelled from a size of a catchment to a region at climate models. The reason for this is that atmospheric circulations and factors that cause the changes in temperature and precipitation often occur at a large scale. Meanwhile, hydrological

characteristics (e.g., stream flow) are considered to be a result of the complex interactions between topography, soil types, climate and vegetation. Therefore, investigations of feedback processes between hydrological and meteorological components should be implemented at a scale in which physical processes occur (e.g., Mekong delta region, Vietnam ~39.000 square kilometres). Furthermore, a coupled climate and hydrological model would be better for these researches. A working strategy is given the following section. For a catchment as Thi Vai, it is still a great challenge to assess feedback processes due to (1) a too small catchment size and (2) a short series of available data. Consequently, such an investigation cannot be carried out for this catchment.

8.2 Interaction of meteorological and water balance effects

In this section, an overview of interactions between meteorological factors and the water balance effects is made as shown in Figure 8.1. The nature of links and feedbacks are identified from these interactions. Briefly, feedback processes are the following:

(1) Obviously, global as well as local precipitation and temperature conditions directly affect the surface and ground water balance as illustrated in this study.

(2) The surface and ground water balance represent the water storage of the soil. This is a key to define the type of land use and vegetation over a region. In turn, the changes in vegetation and land use cause changes in the cycle of surface and ground water and heat (e.g., stream flow rates to a river, soil moisture storage) via the processes of interception of precipitation and evapotranspiration as examples.

(3) Evapotranspiration is strongly influenced by surface land use and vegetation conditions. Different types of land use and vegetation have different values for surface albedo and roughness, physical mechanism of leaf, root depth, transpiration and canopy water evaporation. As a result, evapotranspiration rates are different. For example, evapotranspiration rates of trees are different from those of bare soil.

(4) Changes of evapotranspiration determine the changes of meteorological variables due to rising air condenses out clouds caused precipitation. In turn, changes of meteorological conditions influence the evapotranspiration rates via the heating of land surface or air motions.

(5) The land use and vegetation define the surface albedo and roughness. These factors are very important for the exchange of atmospheric and surface fluxes. As a result, meteorological conditions vary. On the other hand, the type of land use and vegetation depend on meteorological conditions like temperature and precipitation.

(6) Surface and ground water regimes determine the evapotranspiration rates. This problem is described in a large number of hydrological documents. In turn, interactions of precipitation and potential evapotranspiration are keys to identify soil moisture that directly influence surface and ground water balance.

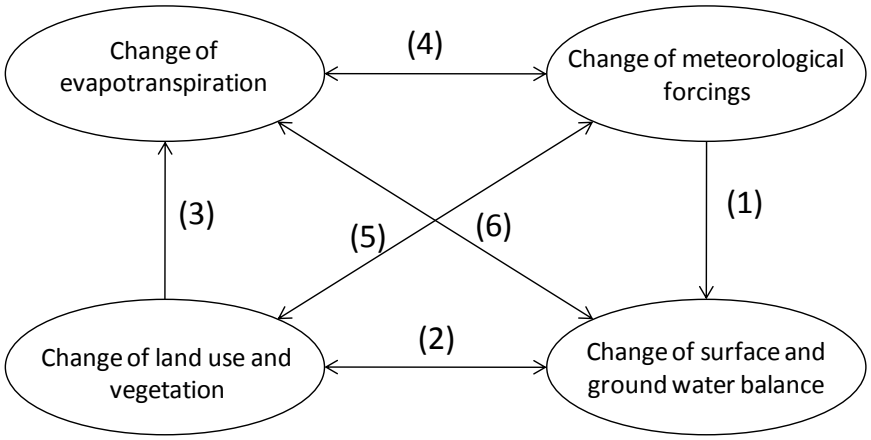

Figure 8.1: Interaction of meteorological components and the water balance and their feedbacks.

The model of interactions of meteorological components and the water balance becomes more complex if anthropogenic effects are considered. Anthropogenic factors mainly affect changes of land use, vegetation and water balance in surface and ground. In the opposite direction, changes of vegetation and water balance would likely affect via a given threshold. This threshold potentially depends on the earth capacity.

8.3 Working strategy

A brief description of this idea can be visualized as follows: Development of different scenarios of changes in the land use should be added in the land surface parameterization models. Then, climate models could be restarted with these scenarios. The output of the models can be used as input for a water balance model with the same land use scenarios. So, the sensitivity of changes in land use is tested in both the climate models and a water balance model. Consequently, changes in the output of climate and hydrological models are explored following the scenarios of land use. Finally, feedback processes can be analysed because changes in land use influence the exchange of water, surface energy fluxes and atmosphere.
A detail in working strategy is drawn as the following steps:

Step 1: Quantification of the variability of land use and vegetation using the real land use and vegetation data from remote sensing, surveys or available data from different sources (e.g., Moderate Resolution Imaging Spectroradiometer data) needs to be done.

Step 2: The quantified land use and vegetation maps at different time scales from step 1 are used for climate models (e.g., RegCM or CWRF) and for a water balance model (e.g., PANTA RHEI). A subroutine step needs to be included so that the land use and vegetation data can be processed at a global scale for climate models and at the local scale for a water balance model.

Step 3: An assumption for an increase or decrease in stream flow should be made a coupled climate and water balance model.

Step 4: Estimation of relationship between changes in local land use and changed stream flow in space and time within the interest of area. To do this, more than two periods with different land use should be analysed.

Step 5: An adjustment of land use would be done with the change in land use and vegetation parts from step 4.

Step 6: Restart a coupled climate and water balance model. The changes in meteorological components would be compared with the changes in hydrological characteristics.

Expected results would mainly be scenarios of land use and vegetation development, variability of meteorological and hydrological variables in time and space. A series of maps described the relationship between changes in land use, vegetation and hydrological parameters for a catchment in time would be given.

9 CONCLUSIONS AND RECOMMENDATIONS

9.1 Conclusions

Even though surface air temperature has apparently increased all over the world, its degree of change depends on local conditions. The increase in temperature directly affects the global heat budget that is a cause of changes in evapotranspiration, precipitation and wind regimes. Therefore, extreme flood events will potentially occur more often in many regions of the world. Under such circumstances, projecting potential flood events will be of great importance for the sustainability of development projects in a range of socioeconomic sectors, such as agriculture and water supply. So far, however, one of the big challenges related to climate change in developing countries like Vietnam is the inhomogeneity of the hydrometeorological observation system in both space and time. This considerably contributes to the uncertainties in the climate and hydrological models. Furthermore, there is a lack of studies dealing with climate change and flood issues in a small basin like the Thi Vai River basin.

The Thi Vai basin is one of the most representative basins for coastal regions in southern Vietnam in terms of sustainable coastal development, mangrove biosphere reserves, and economic expansion goals. Coastal regions are particularly vulnerable to natural disasters such as tropical cyclones, tsunamis and sea level rise, especially in the context of observed climatological changes in Vietnam. Considering these issues, in this thesis the present and potential future local climatic conditions are analysed. Furthermore, trends in observed climatic fields are investigated at the catchment scale.

For the quantification of potential changes in stream flow under the SRES A1B scenario, the following steps are carried out: (i) Regional climate simulations are performed for the periods 1961-1990, 1981-2010 and 2071-2100 with a horizontal grid resolution of 10 km x 10 km, which is the highest resolution that can be reached using a hydrostatic climate model. Accordingly, potential far-future changes of precipitation, temperature and other meteorological variables could be analysed on the finest resolution. (ii) Uncertainties in the dynamical climate modeling are reduced by applying statistical downscaling to the output of the Regional Climate Model. (iii) The potential impacts of climate change on the stream flow of the Thi Vai basin are quantified for the far future using the hydrologic model PANTA RHEI. (iv) Strategy for future analyses of the reverse effects of changes in the water balance on the outputs of downscaling models were made.

The results of this study are consistent with those of some previous studies for different climate regions in Vietnam (MONRE, 2009; MONRE, 2012a; Phan, 2010; Nguyen *et al.*, 2010). A significant difference between the observed hydrometeorological features and those that are projected for the future is found. This indicates that climate change plays an important role for changes in stream flow in the Thi Vai River basin.

The main findings of this thesis are:

(1) The review in chapter 2 provides the “state of the art” in dynamic-statistical downscaling technology at a variety of scales. Downscaling technologies are evaluated and a brief description of

hydrological models is given. The strengths, weaknesses and uncertainties of climate models are provided. This is very important for performing the climate simulations which are then used to force the hydrological model.

(2) In chapter 3 and chapter 4, the local climatic conditions and obtained datasets (point and raster) are analysed in order to select a dataset that is used as initial and lateral boundary condition for the regional climate model. Furthermore, this is fundamental to interpret the causes of floods and the local climate projections for the far future in relation to the present climate conditions.

(3) For the Thi Vai catchment, the present climate variability is investigated in order to identify observed trends in climate data series. The analysis of monthly, seasonal and annual precipitation shows a decreasing trend for August and June and a decreasing trend for the rainfall amount during the rainy season, except for an increasing trend in May. During the dry season, an increasing trend is observed at all stations at given significant or insignificant levels. The magnitude of positive or negative trends varies from station to station.

(4) Significant positive and negative trends are observed at most stations for the maximum one, three-, five- and seven-days rainfall. This is similar to the analysis results of maximum number of consecutive wet and dry days, which show a significant positive trend at the stations Hoc Mon and Thong Nhat for the maximum number of consecutive wet days, and a significant negative trend at the stations Vung Tau, Long Thanh, Bien Hoa and Binh Chanh for maximum number of consecutive dry days.

(5) The primary aim of the downscaling procedure is to develop a scenario of climate change at high resolution that can be used for hydrological modeling. Dynamic-statistical downscaling is improved to overcome the coarse resolution issues of GCMs and RCMs (see chapter 2). The Model Output Statistics (MOS) and Two-Step Model (TSM) technologies are coupled with the regional climate model RegCM4. The climate simulations for the past (1981-2010) are performed with three self-nesting steps of RegCM4 nested in the ERA-Interim reanalysis dataset. The ability of the climate model to simulate the observed climate is evaluated based on the mean annual cycle, the seasonal climatology as well as on the monthly and daily scale for the Thi Vai catchment. The model output is evaluated by weather station data, interpolated to a 10 km resolution grid. The CRU, ERA-Interim, TRMM, GPCC and Apthrodite datasets are used to evaluate the model performance for temperature and precipitation.

(6) The results of the climate simulations show a warm bias in temperature and wet bias in precipitation when RegCM4 is nested to the ERA-Interim reanalysis dataset. Over the Thi Vai River catchment, the simulated pattern and intensity of temperature and precipitation correspond to those of the observation data, especially in heavy rainfall and heat centers. This implies that RegCM4 is able to act for the climatic features. Furthermore, it can be used to simulate past and future climate. The method of three self-nesting steps in RegCM4 is satisfactorily performed for temperature and precipitation for a small basin located in the tropical coastal zone.

(7) With the MOS approach, the level of accuracy and the degree of correlation between downscaled and observed daily temperature data is enhanced. In the Thi Vai River basin, surface air temperature increases during 2071-2100. In the period between 2071 and 2080, the air temperature is projected to increase by about 1.5 ^{o}C in January and nearly 3 ^{o}C in June. In the period 2081-2090, the air temperature may be 2 and 3^{o}C higher in January and May respectively. The simulated air temperature during the period 2081-2090 is higher than that one during the period 2071-2080. The strongest change in temperature may reach approximately 4 ^{o}C in May in the last ten years of the 21st century (2091-2100). This indicates that climate change signals are very clear in case of projected temperature.

(8) In comparison with the reference period 1961-1990, the projected seasonal warming amounts to +1.9 ^{o}C in winter, +2.3 ^{o}C in spring, +2.3 ^{o}C in summer and +2.3 ^{o}C in autumn for the period 2071-2080; whereas for the period 2081-2090 it is 2.7 ^{o}C, 3.2 ^{o}C, 2.8 ^{o}C and 3.0^{o}C, respectively. In the last ten years of the 21st century, these changes amount to 3.1 ^{o}C, 3.7 ^{o}C, 3.1 ^{o}C and 3.5 ^{o}C in winter, spring, summer and autumn, respectively.

(9) Without TSM, the downscaled results illustrate that RegCM4 simulations are not good for daily precipitation over the catchment. With TSM however, both frequency and intensity of daily precipitation are improved. Until the end of the 21st century, the projected climate change over the Thi Vai catchment is transient in winter and spring season, whereas wetter conditions are projected for summer whereas for autumn drier conditions are simulated. On a monthly basis, the projected rise in precipitation is greatest in July (about 1.5 mm/day). Contrary to this, the change towards drier conditions is greatest in October (nearly -1.5 mm/day). For the end of the 21st century, the greatest decrease in precipitation is projected for October.

(10) In comparison with the reference period 1961-1990, the projected seasonal precipitation may slightly change during a 30-year period in the far future (2071-2100). The projected precipitation changes amount to -2.4% in winter, -0.5% in spring, +5.9% in summer and -8.9% in autumn. For the period 2071-2080, the projected precipitation changes are +13% in winter, +8% in spring, +3.3% in summer and -12.6% in autumn; for the period 2081-2090 the changes amount to -8.6%; -4%; +7.1%, and -3.2% for the different seasons. For the last decade 2091-2100, these changes are -12%, -5.6%, 7.1%, and -10.7% in winter, spring, summer and autumn, respectively.

(11) The simulations of the Thi Vai river stream flow are investigated for periods of over 30 years in the past and the future by using the hydrological model PANTA RHEI which uses the output of dynamic-statistical downscaling as input data. Although the peak flows are not accurately captured, the simulated stream flow generally fits well the measured data. The model simulations reveal that stream flow is strongly sensitive to the soil moisture parameter.

(12) The period 1961-1990 is used as a reference period. For a 30-years period in far future (2071-2100) the simulated seasonal stream flow changes are quantified at three hydrometric measurement stations. At the station Binh Son, the potential stream flow changes amount to -5.0% in winter, -1.1% in spring, +7.8% in summer and -13.6% in autumn. For the station Cau Vac these changes are: -21.9% in winter, -10.1% in spring, +3.2% in summer and -21.9% in autumn. At the station Suoi Ca, these

potential changes amount to -11.3% in winter, -6.5% in spring, +4.5% in summer and -33.4% in autumn.

(13) The projection of future stream flow using the SRES A1B scenario shows that even if the amount of precipitation only changes slightly, river stream flow significantly changes when the air temperature rises. The spring precipitation is projected to decrease by just 0.5%, whereas stream flow in spring is projected to decrease by around 5%. This reveals that the changes in stream flow are induced by the changes in precipitation.

9.2 Recommendations

The major sources of uncertainty in this project are (i) insufficient terrestrial meteorological observations, (ii) estimation technologies of missing records, (iii) greenhouse gas emission scenario, (iv) parameterizations and resolutions in the dynamical downscaling model, (v) post-processing technologies and (vi) the hydrological model. The uncertainties from land use and soil data and GIS pre- and post-processing are not discussed in this study.

Insufficient terrestrial meteorological observations are the most important source of uncertainty. This lack of data limits the ability of hydrological model to reproduce the hydrological characteristics in the catchment. Moreover, the evaluation of meteorological and hydrological modeling performance was deficient.

In the climate modeling, the greatest source of uncertainty is the unpredictability of greenhouse gas emissions in the future. The reason for this is that all available emission scenarios are based on the different assumptions (see chapter 4). For dynamical climate models, a variety of uncertainty sources, such as epistemological and ontological uncertainties, is presented by Foley (2010). Besides that, the uncertainties in the hydrological arise from the hydrological model components and their parameters (Kay *et al.*, 2009).

A hydrometeorological database system is very important for hydrologic projects. Within this thesis, however, observation data that is needed for model simulation and validation is limited. Therefore, the extension of data collection including additional meteorological observation stations and stream flow gauges is highly recommended to achieve a higher homogeneity of data. A longer stream flow time series data would be especially valuable to evaluate the performance of hydrological models.

The greatest challenge when applying climate model simulations for hydrological projects is the selection and combination of downscaling methods. This is directly associated with the uncertainty of model simulations. Therefore, it is recommended that a combination of MOS, TSM and other dynamical models like COSMO or the Climate-Weather Research and Forecasting Model (CWRF) should be tested.

As climate change is a very complex topic, the results and findings presented within this study are just an example of potential futures. With more data and time, the projections will be more realistic. For this, continuous efforts for translating the results of the different climate models and scenarios into potential impacts are extremely important. The latest high emission scenario (e.g., RCP8.5)

should be added. Moreover, the choice of the baseline period should be adjusted because extreme weather phenomena have increased in the recent years.

Regarding the application of regional climate models and hydrological models to a small basin within the tropical region, several catchments or multiple rivers located in different regions like rural, urban or mountain areas should be investigated, especially in Central Vietnam where rivers are characterised by short length and steep slopes.

Within this project, possible reverse effects of changed water balance on meteorological components could not be studied. Therefore, further research projects should focus on the feedback of land use and land cover change to meteorological and hydrological characteristics with the help of the conceptual approach developed in this thesis. Based on this, better results for the reverse effects can be obtained. The influences of land use and land cover change, artificial nature structures like reservoirs and human activities on hydrological and meteorological characteristics should be investigated. Furthermore, investigations of microclimate and hydroclimate scale should be implemented. To do this work however, the costs of human, time and measurement device are relatively large.

Last but not least, a complement of the model chain by a hydraulic model, which provides water levels of the surface flow simulated by the hydrological model, should be considered. In doing so, the combined hydrological and hydraulic characteristics can be quantified for both unaffected and affected areas with tidal influences.

REFERENCES

Abbott, M. B., Bathurst, J. C., Cunge, J. A., O'connell, P. E., & Rasmussen, J. (1986). “An introduction to the European Hydrological System—Systeme Hydrologique Europeen,“SHE”, 2: Structure of a physically-based, distributed modelling system.” Journal of hydrology, 87(1), 61-77.

ADB (2009). "The economics of climate change in Southeast Asia: a regional review." Asian Development Bank.

Aksoy, H. (2000). “Use of gamma distribution in hydrological analysis. ” Turkish Journal of Engineering and Environmental Sciences, 24(6), 419-428.

Anandhi, A., Srinivas, V. V., Kumar, D. N., & Nanjundiah, R. S. (2009). “Role of predictors in downscaling surface temperature to river basin in India for IPCC SRES scenarios using support vector machine.” International Journal of Climatology, 29(4), 583-603.

Anderson, R. L. (1942). “Distribution of the serial correlation coefficient.” The Annals of Mathematical Statistics, 13(1), 1-13.

Arnell, N. W. (1999). "The effect of climate change on hydrological regimes in Europe: a continental perspective." Global environmental change 9(1): 5-23.

ASCE (1996). "Hydrology Handbook." American Society of Civil Engineers, New York.

Basseville, M., & Nikiforov, I. V. (1993). “Detection of abrupt changes: theory and application.” Prentice Hall Englewood Cliffs.

Behrendt, H., & Opitz, D. (1999). “Retention of nutrients in river systems: dependence on specific runoff and hydraulic load. In Man and River Systems (pp. 111-122).“ Springer Netherlands.

Benestad, R. E., Hanssen-Bauer, I., & Chen, D. (2008). “Empirical-statistical downscaling. Singapore: World Scientific Publishing Company Incorporated.”

Bjerknes, V. (1904). "Das Problem der Wettervorsage, betrachtet vom Standpunkte der Mechanik und der Physik.“ (English translation by Yale Mintz, Los Angeles, 1954). Meteor. Z , 21, 1-7.

Blunden, J., & Arndt, D. S. (2015). “State of the Climate in 2014.” Bulletin of the American Meteorological Society, 96(7), ES1-ES32.

Boer, G. (1995). "A hybrid moisture variable suitable for spectral GCMs." Research Activities in Atmospheric and Oceanic Modelling. WGNE Report 21.

Boggild, C.E., Knudby, C.J., Knudsen, M.B., & Starzer, W. (1999). “Snowmelt and runoff modelling of an Arctic hydrological basin in west Greenland.” Hydrological Processes, 13: 1989–2002.

Bonsal, B., Zhang, X., Vincent, L., & Hogg, W. (2001). "Characteristics of daily and extreme temperatures over Canada." Journal of Climate 14(9): 1959-1976.

Borah, D. K., Bera, M., & Xia, R. (2004). “Storm event flow and sediment simulations in agricultural watersheds using DWSM.” Transactions of the ASAE, 47(5), 1539.

Bradley, R. S., Diaz, H. F., Eischeid, J. K., Jones, P. D., Kelly, P. M., & Goodess, C. M. (1987). “Precipitation fluctuations over Northern Hemisphere land areas since the mid-19th century.” Science, 237(4811), 171-175.

Bretherton, C. S., Smith, C., & Wallace, J. M. (1992). “An intercomparison of methods for finding coupled patterns in climate data.” Journal of climate, 5(6), 541-560.

Brooks, H. E., & Doswell III, C. A. (1996). “A comparison of measures-oriented and distributions-oriented approaches to forecast verification.” Weather and forecasting, 11(3), 288-303.

Burrough, P. A., McDonnell, R. A., & Lloyd, C. D. (1998). “Principles of geographical information systems.” Oxford University Press.

Busuioc, A., & Von Storch, H. (1996). “Changes in the winter precipitation in Romania and its relation to the large-scale circulation.” Tellus A, 48(4), 538-552.

Busuioc, A., Tomozeiu, R., & Cacciamani, C. (2008). “Statistical downscaling model based on canonical correlation analysis for winter extreme precipitation events in the Emilia-Romagna region.“ International Journal of Climatology, 28(4), 449-464.

Cess, R. D. (1978). "Biosphere-albedo feedback and climate modeling." Journal of the Atmospheric Sciences 35.9: 1765-1768.

Chapman, T. (1994). "Stochastic models for daily rainfall." Water Down Under 94: Surface Hydrology and Water Resources Papers; Preprints of Papers: 7.

Charney, J. G., Fjörtoft, R., & Neumann, J. V. (1950). “Numerical integration of the barotropic vorticity equation.” Tellus, 2(4), 237-254.

Chen, Y., Ebert, E. E., Walsh, K. J., & Davidson, N. E. (2013). “Evaluation of TRMM 3B42 precipitation estimates of tropical cyclone rainfall using PACRAIN data.” Journal of Geophysical Research: Atmospheres, 118(5), 2184-2196.

Chew, C. Y., Moore, L. W., & Smith, R. H. (1991). “Hydrological simulation of Tennessee's north Reelfoot Creek watershed.” Research Journal of the Water Pollution Control Federation, 10-16.

Chiles, J. P., & Delfiner, P. (2009). “Geostatistics: modeling spatial uncertainty (Vol. 497).” John Wiley & Sons.

Chin, E. H., & Miller, J. F. (1980). “On the conditional distribution of daily precipitation amounts.” Monthly Weather Review, 108(9), 1462-1464.

Chow, V. T., Maidment, D. R., & Mays, L. W. (1988). “Applied hydrology.”

COMET (2016). “Introduction to Tropical Meteorology.”

Cressie, N. (1990). "The origins of kriging." Mathematical geology 22(3): 239-252.

Cressman, G. P. (1959). "An operational objective analysis system." Monthly Weather Review 87(10): 367-374.

Dee, D. P., Uppala, S. M., Simmons, A. J., Berrisford, P., Poli, P., Kobayashi, S., Andrae, U., Balmaseda, M., Balsamo S., & Bechtold, P. (2011). “The ERA-Interim reanalysis: Configuration and performance of the data assimilation system.” Quarterly Journal of the Royal Meteorological Society, 137(656), 553-597.

Diallo, I., Giorgi, F., Sukumaran, S., Stordal, F., & Giuliani, G. (2014). "Evaluation of RegCM4 driven by CAM4 over Southern Africa: mean climatology, interannual variability and daily extremes of wet season temperature and precipitation." Theoretical and Applied Climatology 1: 193.

Diaz, H. F., Bradley, R., & Eischeid, J. (1989). "Precipitation fluctuations over global land areas since the late 1800's." Journal of Geophysical Research: Atmospheres (1984–2012) 94(D1): 1195-1210.

Dickinson, R. E., Errico, R. M., Giorgi, F., & Bates, G. T. (1989). "A regional climate model for the western United States." Climatic Change 15(3): 383-422.

Dickinson, R. E., Kennedy, P., & Henderson-Sellers, A. (1993). "Biosphere-atmosphere transfer scheme (BATS) version 1e as coupled to the NCAR community climate model." National Center for Atmospheric Research, Climate and Global Dynamics Division.

Dirks, K., Hay, J., Stow, C., & Harris, D. (1998). "High-resolution studies of rainfall on Norfolk Island: Part II: Interpolation of rainfall data." Journal of Hydrology 208(3): 187-193.

DOE (1996). "Review of the potential effects of climate change in the United Kingdom." HMSO, London. Department of the Environment.

DONRE (2015). "Atlas of the Dong Nai Province."

Dosio, A., Paruolo, P.,& Rojas, R. (2012). "Bias correction of the ENSEMBLES high resolution climate change projections for use by impact models: Analysis of the climate change signal." Journal of Geophysical Research: Atmospheres (1984–2012) 117(D17).

Echaabi, J., Trochu, F., & Gauvin, R. (1995). "A general strength theory for composite materials based on Dual Kriging interpolation." Journal of reinforced plastics and composites 14(3): 211-232.

Efron, B., & Tibshirani, R. J. (1994). "An introduction to the bootstrap." CRC press.

Ehret, U., Zehe, E., Wulfmeyer, V., Warrach-Sagi, K., & Liebert, J. (2012). "HESS Opinions" Should we apply bias correction to global and regional climate model data?"." Hydrology and Earth System Sciences Discussions 9(4): 5355-5387.

Elguindi, N., Bi, X., Giorgi, F., Nagarajan, B., Pal, J., Solmon, F., Rauscher, S., Zakey, A., & Giuliani, G. (2011). "Regional climatic model RegCM user manual version 4.1." ITCP, Trieste, Italy.

Emanuel, K. A. (1991). "A scheme for representing cumulus convection in large-scale models." Journal of the Atmospheric Sciences 48(21): 2313-2329.

Enke, W., & Spekat, A. (1997). "Downscaling climate model outputs into local and regional weather elements by classification and regression." Climate Research 8(3): 195-207.

Exner, F. M. (1908). "Uber eine erste Annäherung zur Vorausberechnung synoptischer Wetterkarten." Meteor. Zeit, 25, 57-67.

Feser, F., Rockel, B., von Storch, H., Winterfeldt, J., and M. Zahn (2011). "Regional climate models add value to global model data: a review and selected examples." Bulletin of the American Meteorological Society 92(9): 1181-1192.

Flato, G. (2005). "The third generation Coupled Global Climate Model (CGCM3)." Canadian Centre for Climate Modelling and Analysis, Victoria, BC, Canada.

Foley, A. M. (2010). "Uncertainty in regional climate modelling: A review." Progress in Physical Geography.

Förster, K. (2013). "Detaillierte Nachbildung von Schneeprozessen in der hydrologischen Modellierung." Dissertation. Abteilung Hydrologie, Wasserwirtschaft und Gewässerschutz am Leichtweiß-Institut für Wasserbau, Technische Universität Braunschweig.

Förster, K., Meon, G., Marke, T., & Strasser, U. (2014). “Effect of meteorological forcing and snow model complexity on hydrological simulations in the Sieber catchment (Harz Mountains, Germany).” Hydrol. Earth Syst. Sci., 18, 4703–4720.

Fowler, H., Blenkinsop, S., & Tebaldi, C. (2007). "Linking climate change modelling to impacts studies: recent advances in downscaling techniques for hydrological modelling." International Journal of Climatology 27(12): 1547-1578.

Frei, C., & Schär, C. (2001). "Detection probability of trends in rare events: Theory and application to heavy precipitation in the Alpine region." Journal of Climate 14(7): 1568-1584.

GCOS (2010). “Implementation plan for the global observing system for climate in support of the UNFCCC (2010 update).” GCOS Rep. 138, 186 pp.

Gerrits, A., Pfister L., & Savenije, H. (2010). "Spatial and temporal variability of canopy and forest floor interception in a beech forest." Hydrological processes 24(21): 3011-3025.

Giang, N. (2014). "Overview of meteorological stations and rain gauges in Vietnam." Resources and Environment.

Giorgi, F. (1990). "Simulation of regional climate using a limited area model nested in a general circulation model." Journal of Climate 3(9): 941-963.

Giorgi, F. (2006). “Regional climate modeling: Status and perspectives.” Journal de Physique IV (Proceedings), EDP sciences.

Giorgi, F., & Anyah, R. (2012). "The road towards RegCM4." Climate Research 52(1): 3-6.

Giorgi, F., Christensen, J., Hulme, M., Von Storch, H., Whetton, P., Jones, R., Mearns, L., Fu, C., Arritt, R., & Bates, B. (2001). "Regional climate information-evaluation and projections." Climate Change 2001: The Scientific Basis. Contribution of Working Group to the Third Assessment Report of the Intergouvernmental Panel on Climate Change [Houghton, JT et al.(eds)]. Cambridge University Press, Cambridge, United Kongdom and New York, US.

Giorgi, F., Jones, C., & Asrar, G. R. (2009). "Addressing climate information needs at the regional level: the CORDEX framework." World Meteorological Organization (WMO) Bulletin 58(3): 175.

Giorgi, F., Marinucci, M. R., & Bates, G. T. (1993). "Development of a second-generation regional climate model (RegCM2). Part I: Boundary-layer and radiative transfer processes." Monthly Weather Review 121(10): 2794-2813.

Giorgi, F., Marinucci, M. R., & Visconti, G. (1990). "Use of a limited-area model nested in a general circulation model for regional climate simulation over Europe." Journal of Geophysical Research: Atmospheres (1984–2012) 95(D11): 18413-18431.

Giorgi, F., Marinucci, M. R., Bates, G. T., & De Canio, G. (1993). "Development of a second-generation regional climate model (RegCM2). Part II: Convective processes and assimilation of lateral boundary conditions." Monthly Weather Review 121(10): 2814-2832.

Glahn, H. R., & Lowry, D. A. (1972). "The use of model output statistics (MOS) in objective weather forecasting." Journal of applied meteorology 11(8): 1203-1211.

Gocic, M., & Trajkovic, S. (2013). "Analysis of changes in meteorological variables using Mann-Kendall and Sen's slope estimator statistical tests in Serbia." Global and Planetary Change 100: 172-182.

Goodess, C. (2005). "STARDEX–Downscaling climate extremes." UEA, Norwich.

Goosse H., Barriat, P.Y., Lefebvre, W., Loutre, M.F., & Zunz, V. (2008-2010). “Introduction to climate dynamics and climate modeling”.

Goovaerts, P. (1997). “Geostatistics for natural resources evaluation.” Oxford university press.

Goovaerts, P. (2000). "Geostatistical approaches for incorporating elevation into the spatial interpolation of rainfall." Journal of hydrology 228(1): 113-129.

Grell, G. A., Dudhia, J., & Stauffer, D. R. (1994). "A description of the fifth-generation Penn State/NCAR mesoscale model (MM5)."

Gruza, G., Rankova, E., Razuvaev, V., & Bulygina, O. (1999). "Indicators of climate change for the Russian Federation." Climatic Change 42(1): 219-242.

GSO (2005). “Statistical annual publication 2005.” General Statistics Office of Vietnam.

Hansen, J., Lacis, A., Rind, D., Russell, G., Stone, P., Fung, I., Ruedy, R., & Lerner, J. (1984). “Climate sensitivity: Analysis of feedback mechanisms.” Climate processes and climate sensitivity, pp.130-163. Harding, R., & Warnaars, T. (2011). “Water and global change. The WATCH Project Outreach Report.”

Hansen, J.W., Challinor, A., Ines, A., Wheeler, T., & Moronet, V. (2006). “Translating forecasts into agricultural terms: advances and challenger.” Clim. Res. 33, 27-41.

Harpham, C., & Wilby, R. L. (2005). "Multi-site downscaling of heavy daily precipitation occurrence and amounts." Journal of Hydrology 312(1): 235-255.

Harris, I., Jones, P., Osborn, T., & Lister, D. (2014). "Updated high-resolution grids of monthly climatic observations–the CRU TS3. 10 Dataset." International Journal of Climatology 34(3): 623-642.

Hay, L. E., Wilby, R. L., & Leavesley, G. H. (2000). “A comparison of delta change and downscaled GCM scenarios for three mounfainous basins in the United States.” Wiley Online Library.

Heino, R., Brázdil, R., Førland, E., Tuomenvirta, H., Alexandersson, H., Beniston, M., Pfister, C., Rebetez, M., Rosenhagen, G., & Rösner, S. (1999). “Progress in the study of climatic extremes in Northern and Central Europe.” Weather and Climate Extremes, Springer**:** 151-181.

Helsel, D. R., & Hirsch, R. M. (1992). “Statistical methods in water resources.” Elsevier.

Hempel, S., Frieler, K., Warszawski, L., Schewe, J., & Piontek, F. (2013). A trend-preserving bias correction–the ISI-MIP approach. Earth System Dynamics, 4(2), 219-236.Hevesi, J. A., J. D. Istok and A. L. Flint (1992). "Precipitation estimation in mountainous terrain using multivariate geostatistics. Part I: structural analysis." Journal of applied meteorology 31(7): 661-676.

Hengl, T. (2007). "A Practical Guide to Geostatistical Mapping of Environmental Variables." 165.

Hengl, T., Heuvelink, G., & Rossiter, D. G. (2007). "About regression-kriging: from equations to case studies." Computers & Geosciences 33(10): 1301-1315.

Hewitson, B. C., & Crane, R. G. (1996). "Climate downscaling: Techniques and application."

Hewitt, C.D., & Griggs, D.J. (2004). “Ensembles-based predictions: Climate changes and their impacts.” Eos, 85, 566.

Ho, T. M. H. (2008). “Performance of seasonal meteorological simulations for Vietnam using hydrodynamic-statistical approaches. ” Dissertation (in Vietnamese)

Holdaway, M. R. (1996). "Spatial modeling and interpolation of monthly temperature using kriging." Climate Research 6(3): 215-225.

Holton, J. R., & Hakim, G. J. (2013). “An introduction to dynamic meteorology.” Academic press.

Holtslag, A., De Bruijn, E., & Pan, H. (1990). "A high resolution air mass transformation model for short-range weather forecasting." Monthly Weather Review 118(8): 1561-1575.

Horton, R. E. (1919). "Rainfall interception." Monthly weather review 47(9): 603-623.

Hosseini, E., Gallich, J., & Caron, J. (1993). "Comparison of several interpolatiors for smoothing hydraulic conductivity data in South-West Iran." Transactions of American society of agriculture engineers ASAE.

Houghton, J. T., & Callander, B. A. (1992). Climate change 1992. Cambridge University Press.

Houze Jr, R. A. (1993). "Cloud dynamics, 573 pp." Academic, San Diego, Calif.

Houze, R. A. (1997). “Stratiform precipitation in regions of convection: A meteorological paradox?.” Bull. Amer. Met. Soc., 78, 2179-2196.

Huffman, G. J., & Bolvin, D. T. (2013). "TRMM and other data precipitation data set documentation." NASA, Greenbelt, USA: 1-40.

Hughes, J. P., Guttorp, P., & Charles, S. P. (1997). "A nonhomogeneous hidden Markov model for precipitation."

Huth, R. (1999). "Statistical downscaling in central Europe: evaluation of methods and potential predictors." Climate Research 13(2): 91-101.

IMHEN and UNDP (2015). “Special Report on Managing the Risks of Extreme Events and Disasters to Advance Climate Change Adaptation for Vietnam.”

Ines, A. V., & Hansen, J. W. (2006). "Bias correction of daily GCM rainfall for crop simulation studies." Agricultural and forest meteorology 138(1): 44-53.

IPC (2014). http://invest-bariavungtau.gov.vn/en/the-necessary-of-co-expoliting-cai-mep-thi-vai-port-group-3163.html/.

IPCC (1990). “Climate Change 1990: The IPCC Scientific Assessment.” Houghton JT, Jenkins G, Ephraums JJ eds, 1, 990.

IPCC (1996). “Climate Change 1995: The Science of Climate Change. Contribution of Working Group I to the Second Assessment Report of the Intergovernmental Panel on Climate Change.” [J. T. Houghton., L. G. Meira . A. Callander, N. Harris, A. Kattenberg and K. Maskell (eds.)]. Cambridge University Press, Cambridge, United Kingdom and New York, NY, USA, 572 pp.

IPCC (2001). “Climate Change 2001: The Scientifi Basis. Contribution of Working Group I to the Third Assessment Report of the Intergovernmental Panel on Climate Change.” [J. T. Houghton, Y. Ding, D. J. Griggs, M. Noquer, P. J. van der Linden, X. Dai, K. Maskell and C. A. Johnson (eds.)]. Cambridge University Press, Cambridge, United Kingdom and New York, NY, USA, 881 pp.

IPCC (2007). “Climate Change 2007: The Physical Science Basis. Contribution of Working Group I to the Fourth Assessment Report of the Intergovernmental Panel on Climate Change.”

[Solomon, S., D. Qin, M. Manning, Z. Chen, M. Marquis, K. B. Averyt, M. Tignor and H. L. Miller (eds.)]. Cambridge University Press, Cambridge, United Kingdom and New York, NY, USA, 996 pp.

IPCC (2013). "Climate Change 2013: The Physical Science Basis. Contribution of Working Group I to the Fifth Assessment Report of the Intergovernmental Panel on Climate Change." [Stocker, T.F., D. Qin, G.-K. Plattner, M. Tignor, S.K. Allen, J. Boschung, A. Nauels, Y. Xia, V. Bex and P.M. Midgley (eds.)]. Cambridge University Press, Cambridge, United Kingdom and New York, NY, USA, 1535 pp.

Isaaks, E. H, & Srivastava, R. M. (1989). "An introduction to applied geostatistics."

Iwashima, T., & Yamamoto, R. (1993). "A statistical analysis of the extreme events: Long-term trend of heavy daily precipitation." Journal of the Meteorological Society of Japan 71(5): 637-640.

Jeong, D. I., St-Hilaire, A., Ouarda, T. B., & Gachon, P. (2012). "CGCM3 predictors used for daily temperature and precipitation downscaling in Southern Québec, Canada." Theoretical and applied climatology 107(3-4): 389-406.

Jolliffe, I. T., & Stephenson, D. B. (2012). "Forecast verification: a practitioner's guide in atmospheric science." John Wiley & Sons.

Jonathan, A. (2003). "Vegetation–Climate Interaction: How Vegetation Makes the Global Environment."

Jones, J. W., Colwick, R. E., & Threadgill, E. D. (1972). "A simulated environmental model of temperature, evaporation, rainfall and soil moisture." Trans. ASAE 15: 366-372.

Jones, P. D., & Harris, I. (2013). "CRU TS3.21: Climatic Research Unit (CRU) Times-Series (TS) Version 3.21 of High Resolution Gridded Data of Month by month Variation in Climte (Jan 1901-Dec-2012)." (NCAS British Atmospheric Data Center).

Jones, P., Horton, E., Folland, C., Hulme, M., Parker, D., & Basnett, T. (1999). "The use of indices to identify changes in climatic extremes. Weather and Climate Extremes." Springer**:** 131-149.

Jones, R., Murphy, J., & Noguer, M. (1995). "Simulation of climate change over europe using a nested regional-climate model. I: Assessment of control climate, including sensitivity to location of lateral boundaries." Quarterly Journal of the Royal Meteorological Society 121(526): 1413-1449.

Jones, R.G., Noguer, M., Hassell, D.C., Hudson, D., Wilson, S.S., Jenkins, G.J. and Mitchell, J.F.B. (2004) Generating high resolution climate change scenarios using PRECIS, Met Office Hadley Centre, Exeter, UK, 40pp.

Journel, A. G., & Deutsch, C. V. (1992). "GSLIB, Geostatistical Software Library and User's Guide." New York, Oxford University Press.

Kalnay, E., & Coauthors (1996). "The NCEP/NCAR 40-Year Reanalysis Project". Bull. Amer. Meteor. Soc., 77, 437–471.

Karl, T. R., & Knight, R. W. (1998). "Secular trends of precipitation amount, frequency, and intensity in the United States." Bulletin of the American Meteorological society 79(2): 231-241.

Kay, A. L., Davies, H. N., Bell, V. A., & Jones, R. G. (2009). “Comparison of uncertainty sources for climate change impacts: flood frequency in England.” Climatic Change, 92(1-2), 41-63.

Keil, C., & Craig, G. C. (2009). "A displacement and amplitude score employing an optical flow technique." Weather and Forecasting 24(5): 1297-1308.

Kendall, M. G. (1948). "Rank correlation methods."

Khromov, S. P. (1957). "Die Geographische Verbreitung der Monsune Petermanns Geogr.": Mitt., 101, pp. 234–237.

Kiehl, J. T., Hack, J. J., Bonan, G. B., Boville, B. A., & Briegleb, B. P. (1996). “Description of the NCAR Community Climate Model (CCM3).” Technical Note, National Center for Atmospheric Research, Boulder, CO (United States). Climate and Global Dynamics Div.

Kienzle, S. W., & Schulze, R. E. (1992). “A simulation model to assess the effect of afforestation on ground-water resources in deep sandy soils.” Water S. A., 18(4), 265-272.

Kieu, T.X., Tran, N. A., Le, C. T., & Phan, V. T. (2000). “Tests on the RegCM performance to simulate precipitation for Vietnam.” Vietnam Hydrometeorological Journal, Nr. 7 (475), pp. 10-18, 2000. (in Vietnamese)

Kim, J., Chang, J., Baker, N., Wilks, D., & Gates, W. (1984). "The statistical problem of climate inversion: Determination of the relationship between local and large-scale climate." Monthly Weather Review 112(10): 2069-2077.

Kittredge, J. (1948). ”Forest influences: The effects of woody vegetation on climate, water, and soil, with applications to the conservation of water and the control of floods and erosion.”

Klein, W. (1948). "Winter precipitation as related to the 700-millibar circulation."

Klein, W. H., & Bloom, H. J. (1987). "Specification of monthly precipitation over the United States from the surrounding 700 mb height field." Monthly weather review **115**(9): 2118-2132.

Klein, W. H., Lewis, B. M., & Enger, I. (1959). "Objective prediction of five-day mean temperatures during winter." Journal of Meteorology 16(6): 672-682.

Krause, P. (2002). “Quantifying the impact of land use changes on the water balance of large catchments using the J2000 model.” Physics and Chemistry of the Earth, 27(9–10): 663–673.

Krause, P., Boyle, D., & Bäse, F. (2005). "Comparison of different efficiency criteria for hydrological model assessment." Advances in Geosciences 5: 89-97.

Kreye, P. (2015). “Mesoskalige Bodenwasserhaushaltsmodellierung mit Nutzung von Grundwassermessungen und satellitenbasierten Bodenfeuchtedaten.“ Dissertation. Abteilung Hydrologie, Wasserwirtschaft und Gewässerschutz am Leichtweiß-Institut für Wasserbau, Technische Universität Braunschweig. 2015.

Krysanova, V., Müller-Wohlfeil, D.-I., & Becker, A. (1998). “Development and test of a spatially distributed hydrological/water quality model for mesoscale watersheds.” Ecological Modelling, 106 (2–3): 261–289.

Kuo, H. L. (1974). “Further studies of the parameterization of the influence of cumulus convection on large-scale flow.” Journal of the Atmospheric Sciences, 31(5), 1232-1240.

Lafon, T., Dadson, S., Buys, G., & Prudhomme, C. (2013). "Bias correction of daily precipitation simulated by a regional climate model: a comparison of methods." International Journal of Climatology 33(6): 1367-1381.

Lam, N. S.-N. (1983). "Spatial interpolation methods: A review." The American Cartographer 10(2): 129-150.

Laslett, G., McBratney, A., Pahl, P. J., & Hutchinson, M. (1987). "Comparison of several spatial prediction methods for soil pH." Journal of Soil Science 38(2): 325-341.

Leander, R., & Buishand, T. A. (2007). "Resampling of regional climate model output for the simulation of extreme river flows." Journal of Hydrology 332(3): 487-496.

Lenderink, G., Buishand, A., & Deursen, W. v. (2007). "Estimates of future discharges of the river Rhine using two scenario methodologies: direct versus delta approach." Hydrology and Earth System Sciences 11(3): 1145-1159.

Li, J., & Australia, G. (2008). "A review of spatial interpolation methods for environmental scientists." Geoscience Australia Canberra.

Loo, Y. Y., Billa, L., & Singh, A. (2014). "Effect of climate change on seasonal monsoon in Asia and its impact on the variability of monsoon rainfall in Southeast Asia." Geoscience Frontiers.

Lorenz, E. N. (1955). "Available potential energy and the maintenance of the general circulation". Tellus, 7, 157-167.

Lorenz, M. (2015). "Entwicklung eines ökohydrologischen Modellsystems auf der Einzugsgebietsskala und Anwendung in den sommerfeuchten Tropen." Dissertation. Abteilung Hydrologie, Wasserwirtschaft und Gewässerschutz am Leichtweiß-Institut für Wasserbau, Technische Universität Braunschweig. 2015.

Lorenz, P., & Jacob, D. (2005). "Influence of regional scale information on the global circulation: A two-way nesting climate simulation." Geophysical research letters 32(18).

Loucks, D. P., Van Beek, E., Stedinger, J. R., Dijkman, J. P., & Villars, M. T. (2005). "Water resources systems planning and management: an introduction to methods, models and applications." Paris: UNESCO.

Luong, M. T. (2010). "The influences of buffer zone and resolution on the climate simulations for Vietnam and adjacent areas." Thesis Master of Science.

Luterbacher, J., Dietrich, D., Xoplaki, E., Grosjean, M., & Wanner, H. (2004). "European seasonal and annual temperature variability, trends, and extremes since 1500." Science 303(5663): 1499-1503.

LWI-HYWAG and IFW (2012). "Panta Rhei Benutzerhandbuch - Programmdokumentation zur hydrologischen Modellsoftware (unveröffentlicht), Braunschweig."

Ly, S., Charles, C., & Degre, A. (2011). "Geostatistical interpolation of daily rainfall at catchment scale: the use of several variogram models in the Ourthe and Ambleve catchments, Belgium." Hydrology & Earth System Sciences 15(7).

Maniak, U. (1997). "Hydrologie und Wasserwirtschaft: Eine Einführung für Bauingenieure." 4 Aufl. Springer-Verlag.

Mann, H. B. (1945). "Nonparametric tests against trend." Econometrica: Journal of the Econometric Society: 245-259.

Manton, M., Della-Marta, P., Haylock, M., Hennessy, K., Nicholls, N., Chambers, L., Collins, D., Daw, G., Finet, A., & Gunawan, D. (2001). "Trends in extreme daily rainfall and temperature in Southeast Asia and the South Pacific: 1961–1998." International Journal of Climatology 21(3): 269-284.

Maraun, D., Wetterhall, F., Ireson, A., Chandler, R., Kendon, E., Widmann, M., Brienen, S., Rust, H., Sauter, T., & Themeßl, M. (2010). "Precipitation downscaling under climate change: Recent developments to bridge the gap between dynamical models and the end user." Reviews of Geophysics 48(3).

Margules, M. (1904). "Über die Beziehung zwischen Barometerschwankungen und Kontinuit ätsgleichung." Ludwig Boltzmann Festschrift. Leipzig, J. A. Barth,: Pp. 585–589

Marzban, C., Sandgathe, S., & Kalnay, E. (2006). "MOS, perfect prog, and reanalysis." Monthly weather review 134(2): 657-663.

Matheron, G. (1962). "Traité de geostatisque appliquée, vol. I: Memoires du Bureau de Recherches Géologiques et Miniéres." no 14(Editions Technip, Paris): 333 pp.

Matheron, G. (1971). "The theory of regionalized variables and its applications (Vol. 5, p. 211pp)." École national supérieure des mines.

McGregor, J. (1997). "Regional climate modelling." Meteorology and Atmospheric Physics **63**(1-2): 105-117.

Meon G., Pätsch M., Phuoc N.V., Quan N.H. (eds.) (2014). "EWATEC-COAST: Technologies for Environmental and Water Protection of Coastal Zones in Vietnam." Contributions to 4thInternational Conference for Environment and Natural Resources, ICENR 2014. Cuvillier, Göttingen, Germany.

Michaels, P. J., Bailing, R., Vose, R. S., & Knappenberger, P. C. (1998). "Analysis of trends in the variability of daily and monthly historical temperature measurements." Climate Research 10(1): 27-33.

Michelangeli, P. A., Vrac, M., & Loukos, H. (2009). "Probabilistic downscaling approaches: Application to wind cumulative distribution functions." Geophysical Research Letters 36(11).

MONRE (2006). " The state of water environment in 3 river basins of Cau, Nhue-Day and Dong Nai river system." Environment report of Vietnam.

MONRE (2008). "National Target Program to respond to climate change (Implementing the Government's Resolution No. 60/2007/NQ-CP dated 3rd December 2007." Ministry of Natural Resources and Environment, Vietnam.

MONRE (2009). "Climate change, sea level rise scenarios for Vietnam." Ministry of Natural Resources and Environment, Vietnam.

MONRE (2011). "The National strategy on climate change (Implementing the Government's Decision No. 2139/QĐ-TTg dated 5th December 2011."

MONRE (2012a). "Climate change scenarios and sea level rise for Vietnam." Ministry of Natural Resources and Environment, Vietnam

MONRE (2012b). "National strategy on climate change." Ministry of Natural Resources and Environment, Vietnam.

Monteith, J. (1965). “Evaporation and environment”. Symp. Soc. Exp. Biol.

Moriasi, D., Arnold, J., Van Liew, M., Bingner, R., Harmel, R., & Veith, T. (2007). "Model evaluation guidelines for systematic quantification of accuracy in watershed simulations." Trans. Asabe 50(3): 885-900.

Murphy, A. H., & Winkler, R. L. (1987). "A general framework for forecast verification." Monthly Weather Review 115(7): 1330-1338.

Murphy, A. H., Brown, B. G., & Chen, Y.-s. (1989). "Diagnostic verification of temperature forecasts." Weather and Forecasting 4(4): 485-501.

Murphy, J. M., Sexton, D. M. H., Jenkins, G. J., Booth, B. B. B., Brown, C. C., Clark, R. T., & Brown, S. J. (2009). “UK climate projections science report: climate change projections.” Meteorological Office Hadley Centre.

Nash, J., & Sutcliffe, J. V. (1970). "River flow forecasting through conceptual models part I—A discussion of principles." Journal of hydrology 10(3): 282-290.

Neng Liew, J., Tangang, F., Tieh Ngai, S., Chung, J. X., Narisma, G., Cruz, F. A., Phan, V. T., Ngo, D. T., Santisirisomboon, J., Milindalekha, J., & Singhruck, P. (2015). “Performance of ICTP's RegCM4 in Simulating the Rainfall Characteristics over the CORDEX-SEA Domain.” In EGU General Assembly Conference Abstracts (Vol. 17, p. 3125).

Nguyen D. N. (2007). “Impacts of ENSO on weather, climate, environment and socio-economic in Vietnam.” National conference in biodiversity and climate change, Hanoi (in Vietnamese)

Nguyen, D. N. (2002). "Impacts of ENSO on weather, climate, environment and socio-economic in Vietnam." (in Vietnamese)

Nguyen, D. N. (2008). "Climate change." Scientific and Technical Publishing House, Ha Noi. (in Vietnamese)

Nguyen, D. N. (2009). "Challenges of Climate change to the economic development, Vietnam." Environmental economics journal 01(10). (in Vietnamese)

Nguyen, D. N., Nguyen, T. H. (2004). “Climate and Climate Resources of Vietnam.” Agriculture Publishing House, Hanoi (in Vietnamese)

Nguyen, D. T., Takagi, H., & Esteban, M. (2014). “Coastal Disasters and Climate Change in Vietnam: Engineering and Planning Perspectives.” Elsevier.

Nguyen, H. N., Hoang, M. H., England, S. B., Usher, P., & Glantz, M. (1992). “The Potential socio-economic effects of climate change on Vietnam.”

Nguyen, Q. T., Phan, V. T., & Ngo, D. T. (2012). “Performance of RegCM3 with different convective precipitation schemes in seasonal simulation.” Scientific Journal of Vietnam National University (in Vietnamese)

Nguyen, V. L. (2007). "Preliminary results in climate change in Vietnam." Hydrometeorological journal, Vietnam 560(33). (in Vietnamese)

Nguyen, V. T., & Le, V. T. (2004). “Experiments on installing the regional climate model RegCM for Vietnam.” Journal of Hydrometeorological Institute of Vietnam. (in Vietnamese)

Nguyen, V. T., Nguyen, T. H., Tran, T., Pham, T. T. H., Nguyen, T. L., Vu, V. T. (2010). “Climate change and its impacts in Vietnam.”

Nijssen, B., Haddeland, I., & Lettenmaier, D. P. (1997). “Point evaluation of a surface hydrology model for BOREAS.” Journal of Geophysical Research. D. Atmospheres, 102, 29.

Oleson, K., & Dai, Y. (2004). “Technical description of the community land model (CLM)." NCAR Technical Note TN-461 STR, 174pp.

Oreskes, N., Shrader-Frechette, K., & Belitz, K. (1994). "Verification, validation, and confirmation of numerical models in the earth sciences." Science 263(5147): 641-646.

Parker, D., Jones, P., Folland, C., & Bevan, A. (1994). "Interdecadal changes of surface temperature since the late nineteenth century." Journal of Geophysical Research: Atmospheres (1984–2012) 99(D7): 14373-14399.

Perkey, D. J., & Maddox, R. A. (1985). “A numerical investigation of a mesoscale convective system.” Monthly weather review, 113(4), 553-566.

Phan, V. T. (2005). "An investigation of the sensitivity of the RegCM2 model to topography and land surface conditions." Scientific project, Vietnam National University. (in Vietnamese)

Phan, V. T. (2008). “Implementation of Regional Climate Model for seasonal simulation/prediction of surface climate fields for development planning and disaster prevention.” Main Point Project of Vietnam National University, Hanoi. Code QGTD06.05 (2006-2008). (in Vietnamese)

Phan, V. T. (2010). “Impacts of Global Climate Change on Extreme Climate Events over Vietnam, Predictability and Adaptation Stategies.” National Project. Code KC.08.29/06-10 (2009-2010). (in Vietnamese)

Phan, V. T., & Ho, T. M. H. (2008). “An investigation of the sensitivity of the Regional Climate Model (RegCM3). Part II: Effects of Convective Parameterizations on the Seasonal Climate Simulations over Vietnam and South East Asian Region.” Submitted to Journal of Hydrometeorology, Aug. 2008. (In Vietnamese)

Phillips, N. A. (1956). “The general circulation of the atmosphere: A numerical experiment”. Quart. I. Roy. Meteor Soc., 82, 123-164.

Phillips, N. A., & Shukla, J. (1973). “On the strategy of combining coarse and fine grid meshes in numerical weather predictions.” J. Appl. Meteorol., 12, 763–770.

Piani, C., Haerter, J. O., & Coppola, E. (2010). “Statistical bias correction for daily precipitation in regional climate models over Europe.” Theoretical and Applied Climatology, 99(1-2), 187-192.

Piani, C., Weedon, G. P., Best, M., Gomes, S. M., Viterbo, P., Hagemann, S., & Haerter, J. O. (2010). “Statistical bias correction of global simulated daily precipitation and temperature for the application of hydrological models.” Journal of Hydrology, 395(3), 199-215.

Plummer, D., Caya, D., Frigon, A., Côté, H., Giguère, M., Paquin, D., Biner, S., Harvey, R., & De Elia, R. (2006). "Climate and climate change over North America as simulated by the Canadian RCM." Journal of Climate 19(13): 3112-3132.

Plummer, N., Salinger, M. J., Nicholls, N., Suppiah, R., Hennessy, K. J., Leighton, R. M., Trewin, B., Page, C. M., & Lough, J. M. (1999). “Changes in climate extremes over the Australian region

and New Zealand during the twentieth century." Weather and Climate Extremes, Springer**:** 183-202.

Ponce, V. M., & Hawkins, R. H. (1996). "Runoff curve number: Has it reached maturity?" Journal of hydrologic engineering 1(1): 11-19. Press, Cambridge, UK.

Priestley, C., & Taylor, R. (1972). "On the assessment of surface heat flux and evaporation using large-scale parameters." Monthly weather review 100(2): 81-92.

Prudhomme, C., Reynard, N., & Crooks, S. (2002). "Downscaling of global climate models for flood frequency analysis: where are we now?" Hydrological processes 16(6): 1137-1150.

Randall, D. A. (2000). "General circulation model development: past, present, and future." Academic Press.

Reboita, M. S., da Rocha, R. P., Dias, C. G., & Ynoue, R. Y. (2014). "Climate projections for South America: RegCM3 driven by HadCM3 and ECHAM5." Advances in Meteorology 2014.

Richardson, L. F. (1922). "Weather Prediction by Numerical Process." Cambridge University

Riedel, G. (2004). "Ein hydrologisches Modell für tidebeeinflusste Flussgebiete." Dissertation (Technische Universität Braunschweig, Braunschweig).

Riedel, G., Meon, G., Förster, K., Lange, S., Liechtenberg, T., & Anhalt, M. (2011). "Panta Rhei - Hydrologisches Modellsystem für Forschung und Praxis in Niedersachsen." Hydrolo-gie und Wasserwirtschaft - von der Theorie zur Praxis Beiträge zum Tag der Hydro-logie am 24./25.

Roer, I., Zemp, M., & van Woerden, J. (2008). "Global glacier changes: facts and figures." UNEP/Earthprint.

Rojas, M. (2006). "Multiply nested regional climate simulation for southern South America: Sensitivity to model resolution." Monthly weather review 134(8): 2208-2223.

Rosenthal, W. D., Srinivasan, R., & Arnold, J. G. (1995). "Alternative river management using a linked GIS-hydrology model." Transactions of the ASAE, 38(3), 783-790

Rouse, W. R., Douglas, M. S., Hecky, R. E., Hershey, A. E., Kling, G. W., Lesack, L., Marsh, P., McDonald, M., Nicholson, B. J., & Roulet, N. T. (1997). "Effects of climate change on the freshwaters of arctic and subarctic North America." Hydrological Processes 11(8): 873-902.

Ruddiman, W.F. (2007). "Earth's Climate: Past and Future". W.H. Freeman, 2 ed., 388 pp.

Rudra, R.P., Dickinson, W.T., Wall, G.J. (1985). "Application of the CREAMS model in southern Ontario conditions", Transactions of the ASAE, 28(4): 1233–1240

Rummukainen, M. (1997). "Methods for statistical downscaling of GCM simulations." SMHI Rapporter. Meteorologi och Klimatologi (Sweden). no. 80.

Rummukainen, M. (2010). "State-of-the-art with Regional Climate Models." Wiley Interdisciplinary Reviews: Climate Change 1(1): 82-96.

Sachindra, D., Huang, F., Barton, A., & Perera, B. (2013). "Least square support vector and multi-linear regression for statistically downscaling general circulation model outputs to catchment streamflows." International Journal of Climatology 33(5): 1087-1106.

Savenije, H. H. (2004). "The importance of interception and why we should delete the term evapotranspiration from our vocabulary." Hydrological Processes 18(8): 1507-1511.

Schmidli, J., Frei, C., & Vidale, P. L. (2006). "Downscaling from GCM precipitation: a benchmark for dynamical and statistical downscaling methods." International journal of climatology **26**(5): 679-689.

Schmidt, M., & Lipson, H. (2009). "Distilling free-form natural laws from experimental data." science 324(5923): 81-85.

Schneider, U., Becker, A., Finger, P., Meyer-Christoffer, A., Rudolf, B., & Ziese, M. (2011). "GPCC full data reanalysis version 6.0 at 0.5: monthly land-surface precipitation from rain-gauges built on GTS-based and historic data." doi: 10.5676/DWD_GPCC." FD_M_V6_050.

Schneider, U., Becker, A., Finger, P., Meyer-Christoffer, A., Ziese, M., & Rudolf, B. (2014). "GPCC's new land surface precipitation climatology based on quality-controlled in situ data and its role in quantifying the global water cycle." Theoretical and Applied Climatology 115(1-2): 15-40.

Schönwiese C. D., Fuchs, T., & Denhard, M. (1994). "Observed climate change in Europe 1891-1990." Meteorol Zeitschrift NF 3 22.

Schönwiese, C.-D., Stähler, U., & Birrong, W. (1990). "Temperature and precipitation trends in Europe and their possible link with greenhouse-induced climatic change." Theoretical and Applied Climatology 41(3): 173-175.

Schoof, J. T., & Pryor, S. (2001). "Downscaling temperature and precipitation: A comparison of regression-based methods and artificial neural networks." International Journal of Climatology 21(7): 773-790.

SCS (1972). "National Engineering Handbook." U. S. Soil Conservation Service. Section 4, Hydrology, U.S. Dept. of Agriculture, available from U.S. Government Printing Office, Washington, D.C.,

Semenov, M. A., & Barrow, A. "LARS-WG (2002): A Stochastic Weather Generator for Use in Climate Impact Studies." User Manual, Hertfordshire, UK.

Semenov, M. A., Brooks, R. J., Barrow, E. M., & Richardson, C. W. (1998). Comparison of the WGEN and LARS-WG stochastic weather generators for diverse climates. Climate research, 10(2), 95-107.

Sen, P. K. (1968). "Estimates of the regression coefficient based on Kendall's tau." Journal of the American Statistical Association 63(324): 1379-1389.

Skamarock, W. C., Klemp, J. B., Dudhia, J., Gill, D. O., Barker, D. M., Wang, W., & Powers, J. G. (2005). "A description of the advanced research WRF version 2 (No. NCAR/TN-468+ STR)." National Center For Atmospheric Research Boulder Co Mesoscale and Microscale Meteorology Div.

Stainforth, D. A., Allen, M. R., Tredger, E. R., & Smith, L. A. (2007a). "Confience, Uncertainty and Decision-Support Relevance in Climate Predictions." Philosophical Transactions of the Royal Society, 365, 2145-2161

Stainforth, D. A., Downing, T. E., Washington, R., Lopez, A., & New, M. (2007b). "Issues in the interpretation of climate model ensembles to inform decisions." Philosophical Transactions of the Royal Society A: Mathematical, Physical and Engineering Sciences 365: 2163-2177

Stanski, H. R., Wilson, L. J., & Burrows, W. R. (1989). “Survey of common verification methods in meteorology.” World Meteorological Organization, Geneva.

Stein, M. L. (1999). “Interpolation of spatial data: some theory for kriging.” Springer.

Stensrud, D. J. (2007). “Parameterization schemes: keys to understanding numerical weather prediction models.” Cambridge University Press.

Stephenson, D. B. (2000). "Use of the “odds ratio” for diagnosing forecast skill." Weather and Forecasting 15(2): 221-232.

Steppeler, J., Doms, G., Schättler, U., Bitzer, H. W., Gassmann, A., Damrath, U., & Gregoric, G. (2003). “Meso-gamma scale forecasts using the nonhydrostatic model LM.” Meteorology and atmospheric Physics, 82(1-4), 75-96.

Stocker, T. (2011). “Introduction to climate modelling.” Springer Science & Business Media.

Stone, D. A., Weaver, A. J., & Zwiers, F. W. (2000). "Trends in Canadian precipitation intensity." Atmosphere-Ocean 38(2): 321-347.

Suppiah, B., & Hennessy, K. J. (1995). "Trends in the intensity and frequency of heavy rainfall in tropical Australia and links with the Southern Oscillation." World Meteorological Organization-publicaions-WMO TD: 897-901.

Swank, W. (1968). "The influence of rainfall interception on streamflow."

Taylor, K. E. (2001). "Summarizing multiple aspects of model performance in a single diagram." Journal of Geophysical Research: Atmospheres (1984–2012) 106(D7): 7183-7192.

Taylor, R. G., Scanlon, B., Döll, P., Rodell, M., Van Beek, R., Wada, Y., Longuevergne, L., Leblanc, M., Famiglietti, J. S., & Edmunds, M. (2013). "Ground water and climate change." Nature Climate Change 3(4): 322-329.

Teng, J., Potter, N. J., Chiew, F. H. S., Zhang, L., Wang, B., Vaze, J., & Evans, J. P. (2015)."How does bias correction of regional climate model precipitation affect modelled runoff?." Hydrology and Earth System Sciences, 19 (2), 711-728.

Thiessen, A. H. (1911). "Precipitation averages for large areas." Monthly weather review 39(7): 1082-1089.

Thom, H. C. (1958). “A note on the gamma distribution.” Monthly Weather Review, 86(4), 117-122.

Tran, C.M. (2003). "Tropical synoptic meteorology." National Vietnam Univerisy Publisher.

Tran, Q.D. (2011). "The tendency of summer monsoon characteristics in Vietnam." Journal of Science, Vietnam National University.

Tran, T. L. (2009). "The Climate change impact to economic, prediction, vulnerabilities and adaptive strategies in Vietnam." 11.

Trzaska, S., & Schnarr, E. (2014). "A review of downscaling methods for climate change projections."

Van der Linden, P., & Mitchell, J. (2009). "ENSEMBLES: Climate Change and its Impacts: Summary of research and results from the ENSEMBLES project." Met Office Hadley Centre, FitzRoy Road, Exeter EX1 3PB, UK 160.

Verseghy, D., McFarlane, N., & Lazare, M. (1993). "CLASS—A Canadian land surface scheme for GCMs, II. Vegetation model and coupled runs." International Journal of Climatology 13(4): 347-370.

Viner, D. (2012). "Spatial Downscaling." Retrieved http://www.cccsn.ec.gc.ca/?page=downscaling

Von Storch, H., & Navarra, A. (1995). "Analysis of climate variability: applications of statistical techniques." Springer Science & Business Media.

Vu, T.T (2009). "Study and prediction in sedimentation and erosion changes of Dong Nai – Sai Gon River system under the impacts of flood protection and environmental improvement projects for the Ho Chi Minh region."

Wang, Bin (2006). "The asian monsoon. Springer Science & Business Media".

Warner, T. T. (2010). Numerical weather and climate prediction. Cambridge University Press.

WB (2003). "Vietnam Environment Monitor 2003." World Bank.

Webster, R., & Oliver, M. A. (2007). "Geostatistics for environmental scientists." John Wiley & Sons.

Weibull, W. (1951). "Wide applicability." Journal of applied mechanics.

White, R., & Toumi, R. (2013). "The limitations of bias correcting regional climate model inputs." Geophysical Research Letters 40(12): 2907-2912.

Wilby, R. L., & Wigley, T. (1997). "Downscaling general circulation model output: a review of methods and limitations." Progress in Physical Geography 21(4): 530-548.

Wilby, R. L., Hay, L. E., & Leavesley, G. H. (1999). "A comparison of downscaled and raw GCM output: implications for climate change scenarios in the San Juan River basin, Colorado." Journal of Hydrology 225(1): 67-91.

Wilby, R. L., Wigley, T., Conway, D., Jones, P., Hewitson, B., Main, J., & Wilks, D. (1998). "Statistical downscaling of general circulation model output: a comparison of methods." Water Resources Research 34(11): 2995-3008.

Wilby, R., Charles, S., Zorita, E., Timbal, B., Whetton, P., & Mearns, L. (2004). "Guidelines for use of climate scenarios developed from statistical downscaling methods."

Wilks, D. S. (2006). "On field significance and the false discovery rate." Journal of applied meteorology and climatology, 45(9), 1181-1189.

Wilson, L. J., Burrows, W. R., & Lanzinger, A. (1999). "A strategy for verification of weather element forecasts from an ensemble prediction system." Monthly Weather Review 127(6): 956-970.

WMO (1975). "Intercomparison of Conceptual Models used in Operational Hydrological Forecasting." WMO Operational Hydrology Report no. 7.

WMO (2008). "Guide to Meteorological Instruments and Methods of Observation (WMO-No. 8)." World Meteorological Organisation: Geneva, Switzerland.

WMO-No. 100 (1983)."Guide to Climatological Practices, 2nd ed."

WMO-No. 1069 (2011). "WMO Strategic Plan 2012-2015."

WMO-No. 49 (1988). "Technical Regulations, Vol. I-General Meteorological Standards and Recommended practices; Vol. II-Meteorological Service for International Air Navigation; Vol. III–Hydrology; Vol. IV Quality Management."

Wood, A. W., Leung, L. R., Sridhar, V., & Lettenmaier, D. (2004). "Hydrologic implications of dynamical and statistical approaches to downscaling climate model outputs." Climatic change 62(1-3): 189-216.

Woodcock, F. (1976). "The evaluation of yes/no forecasts for scientific and administrative purposes." Monthly Weather Review 104(10): 1209-1214.

Woolhiser, D. A., & Roldán, J. (1982). "Stochastic daily precipitation models: 2. A comparison of distributions of amounts." Water resources research 18(5): 1461-1468.

Xu, C.-y. (1999). "From GCMs to river flow: a review of downscaling methods and hydrologic modelling approaches." Progress in Physical Geography 23(2): 229-249.

Yafeng, S., Yongping, S., Dongliang, L., Guowei, Z., Yongjian, D. & Ersi, K. (2003). "Discussion on the present climate change from warm-dry to warm-wet in northwest China." Quaternary Sciences 23(2): 152-164.

Yatagai, A., Kamiguchi, K., Arakawa, O., Hamada, A., Yasutomi, N., & Kitoh, A. (2012). "APHRODITE: Constructing a long-term daily gridded precipitation dataset for Asia based on a dense network of rain gauges." Bulletin of the American Meteorological Society 93(9): 1401-1415.

Yin, C. (2011). “Applications of Self-Organizing Maps to Statistical Downscaling of Major Regional Climate Variables.” University of Waikato.

Yu, P.-S., Chen, S.-T., & Chang, I.-F. (2006). "Support vector regression for real-time flood stage forecasting." Journal of Hydrology 328(3): 704-716.

Yue, S., & Wang, C. (2004). "The Mann-Kendall test modified by effective sample size to detect trend in serially correlated hydrological series." Water Resources Management 18(3): 201-218.

Yue, S., Pilon, P., Phinney, B., & Cavadias, G. (2002). "The influence of autocorrelation on the ability to detect trend in hydrological series." Hydrological Processes 16(9): 1807-1829.

Zhang, G. J., & McFarlane, N. A. (1995). "Sensitivity of climate simulations to the parameterization of cumulus convection in the Canadian Climate Centre general circulation model." Atmosphere-Ocean 33(3): 407-446.

Zinke, P. J. (1967). “Forest interception studies in the United States (pp. 137-161).” Forest Hydrology. Oxford, UK: Pergamon Press.

Zorita, E., & Von Storch, H. (1999). "The analog method as a simple statistical downscaling technique: comparison with more complicated methods." Journal of climate 12(8): 2474-2489.

Appendixes

Appendix 1: MK test results

Table A1.1: MK test results for MWD.

Station	Test	Jan	Feb	Mar	Apr	May	Jun	Jul	Aug	Sep	Oct	Nov	Dec	Annual
Vung Tau	Z_{mk}	2.68***	2.14**	1.71*	1.69*	0.78	-0.56	0.15	0.40	0.10	0.11	0.96	1.20	2.03**
	Sen's slope	0.00	0.00	0.00	0.08	0.04	0.00	0.00	0.00	0.00	0.00	0.08	0.04	0.04
Can Gio	Z_{mk}	0.94	0.97	0.88	1.58	2.20**	-0.30	0.00	0.15	-0.45	-0.83	0.82	1.66*	1.28
	Sen's slope	0.00	0.00	0.00	0.04	0.23	0.00	0.00	0.00	-0.04	-0.06	0.04	0.00	0.03
Tan Son Hoa	Z_{mk}	0.68	0.32	2.25**	0.42	0.19	-2.58**	-0.08	-1.58	-0.85	0.66	-1.03	0.11	-0.68
	Sen's slope	0.00	0.00	0.07	0.00	0.00	-0.15	0.00	-0.08	-0.02	0.00	-0.11	0.00	-0.02
Long Thanh	Z_{mk}	0.86	1.50	2.31**	0.84	0.83	-0.01	1.03	0.18	0.49	0.31	-0.37	0.12	0.64
	Sen's slope	0.00	0.00	0.07	0.04	0.12	0.00	0.13	0.00	0.05	0.05	-0.04	0.00	0.08
Bien Hoa	Z_{mk}	2.17**	0.43	2.05**	1.25	-0.26	-0.32	1.08	-0.77	-0.70	-0.33	-0.82	0.21	0.50
	Sen's slope	0.05	0.00	0.09	0.11	0.00	0.00	0.06	-0.06	0.00	0.00	-0.08	0.00	0.02
Tam Thon Hiep	Z_{mk}	2.90***	0.23	0.99	1.82*	1.53	-0.20	1.40	-0.08	-0.27	0.48	0.39	0.99	0.84
	Sen's slope	0.00	0.00	0.00	0.08	0.11	0.00	0.12	0.00	0.00	0.04	0.00	0.00	0.03
Thong Nhat	Z_{mk}	1.43	0.87	1.87*	0.81	2.48**	2.75***	3.16***	2.80***	2.73***	3.48	1.11	1.44	4.61
	Sen's slope	0.00	0.00	0.07	0.05	0.25	0.21	0.38	0.31	0.23	0.33	0.10	0.07	0.18
Cam My	Z_{mk}	2.02**	0.08	1.26	0.78	2.85***	1.12	2.88***	0.62	1.31	0.75	0.88	-1.06	2.40**
	Sen's slope	0.00	0.00	0.00	0.00	0.27	0.11	0.25	0.07	0.10	0.00	0.04	-0.05	0.08
Mac Dinh Chi	Z_{mk}	-0.13	-0.47	1.66*	1.35	0.75	-0.62	-0.04	-0.72	0.64	0.58	-0.75	1.02	0.18
	Sen's slope	0.00	0.00	0.00	0.08	0.09	-0.03	0.00	-0.05	0.00	0.00	-0.07	0.08	0.00
Hoc Mon	Z_{mk}	0.83	1.23	1.00	1.78*	1.19	0.48	0.91	1.17	0.46	2.09**	0.32	1.93*	2.37**
	Sen's slope	0.00	0.00	0.00	0.09	0.15	0.00	0.12	0.13	0.00	0.20	0.00	0.08	0.08

Nha Be	Z_{mk}	1.38	0.59	0.64	0.51	0.54	-1.46	-1.82*	-1.28	-0.74	-1.17	0.31	-1.20	-1.10
	Sen's slope	0.00	0.00	0.00	0.05	0.08	-0.13	-0.23	-0.18	-0.07	-0.12	0.05	-0.13	-0.06
Xuan Loc	Z_{mk}	0.53	1.08	1.35	1.31	1.95*	-0.09	0.80	1.47	-0.24	0.09	1.49	0.24	2.78***
	Sen's slope	0.00	0.00	0.17	0.18	0.32	0.00	0.03	0.16	0.00	0.00	0.29	0.00	0.13
Binh Chanh	Z_{mk}	1.89*	0.61	1.94**	1.08	3.73	0.95	2.91***	0.39	1.08	1.74*	0.64	-0.63	2.85***
	Sen's slope	0.00	0.00	0.00	0.06	0.33	0.11	0.25	0.04	0.10	0.10	0.00	0.00	0.10

*** at significant level of 0.01, ** at significant level of 0.05, and * at significant level of 0.1

Table A1.2: MK test results for MCWD, MCDD, RX1day, RX3day, RX5day and RX7day.

Station	Test	RX1day	RX3day	RX5day	RX7day	MCWD	MCDD
Vung Tau	Z_{mk}	-1.83*	-1.57	-1.24	-1.27	1.02	-2.93***
	Sen's slope	-1.02	-1.55	-0.98	-1.07	0.05	-1.50
Can Gio	Z_{mk}	3.01***	3.14***	2.88***	3.05***	0.66	-1.04
	Sen's slope	2.14	2.80	2.85	3.00	0.00	-0.56
Tan Son Hoa	Z_{mk}	0.88	0.22	-0.95	-0.54	-0.82	-0.48
	Sen's slope	0.31	0.16	-0.66	-0.40	-0.06	-0.28
Long Thanh	Z_{mk}	1.38	1.98**	1.35	1.54	0.29	-2.69***
	Sen's slope	0.72	1.14	0.91	1.25	0.06	-1.05
Bien Hoa	Z_{mk}	-0.40	0.05	-0.25	-0.04	-0.40	-1.85*
	Sen's slope	-0.21	0.03	-0.18	-0.04	0.00	-0.70
Tam Thon Hiep	Z_{mk}	0.99	1.39	1.19	1.87*	0.63	-0.96
	Sen's slope	0.47	0.98	0.77	1.20	0.00	-0.44
Thong Nhat	Z_{mk}	-0.46	-0.75	-0.29	-0.75	1.90*	-1.59
	Sen's slope	-0.68	-0.65	-0.56	-0.66	0.20	-0.92
Cam My	Z_{mk}	1.19	1.07	1.50	0.88	0.98	-1.13
	Sen's slope	0.90	1.54	1.82	1.29	0.07	-0.75
Mac Dinh Chi	Z_{mk}	-1.23	-1.56	-2.43**	-1.60	0.24	-1.23
	Sen's slope	-0.75	-1.30	-1.80	-1.74	0.00	-0.52

Hoc Mon	Z_{mk}	1.52	0.73	0.34	0.85	2.23**	-0.91
	Sen's slope	0.93	0.83	0.51	1.14	0.17	-0.82
Nha Be	Z_{mk}	0.00	0.32	-0.21	-0.14	-1.03	-0.48
	Sen's slope	0.13	0.29	-0.63	-0.53	-0.09	-0.50
Xuan Loc	Z_{mk}	0.27	-0.51	0.03	0.51	0.49	-1.09
	Sen's slope	0.36	-1.13	0.07	0.99	0.13	-1.06
Binh Chanh	Z_{mk}	0.79	0.70	1.22	1.07	0.98	-1.77*
	Sen's slope	0.64	1.12	1.85	1.70	0.07	-1.06

*** at significant level of 0.01, ** at significant level of 0.05, and * at significant level of 0.1

Appendix 2

Table A2.1: Hydrometeorological measurement stations

Nr.	Station	Station code	Coordinates		Elevation (m a.s.l)	Period	Parameters	Temporal resolution
			Latitude (N)	Longitude (E)				
I.	**Meteorological station/ Rain gauge**							
1	Tan Son Hoa	489000	10°49’	106°40’	5	1980-2013	RR, E, T, RHmin, RHmax, RHtb, Sh, Vtd, Td, Vs. CT, TCF	Hourly, daily
2	Vung Tau	489030	10°22’	107°05’	4.1	1978-2013	RR, E, T, RHmin, RHmax, RHtb, Sh, Vtd, P, Td, Vs, CT, TCF	Hourly, daily
3	Long Thanh	30901006	10°27	106°33	41	1978-2013	RR	Daily
4	Can Gio	30906007	10°14’	106°35’	9	1980-2013	RR	Daily
5	Bien Hoa	48896	10°34’	106°29	13	1978-2013	RR, E, T, RHmin, RHmax, RHtb, Sh, Vtd, Td, Vs, CT, TCF	Hourly, daily
6	Tam Thon Hiep	30906022	10°40	106°52	4	1981-2013	RR	Daily
7	Cam My	30901004	10°51	107°09	145	1981-2013	RR	Daily
8	Thong Nhat	30901013	10°57	107°00	61	1981-2010	RR	
9	Nha Be	30906015	10°40’	106°44’	9	1992-2013	RR	Daily
10	Binh Chanh	30906004	10°44’	106°44’	9	1981-2013	RR	Daily
11	Xuan Loc	30901016	10°57’	107°14’	190	1990-2010	RR, E, T, RHmin, RHmax, RHtb, Sh, Vtd, Td, Vs, CT, TCF	Hourly, daily
12	Hoc Mon	30906010	10°46’	106°41’	8	1980-2007	RR	Daily
13	Mac Dinh Chi	30906014	10°48’	106°42’	6	1980-2007	RR	Daily
II.	**Hydrological stations**							
1	Binh Son	Not available	10°47’	107°08’	Not available	2013-present	Q	Every 10 minutes
2	Suoi Ca	Not available	10°44’	107°8’	Not available	2013-present	Q	Every 10 minutes

3	Cau Vac	Not available	$10^{o}40'$	$107^{o}04'$	Not available	2013-present	Q	Every 10 minutes

Note:

TCF: Total Cloud Fraction
CT: Cloud Types
RR: Precipitation
E: Evaporation
T: Temperature
RHmin: Minimum Relative Humidity
RHmax: Maximum Relative Humidity
RHtb: Average Relative Humidity
Sh: Sunshine
Vtd: Observed wind (speed and direction of wind)
Td: dewpoint temperature
Vs: Visibility
Q: Discharge

Appendix 3: Dynamical equations of dynamical model RegCM4

Horizontal Momentum Equations:

$$\frac{\partial p^* u}{\partial t} = -m^2\left(\frac{\partial p^* uu/m}{\partial x} + \frac{\partial p^* vu/m}{\partial y}\right) - \frac{\partial p^* u\dot{\sigma}}{\partial \sigma} - mp^*\left[\frac{RT_v}{(p^*+p_t/\sigma)}\frac{\partial p^*}{\partial x} + \frac{\partial \phi}{\partial x}\right] + fp^* v + F_H u + F_V u \quad \text{(A3.1)}$$

$$\frac{\partial p^* v}{\partial t} = -m^2\left(\frac{\partial p^* uv/m}{\partial x} + \frac{\partial p^* vv/m}{\partial y}\right) - \frac{\partial p^* v\dot{\sigma}}{\partial \sigma} - mp^*\left[\frac{RT_v}{(p^*+p_t/\sigma)}\frac{\partial p^*}{\partial y} + \frac{\partial \phi}{\partial y}\right] + fp^* v + F_H v + F_V v \quad \text{(A3.2)}$$

where:

u and v are the eastward and northward components of velocity

T_v is virtual temperature

Φ is geopotential height

f is the coriolis parameter

R is the gas constant for dry air; m is the map scale factor for either the Polar Stereographic, Lambert Conformal, or Mercator map projection, $\dot{\sigma} = \frac{d\sigma}{dt}$

F_H and F_V represent the effect of horizontal and vertical diffusion, and $p^* = p_s - p_t$.

Continuity and Sigmadot ($\dot{\sigma}$) Equations

$$\frac{\partial p^*}{\partial t} = -m^2\left(\frac{\partial p^* u/m}{\partial x} + \frac{\partial p^* v/m}{\partial y}\right) - \frac{\partial p^* \dot{\sigma}}{\partial \sigma} \quad \text{(A3.3)}$$

The temporal variation of the surface pressure in the model is implemented by:

$$\frac{\partial p^*}{\partial t} = -m^2 \int_0^1 \left(\frac{\partial p^* u/m}{\partial x} + \frac{\partial p^* v/m}{\partial y}\right) d\sigma \quad \text{(A3.4)}$$

At each level in the model, the vertical velocity in sigma coordinates ($\dot{\sigma}$) is calculated based on the vertical integral of Equation 9.4.

$$\dot{\sigma} = -\frac{1}{p^*}\int_0^\sigma \left\{\frac{\partial p^*}{\partial t} + m^2\left(\frac{\partial p^* u/m}{\partial x} + \frac{\partial p^* v/m}{\partial y}\right)\right\} d\sigma' \quad \text{A3.5)}$$

where σ' is a dummy variable of integration and $\dot{\sigma}(\sigma=0) = 0$

Thermodynamic Equation and Equation for Omega (ω)

$$\frac{\partial p^* T}{\partial t} = -m^2\left(\frac{\partial p^* uT/m}{\partial x} + \frac{\partial p^* vT/m}{\partial y}\right) - \frac{\partial p^* T\dot{\sigma}}{\partial \sigma} + \frac{RT_v\omega}{c_{pm}(\sigma+P_t/P_{past})} + \frac{P^* Q}{c_{pm}} + F_H T + F_V T \quad \text{(A3.6)}$$

Where:

c_{pm} is the specific heat for moist air at constant pressure

Q is the diabatic heating

F_HT represents the effect of horizontal diffusion

F_VT represents the effect of vertical mixing and dry convective adjustment

$$\omega = p^*\sigma + \dot{\sigma}\frac{dp^*}{dt} \quad \text{(A3.7)}$$

$$\frac{dp^*}{dt} = \frac{\partial p^*}{\partial t} + m\left[u\frac{\partial p^*}{\partial y} + v\frac{\partial p^*}{\partial y}\right] \quad \text{(A3.8)}$$

$$c_{pm} = c_p(1+0.8q_v) \quad \text{(A3.9)}$$

where:

c_p is the specific heat at constant pressure for dry air and q_v is the mixing ratio of water vapor.

Hydrostatic Equation

The hydrostatic equation is used to compute the geopotential heights from the virtual temperature T_v

$$\frac{\partial\Phi}{\partial\ln(\sigma+\frac{p_t}{p^*})} = -RT_v\left[1+\frac{q_c+q_r}{1+q_v}\right]^{-1} \quad \text{(A3.10)}$$

where:

$T_v=T(1+0.608q_v)$, q_v, q_c, and q_r are the water vapor, cloud water or ice, and rain water or snow, mixing ratios.

Appendix 4

Table A4.1: Comparison of BATS and CLM schemes in RegCM4

	BATs	CLM
Soil texture	FAO Soil Map of the World	IGBP soil dataset
Number of soil layers	3	10
Soil temperature calculation	Force-restore method	Heat diffusion equation
Soil freezing and thawing	Yes	A new frozen soil model (super cooled soil water)
Number of snow layers	1	5
Land use parameters	20 (GLCC)	5 land units, 17 types (PFTs) represent vegetation
Surface datasets	Leaf area index	MODIS products

Appendix 5: Estimation of parameters

Weilbull estimators

The Equation (6.2) can be transformed into a linear form by rearranging the equation and taking logarithms of both sides twice:

$$\mathrm{lnln}\left(\frac{1}{1-\mathrm{F(x)}}\right) = \mathrm{clnx} - \mathrm{clnb} \tag{A5.1}$$

A straight line with slope c and axis intercept b can fit this equation.

Gamma estimators

The shape (α) and scale (β) parameters can be estimated as follow:

Given precipitation value for wet days (x_i, i = 1,n), the likehood function for a gamma distribution can be written as:

$$f_n(x|\alpha,\beta) = \frac{1}{\Gamma^{\mathrm{n}}(\alpha).\beta^{\mathrm{n}\alpha}}\left(\prod_{i=1}^{n} x_i\right)^{\alpha-1} exp\left(-\sum_{i=1}^{n}\frac{x_i}{\alpha}\right) \tag{A5.2}$$

Taking the log, the log-likelihood function of the gamma distribution is the following:

$$l(\alpha,\beta) = -n.\log\left(\Gamma(\alpha)\right) - \mathrm{n}.\,\alpha.\log(\beta) + (\alpha-1)\sum_{\mathrm{i}=1}^{\mathrm{n}}\log(\mathrm{x_i}) - \frac{1}{\beta}\sum_{\mathrm{i}=1}^{\mathrm{n}}\mathrm{x_i} \tag{A5.3}$$

The α and β estimators ($\hat{\alpha}, \hat{\beta}$) are chosen to maximize the log-likelihood function. These values satisfy the following equations:

$$\log(\hat{\alpha}) - \frac{\Gamma'(\hat{\alpha})}{\Gamma(\hat{\alpha})} = \log(\bar{x}) - \frac{\sum_{i=1}^{n}\log(x_i)}{n} \tag{A5.4}$$

$$\hat{\beta} = \frac{1}{\hat{\alpha}}\bar{x} \tag{A5.5}$$

where

Γ' is the derivative of Γ gamma operator

According to Thom's study (Thom, 1957), the final product of the shape and the scale is approximated by the equations:

$$\hat{\alpha} = \frac{1}{4\left(\log(\bar{x}) - \frac{\sum_{i=1}^{n}\log(x_i)}{n}\right)}\left(1 + \sqrt{1 + \frac{4\left(\log(\bar{x}) - \frac{\sum_{i=1}^{n}\log(x_i)}{n}\right)}{3}}\right) \tag{A5.6}$$

$$\hat{\beta} = \frac{1}{\hat{\alpha}}\bar{x} \tag{A5.7}$$

Appendix 6: Definition for the indices

RX1day is the maximum 1-day precipitation. If RR_{ij} is the daily precipitation amount on day i in period j, the maximum 1-day precipitation value for period j is calculated as the following:

$$\mathrm{RX1day_j} = \max\{\mathrm{RR_{ij}}\} \quad \text{(A6.1)}$$

RX3day is the maximum 3-day precipitation. If RR_{ij} is the precipitation amount in 3-day interval i in period j, where i is defined by the last day, and the maximum 3-day values for perid j is calculated as the following:

$$\mathrm{RX3day_j} = \max\left\{\sum_{n=1}^{i} \mathrm{RR_{nj}}\right\} \quad \text{(A6.2)}$$

RX5day is the maximum 5-day precipitation. If RR_{ij} is the precipitation amount in 5-day interval i in period j, where i is defined by the last day, the maximum 5-day values for period j is calculated as the following:

$$\mathrm{RX5day_j} = \max\left\{\sum_{n=1}^{i} \mathrm{RR_{nj}}\right\} \quad \text{(A6.3)}$$

RX7day is the maximum 7-day precipitation. If RR_{ij} is the precipitation amount in 7-day interval i in period j, where i is defined by the last day, the maximum 7-day values for period j is calculated as the following:

$$\mathrm{RX7day_j} = \max\left\{\sum_{n=1}^{i} \mathrm{RR_{nj}}\right\} \quad \text{(A6.4)}$$

MCDD is the number of consecutive dry days. It is calculated as maximum length of dry spell with precipitation amount less than 0.1 mm. Let RR_{ij} be the daily precipitation amount on day i in period j. The count of the largest number of consecutive days where $RR_{ij} < 0.1$ mm is given by the following equation:

$$\mathrm{MCDD_j} = \sum_{i=1}^{n} \mathrm{RRC_i} \quad \text{(A6.5)}$$

where RRC = 1, if $RR_{ij} < 0.1$ mm; else RRC = 0

MCWD is the consecutive wet days. It is calculated as maximum length of wet spell with precipitation amount greater than or equal to 0.1 mm. Let RR_{ij} be the daily precipitation amount on day i in period j. The count of the largest number of consecutive days where $RR_{ij} \geq 0.1$ mm is given by the following equation:

$$\mathrm{MCWD_j} = \sum_{i=1}^{n} \mathrm{RRC_i} \quad \text{(A6.6)}$$

where RRC = 1, if $RR_{ij} \geq 0.1$ mm; else RRC = 0

Appendix 7: Main documents regarding climate change in Vietnam

Legal documents

The important legal documents include:

1998: Vietnam signed the Kyoto protocol on 3 December 1998 and officially ratified the Kyoto protocol on 25 September 2002.

2003: SRV, Socialist Republic of Vietnam & MONRE, Ministry of Natural Resources and environment (2003): Viet Nam - Initial National Communication – Under the United Nations Framework Convention on Climate Change.

2004: National Report on Disaster Risk Reduction in Vietnam, Ha Noi, Vietnam

2004: Sustainable Development Program in Vietnam under Decision No. 153/2004/QD-TTg dated 17 August 2004.

2005: On the implementation of the Kyoto protocol under the United Nations Framework Convention on Climate Change under Instruction No. 35/2005/CT-TTG dated 17 October 2005.

2007: National Strategy for natural Disaster Response, Prevention and Mitigation to 2020 has been approved in November 2007.

2007: The National Target Program to Respond to Climate Change under Decree No. 60/2007/NQ-CP dated 3 December 2007.

2008: Action Plan Framework for Adaptation to Climate Change in the Agriculture and Rural Development Sector Period 2008-2010, approved by the Minister of Agriculture and Rural Development promulgated Decision No. 2730/QD-BNN-KHCN dated 5 September 2008.

2008: The National Target Program to Respond to Climate Change under Decision No. 158/2008/QĐ-TTg dated 2 December 2008.

2011: The National Strategy on Climate Change was approved under Decision No. 2139/QD-TTg dated 5 December 2011.

2012: National committee on Climate Change was founded under Decision No. 43/QD-TTg dated 9 January 2012.

2013: Urban development Plan in Vietnam to Respond to Climate Change 2013-2020 phase under Decision No. 263/QD-TTg dated 31 December 2013.

Climate Change Scenario and Impact Assessment Studies

MONRE (2003). “Vietnamm Initial Communication to the UNFCCC”

IPCC AR4 (2007). “Fourth Assessment Report (AR4)”

MONRE (2009). “Climate Change, Sea Level Rise Scenarios for Vietnam”

ISPONRE (2009). “Vietnam Assessment Report on Climate Change”

MONRE (2010). “Handbook on analysis tools to guide climate change-partnership program Vietnam government and the German GTZ and IFAD.”

IMHEN (2010a). “Impacts of Climate Change on Water Resources and Adaptation Measures”

IMHEN (2010b). “Sea Level Rise-Scenarios and Possible Risk Reduction in Vietnam”

MONRE (2010). “Vietnam’s Second Communication to the UNFCCC”

MONRE (2012). “Climate Change, Sea Level Rise Scenarios for Vietnam”

IPCC AR5 (2013). “Fifth Assessment Report (AR5)”

IMHEN = Institute of Meteorology, Hydrology and Environment; IPCC = Intergovernmental Panel on Climate Change; ISPONRE = The Institute of Strategy and Policy on Natural Resources and Environment; MONRE = Ministry of Natural Resources and Environment; UNFCCC = United Nations Framework Convention on Climate Change.

Appendix 8

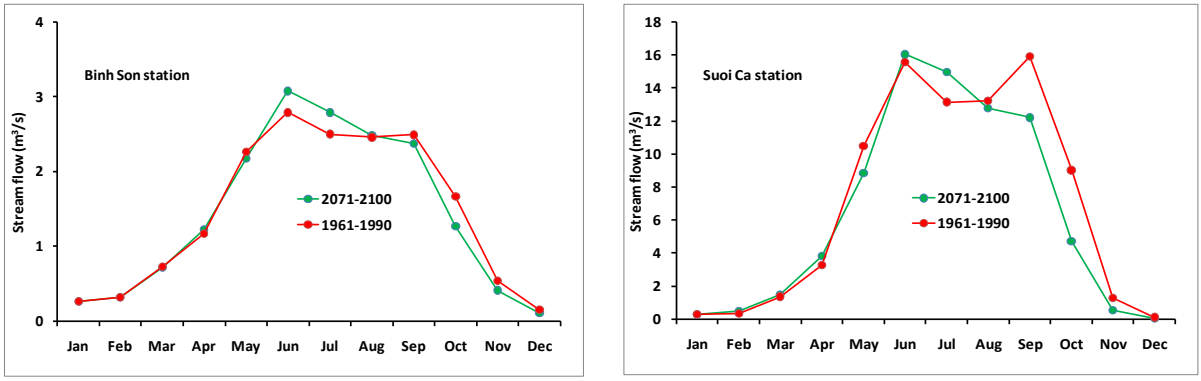

Figure A8.1: Simulated monthly stream flow for the base-line (1961-1990) and for the future (2071-2100) periods for the stations Binh Son and Suoi Ca (m3/s).

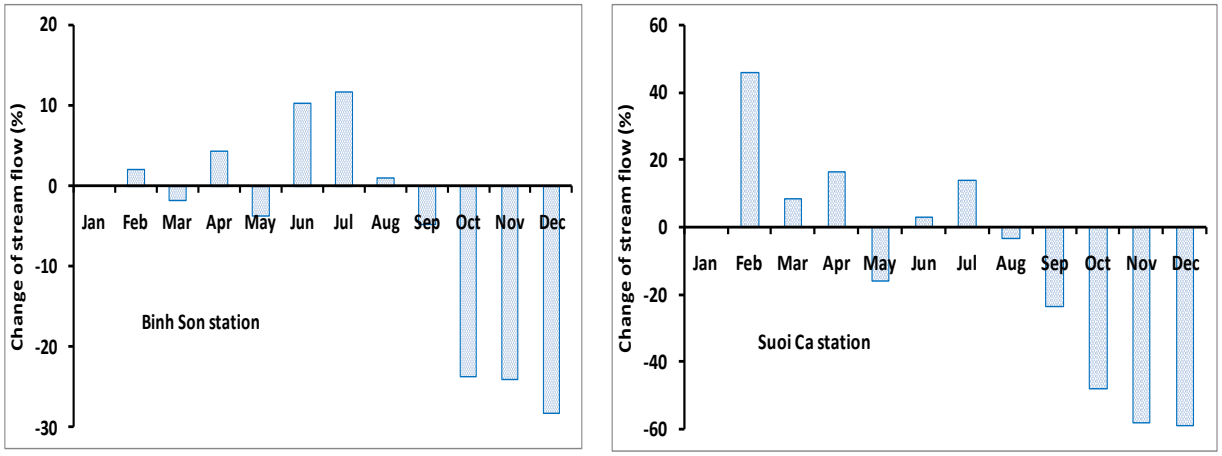

Figure A8.2: Projected monthly stream flow changes (2071-2100 compared to 1961-1990) for the stations Binh Son and Suoi Ca (%).

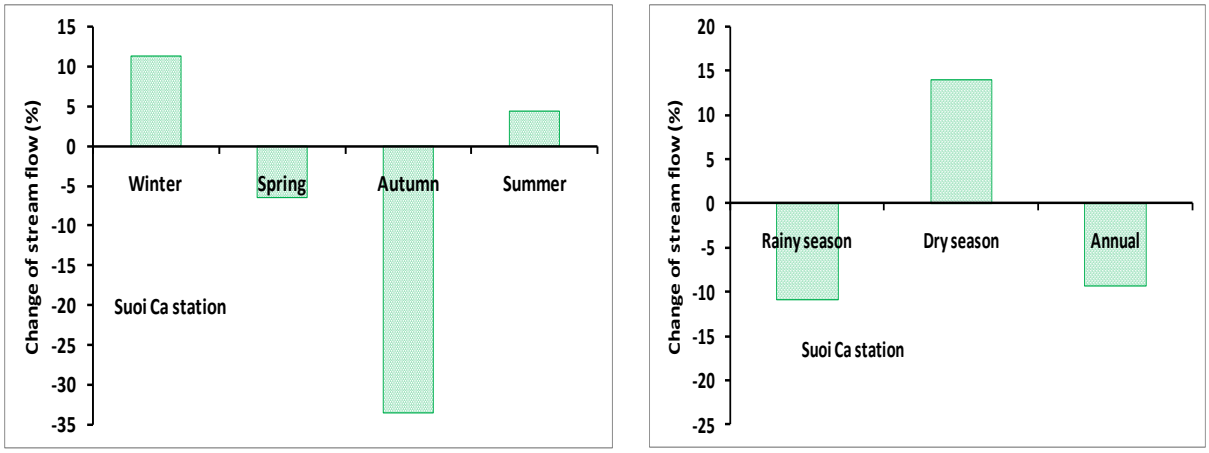

Figure A8.3: Projected seasonal stream flow changes (2071-2100 compared to 1961-1990) for four seasons (left) and for two seasons (right) for the station Suoi Ca (%).

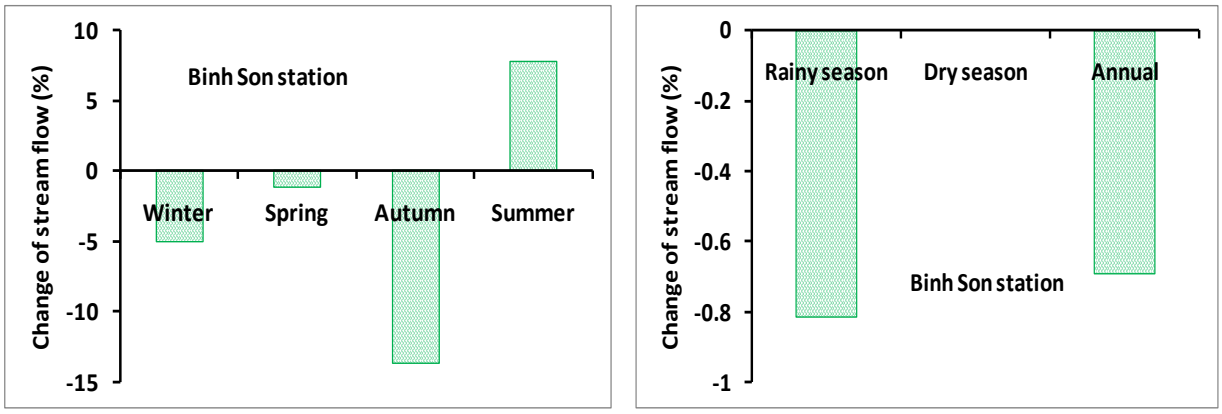

Figure A8.4: Projected seasonal stream flow changes (2071-2100 compared to 1961-1990) for four seasons (left) and for two seasons (right) for the station Binh Son (%).

List of figures

FIGURE 1.1: SCHEME OF THE MAIN STRUCTURE OF THIS THESIS. 8
FIGURE 2.1: "DOWNSCALING" SCHEME FROM COARSE TO FINE RESOLUTION. 10
FIGURE 2.2: THE DEVELOPMENT OF CLIMATE MODELS FROM THE 1970S TO THE PRESENT. 12
FIGURE 2.3: DEVELOPMENT OF CLIMATE MODELS FROM ZERO- TO THREE-DIMENSIONAL MODELS. 13
FIGURE 2.4: REPRESENTATION OF PHYSICAL PROCESSES IN THE THREE-DIMENSIONAL GRID OF AGCMS AND OGCMS, REPRESENTED BY INDIVIDUAL GRID BOXES. 14
FIGURE 2.5: THE NESTING OF A REGIONAL CLIMATE MODEL WITHIN A GLOBAL CLIMATE MODEL. 15
FIGURE 2.6: DOMAINS WITH THE ONE-WAY NESTING MM4 IN A GCM. 16
FIGURE 2.7: THE MM5 MODEL CONFIGURATION: THE DOMAINS AND RESOLUTIONS OF THREE NESTED MODELS. 17
FIGURE 2.8: THE TWO-WAY NESTED SYSTEM. 18
FIGURE 2.9: SCHEME OF THE RELATIONSHIP BETWEEN PREDICTOR AND PREDICTAND IN STATISTICAL DOWNSCALING. 19
FIGURE 2.10: APPROACHES OF STATISTICAL DOWNSCALING. 23
FIGURE 2.11: REPRESENTATION OF A TRANSFER FUNCTION METHOD. 26
FIGURE 2.12: THE VALIDATION AND VERIFICATION PROCESSES FOR A CLIMATE MODEL 28
FIGURE 2.13: CLASSIFICATION SCHEME FOR HYDROLOGICAL MODELS. 30
FIGURE 3.1: THE STUDY AREA RIVER BASIN IN RELATION TO THE MAIN RIVER BASIN IN VIETNAM. 34
FIGURE 3.2: TOPOGRAPHY OF THE STUDY AREA IN RELATION TO THE VIETNAM TOPOGRAPHY. 34
FIGURE 3.3: MONTHLY SUM OF RAINFALL AT THIRTEEN PRECIPITATION MEASURING STATIONS. 35
FIGURE 3.4: MAP OF PRECIPITATION MEASURING STATIONS CLOSE TO THE THAI VAI CATCHMENT. 36
FIGURE 3.5: BOX PLOT DIAGRAMS OF PRECIPITATION AT THE STATIONS LONG THANH, CAM MY, TAM THON HIEP AND THONG NHAT. 37
FIGURE 3.6: ANNUAL PRECIPITATION DISTRIBUTION FOR 13 PRECIPITATION STATIONS IN TIME AND SPACE. 38
FIGURE 3.7: VARIABILITY OF MONTHLY TEMPERATURE AT THE OBSERVATION STATIONS BIEN HOA, VUNG TAU, XUAN LOC AND TAN SON HOA DURING THE DIFFERENT PERIOD. 40
FIGURE 3.8: ATMOSPHERIC PRESSURE AT VUNG TAU STATION DURING 1979-2010. 41
FIGURE 3.9: WINDROSE FOR THE RAINY SEASON AND THE DRY SEASON AT THE STATIONS TAN SON NHAT, XUAN LOC AND VUNG TAU. 42
FIGURE 3.10: VARIABILITY OF MONTHLY EVAPORATION PER DAY AT VUNG TAU STATION DURING 1979-2013. 43
FIGURE 3.11: DAILY VARIABILITY OF HUMIDITY AT BIEN HOA STATION DURING THE PERIOD 1980-2013 43
FIGURE 3.12: LAND USE AND LAND COVER UNITS OF THI VAI RIVER CATCHMENT. 44
FIGURE 3.13: GEOLOGICAL MAP OF THI VAI CATCHMENT. 45
FIGURE 3.14: SOIL MAP OF THE THI VAI CATCHMENT 45
FIGURE 3.15: METEOROLOGICAL STATION: VUNG TAU STATION AND XUAN LOC STATION. 48
FIGURE 3.16: MONITORING LOCATIONS FOR DISCHARGE IN THE THI VAI RIVER CATCHMENT 49
FIGURE 4.1: SCHEMATIC VIEW OF THE COMPONENTS OF THE GLOBAL CLIMATE SYSTEM, THEIR PROCESSES AND INTERACTIONS. 55
FIGURE 4.2: ANOMALIES OF GLOBAL ANNUAL MEAN TEMPERATURES 56
FIGURE 4.3: TREND OF ANNUAL LAND PRECIPITATION IN DIFFERENT PARTS OF THE WORLD FOR 1901 TO 2005 AND 1979 TO 2005 57

FIGURE 4.4: SPATIO-TEMPORAL PATTERNS OF CHANGES IN GLACIER MASS. 58
FIGURE 4.5: THE MONSOON REGIONS OF THE WORLD ARE CLASSIFIED. 60
FIGURE 4.6: AVERAGE POSITION OF TROPICAL CYCLONES AND ITCZ. 61
FIGURE 4.7: VIETNAM TERRITORIAL WATERS AND THE NUMBER OF TCS LANDED BINH THUAN-CA MAU REGION. 62
FIGURE 4.8: RIVER RUN-OFF PER REGION. 66
FIGURE 5.1: AN ILLUSTRATION OF THE INSTRUMENTS THAT COMPRISE THE WMO GLOBAL OBSERVING SYSTEM. 69
FIGURE 5.2: MISSING OBSERVATIONAL DAILY PRECIPITATION BEFORE GAP FILLING. 73
FIGURE 5.3: DOUBLE MASS CURVES FOR THE RAINFALL AT THE STATIONS CAN GIO, CAM MY, MAC DINH CHI AND BINH CHANH 74
FIGURE 5.4: CUMULATIVE SUM CHARTS FOR MEAN TEMPERATURE AT THE STATIONS VUNG TAU AND BIEN HOA DURING 1981-2013. 80
FIGURE 5.5: SPATIAL DISTRIBUTION OF MONTHLY PRECIPITATION TRENDS WITH THE RESULTS OF THE MK TEST AT THE SIGNIFICANT LEVELS 0.1, 0.05 AND 0.01. 81
FIGURE 5.6: SPATIAL DISTRIBUTION OF SEASONAL AND ANNUAL PRECIPITATION TRENDS WITH STATISTICAL TESTS AT DIFFERENT SIGNIFICANT LEVELS 0.1, 0.05 AND 0.01. 83
FIGURE 5.7: MAP OF CONSIDERED PRECIPITATION STATIONS AND CUMULATIVE SUM CHARTS FOR DAILY PRECIPITATION AT THE FOUR STATIONS DURING DIFFERENT PERIOD. 84
FIGURE 5.8: A SCHEMATIC EXAMPLE OF REGRESSION KRIGING: FITTING A VERTICAL CROSS-SECTION WITH ASSUMED DISTRIBUTION OF AN ENVIRONMENTAL VARIABLE IN HORIZONTAL SPACE. 87
FIGURE 5.9: TAYLOR DIAGRAM DISPLAYING A STATISTICAL COMPARISON OF OBSERVATIONS WITH INTERPOLATION METHODS OF PRECIPITATION OVER THE THI VAI RIVER CATCHMENT FROM MAY TO NOVEMBER 2013. 88
FIGURE 5.10: SPATIAL DISTRIBUTION OF PRECIPITATION OVER THE THI VAI CATCHMENT FROM VARIOUS INTERPOLATION TECHNOLOGIES. 89
FIGURE 6.1: THE VERTICAL STRUCTURE WITH 16 LAYERS AS AN EXAMPLE. 93
FIGURE 6.2: TOPOGRAPHIC MAP OF GLOBAL DOMAIN FROM CGCM3. 95
FIGURE 6.3: TOPOGRAPHIC MAP OF THE DOMAINS WITH 30-SECONDS RESOLUTION FROM REGCM4. 95
FIGURE 6.4: SPATIAL DISTRIBUTION OF TEMPERATURE BIASES IN MEAN (1981-2010) FOR FOUR SEASONS. 98
FIGURE 6.5: AVERAGED (1981-2010) AIR TEMPERATURE IN DJF FOR ERA-INTERIM, CRU AND RCM4/ERA-INTERIM. 99
FIGURE 6.6: AVERAGED (1981-2010) AIR TEMPERATURE IN JJA FOR ERA-INTERIM, CRU AND RCM4/ERA-INTERIM. 100
FIGURE 6.7: LATITUDE-TIME PLOTS OF DAILY TEMPERATURE OF THE DRIVING DATA ERA-INTERIM AND RCM4/ERA-INTERIM DURING 1981-2010. 101
FIGURE 6.8: LONGITUDE-TIME PLOTS OF DAILY TEMPERATURE OF THE DRIVING DATA ERA-INTERIM AND RCM4/ERA-INTERIM DURING 1981-2010. 101
FIGURE 6.9: MONTHLY (1981-2010) SURFACE AIR TEMPERATURE OVER THE THI VAI BASIN. 102
FIGURE 6.10: TAYLOR DIAGRAM FOR THE PERFORMANCE OF TEMPERATURE SIMULATION AT THE ANNUAL SCALE FOR THE PERIOD 1981-2010. 103
FIGURE 6.11: SPATIAL DISTRIBUTION OF AVERAGE DAILY PRECIPITATION FOR APHRODITE (1981-2007), TRMM 3B42V7 (1998-2010) AND STATION DATA (1981-2010). 103
FIGURE 6.12: SPATIAL DISTRIBUTION OF PRECIPITATION BIAS FOR FOUR SEASONS. 105

FIGURE 6.13: AVERAGE PRECIPITATION IN MAM FOR RCM4/ERA-INTERIM, APTHRODITE, GPCC AND TRMM. ... 106
FIGURE 6.14: AVERAGE PRECIPITATION IN JJA FOR RCM4/ERA-INTERIM, APTHRODITE, GPCC AND TRMM. 107
FIGURE 6.15: AVERAGE PRECIPITATION IN SON FOR APTHRODITE, GPCC, TRMM AND RCM4/ERA-INTERIM. 107
FIGURE 6.16: LONGITUDE-TIME CONTOUR PLOTS OF DAILY PRECIPITATION FOR A BAND OF LATITUDE 10.3°N - 10.5°N. 108
FIGURE 6.17: DISTRIBUTION OF DAILY PRECIPITATION OVER THI VAI CATCHMENT. 109
FIGURE 6.18: MONTHLY PRECIPITATION OVER THE THI VAI BASIN. 109
FIGURE 6.19: PERFORMANCE OF RAINFALL SIMULATIONS OVER THE DOMAIN OF INTEREST AT THE MONTHLY SCALE. 110
FIGURE 6.20: GRID CELLS OF THE DOMAIN OF INTEREST. 111
FIGURE 6.21: RELATIONSHIP BETWEEN OBSERVED AND DOWNSCALED DAILY TEMPERATURE FOR RCM-OUTPUTS WITHOUT APPLYING MOS AND WITH THE APPLICATION OF MOS 112
FIGURE 6.22: DAILY PRECIPITATION INTENSITY BIAS FOR RCM4/ERA-INTERIM OUTPUTS COMPARED TO INTERPOLATED STATION DATA WITH THE APPLICATION OF TSM AND WITHOUT APPLYING TSM FOR THE PERIOD 1981-2010. 115
FIGURE 6.23: PERFORMANCE OF TSM AT GRID1 CELL: CORRECTED NUMBER OF WET DAYS, CORRECTED MONTHLY PRECIPITATION INTENSITY. 116
FIGURE 6.24: CUMULATIVE DISTRIBUTION OF STATION DATA, RCM4/ERA-INTERIM AND CORRECTED RCM4/ERA-INTERIM PRECIPITATION AT GRID1 CELL IN AUGUST FOR THE PERIOD 1981-2010. 117
FIGURE 6.25: WET DAY FREQUENCY BIAS BETWEEN RCM4/ERA-INTERIM OUTPUT AND OBSERVED DATA WITHOUT APPLYING TSM AND WITH THE APPLICATION OF TSM TO THE RCM4/ERA-INTERIM OUTPUT. 117
FIGURE 6.26: PROJECTED CHANGES OF SEASONAL PRECIPITATION OVER THE THI VAI RIVER BASIN FOR THE PERIOD 2071-2100 COMPARED TO 1961-1990 AND PROJECTED ABSOLUTE PRECIPITATION FOR THE FOUR SEASONS UNDER THE SRES A1B SCENARIO. 119
FIGURE 6.27: PROJECTED CHANGES OF MONTHLY PRECIPITATION OVER THE THI VAI RIVER BASIN FOR THE PERIOD 2071-2100 COMPARED TO 1961-1990 AND PROJECTED ABSOLUTE PRECIPITATION FOR EACH DECADE FROM 2071-2100 UNDER THE SRES A1B SCENARIO. 119
FIGURE 6.28: PROJECTED CHANGES OF SEASONAL TEMPERATURE OVER THE THI VAI RIVER BASIN FOR THE PERIOD 2071-2100 COMPARED TO 1961-1990 AND PROJECTED ABSOLUTE TEMPERATURE VALUES FOR THE DECADES IN 2071-2100 UNDER THE SRES A1B SCENARIO. 121
FIGURE 6.29: MONTHLY TEMPERATURE DIFFERENCE FOR THE DECADES 2071-2100 COMPARED TO 1961-1990 AND PROJECTED ABSOLUTE TEMPERATURE FOR THE DECADES IN 2071-2100 UNDER THE SRES A1B SCENARIO. 121
FIGURE 7.1: MAIN HYDROLOGICAL PROCESSES 123
FIGURE 7.2: SCREENSHOT OF THE WINDOWS IN THE TAB "METEOROLOGICAL STATIONS" IN PANTA RHEI. 124
FIGURE 7.3: FLOW CHART OF MODELING STREAM FLOW IN THE THI VAI RIVER BASIN USING PANTA RHEI. 128
FIGURE 7.4: HYDROGRAPHS OF SIMULATED AND MEASURED DISCHARGE AT THE STATIONS BINH SON, CAU VAC AND SUOI CA USING THE STATION DATA. 130
FIGURE 7.5: A COMPARISON OF REFERENCE STREAM FLOW USING CLIMATE STATION DATA AND DAILY STREAM FLOW SIMULATED WITH DOWNSCALED CLIMATE DATA FOR THE STATIONS BINH SON, SUOI CA AND CAU VAC, 2008-2009. 133
FIGURE 7.6: SIMULATED MONTHLY STREAM FLOW FOR THE BASELINE (1961-1990) AND THE FUTURE (2071-2100) PERIODS FOR THE STATION CAU VAC 134

FIGURE 7.7: SIMULATED MONTHLY STREAM FLOW FOR THE BASE-LINE (1961-1990) AND FOR THE FUTURE (2071-2100) PERIODS FOR THE STATION CAU VAC. 135
FIGURE 7.8: PROJECTED MONTHLY STREAM FLOW CHANGES (2071-2100 COMPARED TO 1961-1990) FOR THE STATION CAU VAC. 136
FIGURE 7.9: PROJECTED CHANGES IN MONTHLY STREAM FLOW (2071-2100 COMPARED TO 1961-1990) FOR THE THI VAI CATCHMENT THI VAI. 136
FIGURE 7.10: SIMULATED SEASONAL STREAM FLOW FOR THE BASELINE (1961-1990) AND THE FUTURE (2071-2100) PERIODS WITH FOUR SEASONS AND TWO SEASONS FOR THE STATION CAU VAC. 138
FIGURE 7.11: PROJECTED CHANGES IN SEASONAL STREAM FLOW (2071-2100 COMPARED TO 1961-1990) FOR FOUR SEASONS AND FOR TWO SEASONS FOR THE STATION CAU VAC. 139
FIGURE 7.12: PROJECTED CHANGES IN SEASONAL STREAM FLOW (2071-2100 COMPARED TO 1961-1990) FOR FOUR SEASONS AND FOR TWO SEASONS FOR THE THI VAI CATCHMENT THI VAI. 140
FIGURE 7.13: PROJECTED STREAM FLOW FOR FUTURE (2071-2100) AT THE OBSERVATION STATIONS. 141
FIGURE 7.14: PROJECTED DIURNAL STREAM FLOW CHANGES (2071-2100 COMPARED TO 1961-1990) FOR THE THI VAI CATCHMENT. 141
FIGURE 8.1: INTERACTION OF METEOROLOGICAL COMPONENTS AND THE WATER BALANCE AND THEIR FEEDBACKS... 146

List of tables

TABLE 2.1: ADVANTAGES AND DISADVANTAGES OF STATISTICAL AND DYNAMICAL DOWNSCALING METHODS. 21
TABLE 2.2: ADVANTAGES AND DISADVANTAGES OF DIFFERENT STATISTICAL DOWNSCALING METHODS. 22
TABLE 2.3: METHODS FOR THE EVALUATION OF NUMERICAL PREDICTION MODEL RESULTS. 27
TABLE 2.4: STATISTICAL EVALUATION INDICES. 28
TABLE 2.5: HYDROLOGICAL MODELS. 30
TABLE 3.1: PRECIPITATION CHARACTERISTICS ARE INVESTIGATED. 35
TABLE 3.2: VALUES FOR RX1DAY, RX3DAY, RX5DAY, AND RX7DAY FOR 13 PRECIPITATION STATIONS NEAR THE THI VAI CATCHMENT. 39
TABLE 3.3: MCWD, MCDD AND MWD FOR 13 PRECIPITATION STATIONS NEAR THE THI VAI CATCHMENT. 39
TABLE 3.4: POPULATION STATISTICS. 46
TABLE 3.5: LISTS OF THE PRECIPITATION MEASURING STATIONS. 47
TABLE 3.6: STRENGTHS AND WEAKNESSES OF DIFFERENT GRIDDED METEOROLOGICAL DATASETS. 51
TABLE 3.7: CHARACTERISTICS OF THE GRIDDED DATASETS USED IN THIS STUDY 53
TABLE 4.1: CHANGES IN TEMPERATURE AND PRECIPITATION DURING 1960-2009 FOR CLIMATE REGIONS IN VIETNAM. 63
TABLE 4.2: IMPACTS OF CLIMATE CHANGE ON SECTORS AND VULNERABILITY OBJECTS. 64
TABLE 4.3: CHANGES IN WATER RESOURCES IN MAJOR RIVER CATCHMENTS CAUSED BY CLIMATE CHANGE A MEDIUM CLIMATE CHANGE SCENARIO B2 IN COMPARISON WITH THE BASELINE PERIOD 1980-1999. 66
TABLE 4.4: OVERVIEW OF GREENHOUSE GASSES, OZONE PRECURSORS AND SULFUR EMISSIONS FOR THE SRES SCENARIO GROUPS BY THE YEAR 2100.. 67
TABLE 5.1: ESTIMATION OF DAILY PRECIPITATION AT CAM MY STATION BY ARITHMETIC AVERAGE METHOD. 71
TABLE 5.2: CORRELATION COEFFICIENTS BETWEEN PRECIPITATION MEASUREMENT STATIONS. 72
TABLE 5.3: ESTIMATION OF DAILY PRECIPITATION AT BINH CHANH STATION BY NORMAL RATIO METHOD. 72
TABLE 5.4: MK TEST FOR TEMPERATURE AT OBSERVATION STATIONS. 79
TABLE 5.5: RESULTS OF SEN'S SLOPE FOR MONTHLY AND ANNUAL PRECIPITATION. 80
TABLE 5.6: RESULTS OF STATISTICAL TESTS FOR SEASONAL AND ANNUAL PRECIPITATION. 82
TABLE 6.1: THE DEVELOPMENT OF THE REGCM MODEL VERSIONS. 90
TABLE 6.2: EXPERIMENTAL CONFIGURATION DESIGN OF LAND SURFACE SCHEMES, DOMAINS AND RESOLUTIONS. 96
TABLE 6.3: CORRELATION COEFFICIENT BETWEEN THE SIMULATED AND OBSERVED TEMPERATURE IN THE PERIOD 1981-2010. 99
TABLE 6.4: LARGE-SCALE PREDICTOR VARIABLES FOR THE "CORRECTION" OF DAILY TEMPERATURE. 111
TABLE 7.1: SELECTED PROCEDURES FOR WATER BUDGET. 128
TABLE 7.2: STATISTICAL EVALUATION INDICES. 129

Abbreviations

ADB	Asian Development Bank
AGCMs	Atmospheric General Circulation Models
ANNs	Artificial neural networks
APTHRODITE	Asian Precipitation-Highly-Resolved Observational Data Integration Towards Evaluation
AS	Arakawa-Schubert: Arakawa-Schubert convection scheme
BATS	Bio-Atmospheric Transfer Scheme version 1e
BMJ	Betts-Miller-Janjic: Betts-Miller-Janjic convection scheme
CCA	Canonical correlation
CCM1	NCAR Community Climate Model version 1
CGCM3	Canadian Centre for Climate Modelling and Analysis (CCCma) Coupled Global Climate Model version 3
CLM	Community Land Model
CORDEX	Coordinated Regional Climate Downscaling Experiment
COSMO	COnsortium for SMall scale Modeling
CRCM	Canadian Regional Climate Model
CRU TS3.21	Climatic Research Unit (CRU) Time-Series (TS) version 3.21
DDM	Dynamical Downscaling Method
DJF	December, January and February
DK	Dual Kriging
ECHAM	An atmospheric general circulation model, developed at the Max Planck Institute for Meteorology.
ECMWF	European Center for Medium Range Weather Forecasts
ERA40	An ECMWF reanalysis of the global atmosphere and surface conditions for 45-years, over the period from September 1957 through August 2002 by ECMWF
ERA-Interim	A global atmospheric reanalysis from 1979 to present
FC	Fritsch-Chappell: Fritsch-Chappell convection scheme
GCMs	Global Climate Models
GHCN	Global Historical Climatology Network
GPCC	Global Precipitation Climatology Centre
HadCM2	Hadley Centre Coupled Model version 2
HadCM3	Hadley Centre Coupled Model version 3
ICTP	International Centre for Theoretical Physics, Italy
IDW	Inverse Distance Weighting
IPCC AR4	IPCC the 4th Assessment Report
IPCC AR5	IPCC the 5th Assessment Report
IPCC FAR	IPCC the First Assessment Report
IPCC SAR	IPCC the Second Assessment Report

IPCC TAR	IPCC the Third Assessment Report
IPCC	Integovernmental Panel on Climate Change
ISI-MIP	Inter-Sectoral Impact Model Intercomparison Project
ITCZ	Internal Tropical Convection Zone
JJA	June, July, and August
LAM	Limited Area Model
LARS-WG	Long Ashton Research Station Weather Generator
LBCs	Lateral Boundary Conditions
MAM	March, April and May
MK	Mann-Kendall
MLR	Multiple linear regression
MM4	Mesoscale Model version 4
MM5	Mesoscale Model version 5
MONRE	Ministry of National Resources and Environment, Vietnam
MOS	Model Output Statistics
MRI/JMA	Meteorological Research Institute of Japan Meteorological Agency
NCAR	National Center for Atmospheric Research (USA)
NCEP	National Center for Environmental Prediction
NOAA	National Oceanographical and Atmospheric Administration
OGCM	Oceanic General Circulation Models
OK	Ordinary Kriging
PCA	Principal Component Analysis
PP	Perfect Prognosis
PR	Precipitation Radar
PRECIS	Providing REgional Climates for Impacts Studies
PSU	Pennsylvania State University
RCMs	Regional Climate Models
REMO	REgional MOdel
RIHN	Research Institute for Humanity and Nature
RK	Regression Kriging
SOM	Self-Organizing Maps
SON	September, October and November
SRES	Special Report on Emission Scenarios
STARDEX	Statistical and Regional dynamical Downscaling of Extremes for European regions
SVD	Singular Value Decomposition
SWAT	Soil and Water Assessment Tool
TCs	Tropical Cyclones
TMI	TRMM Microwave Imager
TRMM	Tropical Rainfall Measuring Mission
TSM	Two-Step Model
TWN	Two Way Nesting

UNFCCC	United Nations Framework Convention on Climate Change
VHMDC	National Hydro-Meteorological Data Center, Vietnam
WGs	Weather Generators
WMO GTS	World Meteorological Organization's (WMO) Global Telecommunications System
WMO	World Meteorological Organization
WRCP	World Climate Research Programme
WWR	World Weather Records